ISBN 978-82-326-2114-9 (printed version)
ISBN 978-82-326-2115-6 (electronic version)
ISSN 1503-8181

Doctoral theses at NTNU, 2017:14

Kristoffer Rist Skøien

Feed Distribution in Large Scale Sea Cage Aquaculture

Experiments, modelling and simulation

Doctoral Thesis
Kristoffer Rist Skøien

NTNU
Norwegian University of
Science and Technology
Faculty of Information Technology,
Mathematics and Electrical Engineering
Department of Engineering Cybernetics

NTNU
Norwegian University of
Science and Technology

Doctoral theses at NTNU, 2017:14

NTNU

NTNU
Norwegian University of
Science and Technology

Kristoffer Rist Skøien

Feed Distribution in Large Scale Sea Cage Aquaculture

Experiments, modelling and simulation

Thesis for the degree of Philosophiae Doctor

Oslo, January 2017

Norwegian University of Science and Technology
Faculty of Information Technology,
Mathematics and Electrical Engineering
Department of Engineering Cybernetics

NTNU
Norwegian University of
Science and Technology

NTNU
Norwegian University of Science and Technology

Thesis for the degree of Philosophiae Doctor

Faculty of Information Technology,
Mathematics and Electrical Engineering
Department of Engineering Cybernetics

ISBN 978-82-326-2114-9 (printed version)
ISBN 978-82-326-2115-6 (electronic version)
ISSN 1503-8181

ITK Report 2017-2-W

Doctoral theses at NTNU, 2017:14

Printed by Skipnes Kommunikasjon as

To my beloved Kristina

Summary

The objective of this thesis was to gain new insight into the process of feeding in large scale sea cage aquaculture and investigate novel methods of feeding in order to increase profitability, welfare and minimize environmental impact.

Compared to livestock farming, Atlantic salmon (*Salmo salar*) farming is a young industry which has experienced an almost exponential growth rate and the product continues to be in high demand. A single cage in Norway may contain more than a 1000 tonnes of fish in the form of 200.000 individuals. Such a figure is difficult to comprehend, but one may draw a parallel to the equivalent of 1600 cows inside a single cage. Feeding of fish kept in sea cages is a complicated endeavour compared to land based farming for a number of reasons. Thousands of individuals co-exist in a single three-dimensional dynamic space, observation is restricted to surface inspections or a submerged camera with limited field of view, feed can not be given to a specific fish and the location of feed is difficult to predict as a consequence of currents and fish induced turbulence. In addition, feed which is not consumed from the time it is distributed over the surface to it passes through the cage represents a direct economic loss and acts as an unnecessary nutrient discharge to the environment. Over 10.000 kg of feed may be administered to a single cage towards the end of a production cycle and is the single largest cost in Norwegian salmon farming. Even though the process of feeding is a complicated one, the systems used to distribute feed are simple. Significant effort has been made in determining the ration size, meal frequency and at what time of day Atlantic salmon should be fed.

This thesis looks into the temporal feed availability on a meal to meal basis and goes into depth with respect to the spatial availability of feed within the sea cage. Many studies on a smaller scale indicate that spatially and temporally restrictive feeding may lead to unequal feed accessibility, loss of growth potential and elevated levels of aggression. With respect to controlling the spatial distribution of feed, it has been shown that current methods cover a small area of the cage surface. In addition, existing methods have limited ability to increase the feed distribution without exhibiting other detrimental effects such as increased pellet breakage. There is also no way of controlling where feed is placed as a consequence of wind

or currents. Experimental results are presented to better understand the dynamics of a feed spreader, a model has been developed and the performance of different spreader designs investigated. Further experimental results for settling rate and diffusion of pellets are presented and have been used to parametrize a full sea cage model. This model enables simulation of environmental factors, feeding methods and fish to predict the effect on central production parameters. Finally, using these two models, different feeding regimes are simulated and the consequent effects on spatiotemporal feed distribution, feed intake and feed loss are commented upon.

It is likely that by increased use of environmental measurements run through feed distribution models and having more adaptable methods of feed placement, one can in the future minimize the environmental impact whilst maintaining high growth rates and good fish welfare.

Preface

This thesis is submitted in partial fulfilment of the requirements for the degree of Philosophiae Doctor (Ph.D.) at NTNU - the Norwegian University of Science and Technology.

This work has been performed at the department of Engineering Cybernetics (ITK) under the supervision of Associate Professor Jo Arve Alfredsen and Adjunct Associate Professor Morten Omholt Alver.

Funding has been provided by NTNU and CREATE - Centre for Research-based Innovation in Aquaculture Technology, SINTEF Sealab, NO-7645 Trondheim, Norway and the Research Council of Norway - grant number 174842. The enclosed work was undertaken from 2012 to 2016.

The results in this thesis are to a large extent applicable to sea cage farming of any species of fish. However, Atlantic salmon (*Salmo salar*) has been used to frame the content as this is the most cultured species in Norway. On certain topics, particularity related to fish behaviour, feeding and aggression, publications based solely on Atlantic salmon were sometimes scarce. Hence, research conducted on other species of the Salmonidae family have been referenced at times. References to papers and manuscripts which are part of this thesis are stated in upper case and underlined Latin lettering. Related experiments are given in underlined numerals. The thesis contains limited programmatic and mathematical details. The reader is invited to consult the enclosed papers for a comprehensive description of the technical specifics.

Kristoffer Rist Skøien - Oslo, January 6, 2017

Acknowledgements

First and foremost I would like to extend my deepest gratitude to my supervisors Associate Professor Jo Arve Alfredsen and Adjunct Associate Professor Morten Omholt Alver. Their input and the discussions between us have been invaluable throughout this period. At times when progress was painstakingly slow, spirits were low and everything seemed to fail, the encouragement and space to gather strength

was greatly appreciated. I am also indebted to Associate Professor Øyvind Stavdahl, Adjunct Professor Harald Martens and Dr. Pål Liljebäck at ITK for valuable input and discussions. Further, I greatly appreciate the collaboration I have had with Dr. Kevin Frank, Andreas Myskja Lien, Dr. Pascal Klebert and Sarah Lundreagan at SINTEF Fisheries and Aquaculture, Finn Victor Willumsen, Guttorm Lange and Terje Bremvåg at ACE, Dr. Turid Synnøve Aas and Dr. Torbjørn Åsgård at Nofima.

I have enjoyed many fine moments with my colleagues and dear friends at ITK. Gaming nights, social gatherings, trips and the general good spirited mood at ITK has been of great value. There are so many I would like to thank for the camaraderie and fun we have had both on and off work. Though, I would especially like to thank Kristian Klausen, Lorenzo Fusini, Artur Zolich, Dr. Hodjat Rahmati, Serge Gale, Dr. Christian Holden and Dr. Torstein Bø for our discussions, assistance with my experiments and the help you provided towards the contents of this thesis. An extra thank you to my office mates, Dr. Martin Føre and Sheng Yan for discussions, ice-cream trips and countless cups of coffee.

I would also like to thank Associate Professor Tim Dempster at the University of Melbourne for allowing me to join him and his team as a visiting researcher. He and many of the Ph.D. students at the school of BioSciences taught me much regarding fish biology and gave me a great stay in Melbourne and Tasmania. A big thank you to Fransica Samsing, Alice Gibbons, Luke Barrett and Daniel Wright.

There are some teachers who deserves an extra thank you for the enthusiasm, knowledge and inspiration they gave me both as a child and adult. Maja Wergeland at Ramstad junior high school, Thomas Christian Philibert at Stabekk upper secondary school, Georg Milvang, Rolf Ingebrigtsen and Dr. Finn Haugen at Oslo University College. A big thank you to Associate Professor Amund Skavhaug and Professor Thor Inge Fossen for supervising my project and master's thesis. The experiences gained from this work contributed significantly to writing publications and this thesis.

I am also greatly indebted to the workshop and technical staff at ITK. Without your assistance, the experiments in this thesis would not have been possible to conduct. Thanks to Torkel Hansen, Stefano Bertelli, Rune Mellingseter, John Olav Horrigmo, Terje Haugen, Per Inge Snildal, Glenn Angell and Daniel Bogen. Also I would like to express my gratitude to the administrative staff at ITK. The help of Tove Kristin Blomset Johnsen, Eva Amdahl, Unni Johansen, Bente Seem Lindquist and Janne Karin Hagen has been greatly appreciated in relation to orders, travels and my duty work at ITK. I hope that the cageball team at ITK keeps going strong. It has been an absolute joy (and pain) playing with you.

A heartfelt thank you to my dearest friends, located in Oslo, Trondheim and the rest of the world. Whether we have met through school, work, common friends, travels or otherwise. We have shared so many great moments together, computer

games, board games, dinners, stag nights, parties, cabin trips, travels, russ and so much more. The stories we have created together and the fun we have had brings a smile to my face every time. I am truly looking forward to all the new experiences we will share through the rest of life.

I would like to proclaim my deepest gratitude to my entire family, especially my mother Hilde, father Espen and brother Lasse. They have been there for me throughout all aspects of life and provided immense support through the sunny and rainy days. My father's interest in electronics is what started my fantastic journey down the engineering path. Finally, my beloved Kristina. I remember well when we decided to journey back to Trondheim and move in together. It has been some great years and I am now looking very much forward to moving back to Oslo with you. Your support through these years, and coming home to your smile after a rough day meant the world to me. We are getting married!

I love you with all my heart.

Contents

List of figures

List of tables

Chapter 1

Introduction

1.1 Atlantic salmon farming in the bigger picture

Agriculture has been practised since 10.000 – 8000 years B.C. (Costa-Pierce, 2008, p.5) and farmed animals have for thousands of years been the primary source of human protein consumption (Vigne, 2011, review by). Today, mainly through pig, chicken and cattle production but also sheep, goat and buffalo (FAO, 2014b). Common for all these species is that farming is done on dry land where processes such as maintaining enclosures, feeding, monitoring and slaughtering are less complex compared to farming fish in an aquatic environment. The earliest evidence of fish aquaculture is from Egypt (Costa-Pierce, 2008, p.8) dating back to 2000 years B.C. With a comparatively brief 60–year history, the amount of farmed Atlantic salmon worldwide is very limited compared to pig, chicken and cattle, but the picture is opposite from a Norwegian perspective (Figure 1.1, 1.2).

With world population on the rise and increased standard of living, the demand for protein is higher than ever. High pollution, global warming and scarcity of resources means that finding sustainable food options is more important than before. This combined with a general elevated awareness and focus on the environment (Ellingsen et al., 2009) drives science to look for new methods of protein production.

Increased use of the oceans may be a possible alternative to expanding land-based animal farming as they offer vast areas of unused space. However, simply continuing to harvest fish from the oceans is not possible as the percentage of overexploited marine fish stock increased from about 10 to 28.8 % from 1974 to 2011 (FAO, 2014a, p.37). In addition, the percentage of fully exploited marine fish stocks was 61.3 % in 2011, which implies that there is no more room for increasing catch rates in these regions and the stocks may even be at risk of declining (FAO, 2014a, p.37). Thus, increased capture of wild fish is not a viable option for meeting the protein demand in many parts of the world. While production from wild

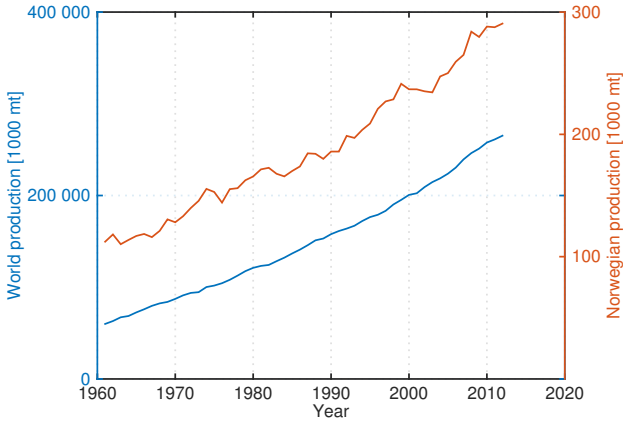

Figure 1.1: The worldwide and Norwegian production of meat from pig, chicken and cattle. Data obtained from FAO (2016b).

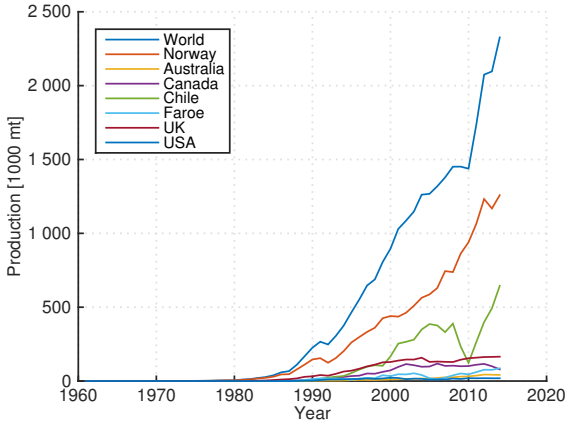

Figure 1.2: Production of farmed Atlantic salmon. Worldwide and a selection of nations based on Oppedal et al. (2011). Data obtained from FAO (2016a).

fisheries has remained stable for some time, aquaculture is one of the most rapidly expanding sectors of animal food production (FAO, 2014a, p.iii). Fish farming can be advantageous as it may reduce pressure on wild stocks, as most of the feed constituents in Norway are of plant origin. However, a percentage of the feed still originates from wild marine sources (Chapter 1.3). Farming also enables selective breeding programmes and provide some influence over the growth environment. Increased food production may also come from feeding farmed fish low quality fish materials, as well as fish by-products and unconventional constituents such as plankton and seaweed.

Worldwide, different species of carp are by far the most common cultured fish, followed by various species of tilapias, cichlids, goldfish, cyprinids and catfishes (FAO, 2012). Atlantic salmon is the most frequently cultured diadromous species and its popularity continues to increase in the world market (FAO, 2014a, p.21). Farming of caged fish was pioneered in Norway at the end of the 1950s and was targeted towards rainbow trout and Atlantic salmon (Grøttum and Beveridge, 2007). The percentage of salmon's share in world fish trade is now 14 % by value and has risen sharply over the last decades which is mostly attributed to increased production of trout and salmon in northern Europe and the Americas (FAO, 2014a, p.58). The rise in popularity combined with a price that is higher compared to most farmed freshwater finfish (FAO, 2014a, p.23) makes Atlantic salmon a popular choice for farmers.

Although a popular commodity, Atlantic salmon farming is not without challenges or controversy. Escapes from fish farms has been a major topic of debate and remains a vigorously discussed issue. Escaped salmon may act as vectors, transferring diseases and parasites to wild stock (Hansen, 2006; Grøttum and Beveridge, 2007). Interbreeding may reduce fitness of wild salmon (McGinnity et al., 2003) and high presence of farmed salmon also makes evaluation of wild stocks difficult (Hansen, 2006).

The Norwegian industry has also been plagued with parasites and diseases such as sea-lice, pancreas disease (PD), infectious salmon anaemia (ISA) and more recently amoebic gill disease (AGD). Some of these may also negatively affect wild fish stocks. These challenges are attacked with vigour by the industry, government and scientists. The industry has seemingly grown more transparent in the latter years, opening up for increased collaboration and discussion. The government has also increased their efforts, not just by introducing rules and legislations, but also by stimulating development and use of new technology through green concessions. In addition, in 2015 the Norwegian directorate of fisheries introduced development concessions ("utviklingstillatelser") which are free but demand considerable levels of innovation.

There are several positive aspects of Atlantic salmon farming. With respect to eco-friendliness, a Swiss report (Buchspies et al., 2011) indicated that for greenhouse gasses alone, farmed Norwegian salmon had slightly higher emission compared with poultry and pork, but much lower compared to lamb, beef and veal production. However, when factoring in nutrient emissions and copper oxide used in anti-fouling agents the emissions are much higher. Feed was by far the most significant contributor to the overall CO_2 production related to production of farmed salmon (Buchspies et al., 2011) as well as energetic input and general emissions (Pelletier and Tyedmers, 2007). Another study by González et al. (2011) showed that the amount of greenhouse gases (kg CO_2 eq./kg food) for Norwegian salmon was comparative to Swedish chicken, lower than pork and much lower

than mutton, lamb and beef. However, the sources in González et al. (2011) were numerous and also factored in transport costs to Sweden. There are many ways of calculating and comparing the environmental impact of different sources of protein against each other making it difficult to draw definitive conclusions. In addition, the diet composition of Atlantic salmon feed has changed dramatically over the last 30 years (Ytrestøyl et al., 2014). Just from 2010-13 there has been a sizeable migration from marine constituents to e.g. vegetable oils, making salmon farming less dependent on use of wild catches for feed production. This does render older studies less valuable for comparison. Overall, it seems that farmed Atlantic salmon may be a viable alternative to several other sources of animal protein with respect to greenhouse gas emissions.

Farming of Atlantic salmon is also a major employer and contributor to the Norwegian economy. In 2015 there were 974 concessions in Norway for salmonids (Atlantic salmon and trout species) of which 86 were research and development concessions (Norwegian Directorate of Fisheries, 2016a). Over 4300 people were directly employed in the grow-out production of these salmonids in 2014 (Norwegian Directorate of Fisheries, 2016b) and a further 1400+ in the production of juveniles (Norwegian Directorate of Fisheries, 2015b). These numbers do not account for the vast number of people involved in transport, equipment production, research and other numerous affiliated traits. The value of slaughtered Norwegian Atlantic salmon was over 44 billion NOK in 2015 (Norwegian Directorate of Fisheries, 2016c, prelim.) corresponding to about 4600 million Euro (31. Dec 2015 exchange rate).

Being a renewable resource, the potential for Atlantic salmon farming is vast given that the challenges associated with all steps of the production process can be properly addressed and solved.

1.2 Growth of farmed Atlantic salmon

The life of an Atlantic salmon starts out as an egg and when hatched the fish is known as an alevin. Being anadromous, the alevins can only survive in fresh water and the first stages of growth are conducted in indoor fresh water tanks. The eggs develop from alevins into fry, parr and finally smolts over the course of 10–16 months at which point they weigh 60–100 g (FHL and EFF, 2011). During this period a wide range of feeds may be presented to the fish, adapted to their current developmental stage (Skretting, 2012). It is in the parr-smolt transition (smoltification) that the physiological, behavioural and morphological changes which adapt the fish to life in a salt water environment take place (Hoar, 1963).

After the juvenile tank-based period, the post-smolts are transferred to sea cages where the marine grow-out phase takes place. During the course of 14–22 months at sea, the fish reach their slaughter weight of 4–6 kg (FHL and EFF,

2011) and are then transported to shore for slaughtering, processing and packaging. A salmon farm typically consist of a central barge which handles feeding and monitoring of 4-16 sea cages (Figure 1.3). Feed is delivered to the barge by ship and loaded into onboard silos. An array of blowers generate compressed air which is first cooled through submerged piping before entering the area below the silos. A series of feeding screws, doser valves and selectors enable several combinations of silos which may contain differently sized or formulated feeds to be routed to the individual sea cages where a feed spreader distributes the feed across the surface (Chapter 3). The blowers provide an airflow of 15–30 m/s which transports the pellets through floating pipes that may be up to 800 m long (Aarseth et al., 2006) to the sea cages. The cages themselves consist of a floating collar commonly made of plastic or steel which keeps the cage afloat and provides a surface for walking the circumference for inspection and maintenance. Rectangular cages tend to have 20–40 m sides and be 20 to 35 m in depth, while circular cages may have circumferences of 90–157 m and can be up to 48 m deep (Oppedal et al., 2011). In Tasmania, even larger circular cages are in use with circumferences up to 240 m. A farm site is often located in the relative shelter of a fjord, which provides some protection from the harsh coastal weather whilst providing sufficient water exchange to allow removal of waste materials and good supply of oxygenated water. Alternatively, and with increasing popularity, a farming site may be situated in more exposed coastal waters but close to shore to facilitate rapid transport of fish, personnel and equipment.

According to Norwegian legislation, a single cage may not hold more than 25 kg/m^3 of fish and a maximum of 200.000 individuals (Norwegian Ministry of Fisheries and Coastal Affairs, 2008).

1.3 The feed pellets

There has been a major shift in how feed was manufactured from when farming first began until the start of the 1980s (Grøttum and Beveridge, 2007). Before this, pellets were often made on site consisting of minced sardines and other low cost fish blended with vitamins, minerals and wheat flour (Grøttum and Beveridge, 2007) typically resulting in feeds with low feed conversion ratio (FCR) and poor water stability. This further evolved from about 1985 to the early 1990s to commercially made dry feeds, and was from 1993 replaced by extruded feed (Grøttum and Beveridge, 2007). Modern feed production has seen a marked shift away from marine constituents. In 1990, about 90 % of Norwegian salmon feed were of marine origin, compared to just 30 % in 2013 (Ytrestøyl et al., 2015). In 2013, the Norwegian feed composition was 18.3 % marine protein, 10.9 % marine oils, 36.7 % plant protein, 19.2 % plant oil and the remainder starch and micro

ingredients (Ytrestøyl et al., 2015). The density of pellets is carefully adapted to achieve a pellet which does not float, and on the other hand sinks slowly such that it remains within the sea cage for as long as possible. Usually, pellets settle at a rate of 6 to 20 cm/s (Paper E).

1.4 Feeding and feed loss

Correct feeding during the marine phase is of critical importance as it is strongly linked to profitability, fish welfare and nutrient discharge. Given an average weight of 5 kg/fish during the final stage of grow-out and with a feed ration of 1 % body weight per day (Oehme et al., 2012) equates to 10 tonnes of feed supplied to each cage every day. On a site level this may equate to as much as 160 tonnes per day. Feed makes up about 50 % of the total farming costs of Atlantic salmon and rainbow trout in Norway (Norwegian Directorate of Fisheries, 2015c; Aas et al., 2011) and some claim up to two-thirds of the total cost. Feed is also the most important contributor to emissions and resource consumption in sea cage salmonid culturing at the farm-gate (Pelletier et al., 2009). Other life cycle assessment studies and environmental analyses of Canadian (Ayer and Tyedmers, 2009) and Norwegian farming (Ellingsen et al., 2009; Buchspies et al., 2011) supports this finding.

With such amounts of feed being distributed on a daily basis just from a single location, utilizing the feed to its maximum potential is of paramount importance. This implies that all feed delivered to the barge should ideally end up being digested by the fish. However, along the way feed may be lost in the form of breakage in the pneumatic transport system (Aarseth, 2004; Aarseth et al., 2006) ending up as dust or feed fragments when entering the sea cage. Dust will be carried away by the wind and causes release of nutrients into the water (Aas et al., 2011). Neither dust or undersized particles have any value as feed (Aas et al., 2011) and are regarded as feed loss.

Not only dust and fragments are lost, but intact pellets may also pass through the sea cage without being consumed. The total feed loss from Norwegian commercial farms is a cumbersome figure to obtain. Uglem et al. (2014) and Taranger et al. (2012) claim that there are no publications on feed loss from commercial farming available. The literature uses a variety of sources when citing feed losses. Table 1.1 summarizes some of the sources which have been widely cited with respect to feed loss. In addition, feed loss of 10 % have been suggested from an anonymous source within the aquaculture industry in 2012.

From Table 1.1: Otterå et al. (2009), Gjøsæter et al. (2008), Cromey et al. (2002) and Milewski (2001) gives numbers on feed loss without providing a clear source of the material. Further, Brooks and Mahnken (2003) states that ≤ 5 % feed

Table 1.1: Feed loss in fish farming

Source	Description	Feed loss	Based on
(Otterå et al., 2009)	Norwegian Salmonids	5 %	Assumption
(Gjøsæter et al., 2008)	Norwegian farming	7 %	Assumption
(Brooks and Mahnken, 2003)	Salmon in net-pens	$\leq$ 5 %	Review
(Cromey et al., 2002)	Marine cage farms	$<$ 5 %	No clear source
(Goulão et al., 2001)	Gilt-head bream *Sparus aurata*	8.3 %	Experiment, bottles (poorly described)
(Milewski, 2001)	Canadian salmon aquaculture	15 % (Claimed to be low)	No clear source
(Findlay and Watling, 1994)	Salmon net-pen aquaculture, Maine, USA	11 % and 5 %. The latter suggested as representative	Experiment, sediment traps
(Seymour and Bergheim, 1991)	Norwegian Atlantic salmon	1/3	Estimate based on FCR
(Thorpe et al., 1990)	500 g Atlantic salmon in sea cage	1.4 % by hand, 40.5 % from localized feeder	Experiment, x-ray markers

loss is probable based on a literature review and Seymour and Bergheim (1991) gives 1/3 feed loss as a plausible figure based on FCR numbers. The remaining entries in Table 1.1 are experimental. However, Goulão et al. (2001) is based on Gilt-head bream (*Sparus aurata*) in Spain and may not be seen as relevant. Goulão et al. (2001) used a series of collector bottles along the sides and bottom of the sea cage but provides no details as to what feeding regime was used or how the final feed loss was calculated. Findlay and Watling (1994) used sediment traps under salmon sea cages and detected 11.0 and 5 % feed wastage. However, the authors claimed this to be a high figure and recommended a middle value of 5 % feed wastage especially for hand-fed farms. Thorpe et al. (1990) used x-ray opaque balls to detect the amount of feed eaten by one year old Atlantic salmon in a 8×8×4

m sea cage. 1.4 % feed loss was observed from hand feeding and 40.5 % from a sharply localized automated feeder.

In summary, to the author's knowledge there are no recent experiments from large scale aquaculture using modern production methods that accurately quantify the feed loss from a sea cage. However, there are other indicators of feed loss as well. An experiment across nine farms in three different Norwegian regions (Dempster et al., 2011) showed that aggregations of wild fish in the vicinity of a single farm might be as high as 10.2 mt only considering four species. Aggregations of just Saithe (*Pollachius virens*) were calculated to consume 1.4 % of the total feed distributed at a farm based on stomach contents (Dempster et al., 2011), and this may even be a low estimate. Since there are no publications suggesting that wild fish eat faecal matter from farms (Taranger et al., 2012) it is likely that waste feed is their primary reason for being in such close proximity to a farm (Tuya et al., 2006). Waste feed may alter the body fat composition of wild fish (Fernandez-Jover et al., 2011) and contribute to increased farm emissions.

FCR describes the amount of feed delivered divided by the round weight gain of the fish. FCR is often stated as biological FCR (bFCR) or economical FCR (eFCR). The former is only based on the actual ingested amount of feed, while the latter is based on the total amount of feed used, and thus takes into account escapees, mortalities and feed loss (Ytrestøyl et al., 2015). A two-month experimental study of Atlantic salmon pre-smolts in cages yielded FCR's as low as 0.89 ± 0.06 and 0.77 ± 0.04 (SEM), the latter using an on-demand feeding method (Noble et al., 2008). This study did not mention any waste pellet collection, and hence waste feed may be part of this FCR. Another experiment on post-smolts in tanks with waste pellet recovery yielded a bFCR of 0.80 for the control feed and 0.77 for an experimental feed (Øverland et al., 2009). As a final example, a 12-month tank experiment from 0.3 kg initial fish weight to 4 kg with waste feed collection observed a bFCR < 0.8 at many intervals during the experiment (Torstensen et al., 2008). Even though a given optimal bFCR is determined, this may be impossible to achieve in practice as the fish's feed conversion efficiency is linked to both their size and water temperature (Handeland et al., 2008). On the other hand, Norwegian reports state the eFCR. Based on reported numbers from 88 farming companies (Norwegian Directorate of Fisheries, 2015a) from 2014, Norwegian salmon and trout farms had an average eFCR of 1.22 ± 0.21. This is considerably higher than the experimental bFCRs indicated above, but the values are not directly comparable as mortalities, escapees and feed loss is difficult to quantify. Regardless, the variations between companies are also substantial, ranging from an eFCR of 0.67 to 1.73. This may indicate differences in escapes, onset of diseases, different diet compositions, mortality or feeding practices. As these factors are all part of the eFCR figure, it is impossible to attribute the differences to feeding or feed loss, but there is a large potential for improvement and likely that optimized feeding can reduce overall

eFCR.

Feed loss should be kept to a minimum as it may significantly affect total waste output (Cho and Bureau, 2001), be a considerable source of economic loss for the farmer and is a waste of valuable resources (Alfredsen et al., 2007). Even though there seems to have been a significant improvement in feed utilization, the introduction of new knowledge and technologies may assist in further reducing the feed loss.

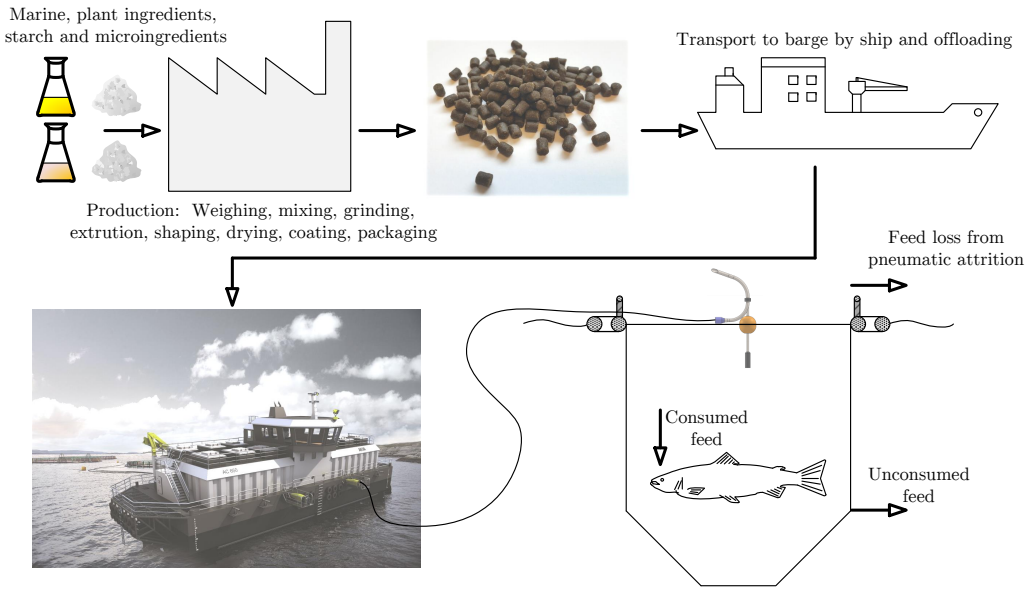

Figure 1.3: Life cycle of feed. Feed loss which occurs during the manufacturing or transport process is not considered in this thesis. Barge image: Creative Commons license, CC-BY-NC-ND, with permission from AKVA group.

The life cycle of feed pellets is illustrated in Figure 1.3. The pellets are produced at large factories near the coast where the ingredients go through a process of weighing, mixing, grinding, extrusion, shaping, drying, coating and packaging. Ships then distribute the feed to farm sites along the coast. Arriving on site, the feed is offloaded to the barge into one or more silos and distributed to the cages using the aforementioned feeding system. At the center of the sea cage is a rotary pneumatic spreader (Chapter 3) responsible for distributing the feed over the water surface of the cage. This kind of rotary floating design is commonly used both in Norway but also at other salmon farms around the world, although other methods of feed distribution are also being used. Despite that feed breakage and creation of dust occurs between the stages of production and offloading into the barge, it is regarded as outside the scope of this study, and we assume that all pellets are

intact as they are fed into the airstream. Figure 1.3 depicts the first stage of feed loss which is the breakage and attrition that occurs during the pneumatic transport and in the spreader itself. Intact pellets and larger fragments pass through the cage and are mostly consumed. Some feed loss occurs through the sides and bottom of the sea cage where it is either eaten by wild fish, carried away by currents or settle on the sea floor.

1.5 Spatiotemporal feed distribution

The arguably most complex and important part of the feeding process takes place inside the sea cage where interactions between individual fish, the environment and feed occurs. Numerous studies have been undertaken in order to gain insight into the complex effects of feeding on salmonid behaviour (crowding, stress, swimming speed and depth), inter-fish behaviour (aggression, dominance, defending of food supply, hierarchies, attacks) and other factors such as growth (total growth and growth variation), feed utilization and feed loss. Salmonid behaviour during feeding is a convoluted combination of biotic factors (e.g. predation risk, competition levels and hunger) as well as environmental factors (e.g. light, temperature, current) (Juell, 1995). It is known that suboptimal feed intake is related to both reduced and inefficient growth in Atlantic salmon (Einen et al., 1999), and the spatial and temporal feed distribution as well as the amount of feed delivered is key in determining feed availability (Juell, 1995). Feed availability is a deciding factor with respect to efficient production (Juell, 1995), and feed should be spatiotemporally unrestricted so the fish may forage according to their own desired manner and preferences (Talbot et al., 1999). Similar conclusions were reached by Olla et al. (1992), and low food availability may also increase size differences and elevate aggression levels. A sharply localized feed delivery renders the food supply defensible by dominant individuals (Juell, 1995) which may lead to dominance hierarchies and high levels of agonistic behaviour, especially when underfed (Olla et al., 1992). Feeding suboptimally can lead to increased discharge of nutrients (Einen et al., 1995) as well as heightened aggression levels and higher variability in growth (Davis and Olla, 1987; Talbot, 1993; Thorpe and Cho, 1995). Another study (Noble et al., 2008) found no variations in growth as a result of restricted ration size, but still observed reduced overall growth and more fin damage. On the other hand, Ryer and Olla (1996) witnessed larger variations in growth as a result of a spatiotemporally localized feed delivery regime as opposed to distributed. Fish of inhomogeneous size are not desirable as the price point for a certain size may be higher, differently sized fish in the same cage may require differently sized pellets and size differences may thus be amplified.

Many salmonid studies, which have mostly been conducted in smaller scales

than full sized sea cages, show strong links between aggression and access to feed (Fenderson et al., 1968; Symons, 1971; Jobling, 1985; Talbot et al., 1999; Noble et al., 2007a,b; Rasmussen et al., 2007; Noble et al., 2008), summarized by Talbot (1993), Ruzzante (1994), Attia et al. (2012) and Brännäs et al. (2005). Aggression should indubitably be avoided as it is a serious welfare issue and is known to play a role in increased fin damage and mortality (López-Olmeda et al., 2012).

Another study by Aas et al. (2015) did not show increased levels of fin damage or growth variations as a result of a spatiotemporally localized versus distributed feeding regime in a tank. However, the weight gain of the fish in Aas et al. (2015) was too limited to draw definite conclusions regarding growth, and the differences in spatial distribution may have been too subtle to detect any variations. Harwood et al. (2003) performed a study in a stream where dominance relationships between fish were determined before they were released into the wild. No correlation was observed between status and growth which was attributed to good spatiotemporal availability of feed, interspecific interactions, different habitats or predators being present. Fish do show a range of behavioural responses in order to adapt to a given feeding system (Talbot, 1993; Thorpe and Cho, 1995; Talbot et al., 1999; López-Olmeda et al., 2012) which may render them more robust to suboptimal feeding regimes.

The effect of a given feeding regime in full scale salmonid sea cage aquaculture on central production indicators such as feed loss, aggression, dominance, hierarchies, satiation, total growth, growth variation and feed loss is still far from completely understood. No full scale experiments investigating this subject have been conducted, which is likely due to the enormous economical and potential welfare risks that are involved. However, a thorough full scale publicly available study of the consequences of a given feeding regime may prove highly valuable to the industry.

Despite the absence of full scale studies, smaller scale experiments, reviews and simulations indicate that maximizing the spatial and temporal feed delivery promotes growth and keeps agonistic behaviour to a minimum (Thorpe et al., 1990; Ryer and Olla, 1991; Olla et al., 1992; Thomassen and Lekang, 1993; Juell, 1995; Thorpe and Cho, 1995; Kadri et al., 1996; Ryer and Olla, 1996; Alver et al., 2004; Attia et al., 2012).

1.6 Objectives

The Norwegian salmon farming industry has seen major technological advances since it first begun in the late 1950s. Increased awareness, regulations, research, openness and cooperation has shifted Norwegian salmon farming away from a state of free-for-all into a more streamlined, efficient and environmentally concious

industry. However, as stated above, there are still major unsolved challenges with respect to diseases and parasites, escapes, welfare and feeding.

This thesis focuses on the optimization of feeding through use of tools from the cybernetic toolbox. The mechanics of feed delivery have progressed from hand-feeding individual cages based on observed surface activity to the feeding systems outlined above. Despite these technological advancements, controlling and distributing feed is still a fairly low-tech operation. As argued in the previous sections, it is likely that the ration size, spatial and temporal delivery of feed is of importance. However, the industry has focused on ration size, meal frequency and duration, not short-term (within meal) temporality or spatial distribution.

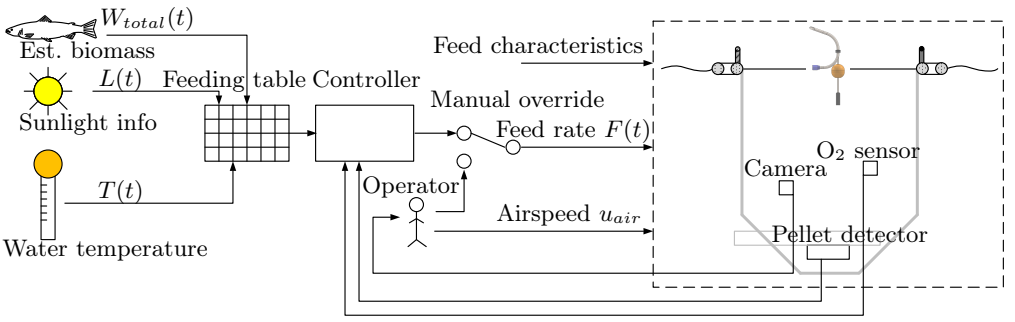

Figure 1.4: Conceptual sketch of feeding system. Artificial lights may as well be a control input which is not depicted here.

Figure 1.4 presents a conceptual sketch of a feeding system. Based on a total biomass estimate as well as feed forward measurements of daylight and water temperature, the feeding system uses a feed table to calculate the daily ration. This information is fed into a controller which may use additional information from an O_2 sensor and/or a pellet loss detector to adjust feeding if the dissolved oxygen level becomes too low or pellet loss is above a certain threshold. More intelligent systems may use an acoustic sensor to detect pellet loss or the swimming depth of fish as this is often correlated with their satiation level (Fernö et al., 1995). A cage is often equipped with an upwards-facing camera relocatable in the dominant current direction and depth. This allows inspection of a limited cage volume and provides some observability of the fish's activity level, swimming depth and feed loss. An operator is able to override or adjust the parameters of the feeding system based on visual feedback from the surface, the submerged camera, data from alternative sensors and personal knowledge. Some sites rely solely on the operator to control feeding.

Many variations exist of the logic depicted in Figure 1.4, but there are two properties which are common for almost all feeding systems. Firstly, the number of control inputs are highly restricted. Considering that the spatiotemporal feed

distribution may be of significant importance, it is odd that all spreaders are fixed in place with no means of controlling the feed distribution across the surface according to the position of the fish, wind and water current. Paper E showed that different densities and sizes of pellets affects settling rates and spatial distribution. However, switching between pellet types in order to achieve a given spatiotemporal feed distribution is cumbersome, and size and nutritional requirements take precedence during day-to-day farming. The feeding rate does give the ability to influence the temporality of feed within the sea cage, but has presumably no or little effect on the spatial distribution. Using a conventional rotary spreader the airspeed may be increased to enlarge the pellet coverage across the surface area (Oehme et al., 2012, G). However, this must be done with caution as it increases pellet breakage (Aarseth, 2004; Aarseth et al., 2006), and still provides no way of placing pellets at a given location. The other common trait of farming systems is that neither the feeding system or farmer possesses a full picture of the ongoing dynamics within the sea cage. A camera only provides a limited field of view into the process, and sensors often provide point readings only. Acoustic sensors may provide a 2D or 3D view into the process, but have yet to be frequently used in sea cage farming. Even if a vast number of sensors were introduced, the farmer would still to a large extent be left with the daunting task of analysing all the sensor data, interpreting their relevance and making the optimal decisions.

As a result, Atlantic salmon farming is often to a large extent performed using straightforward methods with considerable subjective involvement. Although this may often produce satisfactory results in terms of FCR and growth rate, it is likely that the limited and often cluttered sensor information from the process complicates decision-making. Control inputs are usually restricted to feed amount, meal timing, airspeed and submerged lights, which may prove insufficient in terms of adapting feed placement with respect to the position of the fish, wind and currents (Paper I). A more advanced and automated option exists, *precision livestock farming* (PLF) which Wathes et al. (2008) defined as "the management of livestock production using the principles and technology of process engineering". Through the use of sensors and models such as model predictive control (MPC), inputs to the biological process such as light, heat, ventilation and feeding can be automatically controlled. Although measurements may be difficult to obtain and many of the variables in sea cage farming are uncontrollable, several elements of the PLF concept may be successfully applied.

The findings presented in this thesis will contribute to our understanding of the farming process. Through modelling and simulation, different methods of feed distribution can be simulated and the effect on central production parameters may be estimated and investigated. In the end, some of the presented results may represent components in an online MPC/PLF system using only a few sensors together with numerical models to predict the state of a vast number of parameters

inside the sea cage. The results could then be presented in an intuitive manner to the farmer, aiding in decision making and providing control inputs to the feeding system with respect to not only feed amount but also feed placement. In this way, the appropriate amount of feed may be presented to the fish in a spatiotemporally optimal way, potentially resulting in increased welfare, promoting rapid growth and keeping feed loss to a minimum.

Chapter 2

Scope and contributions

2.1 Main contributions

This section outlines the main contributions of this thesis.

2.1.1 Contributions in relation to Chapter 3, The feed spreader

- An attitude measuring system (AMS 1.0) was developed and used to measure the motion of a pneumatic rotary spreader during operation without feed (Paper A). This experiment (4) provided new insight into the behaviour of the rotary spreader, and attitude data from this experiment was used in subsequent simulations.
- A robotic and extrinsic ballistic spreader model was developed and presented in Paper C. Based on the *CF90 Double* rotary spreader (AKVA group, Bryne, Norway) this model enables simulations of different spreader configurations, airspeeds and pellet types and the consequent effects on the 2D surface distribution.
- This model was further developed and the effect of wind was added in Paper F. As part of this publication, a new experiment was undertaken using Styrofoam boxes to collect pellets across the surface (Experiment 5) to parameterize the model.
- In Paper G a quadcopter was used to record the 2D pellet distribution from a pneumatic spreader (Experiment 8). This experiment also featured a completely new version of the attitude measurement system (AMS 2.0), making it the first study to record both the attitude and surface distribution from a spreader at the same time. This paper also presented computer vision (CV) algorithms to detect the spreader position and rotation within the image and determine the position of pellet impacts in relation to the spreader.

- Paper I is the final publication related to the spreader and is a simulation study, investigating the effects of different spreader configurations on the surface distribution. The model was parametrized and validated based on the results from Paper G. This study compared the effects of different airspeeds, having an optimal initial pellet trajectory and introduced the concept of a motorized spreader in order to maximize the spatial surface coverage whilst keeping pellet breakage to a minimum.

2.1.2 Contributions in relation to Chapter 4, Pellet detection

- In order to count pellets in subsequent experiments, a physical submersible pellet detector was constructed along with a computer vision solution to accurately track and count pellets passing through a control volume (Paper B). A small scale experiment (3) was conducted using different pellets to determine the performance of the pellet detector. Using a Kalman filter for pellet tracking, the detector was able to accurately quantify the number of passing pellets as well as possessing means of separating feed pellets from fecal particles. This device may be used for pellet counting in tank based aquaculture, count any kind of dilute particulate flow in pipes or may be deployed in sea cages to quantify the number of pellets passing through a limited volume. It may also be used to accurately determine the settling rate of passing particles.

2.1.3 Contributions in relation to Chapter 5, Sea cage dynamics

- A sizeable experimental study was carried out in Paper E where the diffusion and settling rate of 12 different pellet types (four sizes, three densities) was determined. (Experiment 1 and 2 respectively). This was the first study to determine the natural diffusion of pellets in stationary water which is a central parameter in all sea cage and deposition models. The results can be used to parametrize models involving the diffusion of pellets.
- Paper D presents a significant expansion to the original sea cage model by Alver et al. (2004). This paper revolves around a new 3D model description, takes into account factors such as fish behaviour, appetite, pellet diffusion, advection and environmental factors such as water temperature and dissolved O_2. This model enables simulation of different stocking densities, fish sizes, currents, feed types and the consequent effects on spatial feed availability, satiation and feed loss. Results from Paper E was used to determine pellet settling rate and diffusion in the model.
- Paper I unifies all the listed contributions by merging the spreader and subsurface model. Different spreader configurations were simulated, such as

the default spreader, a motorized design and a relocatable spreader as well as point feeding and the other extreme, a perfectly homogeneous feed coverage across the entire surface. The consequent results on central production parameters such as aggression indicators, satiation and feed loss are discussed. This study gives new insight into the effect of different feeding regimes on growth, welfare and feed loss.

2.2 List of publications

The underlying work of this thesis has resulted in the following publications, listed by type and chronologically sorted by date of publication. See Figure 2.1 for a graphical overview.

Journals

Paper D: (Alver et al., 2016) Alver, M. O., Skøien, K. R., Føre, M., Aas, T. S., Oehme, M., and Alfredsen, J. A. Modelling of surface and 3D pellet distribution in Atlantic salmon (*Salmo salar* L.) cages. *Aquacultural Engineering*, 72-73:20–29, 2016. ISSN 0144-8609. doi: http://dx.doi.org/10.1016/j.aquaeng.2016.03.003

Paper E: (Skøien et al., 2016a) Skøien, K. R., Aas, T. S., Alver, M. O., Romarheim, O. H., and Alfredsen, J. A. Intrinsic settling rate and spatial diffusion properties of extruded fish feed pellets. *Aquacultural Engineering*, 74:30–37, 2016a. ISSN 0144-8609. doi: http://dx.doi.org/10.1016/j.aquaeng.2016.05.001

Paper G: (Skøien et al., 2016e) Skøien, K. R., Alver, M. O., Zolich, A. P., and Alfredsen, J. A. Feed spreaders in sea cage aquaculture - Motion characterization and measurement of spatial pellet distribution using an unmanned aerial vehicle. *Computers and Electronics in Agriculture*, 129:27 – 36, 2016e. ISSN 0168-1699. doi: http://dx.doi.org/10.1016/j.compag.2016.08.020

Paper H: (Skøien et al., 2016b) Skøien, K. R., Alver, M. O., and Alfredsen, J. A. Modelling and simulation of rotary feed spreaders with application to sea cage aquaculture - a study of common and alternative designs (manuscript). 2016b

Paper I: (Skøien et al., 2016c) Skøien, K. R., Alver, M. O., and Alfredsen, J. A. Optimizing feed delivery in salmon sea cage culture for growth and fish welfare - a simulation study (manuscript). 2016c

International conferences

Paper A: (Skøien and Alfredsen, 2014) Skøien, K. R. and Alfredsen, J. A. Feeding of large-scale fish farms: Motion characterization of a pneumatic rotor feed spreader. In *Oceans - St. John's, 2014*, pages 1–7, Sept 2014. doi: http://dx.doi.org/10.1109/OCEANS.2014.7003103

Paper B: (Skøien et al., 2014a) Skøien, K. R., Alver, M. O., and Alfredsen, J. A. A computer vision approach for detection and quantification of feed particles in marine fish farms. In *2014 IEEE International Conference on Image*

Processing (ICIP), pages 1648–1652, Oct 2014a. doi: http://dx.doi.org/10.1109/ICIP.2014.7025330

Paper C: (Skøien et al., 2015) Skøien, K. R., Alver, M. O., and Alfredsen, J. A. Modelling spatial surface pellet distribution from rotary pneumatic feed spreaders. In *23th Mediterranean Conference on Control and Automation (MED)*, pages 883–888, June 2015. doi: http://dx.doi.org/10.1109/MED.2015.7158857

Paper F: (Skøien et al., 2016d) Skøien, K. R., Alver, M. O., Lundregan, S., Frank, K., and Alfredsen, J. A. Effects of wind on surface feed distribution in sea cage aquaculture: A simulation study (in press). In *European Control Conference ECC16*, 2016d

Related publications, reports, posters and presentations not considered for inclusion in this thesis

(Skøien et al., 2013b) Skøien, K. R., Alver, M. O., Føre, M., Solvang-Garten, T., Aas, T. S., and Åsgård, T. E. Modelling and measurement of feed concentrations in salmon cages – tools for optimization of feeding. Abstract and presentation. *Presented at European Aquaculture Society (EAS 2013)*, 2013b

(Skøien et al., 2013c) Skøien, K. R., Alver, M. O., Føre, M., Solvang-Garten, T., Aas, T. S., Åsgård, T. E., and Alfredsen, J. A. Pellet distribution modelling: a tool for improved feed delivery in sea cages. Technical report, International Aquafeed, 2013c

(Skøien et al., 2013a) Skøien, K. R., Alver, M. O., Føre, M., Solvang-Garten, T., Aas, T. S., Åsgård, T., and Alfredsen, J. A. Modellbasert pelletplassering i stormerd - neste skritt? Presentation. In *TEKMAR*, 2013a

(Skøien et al., 2014b) Skøien, K. R., Alver, M. O., Føre, M., and Alfredsen, J. A. Modellbasert fôrdistribusjon i oppdrett. *Fiskeri og havbruk (Addition to Teknisk Ukeblad)*, page 14, 2014b

(Aas et al., 2015) Aas, T. S., Ytrestøyl, T., Åsgård, T. E., Skøien, K. R., Alver, M. O., and Alfredsen, J. A. Feed intake in Atlantic salmon fed with two different spreading patterns of feed. Technical report, Nofima, 2015

(Zolich et al., 2016) Zolich, A., Alfredsen, J. A., Johansen, T. A., and Skøien, K. R. A communication bridge between underwater sensors and unmanned vehicles using a surface wireless sensor network – design and validation. In *OCEANS 2016* -

Shanghai, pages 1–9, April 2016. doi: http://dx.doi.org/10.1109/OCEANSAP.2016.7485493

Presentations at Centre for Research-based Innovation in Aquaculture Technology (CREATE) annual meeting 2013 and 2014.

Poster presentation at the Department of Engineering Cybernetics 60-year anniversary, 2014.

2.3 List of experiments

Table 2.1 presents an overview and brief description of the experiments performed as part of or related to this thesis as outlined in Chapter 2.1. Experiment 6 has not yet been published, but preliminary results from the high speed camera mounted at the outlet pipe of the spreader have been used to parametrize the spreader model (Paper H). Data from Experiment 7 is still being analysed, and the results used to create and test a fully automatic method of quantifying the surface pattern from a spreader using an unmanned aerial vehicle (UAV). Remaining experiments are elaborated upon in their respective chapters.

Table 2.1: Overview of experiments

	Description	Time	Publi-ca-tion	Responsible
1	Determining the diffusion of 12 different pellet types in a tank of stationary water. Nofima, Sunndalsøra.	June 13	E	Skøien K. R.
2	Measuring the settling rate of the 12 different pellet types. NTNU, Trondheim	Oct. 13	E	Skøien K. R
3	Tuning and testing the pellet detector with laboratory made pellets. NTNU, Trondheim.	Jan. 14	B	Skøien K. R.
4	First spreader attitude measurements at Korsneset, Halsa.	June 14	A	Skøien K. R.
5	Measuring the 2D surface coverage of a feed sprader using two rows of Styrofoam boxes at Rataran, Frøya.	Aug. 14	F	Lundregan S.
6	Using a high speed camera on the outlet pipe of the spreader to determine pellet speed and angle. Korsneset, Halsa.	Aug. 15	TBP	Lien, A. M.
7	Using both Styrofoam boxes and a quadcopter to verify and develop a fully automatic pellet detection method using an AUV. Korsneset, Halsa.	Aug. 15	TBP	Lien, A. M.
8	Second spreader attitude measurement and quadcopter filming pellet impacts, Korsneset, Halsa.	Nov. 15	G	Skøien K. R.

TBP: To be published

2.4 Relation between publications

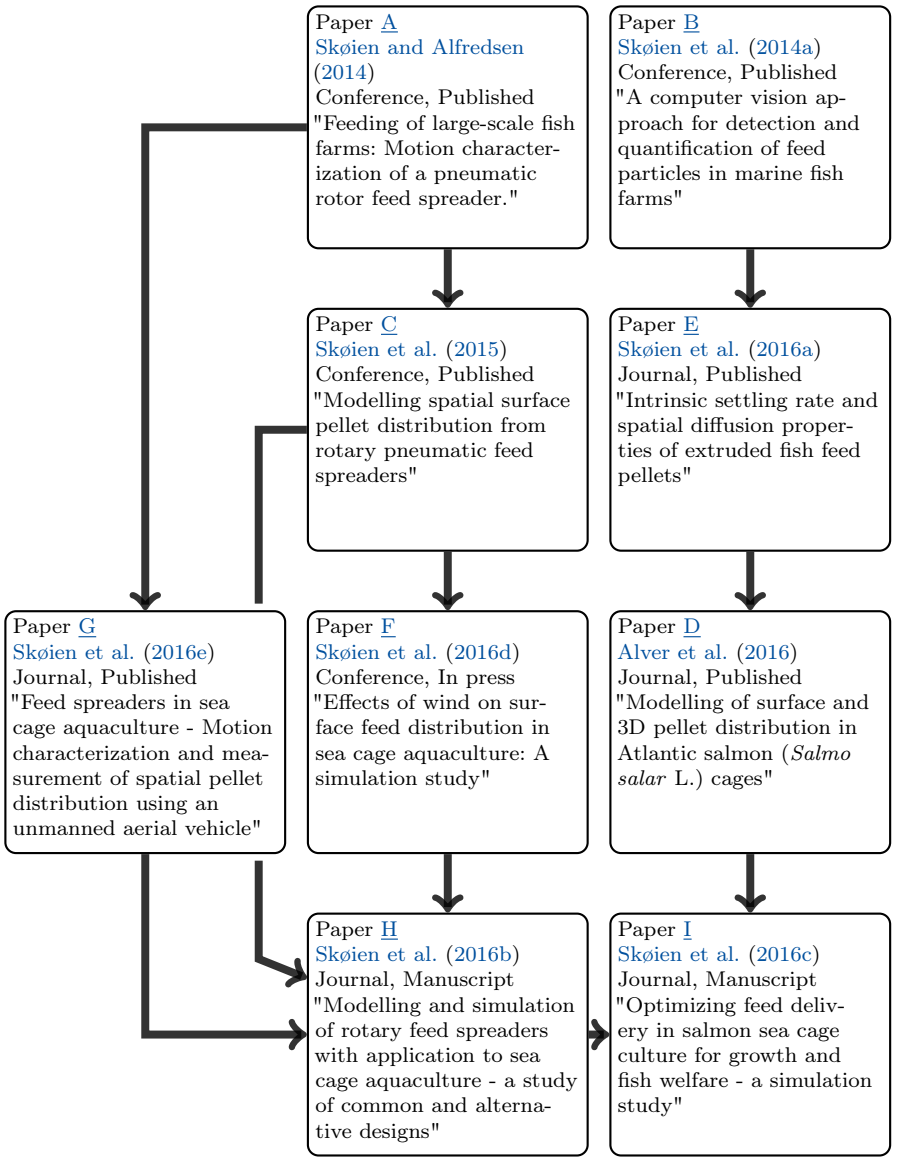

Figure 2.1: Causality of publications

2.5 Thesis outline

- **Chapter 1** gives a general introduction to fish farming. It also highlights some of the present day challenges with respect to feeding based on existing literature.
- **Chapter 2** states the scope of this thesis as well as listing the included publications.
- **Chapter 3** presents experimental results where the behaviour of a rotary spreader was investigated with respect to attitude and pellet throw. This chapter further presents the robotic and ballistic spreader model, model verification and simulation results.
  Publications related to this chapter: A, C, F, G, H.
- **Chapter 4** summarizes the hardware and computer vision solution for tracking and counting feed pellets.
  Publications related to this chapter: B.
- **Chapter 5** describes the three dimensional sea cage model which involves the fish and feed. This chapter also includes the experiments conducted to determine the settling rate and diffusion of several pellet types. Finally, the spreader model is combined with the sea cage model and the results discussed.
  Publications related to this chapter: D, E, I.
- **Chapter 6** concludes this thesis and states possible further work.
- **Chapter 7** lists all the published, submitted and manuscript material included in this thesis.

Chapter 3

The feed spreader

3.1 Background

Figure 3.1 depicts a *CF90 Double* (AKVA group, Bryne, Norway) rotary spreader inside a sea cage. This type of floating design is commonly used both in Norway and other countries although many variations exist. The basic principle is based on a floatation device, a connection to the feed pipe and a ball bearing allowing the center and outlet pipe of the spreader to turn. The airflow combined with the spiral shape and angled cut of the outlet pipe produces a torque around the vertical axis, causing the spreader to rotate. Both the rotation and pellet throw are driven by the same airflow. The *CF90 Double* features a submerged counterweight to maintain an upright position, whilst other designs may use a larger hexagonal shaped base for stability. Rotary spreaders are not the only means of feed distribution. Some spreaders may be be suspended upside-down over the sea cage and certain locations use a "spoon" spreader where there is no rotation but rather a flat spout distributing the feed across the surface in a Chinese fan shape. Some use completely different methods all together, such as submerged feeding where water is used as the conveying medium with floating feed which enter the cage at the bottom.

The pneumatic rotary spreader was chosen as the topic of study for three main reasons: Its widespread use, the fact that very limited work had been conducted on such a crucial part of the farming system and the appearance of a study by Oehme et al. (2012) which raised questions with respect to the performance of such a design. Oehme et al. (2012) used two rows of Styrofoam boxes with the spreader in the centre, arranged in a single line to determine the spatial feed distribution. Across two different spreaders, outlet pipe tilt configurations and airspeeds, the experiment showed that the spreaders portrayed an annular distribution pattern, concentrated to one side, covering just 6.1 to 26.8 % of the surface area with

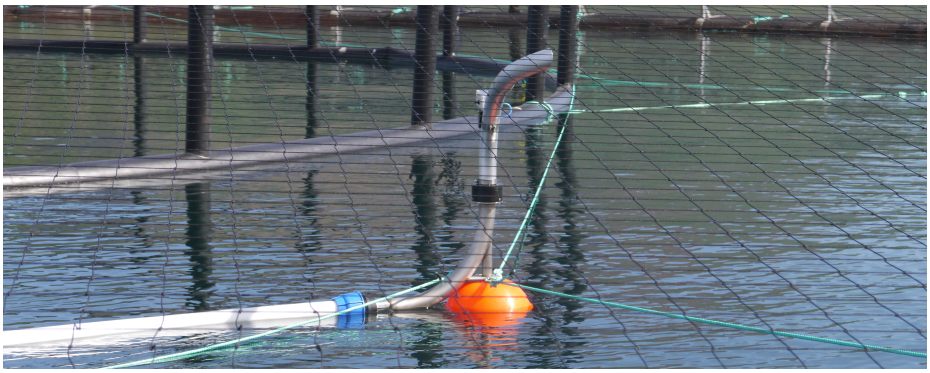

Figure 3.1: A rotary spreader in a sea cage attached to the floating collar. The spreader is typically located inside the hamster wheel, seen in the top left.

respect to a 157 m circumference sea cage (H). Even at 30 m/s airspeed pellets covered just 1/3 of the cage diameter. Surface coverage was greatest at the highest airspeed, but this presents problems such as increased pellet breakage (Aarseth, 2004; Aarseth et al., 2006) elevated energy expenditure and cooling demands (H). The surface feed distribution pattern generated by the spreader seeds the spatial sub-surface distribution, and the effects of surface coverage are discussed in detail in Chapter 5.

This chapter first presents experimental results from both attitude measurements of the spreader, high speed camera recordings of pellets exiting the outlet pipe as well as surface distribution measurements. Results from these empirical studies provided new insight into spreader behaviour, performance and contributed with valuable data for parametrization of a spreader model (Chapter 3.5). An alternative method of determining the surface distribution using an UAV is presented in Chapter 3.4.2 (Paper G). This chapter further explains the fundamentals of the spreader model which is introduced in Chapter 3.5 and presents simulation results from existing as well as alternative designs.

3.1.1 Objectives

It is clear that our understanding of rotary spreaders is limited. Through modelling and simulation it is possible to investigate alternative designs and the consequent effect on production parameters. It was desirable to measure the attitude of a spreader during operation to better understand spreader behaviour and these measurements could be used as simulation input for kinematic models or verification data for kinetic models.

The second objective was to develop a spreader model, parametrize it and verify the results. Through the use of models, researchers and equipment producers may

vary different aspects of the design and investigate the resulting feed distribution pattern. The spatial surface feed pattern is not especially important or explanatory on its own, but the relation to relevant production parameters are discussed in Chapter 5.

3.2 Reference systems

Figure 3.2 illustrates the reference systems and notation which have been used in this thesis and the publications. All systems are right-handed and chosen in accordance with Fossen (2011). The base frame $\{O_a\} = (x_a,y_a,z_a)$ is located at the center of the sea cage at the position of the spreader, considered stationary, inertial and defined in accordance with the North-East-Down (NED) definition. That is x_a points towards true north, y_a points east and z_a down into the center of the earth perpendicular to the x_a, y_a water plane. For simplicity, the feed pipe is considered to always point directly north, away from the spreader. $\{O_b\} =$

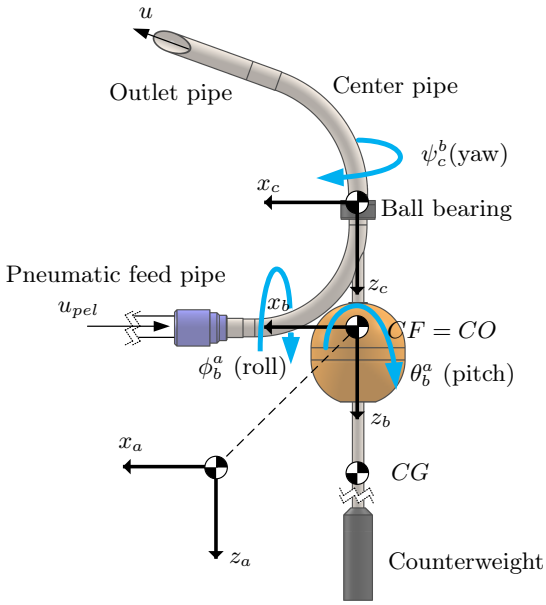

Figure 3.2: Feed spreader and systems of reference.

(x_b,y_b,z_b) is the center of origin (CO) body reference system attached at the center of the water plane area (center of flotation, CF) which is the point the spreader rolls and pitches about (Fossen, 2011). To simplify, the water plane area of the feed pipe is not considered and hence the $(CF) = (CO)$. Finally, $\{O_c\} = (x_c,y_c,z_c)$ is fixed to the lower end of the center pipe which rotates. $\mathbf{\Theta}_b^a = \begin{bmatrix}\phi_b^a & \theta_b^a & \psi_b^a\end{bmatrix}^T$

$\in \mathcal{S}^3$ is the roll, pitch and yaw of $\{O_b\}$ with respect to $\{O_a\}$ given in Euler angles. Similarly, the attitude between $\{O_b\}$ and $\{O_c\}$ is given as $\mathbf{\Theta}_c^b = \begin{bmatrix}\phi_c^b & \theta_c^b & \psi_c^b\end{bmatrix}^T \in \mathcal{S}^3$. The spreader position is given by a vector from O_a to O_b in the $\{O_a\}$ frame $\boldsymbol{o}_b^a = \begin{bmatrix}x_b^a & y_b^a & z_b^a\end{bmatrix}^T \in \mathbb{R}^3$. In accordance with Paper C the translation and rotation of this system can be represented by

$$^*\boldsymbol{o}_b^a = \begin{bmatrix}0 & 0 & 0\end{bmatrix}^T \tag{3.1a}$$

$$\mathbf{\Theta}_b^a = \begin{bmatrix}\phi_b^a & \theta_b^a & 0\end{bmatrix}^T \in \mathcal{S}^2 \tag{3.1b}$$

$$\mathbf{\Theta}_c^b = \begin{bmatrix}0 & 0 & \psi_c^b\end{bmatrix}^T \in \mathcal{S} \tag{3.1c}$$

where * denotes a constant variable. The spreader translation and base yaw can be neglected due to moorings and wave effects averaging out over time. For future reference, at $\psi_c^b = 0$ which is the current position of the center pipe in Figure 3.2 the spreader is in a "U" configuration. This is easily distinguishable by the "U"-shaped path pellets have to traverse through the spreader. On the other hand, when the outlet pipe is rotated away from the feed pipe at $\psi_c^b = -180° = 180°$ will be known as an "S" configuration.

3.3 Attitude measurement

3.3.1 Attitude measurement system 1.0

Figure 3.3 shows the first version of the attitude measurement system used to characterize the spreader motion in Experiment 4. The device consisted of a self contained attitude and heading reference system (AHRS), storing attitude data to a microSD card with a custom made power supply device with wireless control. The wireless solution enabled activation and stopping of the device from distances over a kilometre away, making synchronization between the feeding- and logging system simple. Experiments were conducted at 15, 20, 25 and 30 m/s airspeed in triplicates. Figure 3.5 shows the roll, pitch and yaw of the spreader at 15 m/s airspeed from a single replicate.

The sensor was mounted to the center pipe of the spreader, hence the obtained Euler angles were on the form $\mathbf{\Theta}_s^a$ where s denotes the sensor. From assumptions in Paper A, it was stated that the sensor described the center pipe attitude $\mathbf{\Theta}_s^a = \mathbf{\Theta}_c^a$. Since the only degree of freedom (DOF) between $\{O_b\}$ and $\{O_c\}$ is ψ_c^b, $\mathbf{\Theta}_c^a$ was used to describe ϕ_b^a, θ_b^a and ψ_c^b.

In Figure 3.5: from t=0 to t=20 the internal Kalman filter of the sensor stabilizes. Further, from t=20 to t=60 the yaw is fairly stable, and the effect of waves on the roll and pitch can be clearly seen. At t=60 the blower starts which rapidly produces a fairly constant angular velocity in ψ_c^b. This again affects the roll and pitch which portray a sinusodial pattern overlaid with wave induced noise.

Figure 3.3: Attitude measurement system (AMS) 1.0 mounted to the center pipe of the spreader.

Figure 3.4: Attitude measurement system (AMS) 2.0 mounted to the base of the spreader with an additional rotary encoder.

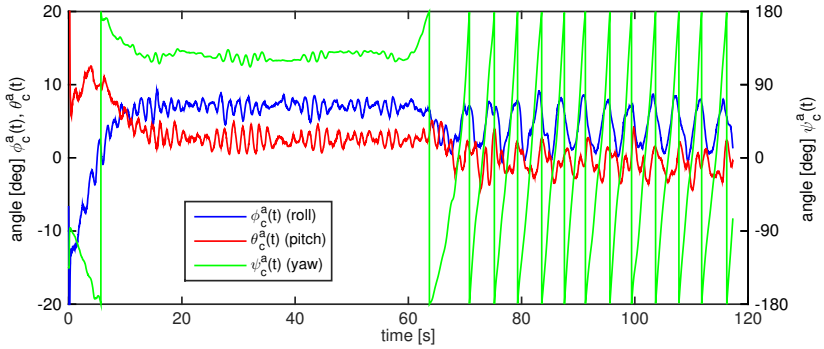

Figure 3.5: Spreader attitude, roll, pitch and yaw at 15 m/s airspeed, obtained from the attitude measurement system 1.0. The blower was started at t=60 s. © 2014 IEEE based on A.

3.3.2 Attitude measurement system 2.0

It was decided to perform another attitude measurement experiment for two reasons. First and foremost, for the purpose of model parametrization and validation it would be beneficial to have both attitude as well as pellet distribution data from the same experiment. Secondly, as the first AMS system was mounted on the center pipe of the spreader, the system was sensitive to centripetal accelerations about ψ_c^b, but also due to the distance from CO to the sensor of about 1 metre,

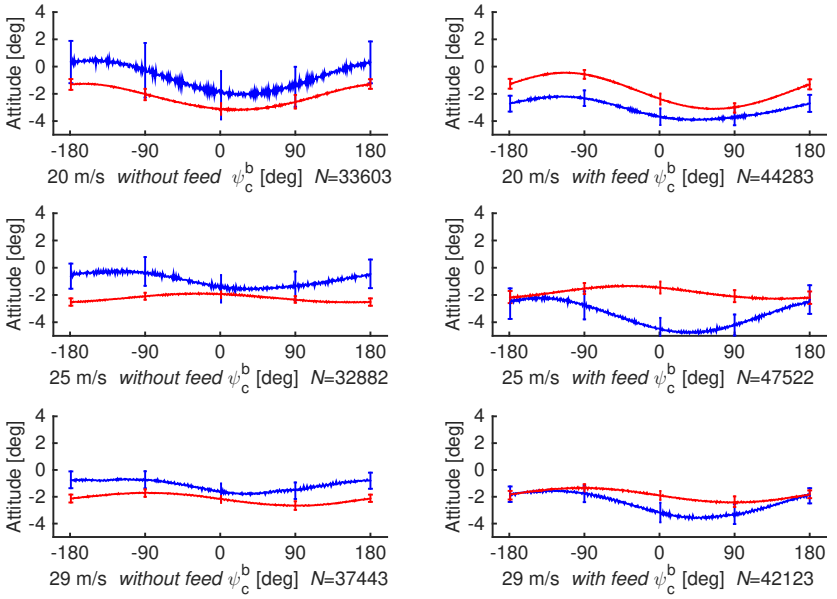

Figure 3.6: Attitude data from AMS 2.0 from G given as a function of center pipe yaw. Roll $\phi_b^a(\psi_c^b)$ given in blue and pitch $\theta_b^a(\psi_c^b)$ in red. ± 1 SD error bars at 90° intervals. Experiments performed in triplicate, N denotes total number of samples.

centripetal accelerations from ψ_b^a and θ_b^a could also have some impact on the results. In A, some attitude drift could be observed in cases with high angular velocity. It was therefore decided to construct a AMS 2.0 which should be situated closer to CO and mounted to the body of the spreader with an external rotary encoder to measure ψ_c^b.

Figure 3.4 shows the AMS 2.0 mounted to the spreader. The waterproof rotary encoder with a 1:1 belt drive is visible in the top left and the AHRS (MTi-G, Xsens, Enschede, the Netherlands) enclosed in a waterproof housing at the lower right side. The AMS 2.0 was used as part of Experiment 8 and used to obtain spreader attitude both without and with feed in the system. Main results are presented in Figure 3.6.

3.3.3 Results

From Figure 3.6 it is evident that the spreader sat quite stably in the water almost at a perfectly vertical attitude. There seems to be a significant shift in mean roll between the *without feed* and *with feed* experiments, but this was attributed to between day variations. Wind and currents may easily affect the long feed pipe and produce a torque which manifests itself as a roll offset. This effect was not

witnessed in pitch which was stable through all experiments. Based on results from both AMS 1.0 and 2.0, G stated that general average attitude values may be given by $-5^\circ \leqslant \bar{\phi}_b^a \leqslant 5^\circ$ and $-2.2^\circ \leqslant \bar{\theta}_b^a \leqslant 1^\circ$.

3.4 Surface pellet distribution measurements

3.4.1 Expanding on earlier empirical results

In order to verify the surface distribution results from a spreader model, experimental data had to be obtained. The first experiment which quantified the surface distribution pattern from a rotary spreader was performed by Oehme et al. (2012). Although this experiment was comprehensive and described in detail, it did not specify the orientation of the boxes in relation to the spreader. In addition, Oehme et al. (2012) only captured pellets along a single line giving limited spatial information.

In a project led by SINTEF and S. Lundregan, a new experiment (5) was conducted where the Styrofoam box setup was expanded to two rows, effectively capturing pellets in a cross formation with known orientation. The experiment used two different spreaders, 16 and 20 m/s airspeed and two tilt configurations of the outlet pipe. The experiment confirmed and expanded upon the results from Oehme et al. (2012) with the surface distribution often being more concentrated and close to the spreader on one side, whilst being more distant and distributed on the opposite side. The data from this experiment are still not published in full, but a limited part of the experiment was presented and used to parametrize and validate the spreader model in Paper F.

3.4.2 Determining surface pellet distribution using an UAV

Although the Styrofoam box method used by Oehme et al. (2012) and F is a straightforward and accurate method of determining surface pellet distribution, it does have several drawbacks. Since most of the pellets land outside the boxes, the spatial resolution is severely limited. The box method is also fairly expensive, it is cumbersome to maintain proper alignment with the spreader, personnel must be inside the cage at almost all times and photographing the contents and emptying boxes after each replicate is a laborious task.

In order to investigate the possibility of using an UAV to observe pellet impacts across the cage surface, Experiment 8 was undertaken. The AMS 2.0 was also included in this experiment to obtain matching attitude and surface data. Using a quadrotor UAV (Phantom 2 Vision+, DJI, Shenzhen, China) pellet impacts were recorded from an altitude of 30–36 m using a three axis gimbal stabilized 1080×1920 pixel camera. 20, 25 and 29 m/s airspeed was used, key feeding system

parameters recorded at the barge, feeding was performed at 10 kg/min and all experiments performed in triplicate.

After applying some basic calibration and thresholding image preprocessing techniques (G) the spreader position was determined from the mooring ropes, visible in Figure 3.7. $\{O_u\} = (x_u, y_u)$ in Figure 3.7 denotes the planar camera coordinates from the UAV given in pixels. Using a Canny edge detector (Canny, 1986) and Hough transform (Hough and Paul, 1962), parametric line descriptors were extracted from the image, the results low pass filtered and the intersection of the two lines most probably representing mooring ropes determined analytically. Spreader and pellet impact positions were transformed from $\{O_u\}$ to $\{O_a\}$ through a process detailed in Paper G. The two lines with highest probability of being mooring ropes are indicated with solid red lines in Figure 3.7 and the detected spreader position marked with a red cross. The dotted red line shows the direction of $+x_a$, and the yellow dotted cross is the area in which pellet impacts were recorded in accordance with previous Styrofoam box experiments (Paper F). All yellow lines have been low pass filtered to smooth the position and rotation estimates of the spreader.

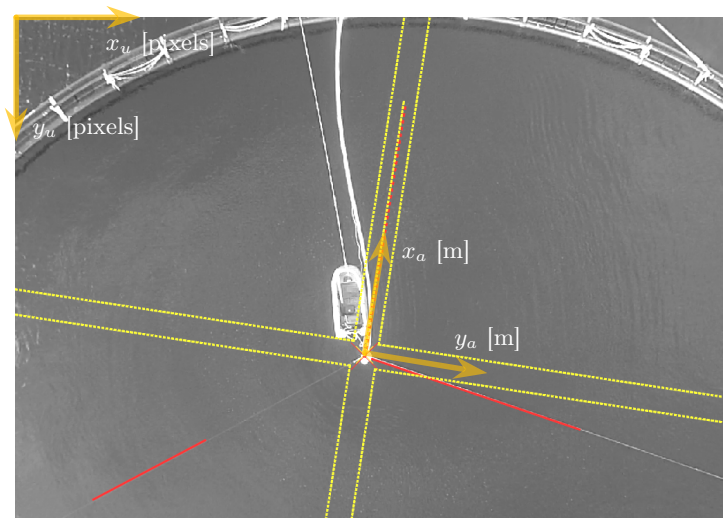

Figure 3.7: Aerial view of sea cage from the UAV. The spreader is located in the center of the image next to a support dinghy used for the experiment. The three mooring ropes are readily visible, and the two superimposed red lines are the results from the CV algorithm. The dotted red line is the direction of the feed pipe in the current image and the yellow dotted line is identical but low pass filtered. The yellow cross is indicative of Styrofoam box placement in earlier experiments.

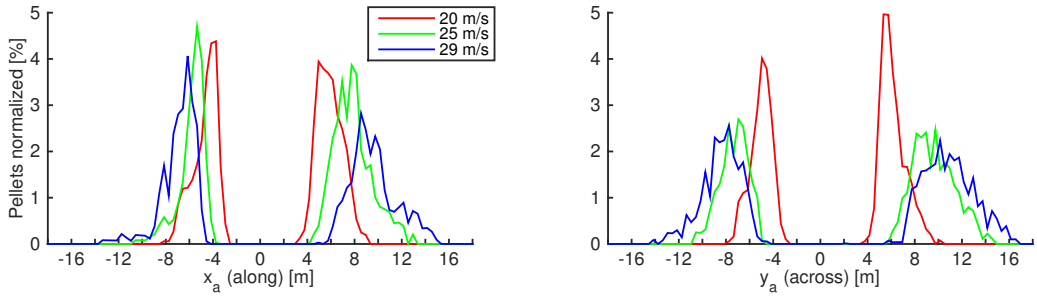

Figure 3.8: Surface pellet distribution extracted from UAV images (G) at 20, 25 and 29 m/s airspeed. Pellets were sampled from a cross-shaped area in accordance with the Styrofoam box method used in F.

3.4.3 Results and discussion

Figure 3.8 presents the surface pellet distributions obtained from the UAV videos and the proposed CV method. The results are similar to what was observed by Oehme et al. (2012) and Paper F in Experiment 5. As airspeed increases, the average pellet throw is longer and larger coverage is obtained with more uniform distribution. Especially along x_a, the annular distribution is skewed to one side as was observed in previous experiments.

Overall, the proposed UAV and CV solution showed promising results, and the process of collecting data in the field was significantly simplified. Especially the ability to run one replicate right after another saved a great deal of time and effort as there was no photographing or emptying of boxes involved. However, two significant improvements could be made to the proposed solution. Firstly, the lack of a visual reference system in the water plane complicated computation of UAV altitude. The height was calculated back from the vertical supports between the floating collar and handrail of the sea cage which is visible in the upper part of Figure 3.7. No method has yet been developed to track these vertical supports through the video sequence, hence, altitude was based on the first frame of each recording where the supports were manually identified. GPS based altitude was considered too inaccurate for the problem at hand as static offsets were observed. However, the flight logs showed that the UAV maintained a very constant altitude throughout each flight. For future experiments, a floating reference system such as a chequerboard is highly recommended. Secondly, the detection of pellet impacts was performed manually which was a time consuming process. Thus, manual detection was restricted to the dotted cross shaped area in Figure 3.7. Attempts were made to automate this procedure, but waves caused a highly dynamic background of light and dark areas as well as sea gulls heavily occluding the water surface at times. Efforts are being made to resolve the latter issue based on the results from

Experiment 7. Experiment 7 also featured use of Styrofoam boxes together with the UAV enabling the results to be compared to a ground truth dataset.

3.4.4 High speed recording

The final piece of empirical data was obtained in Experiment 6 where a high speed camera was attached to the outlet pipe of the spreader (Frank K., 2016, pers. comm.). The recordings captured both the speed of pellets as well as information regarding the exit angle from the spreader. Experiments were conducted across different airspeeds with the spreader in both "U" and "S" configuration. A full analysis and subsequent publication of this experiment will likely be completed by the end of 2016. Preliminary results are presented in Paper H and were used to parametrize the spreader model presented in Chapter 3.5.

3.5 The spreader model

3.5.1 Model development

A robotic (forward kinematic) and ballistic spreader model was first introduced in C where several parameters were tuned based on the experimental results from Oehme et al. (2012). Based on empirical attitude data from Experiment 4 as well as a given airspeed, the model was able to simulate a 2D surface pellet distribution pattern. The model was further refined with the introduction of wind in the equations, and additional joints were added to represent the angular variability at the origin of the ballistic trajectory (Paper F). This extension also included a more accurate description of the ballistic model, an adjustment to the pellet speed as a function of ψ_c^b ("U" and "S" configuration) as well as the inclusion of a dynamic drag coefficient. This publication also featured Experiment 5 where two rows of Styrofoam boxes were used to further parametrize the model. The final version is presented in H where the high speed (Chapter 3.4.4, Experiment 6) recordings were used to further tune the model, and the resulting surface distribution simulation results compared to the empirical data from the UAV (Chapter 3.4.2). Using the Jacobian, this version also considered the linear velocity components of the outlet pipe.

3.5.2 Model overview

This section briefly introduces the model. Comprehensive descriptions are available from Paper C, F and H.

The model is founded on a forward kinematic description of the spreader based on the Denavit-Hartenberg (DH) convention, determining the outlet opening (the

ballistic origin) in relation to $\{O_a\}$. From Spong et al. (2006); Siciliano et al. (2009) the spreader base was given as $\{O_0\} = \{O_a\}$ to the last joint (n) $\{O_n\}$ to separate between the forward kinematic model with numeric super- and subscripts and general reference systems with Latin alphabetical notation. The rotation and translation of $\{O_n\}$ with respect to $\{O_0\}$ in the $\{O_0\}$ frame can be derived by (Spong et al., 2006):

$$\boldsymbol{H} = \begin{bmatrix} \boldsymbol{R}_n^0 & \boldsymbol{o}_n^0 \\ \boldsymbol{0}_{1\times 3} & 1 \end{bmatrix} \tag{3.2}$$

$\boldsymbol{R}_n^0$ is a 3×3 rotation matrix and $\boldsymbol{o}_n^0$ is a translation vector. Let $\boldsymbol{q}$ be a vector of joint variables

$$\boldsymbol{q} = \begin{bmatrix} q_1 & \cdots & q_n \end{bmatrix}^T \tag{3.3}$$

where $q_i = \theta_i$ represents a revolute joint or alternatively $q_i = d_i$ for a prismatic joint (Siciliano et al., 2009). The system can be represented by a transformation matrix $\boldsymbol{T}$

$$\boldsymbol{H} = \boldsymbol{T}_n^0(\boldsymbol{q}) = \prod_{i=1}^{n} \boldsymbol{A}_i^{i-1}(q_i) \tag{3.4}$$

For each joint

$$\boldsymbol{A}_i^{i-1}(q_i) = \begin{bmatrix} \boldsymbol{R}_i^{i-1}(q_i) & \boldsymbol{o}_i^{i-1}(q_i) \\ \boldsymbol{0}_{1\times 3} & 1 \end{bmatrix} \tag{3.5}$$

From Paper H, the ballistic origin vector can be obtained by

$$\boldsymbol{\xi} = \begin{bmatrix} \xi_x & \xi_y & \xi_z \end{bmatrix}^T = \boldsymbol{o}_n^{n-2} = \boldsymbol{o}_n^0 - \boldsymbol{o}_{n-2}^0 \tag{3.6}$$

since the last two joints describe the variability in the origin of the ballistic path. $\boldsymbol{\xi}$ is finally normalized $\hat{\boldsymbol{\xi}} = \boldsymbol{\xi}/||\boldsymbol{\xi}||$ (C), multiplied by the pellet speed u at the outlet pipe and linear velocities added to obtain the final velocity components (H)

$$\boldsymbol{v} = \begin{bmatrix} v_x & v_y & v_z \end{bmatrix}^T = \hat{\boldsymbol{\xi}} u + \dot{\boldsymbol{o}}_n^0 \tag{3.7}$$

The extrinsic ballistic trajectory model of pellets is more involved and may be obtained from Paper H, as well as the modelled speed reduction from pellets entering the spreader (u_{pel}) to exiting the spreader (u) as a consequence of the retarding effect of the "S" configuration as opposed to "U".

Figure 3.9 presents a visualization of the proposed spreader model. The static joints denoted θ_{cnt}, θ_{cur} are based on the *CF90 Double* rotary spreader, and the static but manually adjustable twist $\theta_{twi} = 0$ gives the ability to alter the angle which pellets exit the spreader during assembly (named "tilt" in Oehme et al. (2012)). $\theta_{w,vert}$ and $\theta_{w,horz}$ models the angular origin variability, and the parameterization based on Experiment 6 (Paper H).

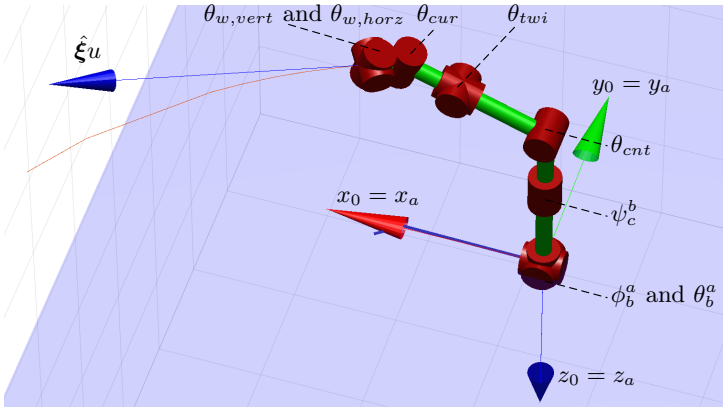

Figure 3.9: The spreader model visualized by the RVC Toolbox (Corke, 2011). In this depicted configuration, $\phi_b^a = 0$, $\theta_b^a = 0$ and $\psi_c^b = 0$ identical to Figure 3.2. In this figure there are no linear accelerations, hence the origin vector $\boldsymbol{v} = \hat{\boldsymbol{\xi}}u$. The red line shows the ballistic trajectory of a pellet.

3.6 Results and discussion

In Paper H the concept of a motorized spreader was introduced. This involved straightening the last bend of the spreader ($\theta_{cur} = 0$) so the airflow no longer contributes to the rotation, and instead driving the rotary action using a separate pneumatic or hydraulic motor. The non-motorized baseline scenario where $\dot{\psi}_c^b$ was 39.5 RPM, 20 m/s airspeed, yielded a mean throw length of 5.5 ± 1.1 m and a surface coverage of 14 %. Increasing the angular velocity using the aforementioned motor configuration to 80 and 160 RPM yielded coverage and average throw lengths of 20.4 %, 7.5 ± 1.2 m and 27.4 %, 9.6 ± 1.4 m respectively with respect to a 157 m circumference sea cage (Paper H). Simulation results are shown in Figure 3.10. This whilst maintaining a low airspeed of 20 m/s. This paper also introduced an optimal ballistic spreader, where the center pipe bend ($\theta_{cnt} = 45°$) to increase the pellet throw length. This simulated design alteration also showed improved performance compared to the baseline scenario, both for surface coverage and average throw length (Paper H).

Figure 3.11 and 3.12 show two simulated scenarios from the spreader model with 0 and 10 m/s wind along $+x_a$ respectively. The angular velocity was set to $\dot{\psi}_c^b = 55.7$ RPM based on a 25 m/s airspeed scenario and $u_{pel} = 12.5$ m/s.

Model performance was verified to a certain degree in Paper H. Figure 3.13 presents a comparison between the spreader model and the experimental surface coverage obtained from the UAV (G). Three different airspeeds were used, 20, 25 and 29 m/s, which corresponded to 39, 55 and 75 RPM angular velocity respectively.

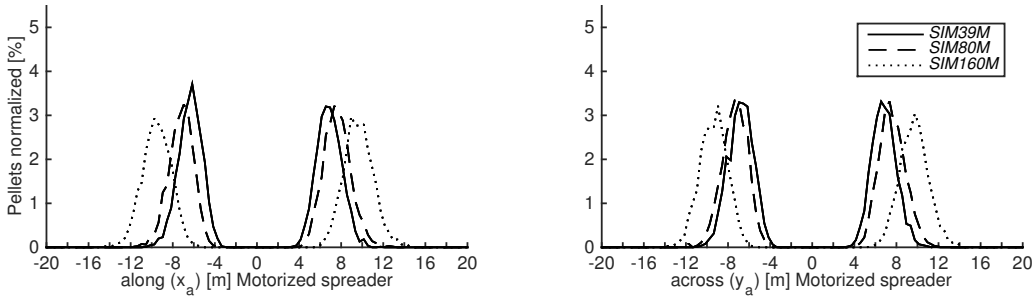

Figure 3.10: Results from experiments using a spreader where the rotation is driven by an external motor. Plot from virtual 40 × 80 cm Styrofoam boxes in a cross formation according to earlier experiments. Showing throw along x_a and y_a for a motorized spreader running at 39, 80 and 160 RPM. Figure have been normalized across all boxes. Figure from Paper H.

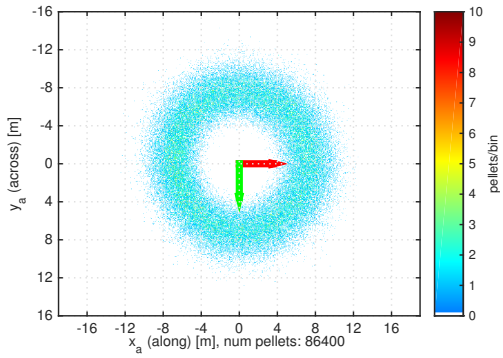

Figure 3.11: Simulated surface distribution at 0 m/s wind

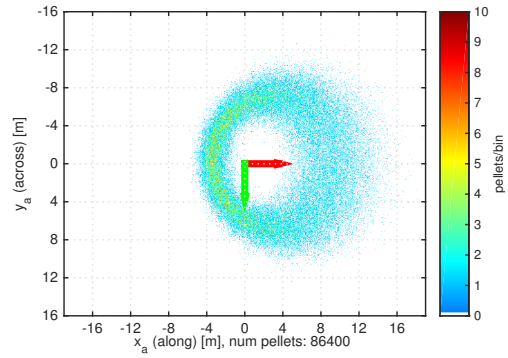

Figure 3.12: Simulated surface distribution at 10 m/s wind along $+x_a$.

In addition, verification was also attempted at an extreme roll angle of -16.4°. This angle was obtained in Experiment 8 by using a rope to pull the spreader down. Since a full model of the pneumatic transport process does not exist, the pellet speed into the spreader (u_{pel}) was tuned to minimize the difference between the simulations and empirical results. For the attitude, AMS 2.0 data from G was used as input for the simulations, describing the roll and pitch of the spreader represented by the spherical joint at the base of the spreader model.

Since attitude data was used and u_{pel} was tuned, the results may not act as a full model validation. However, the good correspondence (Figure 3.13) does indicate that the forward kinematic model, the retardation model as a function of ψ_c^b, the outlet initial trajectory angle model and ballistic model performed well and are able to replicate the dynamics of the physical system. For the extreme roll

offset scenario, the model showed reduced performance. This may have been due to the fact that data could only be collected from a single replicate and the large roll inducing unknown effects which are not considered by the model (H).

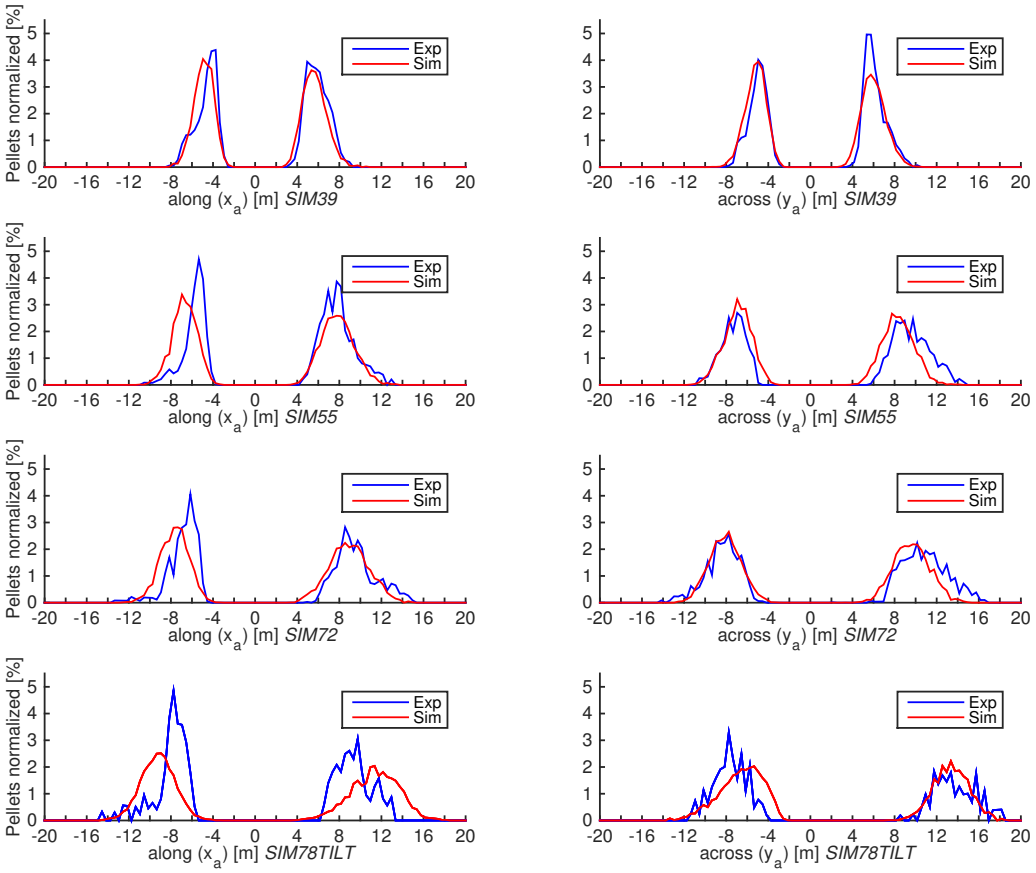

Figure 3.13: Model validation, figure from H. The blue lines are the experimental results sampled from a cross pattern in accordance with the Styrofoam box method, and red indicates the simulated results. 39, 55, 72 and 78 is the angular velocity of the spreader [RPM]. In *TILT* the spreader was forced to a roll offset of -16.4°.

There are some aspects of the model which would benefit from further development. A full fluid model of the pneumatic pellet transport process from barge to spreader would have added significant versatility. Based on the airspeed and pressure which is measured at the barge, pellet type and feed pipe length, such a model could be able to predict the actual pellet speed at the spreader. However, modelling such a multiparticle transport system may become highly complex (Klinzing et al., 2010) as factors such as both horizontal and vertical transport must be considered,

as well as drag, friction, compressibility, collisions and electrostatics to obtain the desired accuracy (Paper H). A full kinetic model would also give the ability to simulate without the need of AHRS data, enabled significant alterations to the basic design and still produced valid results. Development of a kinetic model has been started, and the results will be validated against the attitude data from AMS 2.0.

Chapter 4

Pellet detection

4.1 Background

The concept of detecting feed loss as a means to control feeding is not a novel one. It is based on fish congregating at the location of the spreader when feed is first introduced and at this point most of the feed is consumed. As satiation gradually sets in, fish will lose interest in the pellets and feed loss increases.

Foster et al. (1995) presented a downwards facing camera with algorithms for pellet detection, classification and counting. Overall, Forster (1995) stated that their solution had an accuracy of ±10 %. Another method was suggested by Parsonage (2001) and further analysed in Parsonage and Petrell (2003) using algorithms on recordings from upwards facing cameras which are often already present in sea cages. Such a solution can use existing cameras and the operator is able to observe the behaviour of the fish without introducing more equipment into the sea cage. Static validation experiments in Parsonage (2001) showed that the solution both over- and underestimated the actual number of pellets (size>30 pixels) with an average detection rate of 84 %.

Pellet loss is usually observed manually through a submerged camera and used to reduce or stop feeding. This is a tedious process which also lends itself susceptible to subjective evaluation based on a very limited view of the sea cage. This is however highly prioritized as it is of significant importance to reduce feed loss and thus profitability. Arguably, this monotonous assignment could be automated to free personnel for other tasks.

4.1.1 Objectives and chapter contents

It was desirable to investigate if a more accurate system could be constructed based on a submerged camera, modern hardware and computer vision algorithms. The system had to be compact enough to fit inside a tank in order to perform

Experiment 1 and 2 (Chapter 5), and the accuracy needed to be far superior compared to the previously cited solutions. As opposed to Parsonage (2001) and Forster (1995) which were dependent on daylight, the system had to be operable both indoors, outdoors, in dark and bright conditions.

4.2 Materials and methods

This section outlines the hardware and software solutions in brief as a detailed description is available from Paper B.

4.2.1 Hardware

Based on the sketch in Figure 4.1 a fully enclosed submersible pellet detector was constructed (Figure 4.2). The detector consists of a 1288×964 pixel gigabit

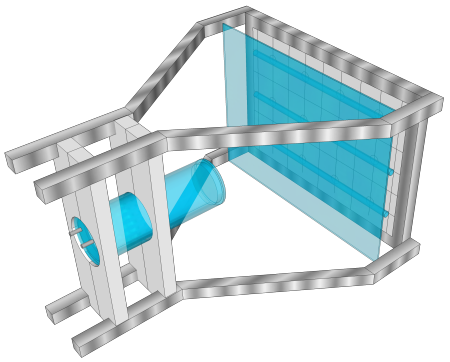

Figure 4.1: 3D sketch of pellet detector

Figure 4.2: Finished pellet detector.

Ethernet camera (FL3-GE-13S2C-CS, Point Grey Research, Inc., BC, Canada) enclosed in a custom made waterproof housing aimed at a uniformly lit translucent background (Paper B). A funnel determines the horizontal detection area and guides pellets into the detection volume. An umbilical transfers power and data to a topside computer which is capable of counting from one detector in real time or record images from five detectors simultaneously for post processing.

4.2.2 Software

The system was implemented in C++ using OpenCV (Bradski, 2000). Since the funnel releases pellets at a uniform distance away from the camera along the principal axis (z) and the motion in z is bounded in one direction by the translucent

Occlusion	Actual	Algorithm result	
		Counted	Percent
None	52	52	100 %
Low	173	176	101.7 %
High	158	154	97.5 %

Table 4.1: The number of counted pellets by the detector and the actual number of pellets which passed through the control volume from Paper E.

Pellet type	Real	Classified as		Percent
		6L	*12H*	
6L	62	56	6	90.3 %
12H	105	9	96	91.4 %

Table 4.2: Algorithm classification of pellet type based on settling rate only. Taken across all levels of occlusion. *6L* pellet type used to simulate faecal particles. From Paper E.

plastic background, the pellet position $\boldsymbol{s}_{k,n}$ and velocity $\boldsymbol{v}_{k,n}$ was considered planar. Hence $\boldsymbol{s}_{k,n} = \begin{bmatrix} s_{k,x} & s_{k,y} \end{bmatrix}^T \in \mathbb{R}^2$, $\boldsymbol{v}_{k,n} = \begin{bmatrix} v_{k,x} & v_{k,y} \end{bmatrix}^T \in \mathbb{R}^2$ where k is a given frame and n the current blob (an object detected in the image as a potential pellet). Due to the uniform and constant lighting, fixed global thresholding was used to convert the image to binary before border following was used (Suzuki and Abe, 1985) to extract blob contours. Blobs were then filtered by size and a Kalman filter initiated to predict the position of a blob in frame $k+1$. Predicted position ($\hat{\boldsymbol{s}}_{k,n}$) and measured positions ($\boldsymbol{s}_{k,n}$) were matched using the Kuhn-Munkres algorithm (Kuhn, 1955; Munkres, 1957) and thus iteratively tracked through the field of view. Blobs with an average settling rate above a certain threshold were classified as pellets and the ones below were filtered out as debris/faecal particles.

4.3 Results and discussion

In Experiment 3 (B) both 6 and 12 mm diameter pellets with low and high density, *6L*, *6H*, *12L* and *12H* was used to determine the performance of the proposed solution. Table 4.1 lists the number of pellets passing through the control volume of the pellet detector and the number of counted pellets. Occlusion for a given pellet drop (replicate) was classified into three levels. *None* – no occlusions in the pellet drop, *Low* – one or two instances of pellet pairs occluding one another during the drop and *high* – three or more occluding pairs.

From Table 4.1 the pellet detector counted the number of pellets perfectly when

there were no occlusions. At *Low* occlusion level the detector slightly overestimated the number of pellets due to pellets leaving and then re-entering the field of view or pellets occluding one another for a period of time and then separating. At *High* level of occlusion the solution underestimated the actual number which was caused by pellets remaining occluded through the field of view. Table 4.2 provides insight into the algorithms ability to separate faecal particles from actual pellets. *6L* pellets with a settling rate of 5.3 ± 1.2 cm/s was used to simulate faecal matter due to the slow settling rate and *12H* (16.6 ± 1.6 cm/s) was used as feed pellets. Across all occlusion levels, the algorithm correctly separated 90.3 % or more of *6L* and *12H* pellets based on settling rate alone.

4.4 Summary

The proposed pellet detector functioned as desired and showed superior accuracy compared to previous solutions (Forster, 1995; Parsonage, 2001). The detector is able to operate under all exterior lighting conditions and the detection area may be adjusted according to funnel size. However, the pellet detector has a comparatively small detection volume compared to the theoretically unlimited reach of both Forster (1995) and Parsonage (2001). Although the detector was intended as a tool for conducting Experiment 1 and 2, it may well be used in sea cages or tank systems. In sea cages the detector will have to be equipped with a large funnel in order to cover a significant section of the sea cage or multiple detectors will have to be used. This will result in increased drag forces on the structure and more equipment inside the cage which may contribute to more difficult inspections and maintenance operations. Rotating sonar solutions which are currently under development may not be as accurate as the detector but have the ability to cover large volumes with a single device. It is likely that such compact single unit solutions will be more appropriate for sea cage use. The pellet detector may on the other hand be more suitable in tank-based aquaculture, counting particles leaving a tank or during pellet manufacturing where accurate measurements of settling rate from a large number of pellets may be required.

Chapter 5

Sea cage dynamics

5.1 Background

In order to make a statement regarding the performance of different spreader designs and methods of feed distribution, the interaction between feed, fish and the environment must be considered. Determining the effect of a given 2D surface feed coverage pattern (Chapter 3) on production parameters such as feed loss and fish satiation is central to this chapter. In order to do this, an existing feed distribution and fish behaviour model was used (Alver et al., 2004), which was improved and expanded (Paper D). The combined use of the spreader and feed distribution model allows researchers to simulate various spreader designs and obtain estimates on the influence on key production parameters.

5.1.1 Objectives and chapter contents

This chapter focuses on experimental results and theoretical modelling of events that transpire beneath the surface of the sea cage. The objectives of this chapter was to improve the performance of the feed distribution model (Alver et al., 2004) by using new empirical results on pellet motion from Paper E, elaborating the model further and expanding it from 2D to 3D (Paper D). Further, the spreader model (Chapter 3.5) are connected to the feed distribution model (Paper D), allowing different spreader designs to be simulated and the consequent effects on central production parameters investigated. Finally, new methods of feed distribution and spreader configurations are simulated and compared to existing methods and their relative performance discussed (Paper I).

5.2 Pellet diffusion and settling rate

5.2.1 Introduction

When modelling the subsurface feeding dynamics of a sea cage the motion of pellets is an essential component. The diffusion of pellets determine how the concentration of feed naturally dilute within the water column which again affects the spatial availability to the fish. The diffusion factor may also affect temporal availability as an extensively distributed feed cloud may be carried out of the sea cage more rapidly compared to a more dense cloud in the center of the sea cage. The settling rate (u_v) is also vital as it influences the temporal feed availability and differences in settling rate affects the spatial opportunity for the fish to feed along the vertical axis.

Ample data exists on the settling rate of feed pellets. Studies by (Findlay and Watling, 1994; Chen et al., 1999; Cromey et al., 2002; Sutherland et al., 2006; Cromey et al., 2009) all determined the settling rate of various fish feeds. In addition, u_v is measured at production as it is vital to avoid floating pellets which would only make the feed available at the surface, as well as too rapidly settling pellets as this would reduce the temporal availability, sinking quickly through the cage.

Diffusion on the other hand seems to be empirically unexplored. This implies that sea cage and waste deposition models such as Gillibrand and Turrell (1997); Cromey et al. (2002); Alver et al. (2004); Cromey et al. (2009) based their diffusion coefficients on various sources and educated estimates and not experimentally derived data obtained from representative feeds. Paper E classified the diffusion of 12 different feed types (3, 6, 9, 12 mm diameter, low (L), medium (M) and high density (H)), and in addition, the settling rate was measured based on a large number of pellets in order to obtain comprehensive matching data for the purpose of modelling and simulation.

5.2.2 Materials and methods

The 12 experimental feeds were specially made for the experiment at Nofima Feed Technology Centre, Bergen. Diet formulation was chosen to represent the average Norwegian feed composition in 2010 (Ytrestøyl et al., 2011). Dry ingredients were mixed and divided into four equal batches and extruded with 2.5, 4.5, 7.2 and 10.0 mm diameter die plate holes (E), and the cutting speed was set to produce pellets with a diameter:height ratio of approximately 1:1. After drying, the four batches were coated with different amounts of oil to obtain three different densities.

The horizontal distribution experiment (1) was conducted at Nofima, Sunndalsøra, using five randomized replicate drops of 40 pellets for each feed released from

a single point into a 2.30 m deep tank of sea water. Pellets settled on a 1×1 m grid and was photographed for each drop. Image analysis was carried out in MATLAB (2014) and statistical analyses made in (SPSS, 2015).

The settling rate experiment (2) was conducted in an indoor tank at NTNU, Trondheim. Due to the large number of pellets, the batch for each replicate were weighed as opposed to counted. 10 randomized drops for each of the 12 pellet types was conducted, and using the pellet detector described in Chapter 4, the number of frames it took pellets to reach a depth of 2.30 m was recorded and the settling rate and settling rate variability calculated.

5.2.3 Results and discussion

Table 5.1 presents the mean distance from the center of mass for all five replicates of each pellet type. The distance was found to be strongly correlated with pellet size. In Table 5.1 the mean distance increases monotonically with pellet size with the exception of *6H* which diffused slightly less compared to *3L*. Using the square root transformed distance, significant differences in diffusion were found (Welch's $F(11,667.228) = 39.859$, $p < .0005$). This was followed by a Games-Howell post-hoc test (E), and no significant differences were found between pellets of the same size. This result showed that pellet size had a significant influence on pellet diffusion and density is of comparatively little importance.

Table 5.1: Pellet diffusion. Mean distance from centre of mass (distance ± SD [mm]). *N* is the number of pellets included in the analysis. Table from Paper E.

Pellet type	Mean distance [mm]			*N*
3H	61	±	43	200
3M	61	±	48	198
3L	70	±	40	191
6H	68	±	40	197
6M	80	±	57	146
6L	89	±	57	48
9H	92	±	48	198
9M	93	±	49	197
9L	95	±	64	167
12H	130	±	70	189
12M	140	±	76	190
12L	119	±	61	145

The settling rate results from E are presented in Table 5.2. As expected, there was a positive correlation between settling rate and density for all pellet sizes.

This was also the case for size, as there was an increasing trend in settling rate with larger pellets. However, during production, only bulk density was measured and hence there may have been differences in specific density between pellets of the same density class (*H, M, L*). A full analysis of significant differences and

Table 5.2: Pellet settling rate (mean ± SD) for all feed types, and number of pellets N. Table from Paper E.

Pellet type	Settling rate (u_v)			N
3H	9.9	±	0.5	506
3M	7.7	±	0.8	435
3L	5.6	±	1.0	376
6H	12.3	±	0.9	329
6M	8.1	±	1.8	250
6L	6.2	±	1.7	84
9H	14.0	±	2.0	254
9M	12.8	±	2.3	214
9L	9.7	±	2.1	186
12H	17.0	±	2.9	192
12M	14.2	±	2.5	186
12L	11.3	±	2.5	177

a comprehensive discussion is available in E. These new diffusion results enable researchers to parametrize models based on empirical results. The data in Table 5.1 was used to determine the diffusion factor κ in Paper D which is central in determining the diffusion and thus the motion of pellets through the sea cage.

5.3 Expanded sea cage model

5.3.1 Model components

To unify the results described so far and derive the effects of different feed distribution patterns on production parameters, a sea cage model was introduced. The first version of this model was presented by Alver et al. (2004) where fish and feed existed in a two dimensional (x, z) grid. A considerable extension to this model was presented in D where the grid describing the sea cage was expanded from two to three dimensions, allowing cage shapes to be more accurately represented. The model takes a 2D surface pattern of feed and calculates the resulting spatiotemporal feed concentration through the sea cage where fish and feed exist in a matrix of equally sized cubical cells. The main equation governing the settling rate, diffusion and advection of pellets as well as added feed and feed ingestion is

given by Equation 5.1 (D).

$$\frac{\partial c}{\partial t} + v_x \frac{\partial c}{\partial x} + v_y \frac{\partial c}{\partial y} + (v_z + u_v)\frac{\partial c}{\partial z} + \kappa \left(\frac{\partial^2}{\partial^2 x} c + \frac{\partial^2}{\partial^2 y} c + \frac{\partial^2}{\partial^2 z} c \right) = u - f_I \quad (5.1)$$

The feed concentration in a given cell is given by $c(x, y, z, t)$, $v_x(x, y, z, t)$, $v_y(x, y, z, t)$, $v_z(x, y, z, t)$ are the velocity components of the water current in x_a, y_a and z_a respectively. a denotes the inertial base frame situated at the surface in the water plane centroid of the sea cage as described in Chapter 3.5. A mask determines the size of the sea cage and cells outside this boundary are set to have a feed concentration of 0. u_v is the settling rate of pellets and κ the feed diffusion factor, both described earlier and based on the results from Paper E. $u(x, y, z, t)$ represents the added feed which is typically given by a feed spreader model. This may alternatively be given by a point source or a perfectly homogeneous distribution across the entire surface for the purpose of reference. Finally, f_I denotes the fish ingestion rate and is modelled as groups of super-individuals, each representing a number of fish which gives a heterogeneous weight distribution across the population (D). Each group has a different feed ingestion rate which is determined by a combination of pellet weight, maximum ingestion rate based on handling and search time, spatial feed distribution, stomach fullness (appetite) and a hierarchical component.

5.3.2 Results and discussion

First, κ was tuned and mean u_v selected from E based on the type of feed pellet used in the simulation. The same value for κ was used both for the vertical and horizontal diffusion which produced Gaussian distributed settling rates that closely matched the experimental results (D). The model was configured to replicate the experimental conditions in Talbot et al. (1999) where feed wastage was monitored in a sea cage measuring 12×12×10 m containing 17.4 tonnes of Atlantic salmon. Using submerged cones for gathering waste and an air-lift collector system, the amount of uneaten feed was determined. Figure 5.1 compares these experimental results with simulations from Alver et al. (2004) and the new model D.

The model was able to predict the main dynamics of pellet distribution as well as feed consumption and loss in a sea cage. Figure 5.1 also indicates that the new model more closely represents the experimental results, which is most easily observable for feed loss during the first seven minutes. Alver et al. (2004) predicted some feed loss just one minute into the meal. On the other hand, D indicated almost no feed loss 0–7 min after first feeding which is more logical, though not entirely quantitatively in accordance with Talbot et al. (1999).

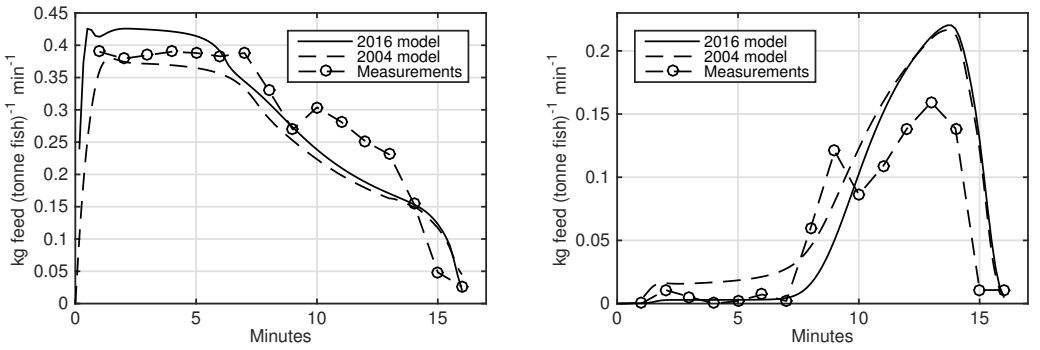

Figure 5.1: Figure based on D comparing the expanded 3D model and the earlier 2D model (Alver et al., 2004) with experimental results from Talbot et al. (1999). The left Figure indicates total feed intake and the right Figure total feed waste.

Overall, the model shows good performance and features an enhancement to the previous 2D version which was attributed to an improved computation of feed ingestion and better estimates of the diffusivity parameter (κ).

5.4 Effects of existing and new methods of feed distribution

With the spreader and sea cage model tuned and verified to a certain extent, Paper I combined the models and investigated different spreader configurations on central parameters such as feed intake, feed loss and aggression. This section presents the preliminary results from this study.

5.4.1 Materials and methods

The spreader model was initialized using the physical attributes of the *CF90 Double* spreader with a perfectly vertical attitude as was deemed realistic by Paper G. A 20 m/s airspeed scenario which corresponded to an actual pellet speed of 9.1 m/s arriving at the base of the spreader was used for the simulations (H). The sea cage model was initialized according to a typical situation encountered during a production cycle in Atlantic salmon sea cage farming. A circular sea cage was used, 157 m diameter (Oppedal et al., 2011) with a cylindrical depth of 40 m and total cone depth of 50 m containing 200.000 fish. Model resolution was set to $\Delta x = 1$, $\Delta y = 1$, $\Delta z = 1$ m, the fish weight was 1.2 ± 0.32 kg scaled up from actual measurements from a farm (0.845 ± 0.224 kg, N=160) distributed across seven groups of super individuals with an initial appetite of 100 % (zero stomach content). A 9 mm pellet size was used which was suitable according to fish size

(Skretting, 2012) with a settling rate of 12.6 cm/s (E) and weight of 0.66 g/pellet (Oehme et al., 2012). Feed was temporally equally distributed over the course of 120 minutes, and a total of 1.1 % of the biomass was delivered which totalled 2.64 tonnes.

Five main scenarios were defined and simulated, as can be viewed in Paper I. $\mathcal{S}_1$ and $\mathcal{S}_2$ acted as opposing references by distributing all the feed into a single cell and covering close to 85 % of the surface with a uniform distribution respectively. $\mathcal{S}_1$ was also run with 0.1 and 0.2 m/s current in the $+x_a$ direction. Further, $\mathcal{S}_3$ is the standard spreader model running at $\dot{\psi}_c^b = 40$ RPM. $\mathcal{S}_4$ used the standard spreader model further, but used the concept of a motorized spreader with an angular velocity of 80 and 160 RPM. $\mathcal{S}_5$ (Figure 5.2) was identical to $\mathcal{S}_3$, however, a 0.1 m/s current in $+x_a$ was introduced. $\mathcal{S}_5$ was further simulated by moving the spreader 5 and 10 m into the direction of current. The consequent feed loss, appetite, volume coverage and global Shannon entropy (GSE) was determined, and Table 5.3 presents the results from Paper I. The Table lists the scenario and the total feed loss throughout the simulation. Min appetite lists the minimum appetite of the sum of all seven fish groups and at what time this occurred. Max diff. appetite gives the largest appetite gap between the group of smallest and largest fish and time of occurrence. Although the model does not model aggression explicitly, a large difference in satiation is an indication of fish groups not having equal feed access which may lead to aggressive behaviour as indicated in Chapter 1.5. The coverage is simply a measure of how many cells contained one or more pellets ($c(x, y, z, t_{steady}) \geq 0.66$ g feed). This metric as well as GSE was obtained without any fish present and taken at time t_{steady} when the model reached a steady state. The coverage does not take into account the actual number of pellets in each cell. E.g. one pellet in every $N - 1$ cells and the final cell containing a large number of pellets will still yield a coverage of 100 %. Hence, GSE (Kam et al., 2013) was introduced which takes the specific contents of each cell into account. A value of zero means that all feed exists within a single cell, and 1 indicates a perfectly homogeneous spatial distribution.

5.4.2 Results and discussion

$\mathcal{S}_1$ yielded the poorest overall results. Feed loss was significantly higher compared to all other scenarios, as well was the min appetite and max diff. appetite. Not surprisingly, adding all the feed in a single cell or at a single location also leads to the lowest volume coverage and GSE. When a current of 0.1 m/s was introduced in $\mathcal{S}_{1,0.1\text{m/s}}$ all metrics improved. The added water flow distributed the feed better and more fish gain access. Interestingly, when this current was further increased to 0.2 m/s all metrics were poorer, most likely due to feed escaping through the cage wall before being consumed. The baseline spreader $\mathcal{S}_3$ and motorized spreader scenarios

Table 5.3: The scenarios and corresponding results. The total feed loss, minimum average appetite across fish groups, the largest difference in appetite between group 1 and 7 given in percent points, percentage of cells within the sea cage containing more than 0.66 g feed (one pellet) and the global Shannon entropy of the spatial feed distribution. The two latter metrics were obtained from simulations without fish present in the sea cage. Table from Paper I.

Scenario	Feed loss [%]	Min appetite [%]	Max diff. appetite [pp]	Coverage [%]	GSE [0,1]
$\mathcal{S}_1$	31.0	6.6 (@125 min)	83.2 (@40 min)	0.7	0.38
$\mathcal{S}_{1,0.1\mathrm{m/s}}$	22.9	4.4 (@123 min)	78.6 (@36 min)	2.6	0.56
$\mathcal{S}_{1,0.2\mathrm{m/s}}$	32.8	6.7 (@122 min)	83.0 (@47 min)	1.6	0.52
$\mathcal{S}_2$	7.2	1.9 (@125 min)	25.4 (@36 min)	85.1	0.99
$\mathcal{S}_3$	7.6	1.9 (@124 min)	59.9 (@34 min)	14.3	0.78
$\mathcal{S}_{4,80\mathrm{RPM}}$	7.2	1.9 (@125 min)	52.1 (@34 min)	20.4	0.82
$\mathcal{S}_{4,160\mathrm{RPM}}$	7.2	1.9 (@125 min)	45.3 (@34 min)	26.8	0.85
$\mathcal{S}_{5,0\mathrm{m}}$	8.7	2.0 (@123 min)	56.0 (@34 min)	18.1	0.81
$\mathcal{S}_{5,5\mathrm{m}}$	8.1	2.0 (@124 min)	56.1 (@34 min)	21.5	0.83
$\mathcal{S}_{5,10\mathrm{m}}$	7.8	1.9 (@124 min)	56.1 (@34 min)	24.4	0.84

$\mathcal{S}_{4,80\mathrm{RPM}}$, $\mathcal{S}_{4,160\mathrm{RPM}}$ had a surface coverage of 16, 23 and 31 % respectively. The feed loss was almost unaffected by the the increased surface coverage as was also the case for min appetite. Max diff. appetite however was reduced from 59.9 pp to 45.3 pp indicating that the fish were able to forage in a more equal and unrestricted manner. Finally, moving the spreader into the current in $\mathcal{S}_{5,0\mathrm{m}}$–$\mathcal{S}_{5,10\mathrm{m}}$ reduced feed loss from 8.7 to 7.8 %. The volume coverage and GSE also increased and remaining metrics remained essentially unaltered.

The results indicated that increasing the spatial surface distribution may allow fish to feed in a more equal manner, possibly reducing aggression, fin damage and mortality. Further, having a spreader which is able to translate along the dominant current direction may reduce feed loss. At first, a reduction from 8.7 to 7.8 % may seem small. However, when considering that 10 tonnes of feed at a value of 11.83 NOK/kg (Norwegian Directorate of Fisheries, 2015c) worth almost 120.000 NOK is introduced into a single cage every day, a small reduction in feed loss quickly amounts to considerable savings. Further economic advantages may also arise from equal feed access. Fish may end up being more uniformly sized which is advantageous in markets where certain sized fish are favourably priced.

A simple fish model was used as outlined in D. More advanced models of fish behaviour and growth have been made such as Føre et al. (2009, 2016) and will

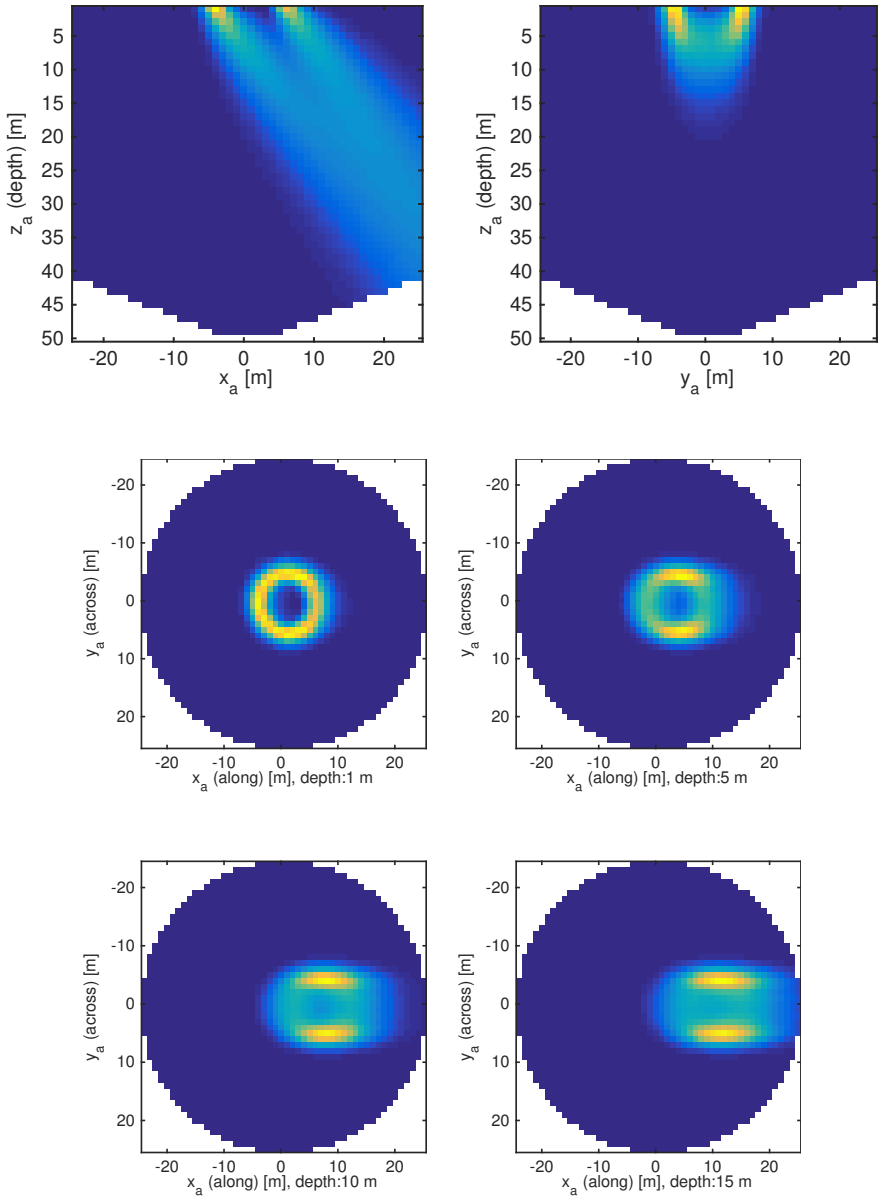

Figure 5.2: Figure based on I. Side and top view of the model running a simulation of scenario $\mathcal{S}_{5,0\mathrm{m}}$. The surface distribution was exported from the spreader model and this particular scenario had no fish.

be incorporated into this model with time. The models have been parametrized and validated from a selection of empirical results. However, there are no full scale experiments which have been undertaken with respect to the effects of localized versus distributed feeding on feed loss and growth leaving this to be desired. Yet, the correspondence with Talbot et al. (1999) does indicate that the quantitative results from the model are reasonable. For the scenarios outlined in this chapter, the fish size, pellet properties and surface feed distribution are dissimilar to the verified scenario. Hence, the numbers may not be exact, but still the large differences in feed loss, appetite and volume coverage for the different scenarios are believed to be viable qualitative indicators when comparing one feeding regime to another.

Chapter 6

Concluding remarks

6.1 Contributions and implications

This thesis has produced results and has implications related to several topics of feeding in large scale sea cage aquaculture. Subjects such as feed spreader design and placement, spreader performance evaluation, feed loss monitoring, pellet behaviour and pellet distribution modelling are linked to spatiotemporal feed distribution which again is related to welfare, feed loss and pollution. The tools presented in this thesis may be used to optimize the feed distribution for improved feed consumption and feed utilization. Some of the tools may also be used to aid the farmer in making more informed decisions with respect to feeding based on an intuitive presentation of sensory data and model predictions. In addition, the tools may also take part as a larger, more autonomous system which will become increasingly important as new farm sites become larger and more exposed far from shore.

The attitude measurements made on the rotary spreader indicated that roll offsets may easily arise from torques which are generated when the spreader is mounted and by forces from the feed pipe. Pitch on the other hand seems to be less susceptible to offsets. This instability is by some claimed to be an intended design feature to increase the pellet distribution. At low airspeeds, the mass of the center and outlet pipe forced the spreader down which resulted in a less favourable ballistic path and reduced surface coverage. At higher speeds, more complex inertial and hydrodynamical forces come into play, making these operational situations difficult to analyse and almost impossible to generalize across different spreader designs. Regardless of this, the mean roll and pitch are always close to vertical (Figure 3.6) implying that this instability has a limited influence on the overall surface distribution pattern. The presented empirical results were used for simulation input and may be used later for verification of a full kinetic feed spreader model.

The proposed spreader model may serve as a tool for researchers and equipment producers to test alternative designs and determine the consequent effects on spatial feed distribution. However, significant deviations from the classic rotary spreader design the model was based upon will have implications on attitude and the angular velocity. This purely kinematic model will become inaccurate if the design strays too far away from what it was based upon. The model does give the ability to experiment with different pellet sizes, wind fields, attitudes, angular velocities, minor alterations to bends/pipe lengths and even motorized spreaders. The model performed in accordance with empirical results and showed that a higher airspeed produced a larger and more uniform pellet distribution. However, this may be undesirable as it causes increased pellet attrition Aarseth (2004); Aarseth et al. (2006) and hence this loss may cancel the beneficial effects of increased spatial distribution. A motorized spreader design was also explored which was able to throw pellets much further even at low airspeeds. Such a design may be realizable through a pneumatic or hydraulic motor and be able to provide increased surface coverage whilst keeping attrition to a minimum.

The pellet detector was able to provide accurate measurements of passing pellets as well as good separation between feed and faecal matter. The device and computer vision algorithm may be applied to a wide range of scenarios where the number of passing particles has to be quantified.

Experimental results from pellet diffusion and settling rate provided new insight into the behaviour of pellets in still water. The results may be of relevance to all sea cage and deposition models which include feed pellets in one form or another. This new data will hopefully lead to more accurate simulation results.

The extended sea cage model provides researchers with a valuable tool where different configurations of fish, feed distributions, pellets and environmental factors can be simulated. This tool is first envisioned as an off-line system where e.g. various feeding regimes can be simulated to determine implications on uniform feed intake, growth and feed loss. Finally, the combined spreader and sea cage model was used to simulate different methods of feed distribution. Results indicated that a large distribution of feed across the surface was beneficial for equal feed access and feeding into the current reduced feed loss.

6.2 Suggestions for future work

With respect to the spreader model, developing a full kinetic model would have greatly improved the model's ability to simulate a wider range of spreader designs. In addition, a model of the pneumatic transport process would have made it possible to predict pellet speed at the spreader as a function of feed pipe parameters, pressure and airspeed at the barge. This would have provided researchers and equipment

producers with a more versatile spreader performance evaluation tool.

The classical rotary spreader has drawbacks such as limited surface coverage and the inability to adapt to changing winds and current. Equipment producers are urged to investigate alternative designs which are able to increase surface coverage without the use of higher conveying airspeed. This may be achieved by a motorized spreader design, air injection after the last bend in the spreader or alternative designs all together. The notion of a relocatable spreader should also be explored. Having the ability to translate the spreader along the dominant current axis may contribute to pellets residing within the sea cage for longer, increasing both the spatial and temporal availability. More advanced solutions may also be envisioned which are able to place pellets in a certain area or sector of the sea cage. This may be beneficial when smolts are first introduced to the sea cage as they may congregate into the current at one location and need to be accustomed to the new feeding regime. Placing feed at a particular location may also be beneficial for larger salmon which tend to aggregate towards the net wall in high water currents (Johansson et al., 2014).

A full scale experiment of localized versus distributed feeding and the consequent effects on growth, injuries and preferably also feed loss is highly desired. The results from such a study would provide some conclusion to the ongoing discussion regarding the benefits of localized versus distributed feeding, and the results may be highly valuable as reference and for further validation of models such as D.

There is also much left to be done with respect to the modelling of dynamics within the sea cage. Føre et al. (2016) took a step forward with integrating both pellet motion (Paper E) through models of feed distribution (Alver et al., 2004, D), fish behaviour (Føre et al., 2009, 2013) and an energetic model. However, there are still many aspects which are yet to be included such as cage deformation (Klebert et al., 2015), diseases (Føre et al., 2016), full integration with the spreader model (C, F, H), use of water currents based on local or regional ocean models and perhaps a more elaborate treatment and further inclusion of environmental drivers (Oppedal et al., 2011). With time, an elaborate model may act as an offline tool, simulating *a priori* scenarios determining the optimal feed distribution method with respect to cage size, fish and location. Ultimately, the simulation tool may be part of an on-line system, providing the farmer with real-time visualization of feed and fish. Such a system could be able to gather information from available sensors, simulate ahead of time and provide the farmer with suggestions for optimal feeding. The system may also be able to position feed optimally with respect to wind, currents and fish placement given that the control inputs are available. This will contribute in moving the industry a step closer to precision livestock farming.

The most challenging part may be to raise interest in such a tool in the industry. Salmon farming in Norway has been a highly profitable business and many tend to use the existing methods because they work "well enough". Atlantic salmon

farming in its simplest form is not very complicated, however, doing it well has proven much more challenging. The industry, equipment producers, scientists and the government have undoubtedly made significant progress in terms of cooperation and stimulated research through common discussion arenas, specialized concessions, government grants and regulations. As Norwegian salmon farming is under heavy criticism, making an extra effort at solving the related challenges will hopefully lead to the business being profitable, humane and environmentally friendly long after the age of fossil fuel extraction.

Chapter 7

Original Publications

This chapter contains seven published papers and two manuscripts.

Paper A Feeding of large-scale fish farms: Motion characterization of a pneumatic rotor feed spreader

(Skøien and Alfredsen, 2014)
Skøien, K. R. and Alfredsen, J. A. Feeding of large-scale fish farms: Motion characterization of a pneumatic rotor feed spreader. In *Oceans - St. John's, 2014*, pages 1–7, Sept 2014. doi: http://dx.doi.org/10.1109/OCEANS.2014.7003103

Feeding of Large-Scale Fish Farms: Motion Characterization of a Pneumatic Rotor Feed Spreader

Kristoffer Rist Skøien
and Jo Arve Alfredsen
Centre for Research-Based Innovation in Aquaculture Technology (CREATE),
Department of Engineering Cybernetics,
Norwegian University of Science and Technology
7491 Trondheim, Norway
Email: kristoffer.rist.skoien@itk.ntnu.no, jo.arve.alfredsen@itk.ntnu.no

***Abstract*—This study presents a wireless attitude heading and reference system (AHRS) adapted for use in marine environments where it was used to characterize the motion of a pneumatic rotary feed spreader representative of designs commonly utilized in large-scale salmon aquaculture. The attitude of the spreader affects the distribution of feed pellets over the cage surface and may have significant influence on the feeding efficiency of fish. Measurement and analysis of the motion were performed over a range of different airspeeds. The results suggested that an angular momentum originating from the connection between the spreader and the feed supply pipe may cause a substantial roll offset. At low airspeeds the yaw angle of the outlet pipe appeared to be most influential on the roll and pitch of the spreader. At higher airspeeds the rotational velocity became increasingly influential. The roll and pitch of the spreader may explain the non-uniform surface pellet distribution observed in a separate study.**

***Keywords*—Aquaculture; Sea Cage; Fish Farming; Fish Feeding; Pneumatic Rotary Feed Spreaders; Modelling; Wireless Inertial Measurement Unit**

I. Introduction

Facilitated by new technology, marine fish farming has experienced rapid growth over the last few decades, and the worldwide production of Atlantic salmon exceeded 2 million tonnes in 2012 [1]. Larger production volumes have led to a more industrialized approach to fish farming and there is currently increased attention towards optimization of the processes and operations involved. One of the major issues is fish feeding and the question of how to distribute feed optimally in space and time within the highly dynamic environment of the sea cage. The cost of pelleted fish feed typically amounts to about 50 % of all farming expenditures of salmon and rainbow trout [2], and with feed loss estimated to 5-7 % [3], [4] there is a substantial economic incentive in improving the feeding process. Moreover, escaping feed can attract wild fish to the cage that may in turn facilitate transmission of diseases between cages and sites [5]. Introduction of wasted salmon feed in the diet of wild fish may also alter their body fat composition [6]. The spatiotemporal distribution of feed within the sea cage is also an important factor, which influences the growth and living environment of the fish. The result of a suboptimal distribution of feed may cause a feed intake that results in inefficient and reduced growth [7], and the availability of feed has been shown to influence the aggressiveness of fish [8], [9], [10], [11], [12], [13]. Based on the aforementioned studies, it is likely that an optimal distribution of fish feed is one that makes feed equally available to all individuals whilst ensuring that no feed is lost. Before inquiring further into how optimal feed distribution can be achieved, more must be known about the performance of current methods of feed distribution.

In salmon farming, feed is brought to the farming site by boat and offloaded into silos on a feed barge which typically handles feed distribution to 4-16 sea cages. An array of blowers propels compressed air through submerged piping to reduce the temperature before entering the silo room where controlled quantities of pelletized feed are released into the airflow. Through a system of pneumatic valves, feed is transported through floating plastic tubes to the individual sea cages. Feed pellets are commonly distributed across the surface using a floating pneumatically driven rotary spreader located near the center of the sea cage (Figure 1). The entire system can be operated from a control room on the feed barge or sometimes remotely from a central control hub which manages several sites.

To facilitate analysis of current and alternative methods of feeding, a mathematical model of the spatiotem-

poral feed distribution inside a sea cage has been developed taking into account physical pellet properties, the feed spread pattern across the cage surface, wind, water current and turbulence, motion of the fish and feeding behavior [14], [15]. The model is used as an evaluation tool in developing new and better methods of feed delivery in large-scale marine fish farms.

II. Problem Statement

The feed spread pattern across the cage surface (feed footprint) must be known in order for the model to make correct calculations of the spatiotemporal feed distribution inside the cage. So far this has been based on data from [16] where the feed footprint of two different rotary feed spreaders were measured directly using collection boxes on the water surface. It is however desirable to expand the current model to include a model of a rotary feed spreader. To validate a spreader model, the inertial forces acting upon the system must be known. In this study we present a compact long-range wireless inertial measurement unit that is specially designed for attachment to a rotary feed spreader for use in marine environments. Based on data from this device, a preliminary analysis of the motion of a rotary feed spreader is performed. The results will be essential in modelling spreader dynamics and facilitate experimentation with current and alternative methods of feed distribution in sea cages.

III. Materials and Methods

A. Pneumatic Rotary Feed Spreader

In this experiment the "CF90 Double" (Figure 1) rotor spreader (Akvasmart, AKVAGroup, Bryne, Norway) was used. This is a representative design for feed spreaders commonly utilized in salmon aquaculture. The spreader design consists of a $90°$ bend where the feed enters and is transported up to the bearing assembly allowing the center pipe to rotate. A shaft extending into the water with a counterweight at the end maintains the spreader in an upright position and counteracts the roll and pitch of the spreader.

The following notation is defined according to [17]. The body reference frame $\{b\}$ is fixed with respect to the main structure of the spreader with its center of origin in the center of the vertical shaft at the water surface. As illustrated in Figure 1, the X_b-axis is defined positive along the feed pipe from the spreader, Y_b to the right with respect to X_b (out of the paper towards the reader) and Z_b down into the water. The rotations about these axes or the attitude of the spreader body is described by the Euler angles $\mathbf{\Theta_{nb}} = [\phi_b \quad \theta_b \quad \psi_b]^T$, roll, pitch and yaw respectively with respect to the *North-East-Down* (NED) inertial reference frame. For simplicity we assume that the feed pipe from the spreader is

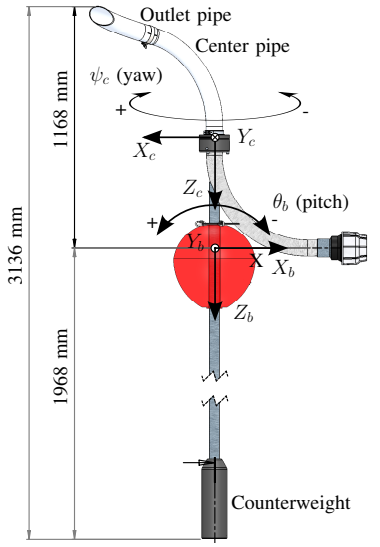

Fig. 1: The "CF90 Double" rotor spreader (AKVAgroup, Bryne, Norway). Air and feed is transported through a pipe (not shown) connected to the flange on the right. The spreader floats on a buoy and is kept upright by the submerged counterweight. A bearing assembly allows for the rotational motion of the center pipe, which is defined as the entire rotating pipe structure including the outlet pipe. At the end of the center pipe is the adjustable outlet pipe used to alter the pellet trajectory. The axes of the reference frames $\{b\}$ at the water level and $\{c\}$ at the center pipe are depicted in the figure. This figure is licensed under a Creative Commons BY-NC-SA license.

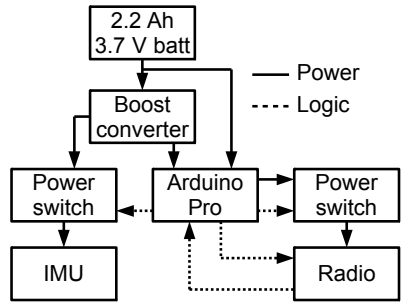

Fig. 2: Block diagram of the measurement unit. This figure is licensed under a Creative Commons BY-NC-SA license.

always directed towards true north. The stiffness of the feed pipe combined with three rope moorings of the spreader to the floating collar of the sea cage restrict the spreaders yaw motion, making $\psi_b = 0$. The reference frame $\{c\}$ is defined at the bottom of the center pipe with axes in identical directions to $\{b\}$. The only degree of freedom between $\{c\}$ and $\{b\}$ is ψ_c. The rotation between these coordinate systems can thus be described by $\mathbf{R_c^b}(\mathbf{\Theta_{bc}})$ where $\mathbf{\Theta_{bc}} = [0 \quad 0 \quad \psi_c]^T$. In this study it is of interest to obtain ϕ_b and θ_b and the yaw angle of the center pipe (ψ_c) not the spreader (ψ_b). Due to the mooring of the spreader it is assumed that there is no horizontal translational motion, and considering the calm weather during the experiment the effects of waves are omitted making the body-fixed linear velocity zero $\mathbf{v_{b/n}^b} = [0 \quad 0 \quad 0]^T$. To reduce the effect of centripetal acceleration, the accelerometers of the attitude heading and reference system (AHRS) were mounted as close to the Z_c axis as possible, making $r \approx 0$, and hence the centripetal acceleration $a_s = r\dot{\psi_c}^2 \approx 0$. The center of mass was also located close to the rotational axis reducing the effect of the added mass on the moment of inertia about the Z_c axis I_{zz}. The effect of centripetal acceleration on the measurements caused by the limited rotations ϕ_b and θ_b are unknown.

B. The Measurement Device

The main components of the system are illustrated in Figure 2. The device runs off a 2.2 Ah 3.7 V (1S) lithium polymer battery connected to a LiPower - Boost Converter (SparkFun Electronics, CO, USA) supplying the system with 5 V whilst providing battery undervoltage protection. At the core of the measurement device is an Arduino Pro equipped with an ATmega328p microcontroller (Atmel, CA, USA) running at 8 MHz with onboard 3.3 V regulator. A voltage divider connected to an internal ADC provides voltage readings from the battery. Two MOSFET switches (TPS2023, Texas Instruments, TX, USA) controls the power supply to the AHRS and radio unit. The radio unit is a 433 MHz transparent frequency shift key (FSK) transceiver produced by 3D Robotics Inc. (CA, USA) based on the HM-TRP module (Hope Microelectronics Ltd., Shenzhen, China) configured for 100 mW 4800 BAUD transmission. The AHRS is a 3-Space Datalogging (YEI Technology, OH, USA) featuring a triaxial gyroscope, accelerometer and magnetometer. It contains a Kalman filter for orientation estimation, real-time clock and MicroSD card for data storage. This device is in itself a fully contained AHRS. During deployment in the sea cage it is difficult to access the sensor. It must be able to operate in standby for days or weeks interrupted by short bursts of logging. These factors called for the described system, which provides long-range remote control and extended standbytime. Via a command set the measurement device can trough a state machine alter its mode of operation between sleep, standby or logging for data capture. While sleeping the microcontroller and wireless link are periodically awakened to enable reception of commands. The AHRS is configured to run at 100 samples/s, sufficient for capturing the dynamics of the spreader, which has a rotational (angular) frequency $\dot{\psi}_c < 4\pi$ rad/s or 120 RPM. Upon receiving a logging command the AHRS performs logging for 120 seconds storing both the final orientation and raw data to the SD card. The hardware was encased in IP67 certified housings and mounted to the center pipe. This yielded a total added mass of 1176 g.

C. Experiment

The experiment was carried out at the facilities of AquaCulture Engineering - "ACE" (Trondheim, Norway) at Korsneset (63.1428° N, 8.2208° E). The rotor spreader was hoisted into a sea-cage and connected to a 90 mm outer diameter polyethylene high-density (PEHD) pipe to the existing Akvasmart (AKVAGroup, Bryne, Norway) feeding system. The length of the feed pipe was approximately 225 m. The airspeed and pressure are sampled with inbuilt sensors at the barge before entering the feed dosing valve where feed is normally added. The airflow exits the barge through a selector valve before entering the PEHD feed pipe to the individual sea cages.

The airspeeds used in this experiment were 15, 20, 25 and 30 m/s corresponding to the blower running at 31, 49, 69 and 88 % power respectively. These values cover the speed settings commonly used in sea cage farming [16]. The experiments were conducted with two methods: "Hot start" (*H*): The blower was set to the desired power and left to stabilize for 60 seconds before logging was performed for 120 s. "Cold start" (*C*): The logging was started without any airflow and after 60 seconds the blower was started at the desired power letting the spreader spin up while logging commenced for a further 60 seconds. The experiments were conducted in the following order during the course of 120 minutes with the labels (reflecting airspeed): 30*H*, 25*H*, 20*H*, 15*H*, 15*C*, 20*C*, 25*C*, 30*C*, each in triplicate.

IV. Results

Prior to conducting the experiments, the center pipe of the spreader was fixed at a yaw angle that corresponds to the outlet pipe pointing along the feed pipe. Yaw readings from this fixed position yielded a $\Delta\psi_b$ giving the yaw of the spreader with respect to North. This was used to rotate the results so that $\psi_c = 0°$ corresponds to the outlet pipe pointing along the feed pipe. The yaw

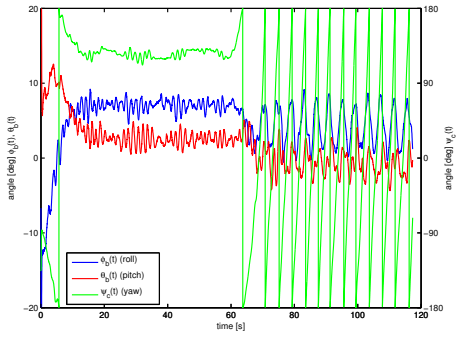

Fig. 3: Roll, pitch and yaw as a function of time from a single 15*C* replicate. The blower was started at t = 60 s. This figure is licensed under a Creative Commons BY-NC-SA license.

position of the outlet pipe in figure 1 thus corresponds $\psi_c = 180° = -180°$. Figure 3 shows $\phi_b(t)$, $\theta_b(t)$ and $\psi_c(t)$ from a single replicate cold start at 15 m/s with the angles rotated into the coordinate systems specified earlier. All rotations are described by YXZ angles. From zero to approximately 20 s the Kalman filter stabilizes, which is most clearly observed from the values of $\phi_b(t)$ and $\theta_b(t)$. The center pipe rotates freely under the influence of wind and waves, which is observable by the fluctuations in $\psi_c(t)$. The rotation of $\psi_c(t)$ from $180°$ to $-180°$ is visible as vertical lines in Figure 3 as a wrap-around. At t = 60 s the blower is started, and the yaw shows a transient response before stabilizing at about 14.6 RPM. After a few seconds, the effect of the center pipe's rotation is manifested in $\phi_b(t)$ and $\theta_b(t)$ resembling a sinusoidal behaviour. The angular velocity was determined to be 14.6, 41.7, 60.8 and 79 RPM for 15, 20, 25 and 30 m/s airspeed respectively.

To get a clearer picture of the variation of the spreader attitude, the center pipe yaw angle was discretized into 360 one degree bins, and for each AHRS sample the roll and tilt readings were added to their respective yaw bins. This yielded an average of N/360 samples in each bin. The contents of each bin were averaged to obtain the results. $\phi_b(\psi_c)$ and $\theta_b(\psi_c)$ at different airspeeds are presented in Figure 4. The clockwise rotation of the spreader corresponds to a left-to-right motion in Figure 4. ± 1 SD error bars are depicted at $90°$ intervals.

The number of samples in each of the graphs in figure 4 differs due to the following reasons: Due to the Kalman filter of the AHRS requiring some time to converge, a visual assessment was made of $\phi_b(t)$ and $\theta_b(t)$ to determine the time needed for the attitude estimation to stabilize. 20 s proved sufficient for the Kalman filter to converge. In addition considering the 60 seconds before the blower was started during cold starts, the first 80 seconds of each log was discarded. The first 80 seconds was also discarded during hot start as the time needed for the Kalman filter to stabilize in these conditions varied markedly. A few seconds was removed at the end of certain logs due to a small number of corrupted samples. One *15H*, one *15C* and one *30C* log had to be discarded due to a SD card malfunction. All logs from 30*H* were discarded as there was evidence of drift in $\phi_b(t)$ and $\theta_b(t)$. This was possibly due to the effects of centripetal acceleration, however, this remains unknown as the internal configuration of the AHRS is proprietary.

V. Discussion

As a reference for the discussion an "*ideal*" spreader is introduced. The *ideal* portrays zero roll and pitch angles and has a constant rotational velocity. The resulting feed distribution across the surface from an *ideal* spreader forms a perfect circle with a uniform feed distribution.

At 15 m/s (Figure 4a) the pitch of the spreader fluctuates around $-0.6°$, which is close to zero as expected. The roll of the spreader has a mean value of $\bar{\phi}_b = 3.5°$, which corresponds well to the visual observations made during the experiment. This deviation from the vertical *ideal* orientation is probably caused by a substantial moment from the feed pipe causing the spreader to sit on the water with a non-zero roll angle. This moment is likely to originate from the mounting procedure between the spreader and feed pipe. A positive roll offset is visible throughout the experiment with $\bar{\phi}_b$ = $3.5°$, $3.7°$, $2.1°$ and $1.2°$ for 15, 20, 25 and 30 m/s respectively. From Figure 4a the roll of the spreader corresponds quite well with the yaw angle of the center pipe. At $\psi_c = -90°$ the mass of the center pipe causes the spreader to reduce its roll angle and increase the roll accordingly at $\psi_c = 90°$. There is a phase lag of about $39°$ between the outlet pipe pointing towards $\psi_c = -90°$ or $\psi_c = 90°$ and the roll angle being at its maximum. This phase lag is far less evident for the pitch angle where maximum pitch corresponds well with $\psi_c = -180° = 180°$ and accordingly the minimum pitch at $\psi_c = 0°$. This difference in phase lag is probably due to the differences in inertia (I) along X_b and Y_b seemingly with $I_{xx} > I_{yy}$ due to the rotational resistance of the feed pipe. This assumption is further strengthened at 20 m/s (Figure 4b) where ϕ_b is less influenced by ψ_c whilst θ_b still is highly influenced by ψ_c. In Figure 4b a phase lag of about $63°$ between θ_b and ψ_c has also appeared. At 25 and 30 m/s (Figure 4c, 4d) ϕ_b and θ_b are almost independent

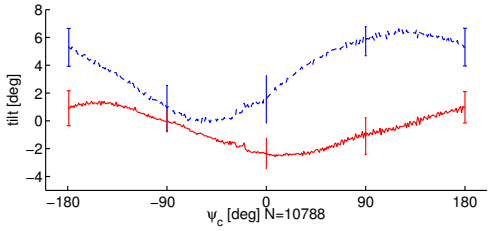

(a) Airspeed = 15 m/s

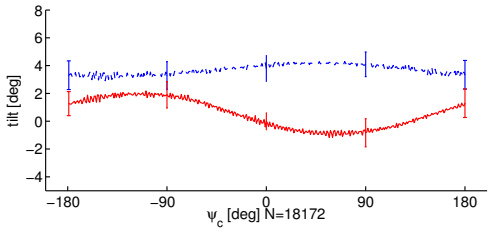

(b) Airspeed = 20 m/s

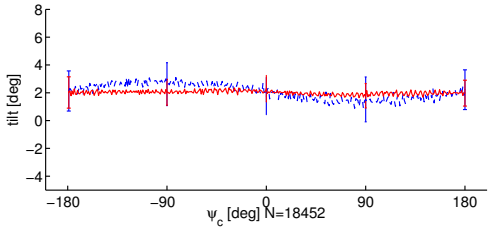

(c) Airspeed = 25 m/s

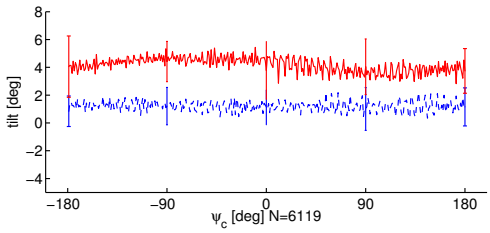

(d) Airspeed = 30 m/s

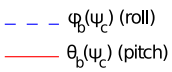

Fig. 4: The roll and tilt of the spreader as a function of yaw at different airspeeds. This figure is licensed under a Creative Commons BY-NC-SA license.

of ψ_c. Inspecting the average roll and pitch $\bar{\phi}_b$ and $\bar{\theta}_b$ from low to high airspeed, $\bar{\phi}_b = 3.5°$, $3.7°$, $2.1°$ and $1.2°$ at 15, 20, 25 and 30 m/s respectively, while $\bar{\theta}_b = -0.6°$, $0.5°$, $2°$ and $4.2°$ at the same airspeeds, $\bar{\phi}_b$ generally decreasing with airspeed whilst $\bar{\theta}_b$ increases. This effect is possibly due to precession related to the gyroscopic effects of the rotating center pipe, which requires further investigation. A reduction in the roll and pitch of the spreader bringing the results closer to *ideal* would probably be observed if a heavier counterweight was mounted and/or a longer shaft leading from the bearing assembly to the counterweight.

To the authors knowledge there are no ballistic models that describe the pellet dispersion across the surface as a function of spreader attitude. To estimate the effects of roll and pitch on the pellet throw a basic ballistic analysis was performed using Equation 1.

$$d = \frac{v_p \cos\alpha}{g}\left(v_p \sin\alpha + \sqrt{(v_p \sin\alpha)^2 + 2gy_0}\right) \quad (1)$$

d is the distance a pellet is thrown from the spreader, α is the angle of the outlet pipe with respect to the water surface, v_p is the speed of the pellet, which is defined as $v_p = 0.55 * v_{air}$ as the pellets have a lower speed than the transport airflow [18]. Further, $g = 9.81$ m/s^2 and the height of the outlet pipe above the water assumed constant $y_0 = 1.168$ m. At 15 m/s we consider the spreader roll at $\psi_c = -90°$ and $\psi_c = 90°$, which are $0.9°$ and $5.7°$ respectively, disregarding the pitch that is close to zero at these yaw angles. Taking into account the top bend of the spreader which is angled $20°$ up from the water, $\alpha = 20.9°$ at $\psi_c = -90°$ and $\alpha = 14.3°$ at $\psi_c = 90°$. According to Equation 1 this yields a throw of 6.7 and 5.9 m respectively. At 30 m/s we consider θ_b to be constant at $4.2°$ and disregard the fairly constant ϕ_b at $1.2°$. Performing a similar analysis at $\psi_c = 0$ and $\psi_c = 180 = -180$ yields $\alpha = 24.2°$ and $\alpha = 15.8°$ respectively. From Equation 1 the corresponding throw lengths are 23.1 and 17.9 m. Through this estimate the effect of the spreader attitude on pellet throw becomes more apparent. The roll and pitch of the spreader affected the throw, which caused it to deviate from the *ideal* where pellets would have been thrown equally long at any yaw angle. At lower airspeeds the roll and pitch of the spreader was highly influenced by the yaw angle resulting in the pellet throw length differing by 0.8 m in the given calculation. At higher airspeeds roll and pitch angles are less influenced by yaw, but the tilt of the spreader causes pellets to be thrown further when $\psi_c = 0$ and shorter (shot down into the water) when the outlet pipe is in the opposite direction.

Comparing these results without feed pellets in the airstream to [16] where feed was involved is not trivial.

Including feed in this study would probably reduce the airspeed and hence the angular velocity of the spreader. Due to the feeding system releasing feed in batches, the system would also likely behave in a more jerky fashion when the continuous airflow is periodically interrupted. [16] does not detail in what direction the pellet collection boxes were placed with respect to the feed pipe making it impossible to determine if the pellet distributions are a function of pitch, roll or a combination. However, the study does state that the boxes were placed in the direction with the largest visible difference in pellet distribution. Basing the comparison from "spreader A - RS-90C" (Akvasmart, AKVAgroup, Bryne, Norway) in [16], which is the spreader most similar to the one used in this study, with tilt up, does yield some possibilities to the link between feed distribution and spreader attitude. Although the two spreader models bear resemblance, the results form [16] show a considerably higher angular velocity for a similar spreader at identical airspeeds with 20, 25 and 30 m/s yielding 71, 98 and 110 RPM respectively. This is likely due to the feed pipe in the present experiment being longer (225 vs. 96 m). We assume that the airspeed and hence the attitude of the spreader are most similar in the case of 30 m/s in this study, corresponding to 79 RPM, and 20 m/s corresponding to 71 RPM in [16]. At 30 m/s (Figure 4d) especially the pitch in this study portrayed a certain deviation from the vertical *ideal*, which might manifest itself to a sharp/dense (shooting down into the water) distribution on one side of the spreader whilst dispersing the feed over a greater area when the outlet pipe is pointed skywards on the opposite side as is reported in [16]. The estimated throw of 23.1 and 17.9 m at 30 m/s in the present study are much greater than the observed values in [16]. This is likely due to the airspeed at the spreader being significantly lower than at the feed barge and Equation 1 not considering the nonlinear damping due to air resistance. However, the pellets in the dispersed direction will be airborne for longer probably causing increased dispersion. The physical behavior of the rotor spreader does show reasonable correspondence with the results in [16] and may explain the witnessed effects in the "dense" and "dispersed" direction.

Further investigation must be made into whether feed influences the attitude of the spreader, and a more comprehensive experiment must be conducted where the feed distribution pattern as well as the attitude of the spreader can be observed jointly. In addition, a more accurate ballistic model should be developed to account for drag, and more accurate estimates of the airspeed at the outlet pipe should be obtained. Depending on the yaw angle, pellets must navigate through different bend configurations from the body of the spreader to the center pipe. The effect of bend configurations must be clarified and analyzed together with the spreader attitude to determine the effect on pellet distribution.

VI. Conclusion

This study presents an addition to an existing AHRS unit for determining the attitude of pneumatic rotary feed spreaders in aquaculture. The device has been used to characterize the behavior of a spreader at different airspeeds in a normal working environment. The results show that the roll and pitch of the feed spreader are influenced by airspeed. Due to the connected feed pipe, it appears that the moment of inertia around the roll axis is greater than around pitch. At low angular speed both the roll and pitch are influenced by the yaw angle of the outlet pipe. At higher speeds, it appears that the roll and pitch angles are mainly governed by the angular velocity and not the angular position, which is possibly due to precession and/or other gyroscopic effects. When mounting the spreader to the feed pipe, care should be exerted so there are no moments present about the roll axis. This will likely result in the spreader standing more vertically and provide a more uniform feed distribution across the surface. A heavier counterweight and/or an elongated shaft from the bearing assembly down to the counterweight would probably aid in stabilizing the spreader. A basic ballistic analysis based on the spreader attitude show that the roll and pitch may account for the uneven distribution patterns observed in a separate study.

Acknowledgment

The authors would like to thank Morten Malm and Ingolf Lygren at AKVAgroup for use of the rotary spreader and assistance during the experiment as well as Per Inge Snildal and Terje Haugen at the workshop at the department of Engineering Cybernetics. Appreciation is also extended to AquaCulture Engineering (ACE) and SalMar for use of their facilities and the assistance at Korsneset.

References

[1] FAO, "Food and Agriculture Organization of the United Nations," Available from http://www.fao.org/fishery/statistics/global-aquaculture-production/en, 2014.

[2] Norwegian Directorate of Fisheries, www.fiskeridir.no, 2012.

[3] C. J. Cromey, T. D. Nickell, and K. D. Black, "Depomod-modelling the deposition and biological effects of waste solids from marine cage farms," *Aquaculture*, vol. 214, no. 1-4, pp. 211 – 239, 2002. [Online]. Available: http://www.sciencedirect.com/science/article/pii/S00448486020036 8X

[4] J. Gjøsæter, H. Otterå, E. Slinde, K. Nedreaas, and A. Ervik, "Effekter av spillfôr på marine organismer," *Kyst og Havbruk*, pp. 52–55, 2008.

[5] T. Dempster, I. Uglem, P. Sanchez-Jerez, D. Fernandez-Jover, J. Bayle-Sempere, R. Nilsen, P. Bjørn *et al.*, "Coastal salmon farms attract large and persistent aggregations of wild fish: an ecosystem effect," *Mar Ecol Prog Ser*, vol. 385, no. 1, p. 14, 2009.

[6] D. Fernandez-Jover, J. A. L. Jimenez, P. Sanchez-Jerez, J. Bayle-Sempere, F. G. Casalduero, F. J. M. Lopez, and T. Dempster, "Changes in body condition and fatty acid composition of wild mediterranean horse mackerel (*Trachurus mediterraneus*, steindachner, 1868) associated to sea cage fish farms," *Marine Environmental Research*, vol. 63, no. 1, pp. 1–18, 2007.

[7] O. Einen, T. Mørkøre, A. M. B. Rørå, and M. S. Thomassen, "Feed ration prior to slaughter—a potential tool for managing product quality of atlantic salmon (salmo salar)," *Aquaculture*, vol. 178, no. 1–2, pp. 149 – 169, 1999. [Online]. Available: http://www.sciencedirect.com/science/article/pii/S004484869900126X

[8] E. Brännäs, U. Berglund, and L.-O. Eriksson, "Time learning and anticipatory activity in groups of arctic charr," *Ethology*, vol. 111, no. 7, pp. 681–692, 2005. [Online]. Available: http://dx.doi.org/10.1111/j.1439-0310.2005.01094.x

[9] J. López-Olmeda, C. Noble, and F. Sánchez-Vázquez, "Does feeding time affect fish welfare?" *Fish Physiology and Biochemistry*, vol. 38, no. 1, pp. 143–152, 2012. [Online]. Available: http://dx.doi.org/10.1007/s10695-011-9523-y

[10] C. Noble, S. Kadri, D. F. Mitchell, and F. A. Huntingford, "Influence of feeding regime on intraspecific competition, fin damage and growth in 1+ atlantic salmon parr (salmo salar l.) held in freshwater production cages," *Aquaculture Research*, vol. 38, no. 11, pp. 1137 – 1143, 2007. [Online]. Available: http://dx.doi.org/10.1111/j.1365-2109.2007.01777.x

[11] C. Noble, K. Mizusawa, K. Suzuki, and M. Tabata, "The effect of differing self-feeding regimes on the growth, behaviour and fin damage of rainbow trout held in groups," *Aquaculture*, vol. 264, no. 1–4, pp. 214 – 222, 2007. [Online]. Available: http://www.sciencedirect.com/science/article/pii/S0044848606009276

[12] D. E. Ruzzante, "Domestication effects on aggressive and schooling behavior in fish," *Aquaculture*, vol. 120, pp. 1 – 24, 1994. [Online]. Available: http://www.sciencedirect.com/science/article/pii/0044848694902178

[13] P. E. K. Symons, "Behavioural adjustment of population density to available food by juvenile atlantic salmon," *Journal of Animal Ecology*, vol. 40, no. 3, pp. pp. 569–587, 1971. [Online]. Available: http://www.jstor.org/stable/3438

[14] M. O. Alver, J. A. Alfredsen, and T. Sigholt, "Dynamic modelling of pellet distribution in atlantic salmon (salmo salar l.) cages," *Aquacultural Engineering*, vol. 31, no. 1-2, pp. 51 – 72, 2004. [Online]. Available: http://www.sciencedirect.com/science/article/pii/S0144860904000056

[15] M. Føre, T. Dempster, J. A. Alfredsen, V. Johansen, and D. Johansson, "Modelling of atlantic salmon (salmo salar l.) behaviour in sea-cages: A lagrangian approach," *Aquaculture*, vol. 288, no. 3–4, pp. 196 – 204, 2009. [Online]. Available: http://www.sciencedirect.com/science/article/pii/S0044848608008533

[16] M. Oehme, T. S. Aas, M. Sørensen, I. Lygren, and T. Åsgård, "Feed pellet distribution in a sea cage using pneumatic feeding system with rotor spreader," *Aquacultural Engineering*, vol. 51, no. 0, pp. 44–52, 11 2012. [Online]. Available: http://www.sciencedirect.com/science/article/pii/S0144860912000568

[17] T. I. Fossen, "Guidance and control of marine craft," *Marine Cybernetics, Trondheim*, 2010.

[18] K. Aarseth, "Attrition of feed pellets during pneumatic conveying: the influence of velocity and bend radius," *Biosystems Engineering*, vol. 89, no. 2, pp. 197 – 213, 2004. [Online]. Available: http://www.sciencedirect.com/science/article/pii/S1537511004001217

Paper B A computer vision approach for detection and quantification of feed particles in marine fish farms

(Skøien et al., 2014a)
Skøien, K. R., Alver, M. O., and Alfredsen, J. A. A computer vision approach for detection and quantification of feed particles in marine fish farms. In *2014 IEEE International Conference on Image Processing (ICIP)*, pages 1648–1652, Oct 2014a. doi: http://dx.doi.org/10.1109/ICIP.2014.7025330

A COMPUTER VISION APPROACH FOR DETECTION AND QUANTIFICATION OF FEED PARTICLES IN MARINE FISH FARMS

Kristoffer Rist Skøien[⋆] *Morten Omholt Alver*[⋆†] *Jo Arve Alfredsen*[⋆]

[⋆]Norwegian Univ. of Science and Technology (NTNU), Dept. of Engineering Cybernetics, NO-7491, Trondheim, Norway
[†]SINTEF Fisheries and Aquaculture AS, P.O. Box 4762 Sluppen, NO-7465, Trondheim, Norway

ABSTRACT

In the realm of marine fish farming, there is increased focus on employing numerical models and tools to optimize production. A model describing the distribution of pelleted fish feed in time and space within a sea cage, a process which is essential for proper fish growth and welfare, has been established, but proper data for model validation have been scarce. A device based on computer vision which is able to accurately quantify the feed density within a specified volume of the sea cage as a function of time was thus developed. This paper describes the physical design of the device, as well as the application and combination of well-established algorithms to reliably detect and quantify feed pellets. Results from tests using realistic feed densities showed that the device was capable of detecting and quantifying with an error of 1.3 %.

Index Terms— Subsea particle quantification, fish feed pellets, Kalman filtering, Hungarian method

1. INTRODUCTION

Marine fish farming is a rapidly expanding industry with worldwide production totaling more than 3.4 million tonnes in 2010 [1]. The bulk of the fish growth is commonly undertaken in large sea cages where the fish are typically fed a diet of pelletized feed particles, and the food is made available to the fish by spreading the sinking feed pellets over the cage surface. The feed pellets have a cylindrical shape with a diameter adapted to the fish size, typically 4-13 mm, and the amount of feed released into one sea cage can amount to several tonnes per day. About 50 % of the costs related to farming of salmon and rainbow trout are spent on feed [2]. Feed loss is estimated at 5-7 % [3, 4], representing a considerable financial loss for the fish farmer as well as a source of negative environmental impacts. To better understand the spatiotemporal distribution of feed, a numerical model describing the transport of feed trough large scale sea cages was developed [5, 6]. The model enables simulation and analysis of the efficiency of different feeding strategies while taking into account factors influencing pellet distribution such as physical pellet properties, spreading patterns, water current, turbulence, fish motion and feeding behavior. The primary motivation for developing the computer vision system presented in the current study was to generate high quality measurements of pellet density and flux at specified locations within a sea cage, which could subsequently be used to validate the feed distribution model and improve model predictions. Solutions involving computer vision to inspect subsurface pellet distribution have been investigated previously [7, 8]. However, these approaches are less suitable to accurately determine the number of pellets passing through a known volume of the sea cage. This is due to their susceptibility to disturbance caused by interfering/occluding fish, and unrestricted detection volume. This paper presents a design for subsea image acquisition in sea cages and an algorithm based on Kalman filtering and bipartite weighted graph cost minimization for accurate pellet quantification.

The research is funded by the Centre for Research-based Innovation in Aquaculture Technology (CREATE), SINTEF Sealab, NO-7465, Trondheim, Norway.

2. HARDWARE

Unlike [7, 8] which depend on natural subsurface light as the source of illumination, the pellet detector presented here uses artificial lighting to obtain high contrast pellet images. The detector is illustrated in Figure 1. A 3×4 grid of 12 white LEDs (Seoul Semiconductors W42180, 6500 K 85 lm 3.8 W) mounted behind a translucent light diffusing plate provides a uniform backlight for the detector. A 1288×964 pixel gigabit Ethernet camera (Point Grey Research, Inc. FL3-GE-13S2C-CS), further reduced with 2×2 pixel binning for increased framerate, is set up to capture 8-bit grayscale images at 56 FPS, and transmits them to a topside computer for processing. The camera is equipped with an adjustable lens (Tamron M13VM308, focus, 3-8 mm, f/1.0-close). The aperture is set as small as possible for greater depth of field, while maintaining adequate light for the camera to obtain sufficiently exposed images at the given frame rate. The diffuser is mounted perpendicular to the principal axis of the camera at a distance of 0.2 m, covering the entire field of view. A funnel guides sinking pellets into the detection volume in front of the camera which is otherwise enclosed on the top and either side. This arrangement prevents influence from fish, it ensures that feed pellets only enter through the top funnel, and it reduces horizontal pellet motion from water currents. The latter may force pellets out of the image along one of the vertical edges, reducing the number of images a pellet is tracked throughout, and thereby negatively influencing the accuracy of the sinking velocity estimation. This configuration renders the camera unaffected by and independent from natural light and allows operation with short shutter times for proper capture of fast sinking pellets.

3. ALGORITHM

The configuration described above provides a stream of images showing pellets as dark objects against a bright background "raining through" the detection volume. Pellets typically have a wobbling motion due to irregularities in their geometry, and, although there is a general vertical path of motion through the detection volume, small deviations e.g. in entry angle cause some pellets to have

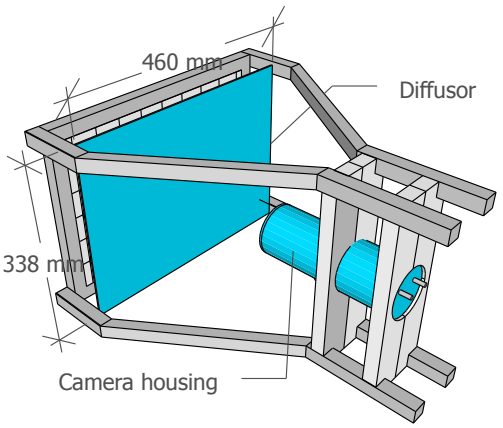

Fig. 1. The pellet detector. The camera is encapsulated in a waterproof housing and directed towards a light diffusing plate. The surrounding cover and top funnel are removed for clarity.

slightly slanting paths. Generally, several pellets will be present in the detection volume at the same time which give rise to situations where pellets collide or occlude each other in varying degree as their paths are crossing. Moreover, foreign objects of varying size, shape and motion such as fish feces may be present in the detection volume. The purpose of the algorithm is to filter out foreign objects based on size and sinking velocity and count the exact number of pellets passing through the detection volume. Based on this, the pellet distribution as function of time can be established, which is the primary output of the algorithm. The position of every pellet is tracked as it sinks through the detection volume, associating each pellet with a set of parameters contained in an instance of a "Blob class" such as ID, Kalman parameters and positional history. This allows for a velocity estimation to be derived based on the positions of a tracked pellet trough the images. Tracking is achieved through prediction of a pellet's position from the current image to the next, then the position of each pellet in the next image is matched to the predicted positions through graph theory and minimization of total Euclidean distance.

The derivation of the algorithm uses the following notation and definitions. A segmented pellet will be referred to as a blob in context of the algorithm. Symbols s, v and a denote position, velocity and acceleration of a blob respectively. The position of a blob is represented by the position s of its centroid. Subscripts $_x$ and $_y$ are used to indicate components along the horizontal and vertical image axis respectively. $\mathbf{I}$ is the identity matrix, while $\mathbf{I}_k$ denotes the current image k. $\hat{s}^-_{n,k+1}$ should be read as the *a priori* estimate of the position of blob n, in image $k+1$. Vectors and matrices are in bold, the latter indicated with capital letters. Vectors of process and measurement noise are given by $\mathbf{w}$ and $\mathbf{v}$. N is the number of blobs, and O the number of predicted blob positions in the image. All calculations are done with reference to the camera coordinate system.

After a new image $\mathbf{I}_k$ is acquired, the image is blurred using a 13×13 normalized box filter to remove imperfections in the particle surface, and then thresholded using a fixed value. Due to the constant uniform light and ample contrast, a global threshold at a fixed value gives sufficient separation between background and pellet. Alternative thresholding methods were tested, such as Otsu's method [9] and local adaptive thresholding [10] based on [11], but were deemed unnecessary. Contours of blobs are then extracted using the Open CV [12] implementation of border following as specified by [13]. The image is divided into two separate areas where the entry zone (Figure 2 (a)) is defined to be the upper 90 % of the area. In this area, blobs enter, are associated with an instance of the Pellet class, and are tracked. The remaining 10 % of the image is designated as the exit-zone. Here the average sinking velocity is calculated, and it is determined whether the blobs should be classified as pellets or feces. Due to the high frame rate, all blobs will reside within the exit-zone for a number of frames before leaving the field of view.

The algorithm determines the position of blobs and their surface area from the contour utilizing the Open CV [12] implementation of Green's theorem [14, pp.485] to establish if blobs pass a certain minimum size requirement. Because of the funnel mounted above the detector, all pellets enter the field of view at approximately the same distance from the camera along the principal axis, making pellets of similar size occupy roughly the same pixel area. If a blob resides in the entry-zone and is above the minimum size limit, an associated instance of the "Blob Class" will be created.

3.1. Prediction

We assume that no water current is present within the enclosed detection volume and model the horizontal acceleration by a random variable $a_x(t) = \mathbf{w}_x(t)$. $\mathbf{w}_x(t)$ is a vector containing white Gaussian noise ($\mathcal{N}(0, \sigma_x^2)$) similar to the method in [15]. Feed pellets in water tend to reach terminal sinking velocity after a few centimeters when hydrodynamic drag cancel out gravitational pull. It is therefore assumed that all pellets have constant velocity upon entering the detectors field of view with their vertical acceleration also modelled by Gaussian white noise ($\mathcal{N}(0, \sigma_y^2)$) $a_y(t) = \mathbf{w}_y(t)$. Unlike [15], these two vectors have different variance (σ_x^2, σ_y^2), as we presume that the horizontal (current induced) noise, and vertical (drag induced) noise have different characteristics. Given these conditions, the following equation from [15] holds for the pellet motion: $\ddot{s}_x(t) = \dot{v}_x(t) = a_x(t) = \mathbf{w}_x(t)$, and $\ddot{s}_y(t) = \dot{v}_y(t) = a_y(t) = \mathbf{w}_y(t)$. Similarly, for the measurement noise $\mathbf{v}(t)$ we also assume influence by white Gaussian noise identical in both directions given by the vectors $\mathbf{v}_x(t)$ and $\mathbf{v}_y(t)$. Position measurements can be expressed as $y_x(t) = s_x(t) + \mathbf{v}_x(t)$, and $y_y(t) = s_y(t) + \mathbf{v}_y(t)$. The complete system can be described with a regular continuous time-invariant state-space model with no control input:

$$\dot{\mathbf{x}}(t) = \mathbf{A}\mathbf{x}(t) + \mathbf{w}(t) \tag{1a}$$
$$\mathbf{y}(t) = \mathbf{H}\mathbf{x}(t) + \mathbf{v}(t) \tag{1b}$$

Where the system matrix $\mathbf{A}$ and output matrix $\mathbf{H}$ are given by

$$\mathbf{A} = \begin{bmatrix} 0 & 0 & 1 & 0 \\ 0 & 0 & 0 & 1 \\ 0 & 0 & 0 & 0 \\ 0 & 0 & 0 & 0 \end{bmatrix} \tag{2} \qquad \mathbf{H} = \begin{bmatrix} 1 & 0 & 0 & 0 \\ 0 & 1 & 0 & 0 \end{bmatrix} \tag{3}$$

with the state vector $\mathbf{x}$

$$\mathbf{x}(t) = \begin{bmatrix} s_x(t) & s_y(t) & v_x(t) & v_y(t) \end{bmatrix}^T \tag{4}$$

and the system and measurement noise terms respectively

$$\mathbf{w}(t) = \begin{bmatrix} 0 & 0 & \mathbf{w}_x(t) & \mathbf{w}_y(t) \end{bmatrix}^T \tag{5a}$$
$$\mathbf{v}(t) = \begin{bmatrix} \mathbf{v}_x(t) & \mathbf{v}_y(t) \end{bmatrix}^T \tag{5b}$$

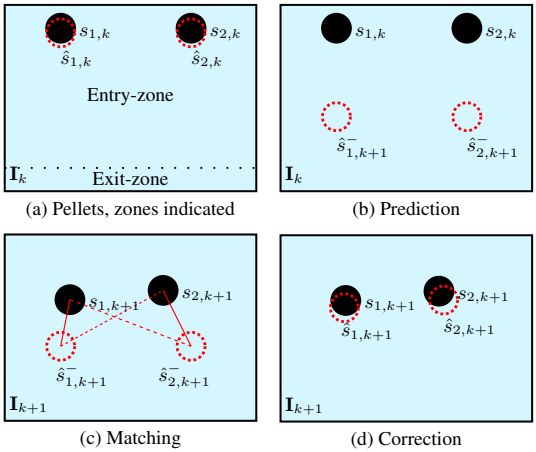

(a) Pellets, zones indicated (b) Prediction

(c) Matching (d) Correction

Fig. 2. Illustration of the prediction, matching, correction process. Back circles indicate pellets travelling trough the field of view, and the dotted circles are predicted positions.

According to [15] and [16, pp.220], the continuous system in (1a) can be discretized into the following system

$$\underbrace{\begin{bmatrix} s_{k+1,x} \\ s_{k+1,y} \\ v_{k+1,x} \\ v_{k+1,y} \end{bmatrix}}_{\mathbf{x}_{k+1}} = \underbrace{\begin{bmatrix} 1 & 0 & \Delta t & 0 \\ 0 & 1 & 0 & \Delta t \\ 0 & 0 & 1 & 0 \\ 0 & 0 & 0 & 1 \end{bmatrix}}_{\mathbf{A}} \underbrace{\begin{bmatrix} s_{k,x} \\ s_{k,y} \\ v_{k,x} \\ v_{k,y} \end{bmatrix}}_{\mathbf{x}_k} + \underbrace{\mathbf{w}_k}_{\text{noise}} \tag{6}$$

Here $\Delta t = 1$ since the algorithm is operating on a frame by frame basis. Initial estimates are given to the Kalman filter, $\hat{\mathbf{x}}_0^- = \begin{bmatrix} s_{0,x} & s_{0,y} & v_{0,x} & v_{0,y} \end{bmatrix}$, where the two first are the initial position of the new blob, and $v_{0,x}$ and $v_{0,y}$ are the initial horizontal and vertical velocities experimentally predetermined based on measurements of the pellets in this study. In this implementation, $v_{0,x} = 0$ since the detection volume is protected from horizontal water currents and $v_{0,y}$ is determined from an average sinking rate of 6 mm low density and 12 mm high density pellets, as 5.9 pixels/frame. The filter was experimentally initialized with $\mathbf{Q} = \mathbf{I} \cdot 0.1$, $\mathbf{R} = \mathbf{I} \cdot 0.1$, and $\mathbf{P}_\mathbf{0}^- = \mathbf{I}$, which are the Kalman process noise, measurement error and estimation error covariance matrices respectively. The system should be tuned for the specific application and imaging system. Measurement error may arise from pellets fluctuating to and from the camera along the principal axis, making the vertical velocity appear different. Also, the imaging process is not perfectly linear (pinhole model), albeit this can be corrected through camera calibration. These factors have been deemed of less importance in this setting, as the quantity of pellets and not their position within the image is the desired output from the algorithm. The reader is referred to [15] for theory regarding Kalman filter initialization, and [17, 18] for further filter details.

3.2. Matching and Correction

All blobs identified in image $\mathbf{I}_{k+1}$ must be matched to their predicted positions from the previous image $\mathbf{I}_k$, ensuring that a given prediction $\hat{s}_o^-$ is corrected with the corresponding blob s_n. This is recognized as a complete weighted bipartite graph problem $G = (U, V, E)$, $|U| = N$, $|V| = O$ being the number of vertices in each of the disjoined sets and the number of edges $|E| = |U||V|$. The edge weights are given by the Euclidean distance between $\hat{s}^-_{1\ldots O}$ and $s_{1\ldots N}$. A cost matrix $\mathbf{C} \in \mathbb{R}^{N \times O}$ holds all the distances. A resulting integer match matrix $\mathbf{M} \in \mathbb{Z}^{N \times O}$ holds ones in positions where there is a matched pair of $\hat{s}_o^-$ and s_n. We want to minimize problem (7), which is based on [19]

$$\min_{\mathbf{M}} \sum_{n=1}^{N} \sum_{o=1}^{O} \mathbf{C}(n,o)\mathbf{M}(n,o) \tag{7a}$$

$$s.t. \sum_{n=1}^{N} \mathbf{M}(n,o) = 1 \qquad \forall o \in O \tag{7b}$$

$$\sum_{o=1}^{O} \mathbf{M}(n,o) = 1 \qquad \forall n \in N \tag{7c}$$

$$\mathbf{M}(n,o) \in \{0,1\} \qquad \forall n \in N, o \in O \tag{7d}$$

$$\mathbf{C}(n,o)\mathbf{M}(n,o) \leq d_{max} \qquad \forall n \in N, o \in O \tag{7e}$$

In term (7e), d_{max} is a upper bound on the distance between the predicted position from $\mathbf{I}_k$, and the measured blob position in $\mathbf{I}_{k+1}$. If any value in $\mathbf{C}(n,o) > d_{max}$, this weight is set to η, which is simply a distance sufficiently large to never occur naturally. This gives the particular combination of $\hat{s}_o^-$ and s_n a very low probability of being part of the optimal match. $d_{max} = 60$ pixels in this implementation. Figure 2 (c) illustrates the possible matches, where the whole lines indicate the optimal match and the dotted lines optional matches. The optimization problem is solved by the Kuhn-Munkres algorithm [20, 21], also known as the Hungarian method implemented by [22]. Given that all position predictions are accurate, there should be a very short distance between $\hat{s}^-_{1\ldots O,k+1}$ and the corresponding blob's measured position $s_{1\ldots N,k+1}$. Now we consider three different options determined by the number of blobs N in the image and the number of predicted blob positions O. If $N = O$ there is an equal number of $\hat{s}^-_{o,k+1}$ and $s_{n,k+1}$. This however, does not imply that all predictions will be corrected. E.g. a new blob may enter, and the prediction of another blob at a different position may still reside within in the entry-zone. $N < O$ indicates that one or more blobs are missing, which might be due to pellets leaving the field of view or being occluded by another pellet. The Khun-Munkres implementation by [22] requires $N \geq O$, hence $O - N$ false blobs or are added with a distance η to all predicted positions, making them the least favorable candidates for correction. Given that a pellet leaves the field of view along one of the vertical edges of the image, this prediction without correction will continue until the Kalman filter predicts that the blob is in the exit-zone, even though out of view. This means that a blob only has to be visible in a single frame for it to pass the size filter and be quantified. Finally, $N > O$ may be an indication of a new pellet entering the field of view, and the Kalman filter will be initialized for this blob in the next image. This could also be due to separation of two pellets which have been occluding one another.

After the optimization, any match to false blobs will be removed. If $\mathbf{C}(n,o)\mathbf{M}(n,o) = \eta \, \forall n \in N, o \in O$ then $\mathbf{M}(n,o) = 0$. In such case, some of the predictions will go uncorrected this iteration, and their position will be predicted for $\mathbf{I}_{k+2}$ as well. When a visible blob reaches the exit-zone, or the predicted position of a blob which is outside the field of view reaches the exit-zone, a final check is performed on the sinking velocity. At this final stage, the average sinking speed is calculated in terms of pixels/frame from the stored position history. This prevents objects outside the desired speed range

being classified as pellets. Depending on the result, counters for pellets or foreign particles are incremented accordingly.

4. RESULTS

The proposed solution was implemented in C++ and OpenCV [12]. A small-scale experiment was conducted to assess the algorithm's ability to quantify pellets, and separate pellets from feces and other foreign objects. The particle detector was placed in a tank, and a batch of feed pellets were released into to the water directly above the detector. The feed pellets had physical properties representative of the average salmon feed used in Norway [23]. Both 6 ± 0.1 mm and 12 ± 0.2 mm diameter pellets with high (H) and low (L) density were used for the experiment. The sinking velocity for the four pellet types: *6L*: $5.3 \pm 1.2\ cm/s$, *6H*: $11.8 \pm 0.9\ cm/s$, *12L*: $9.7 \pm 1.7\ cm/s$ *12H*: $16.6 \pm 1.6\ cm/s$, (measurements made by the manufacturer, N = 20). To mimic foreign particles in the water, such as feces from the fish, we took the following approach: Feces from salmon with a weight of 0.7-1.0 kg has a sinking velocity of $5.3 \pm 0.8\ cm/s$ [24], and larger salmon with a mean weight of 3.39 kg had a fecal sinking rate of $3.2 \pm 1.1\ cm/s$ [3]. These results suggest that sinking velocity may be a factor which enables separation of pellets and fecal matter depending on fish size and diet. To determine the ability to separate pellets from feces, the *6L* pellets are chosen to mimic feces in the classification experiment since they have a settling rate almost identical to the feces of smaller salmon. The low density pellets were released in batches of 10 and 20 at a time, while high density pellets in batches of 8 and 15 to simulate different quantities of pellets in water. A high number of pellets results in increased occlusion. All tests were performed with five replicates in random order, and the algorithm was tuned based on a separate set. Three occlusion levels are defined corresponding to the number of partially or fully occluded pellets in the replicate. *None*: No occlusion for the duration of the replicate. *Low*: One or two pellet pairs occlude one another at some point during the replicate. *High*: Three or more occlusions. Realistically, only *None* and *low* occlusion are likely to occur in practice as pellets may be consumed by fish before reaching the sensor and due to pellets diffusing in water, greatly reducing concentration with increased depth. *High* must be regarded as a stress test, and does not represent normal operating conditions. Where the algorithm miscounted the number of pellets the reason was determined, and three sources of error defined. The signs indicate whether the error contributes to an over- or underestimation of the total count. (1^-) *Occlusion*: A pellet remaining occluded or too close to one or several other pellets throughout the field of view. (2^+) *Join-Separate*: Two pellets are detected and each initialized with an instance of the Blob Class with Kalman prediction. Then the blobs merge into one, making the algorithm capable of updating the predicted position of only one of them, while the estimated position of the remaining occluded pellet is predicted and not corrected for a number of frames. The Kalman predictions are not perfect, and the center of mass of the predicted blob drifts away from the multi-blob cluster. Later, the two blobs separate, causing the algorithm to create an additional instance of the Blob Class. (3^+) *Re-entering*: A pellet leaving of the field of view trough one of the vertical edges and later re-entering, which may result in a double count. The pellet-fecal sinking velocity separation limit was experimentally set to 5.4 pixels/frame. The results are presented in Table 1 and 2.

Occl.	Real	Algorithm result		Error type		
		Counted	Percent	1^-	2^+	3^+
None	52	52	100 %	-	-	-
Low	173	176	101.7 %	-	2	1
High	158	154	97.5 %	5	1	-

Table 1. The number of miscounts and type of error with the level of occlusion being *none*, *low* and *high*.

Pellet type	Real	Classified as		Percent
		6L	*12H*	
6L	62	56	6	90.3 %
12H	105	9	96	91.4 %

Table 2. Classification of pellet type based on sinkrate across all levels of occlusion. The *6L* pellets used to simulate feces.

5. DISCUSSION

The results from Table 1 indicates that the pellet detection algorithm is capable of accurately quantifying the number of feed pellets at different occlusion levels, sink rates and sizes. The combination of the *None* and *Low* pellet density/overlap experiments were deemed as realistic conditions. This combination, disregarding fecal separation gave an overestimation of 1.3 %, *N*=225, 3 positive miscounts. This is an improvement compared to the solution suggested by [8] with a counting accuracy of $\pm 10\%$ (disregarding fecal separation in both solutions). Comparing the results with [7] is not trivial, as it is more focused towards raising an alarm when a given number of pellets are present in the water column rather than quantifying passing pellets. It must however be mentioned that the two previous pellet detectors use an entirely different approach without controlled illumination and with the camera's field of view being substantially larger. In addition, the solution presented here cannot be affected by interfering fish. In the *High* occlusion experiments, the number of pellets are underestimated with 97.5 % of the pellets counted (N=158). It must be noted that errors of both positive and negative nature occurred (Table 1). The main source of error in the *High* experiments is due to pellets overlapping throughout their entire presence while sinking trough the field of view, causing an underestimate. No quantification errors occurred as a result of pellet debris or other waterborne particles during the experiments. With regard to fecal separation, the algorithm is accurate to 90.3 % and 91.4 % in classifying low and high density pellets respectively (Table 2). According to the feed manufacturer, the *6L* and *12H* pellets have sufficiently large difference in sinking velocity that given a normal distribution, no overlap should occur within tree standard deviations of the mean velocity. However, observations suggest that the variations in sinking velocity are much larger in this experiment. This might be caused by the relatively short length of the field of view, or that such a high number of pellets is released into the water simultaneously.

6. CONCLUSION

A high accuracy pellet detector and algorithm has been presented based on well-established theory. The approach provides a level of accuracy that is beyond previous studies, with an error level of 1.3 % using realistic pellet densities and without foreign particles. The pellet detector will serve as a valuable tool for determining spatiotemporal pellet densities within and beneath marine sea cages and data generation for validation of feed distribution models.

7. REFERENCES

[1] FAO, "Food and Agriculture Organization of the United Nations," Available from http://www.fao.org/fishery/statistics/global-aquaculture-production/en, 2013.

[2] Norwegian Directorate of Fisheries, www.fiskeridir.no, 2012.

[3] C. J. Cromey, T. D. Nickell, and K. D. Black, "Depomod-modelling the deposition and biological effects of waste solids from marine cage farms," *Aquaculture*, vol. 214, no. 1-4, pp. 211 – 239, 2002.

[4] J. Gjøsæter, H. Otterå, E. Slinde, K. Nedreaas, and A. Ervik, "Effekter av spillfôr på marine organismer," *Kyst og Havbruk*, pp. 52–55, 2008.

[5] M. O. Alver, J. A. Alfredsen, and T. Sigholt, "Dynamic modelling of pellet distribution in atlantic salmon (salmo salar l.) cages," *Aquacultural Engineering*, vol. 31, no. 1-2, pp. 51 – 72, 2004.

[6] M. Føre, T. Dempster, J. A. Alfredsen, V. Johansen, and D. Johansson, "Modelling of atlantic salmon (salmo salar l.) behaviour in sea-cages: A lagrangian approach," *Aquaculture*, vol. 288, no. 3–4, pp. 196 – 204, 2009.

[7] K. D. Parsonage and R. J. Petrell, "Accuracy of a machine-vision pellet detection system," *Aquacultural Engineering*, vol. 29, no. 3-4, pp. 109 – 123, 2003.

[8] M. Foster, R. Petrell, M. Ito, and R. Ward, "Detection and counting of uneaten food pellets in a sea cage using image analysis," *Aquacultural Engineering*, vol. 14, no. 3, pp. 251 – 269, 1995.

[9] N. Otsu, "A threshold selection method from gray-level histograms," *Automatica*, vol. 11, no. 285-296, pp. 23–27, 1975.

[10] F. Shafait, D. Keysers, and T. M. Breuel, "Efficient implementation of local adaptive thresholding techniques using integral images," *Document Recognition and Retrieval XV*, vol. 6815, no. 1, pp. 681510, 2008.

[11] J. Sauvola and M. Pietikäinen, "Adaptive document image binarization," *Pattern Recognition*, vol. 33, no. 2, pp. 225 – 236, 2000.

[12] G. Bradski, "The OpenCV Library," *Dr. Dobb's Journal of Software Tools*, 2000.

[13] S. Suzuki and K. be, "Topological structural analysis of digitized binary images by border following," *Computer Vision, Graphics, and Image Processing*, vol. 30, no. 1, pp. 32 – 46, 1985.

[14] E. Kreyszig, *Advanced Engineering Mathematics 8th edition*, John Wiley & Sons, ISBN 0-471-15496-2, 1999.

[15] M. Kohler, *Using the Kalman filter to track human interactive motion: modelling and initialization of the Kalman filter for translational motion*, Citeseer, 1997.

[16] R. G. Brown and P. Y. C. Hwang, *Introduction to random signals and applied Kalman filtering*, Wiley, New York, 2nd edition, 1992.

[17] R. E. Kalman et al., "A new approach to linear filtering and prediction problems," *Journal of basic Engineering*, vol. 82, no. 1, pp. 35–45, 1960.

[18] G. Welch and G. Bishop, "An introduction to the kalman filter," 1995.

[19] C. Vasconcelos and B. Rosenhahn, "Bipartite graph matching computation on gpu," in *Energy Minimization Methods in Computer Vision and Pattern Recognition*, D. Cremers, Y. Boykov, A. Blake, and F. Schmidt, Eds., vol. 5681 of *Lecture Notes in Computer Science*, pp. 42–55. Springer Berlin Heidelberg, 2009.

[20] H. W. Kuhn, "The hungarian method for the assignment problem," *Naval research logistics quarterly*, vol. 2, no. 1-2, pp. 83–97, 1955.

[21] J. Munkres, "Algorithms for the assignment and transportation problems," *Journal of the Society for Industrial & Applied Mathematics*, vol. 5, no. 1, pp. 32–38, 1957.

[22] L. Liu and D. A. Shell, "Assessing optimal assignment under uncertainty: An interval-based algorithm," *The International Journal of Robotics Research*, vol. 30, no. 7, pp. 936–953, 2011.

[23] T. Ytrestøyl, T. Aas, G. Berge, B. Hatlen, M. Sørensen, B. Ruyter, M. Thomassen, E. Hognes, F. Ziegler, V. Sund, et al., "Resource utilisation and eco-efficiency of norwegian salmon farming in 2010," *Nofima Report*, vol. 53, no. 2011, pp. 65, 2011.

[24] Y.-S. Chen, M. C. M. Beveridge, and T. C. Telfer, "Settling rate characteristics and nutrient content of the faeces of atlantic salmon, salmo salar l., and the implications for modelling of solid waste dispersion," *Aquaculture Research*, vol. 30, no. 5, pp. 395–398, 1999.

Paper C Modelling spatial surface pellet distribution from rotary pneumatic feed spreaders

(Skøien et al., 2015)
Skøien, K. R., Alver, M. O., and Alfredsen, J. A. Modelling spatial surface pellet distribution from rotary pneumatic feed spreaders. In *23th Mediterranean Conference on Control and Automation (MED)*, pages 883–888, June 2015. doi: http://dx.doi.org/10.1109/MED.2015.7158857

Modelling Spatial Surface Pellet Distribution From Rotary Pneumatic Feed Spreaders

Kristoffer Rist Skøien[1], Morten Omholt Alver[1,2], and Jo Arve Alfredsen[1]

***Abstract*— This paper presents a combined robotic and external ballistic model to predict the feed pellet distribution pattern across the water surface generated by a pneumatic rotary feed spreader commonly used in sea cage aquaculture. Results from experimental studies have been used to parameterize and validate the model. The model can be applied to evaluate spreader performance under varying operational conditions as well as exploring alternative spreader designs and configurations in order to optimize pellet distribution and feed utilization with respect to fish growth and welfare.**

***Index Terms*— Robotics, Ballistics, Aquaculture, Feed Distribution, Rotor Spreader**

I. Introduction

In salmon (*Salmo salar*) sea cage farming, feed is usually distributed to the fish using a pneumatic rotary feed spreader positioned on the surface close to the center of the cage. The pelletized feed is stored in large silos on a barge and transported through flexible tubing to the individual sea cages using compressed air. The distance from the barge to a given cage can be up to 800 m [1]. In 2014, nearly 1.7 million tons of feed worth about €2000 million were administered in this manner in Norwegian salmon and trout aquaculture [2]. A representative rotor spreader is depicted in Figure 1. It usually consists of a flotation device (buoy) and a submerged counterweight maintaining the upright position of the spreader. A ball-bearing separates the base from the center/outlet pipe on the top allowing it to rotate freely. The spreader is itself not actively controlled, the rotary motion is driven by the airflow due to the spiral shape of the outlet pipe. This configuration leads to feed being thrown and spread in an annular pattern across the water surface [3]. See [4, pp.293] for a more comprehensive description of the feeding system. This system is low-cost and low-maintenance due to the absence of electronic components and few moving parts. However, questions have been raised with respect to the performance of such a design. A study by [3] quantified the spatial feed distribution of two different rotary feed spreaders given various tilting of the outlet pipe, airspeeds and pellet size, by placing Styrofoam boxes on the water surface radially along one axis. The boxes were placed along the axis of the largest observed difference in feed distribution with an equal number of boxes on each side of the spreader. Results showed that the spreaders had an annular distribution pattern that covered from 18.2 to 79.8 % of the cage surface given a circular cage with radius 14.5 m (660.5 m^2). However, with the largest sea cages being up to 25 m in radius [5] surface area is almost tripled, giving a surface coverage of just 6.1 to 26.8 %. The annular pattern is also skewed towards one side, referred to by [3] as the *dense* and the *dispersed* direction. Based on these findings [6] created a basic set of equations to determine the surface feed distribution based on airspeed and tilt. An example from these equations are depicted in Figure 2 where the asymmetry of the surface distribution pattern is apparent.

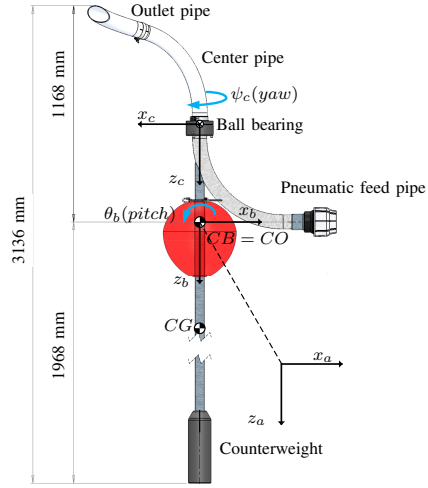

Fig. 1. Model of the "CF90 Double" pneumatic rotor spreader (AKVA-group, Bryne, Norway). The center of buoyancy (CB) coincides with the origin (OB). The base frame $\{a\}$, body fixed $\{b\}$ and the center pipe fixed reference frame $\{c\}$ are depicted in the figure. This figure is licensed under a Creative Commons BY-NC-SA license.

A. Optimal Feed Distribution

The surface feed distribution will seed the spatiotemporal distribution in the water column which in turn may affect how well the fish can access feed, as well as feed loss through the cage wall. Feed loss is estimated to be 5-7 % [7], [8], giving poor utilization of precious resources, and with about 50 % of all costs in salmon and trout farming being feed [9] this feed loss will accumulate to a significant

[1]Faculty of Information Technology, Mathematics and Electrical Engineering, department of Engineering Cybernetics, Norwegian University of Science and Technology NTNU, Trondheim, NO-7491, Norway kristoffer.rist.skoien@itk.ntnu.no, jo.arve.alfredsen@itk.ntnu.no

[2]SINTEF Fisheries and Aquaculture, Trondheim, NO-7465, Norway morten.alver@sintef.no

This research has been funded by the Centre for Research-based Innovation in Aquaculture Technology (CREATE), SINTEF Sealab, Trondheim, NO-7645, Norway.

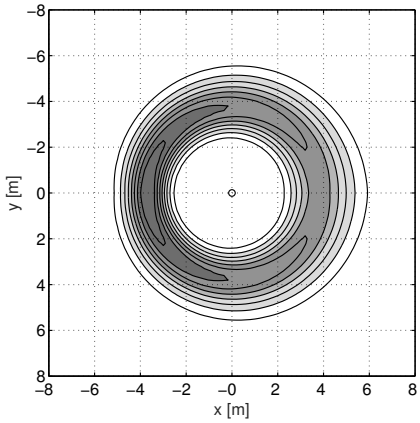

Fig. 2. Example of surface feed distribution from [6]. This result is based on 20 m/s airspeed, a spatial model resolution of 0.2 m with the outlet pipe tilted up.

negative economic impact for the farmer. Suboptimal feed intake is related to inefficient and reduced growth in Atlantic salmon [10]. Little is known about the effect of feed access on fish growth and welfare in large scale sea cages, but in smaller tanks, aggressive behavior related to feed access has been shown [11], [12], [13], [14], [15], [16]. Spatial feed distribution influences equal feed access [17], and the way feed is delivered may lead to monopolization causing uneven feed rations [18] and increased size variability among the fish [19].

These findings suggest that the spatiotemporal feed distribution influences important economic, environmental and welfare issues in large scale fish farming and motivate a further investigation and potential optimization of the feed delivery system. A full sea cage and fish model has been developed [20], [21] giving valuable insight into the complex farming process. Simulations from these studies were later based on the experimentally derived surface feed distributions from [3].

The current study describes the spreader as a robotic manipulator and this is combined with a ballistic model in order to predict surface feed distribution patterns based on different spreader attitudes. Simulations have been run with the joint angles of the robot being based on experiments from [22] which was obtained by using an Attitude Heading and Reference System (AHRS) attached to a rotary spreader. The results have been compared against the experimentally derived surface feed distribution produced by a similar spreader [3]. The model proposed in the current study enables simulations of different rotor spreaders and feed configurations. These results may later be used in the full cage model [20], [21], giving insight into the effects of spreader design on feed loss, fish growth and welfare in sea cages.

II. Spreader Model

A. Spreader Description

The reference frames are based on [23], [24], [25] and defined as follows. The translative and rotational motion of the spreader is characterized with respect to the *North-East-Down* (NED) coordinate system (base frame) $\{O_a\} = (x_a, y_a, z_a)$ (often denoted $\{n\}$) positioned at the center of the sea cage and considered inertial. x_a points towards true *North*, y_a points *East* and z_a *Down* from the x_a, y_a water plane. For simplicity, the pneumatic feed pipe is defined to always point towards true north from the spreader. The body-fixed reference frame $\{O_b\} = (x_b, y_b, z_b)$, and its origin (O_b) is fixed at the center of the counterweight leg at the water level (Figure 1). The orientation of the spreader body with respect to the base frame is given by the Euler angles $\boldsymbol{\Theta}_{ab} = \begin{bmatrix}\phi_b & \theta_b & \psi_b\end{bmatrix}^T \in \mathcal{S}^3$ which is the roll, pitch and yaw respectively using the YXZ rotation sequence. x_b is defined positive along the pneumatic pipe directed away from the spreader, y_b positive to starboard, and z_b downwards as defined in [23]. The center pipe-fixed reference frame $\{O_c\} = (x_c, y_c, z_c)$ is situated on top of the ball-bearing and rotates with the center pipe. The only degree of freedom between $\{O_b\}$ and $\{O_c\}$ is $\boldsymbol{\Theta}_{bc} = \begin{bmatrix}0 & 0 & \psi_c\end{bmatrix}^T$ When the outlet pipe points in the direction of the feed pipe, there is no rotation between $\{O_b\}$ and $\{O_c\}$, $\psi_c = 0$. In this model, it is assumed that only the buoy lies in the water surface, and the feed pipe is not part of the model. Thus, the centroid of the water plane area A_{wp} which the spreader rolls and pitches about [23] is the center of flotation (CF), and is here defined as CO = CF = O_b. The position vector $\boldsymbol{o}_b^a = \begin{bmatrix}x_b^a & y_b^a & z_b^a\end{bmatrix}^T \in \mathbb{R}^3$ gives the distance from O_a to O_b in the $\{O_a\}$ frame. Accordingly, the full position and orientation of the spreader body is given by the six degrees of freedom (6 DOF)

$$\boldsymbol{\eta} = \begin{bmatrix}\boldsymbol{o}_b^a & \boldsymbol{\Theta}_{ab}\end{bmatrix}^T \in \mathbb{R}^3 \times \mathcal{S}^3 \tag{1}$$

Since the spreader is moored to the floating collar of the sea cage, the spreader will be stationary with respect to the rest of the cage and the fish. The cage has some limited translational motion, often most prominent at the turn of the tides, but this will not affect the position of the spreader to the fish. Hence, the spreader is stationary in the horizontal plane $x_b^a = 0$ and $y_b^a = 0$. Waves will affect the vertical translation of the spreader, but it is assumed that this effect will average out over time. The effects of waves are omitted in this study, $z_b^a = 0$. The moorings also prohibit the spreader body from rotating around the z_b-axis. Due to the aforementioned properties, the position of $\{O_b\}$ is given by

$$\boldsymbol{o}_b^a = \begin{bmatrix}0 & 0 & 0\end{bmatrix}^T \tag{2}$$

And the rotations described by the following equations using the YXZ rotation sequence

$$\boldsymbol{\Theta}_{ab} = \begin{bmatrix}\phi_b & \theta_b & 0\end{bmatrix}^T \tag{3a}$$

$$\boldsymbol{\Theta}_{bc} = \begin{bmatrix}0 & 0 & \psi_c\end{bmatrix}^T \tag{3b}$$

This attitude description of the spreader will be useful when applying the experimentally derived attitudes from [22].

B. Forward Kinematics

To determine the position of the outlet opening (end effector) from a given attitude, robotics conventions and forward kinematics are used. In order to adhere to common robotics literature [24], [25], the base frame is given by $\{O_0\}$, and

$$\{O_a\} = (x_a, y_a, z_a) = \{O_0\} = (x_0, y_0, z_0) \tag{4}$$

The position of the outlet opening O_n with respect to the base frame in the base coordinate system is given by $\boldsymbol{o}_n^0 = \begin{bmatrix} x_n^0 & y_n^0 & z_n^0 \end{bmatrix}^T$. The spreader is modelled as a robotic manipulator using the Denavit-Hartenberg (DH) convention [25], [24], viewing the spreader as a series of n joints and $n+1$ links. First, an initial joint aligns z_1 according to the DH convention. The pitch and roll of the spreader is modelled as a spherical wrist with 2 DOF, the yaw rotation of the center pipe acts as a separate revolute joint. The bend of the outlet pipe is modeled as a static revolute joint (Figure 3). Finally, there is a translation from the top bend to the opening of the outlet pipe making $n = 5$ for the spreader. The pitch rotation is performed prior to roll to make it simpler to run simulations on the attitudes from [22] which are described by YXZ angles. The translation and rotation of the spout opening relative to $\{O_0\}$ is given by a homogeneous transformation matrix [24]

$$\boldsymbol{H} = \begin{bmatrix} \boldsymbol{R}_n^0 & \boldsymbol{o}_n^0 \\ \boldsymbol{0}_{1\times 3} & 1 \end{bmatrix} \tag{5}$$

where $\boldsymbol{R}_n^0$ is a 3×3 rotation matrix. $\boldsymbol{H}$ can be described by a series of joints

$$\boldsymbol{H} = \boldsymbol{T}_n^0(\boldsymbol{q}) = \prod_{i=1}^{n} \boldsymbol{A}_i^{i-1}(q_i) \tag{6}$$

$\boldsymbol{T}$ is a transformation matrix, and the general joint variables $\boldsymbol{q} = \begin{bmatrix} q_1 & \cdots & q_n \end{bmatrix}^T$ $q_i = \theta_i$ and $q_i = d_i$ for revolute and prismatic joints respectively [25]. The homogeneous transformation matrix [24] for each joint is given by

$$\boldsymbol{A}_i^{i-1}(q_i) = \begin{bmatrix} \boldsymbol{R}_i^{i-1}(q_i) & \boldsymbol{o}_i^{i-1}(q_i) \\ \boldsymbol{0}_{1\times 3} & 1 \end{bmatrix} \tag{7}$$

The complete attitude of the spreader as a function of the joint variables is given by

$$\boldsymbol{H} = \boldsymbol{A}_1^0(0)\boldsymbol{A}_2^1(\pi/2+\theta_b)\boldsymbol{A}_3^2(\pi/2+\phi_b)\boldsymbol{A}_4^3(\pi/2-\psi_c)\boldsymbol{A}_5^4(0) \tag{8}$$

From $\boldsymbol{H}$, $\boldsymbol{o}_n^0$ and $\boldsymbol{o}_{n-1}^0$ is obtained, which is the translation of the outlet pipe opening and top bend of the spreader respectively. $\boldsymbol{o}_n^0$ is the origin of the ballistic trajectory, and

$$\boldsymbol{\xi} = \begin{bmatrix} \xi_x & \xi_y & \xi_z \end{bmatrix}^T = \boldsymbol{o}_n^{n-1} = \boldsymbol{o}_n^0 - \boldsymbol{o}_{n-1}^0 \tag{9}$$

is the vector along the outlet pipe. This vector is normalized by $\hat{\boldsymbol{\xi}} = \boldsymbol{\xi}/||\boldsymbol{\xi}||$.

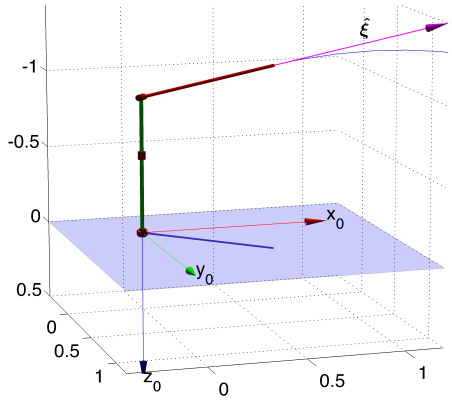

Fig. 3. Visualization of the robot model for $\phi_b = 0$, $\theta_b = 0$ and $\psi_c = \pi/4$. The unit vector $\hat{\boldsymbol{\xi}}$ points away from the outlet pipe and the beginning of a pellet trajectory is shown. The shadow cast by the spreader is visible on the water surface. Visualized by the Robotics Toolbox [26].

III. External Ballistic Model

The speed of pellets u at the outlet pipe of the spreader in relation to the airspeed is given by

$$u = ((0.55u_{air} - 2) + \mathcal{N}(0, \sigma_u^2))k_u \tag{10}$$

consisting of an experimentally derived part, Gaussian white noise and an attenuation parameter k_u. The first term is based on [27] for a 6 mm particle. The airspeed u_{air} was measured using an inbuilt measuring unit at the feed barge. $\sigma_u = 1.86$ is an estimate based on airspeed of 20 and 25 m/s from [27]. It must be noted that there are few data points in [27] as well as the data being slightly bimodal. The speed measurements in [27] are based on a least square fit from experiments with a specific feeding system, and is not concerned with speed reduction caused by bends in the spreader itself or the vertical transport of pellets from sea level to the outlet pipe. $k_u = 0.33$ is an estimated attenuation parameter which accounts for these obstacles in order to achieve better fit with the results from [3]. In order to obtain the individual velocity components at the outlet pipe in the $\{O_0\}$ frame, a velocity vector is introduced by $u = ||\boldsymbol{v}||$ and the components given by

$$\boldsymbol{v} = \begin{bmatrix} v_x & v_y & v_z \end{bmatrix}^T = \hat{\boldsymbol{\xi}} u \tag{11}$$

Hence, $\boldsymbol{v}$ is the velocity vector at the outlet pipe in $\mathbb{R}^3$ with respect to the base frame. The drag due to air resistance on general form is given in Equation 12 based on [28]

$$F_d = -\frac{1}{2} C_{d\infty} \rho_{air} A u^2 \tag{12}$$

The unbounded fluid drag coefficient $C_{d\infty}$ is obtained by approximating the cylindrical shape of the pellet to a sphere. A is the frontal area of the pellet and $C_{d\infty}$ is a function of the Reynolds number [28]

$$R_e = \frac{\rho_{air} u D}{\mu_{air}} \tag{13}$$

where the density $\rho_{air} = 1.2$ kg/m^3 and viscosity $\mu_{air} = 1.8 * 10^{-5}$ Ns/m^2 at $20°C$ according to [28]. In order to determine R_e, the maximum and minimum speed of the pellet must be known. The airspeed from the feed barge is minimum 15 m/s to avoid pipe clogging, and maximum 30 m/s due to performance restrictions and heat generation. Based on Equation 10 and given $\pm 2\sigma_u$, $0.9 < u < 6.2$ m/s. This yields $516 < R_e < 3717$. In this range, the drag coefficient of a sphere is fairly stable [29], hence a fixed value is used, $C_{d\infty} = 0.5$. Equation 12 can be rewritten using Newton's second law, and based on [30] and trivial geometric relations written as the decomposed external ballistic forces

$$F_x = -\kappa v_x ||\boldsymbol{v}|| \quad \Rightarrow \quad \frac{dv_x}{dt} = \frac{-\kappa}{m} v_x ||\boldsymbol{v}|| \tag{14a}$$

$$F_y = -\kappa v_y ||\boldsymbol{v}|| \quad \Rightarrow \quad \frac{dv_y}{dt} = \frac{-\kappa}{m} v_y ||\boldsymbol{v}|| \tag{14b}$$

$$F_z = -\kappa v_z ||\boldsymbol{v}|| + mg \quad \Rightarrow \quad \frac{dv_z}{dt} = \frac{-\kappa}{m} v_z ||\boldsymbol{v}|| + g \tag{14c}$$

Where $\kappa = \frac{1}{2} C_{d\infty} \rho_{air} A$. Futher, three differential equations are defined to describe the relation between pellet position and velocity

$$\frac{ds_x}{dt} = v_x \tag{15a}$$

$$\frac{ds_y}{dt} = v_y \tag{15b}$$

$$\frac{ds_z}{dt} = v_z \tag{15c}$$

These six equations are solved for each pellet using MATLAB [31] and the *ode45* solver. For each pellet the forward kinematics was calculated and the differential equations initialized with $\boldsymbol{v}(0) = \boldsymbol{v}$ and $\boldsymbol{s}(0) = \boldsymbol{o}_n^0$ The solver was terminated when the pellet reached the water surface, $s_z(t) >= 0$ and this t stored as total flight time T. As the pellets are significantly smaller than any of the pipes along the pneumatic path, some random motion is likely to occur during the transport process. At the outlet pipe, pellets exit at moderately different angles and the trajectory may be influenced by wind and collisions between pellets. To account for variability that occurs in the trajectory, noise is added at the end of each pellet impact point with $\sigma_s = 0.25$.

$$s_{x,imp} = s_x(T) + \mathcal{N}(0, T\sigma_s^2) \tag{16a}$$

$$s_{y,imp} = s_y(T) + \mathcal{N}(0, T\sigma_s^2) \tag{16b}$$

IV. Simulation

In [3] experiments were run with $m_{tot} = 10$ kg of feed per replicate. To obtain comparable results, simulations were based on a 9 mm pellet with specific weight $m_p = 0.64 \pm 0.0$ g/pellet [3]. As one pellet is released for each degree of ψ_c in the model, the total number of revolutions was determined by $m_{tot}/(m_p 360) \approx 43$ or 15480 pellets per simulation. The angular velocity of the spout in the pellet distribution experiment [3] was considerably higher for the same airspeeds compared to the AHRS experiments in [22]. This was probably due to the difference in pipe length (96 and 225 m respectively). In order to compare the most similar scenarios, the 20 m/s 71 RPM distribution [3] and 30 m/s 79 RPM AHRS data [22] was compared. In order to drive the motion of the spreader in the simulations the experimental results from [22] was used, which was obtained using 30 m/s airspeed. In the experiment [22], an AHRS was attached to the center pipe of the spreader, giving the attitude

$$\breve{\boldsymbol{\Theta}}_{ac} = \begin{bmatrix} \breve{\phi}_c & \breve{\theta}_c & \breve{\psi}_c \end{bmatrix}^T \tag{17}$$

Where $\breve{}$ denotes a measured variable. Since the only degree of freedom between $\{O_c\}$ and $\{O_b\}$ is ψ_c, and $\psi_b = 0$ the experimentally derived attitudes are used for simulation purposes by stating that $\phi_b = \breve{\phi}_c$, $\theta_b = \breve{\theta}_c$ and $\psi_c = \breve{\psi}_c$

The motion of the spreader at 30 m/s airspeed from [22] is presented in Figure 4.

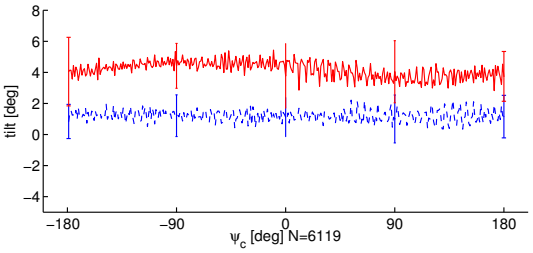

Fig. 4. The average roll $\phi_b(\psi_c)$ lower/blue and pitch $\theta_b(\psi_c)$ upper/red from [22]. YXZ convention, experimentally obtained by an AHRS mounted at the center pipe of the spreader. ± 1 SD bars depicted at 90° intervals. (CC BY-NC-SA).

From Figure 4 it is apparent that the spreader portrays a fairly constant offset in both ϕ_b and θ_b, independent of ψ_c. Based on these values, it is expected that ϕ_b will have little contribution to the pellet distribution pattern. θ_b however, shows that the spreader leans away/back from the feed pipe in $-x_0$ direction. This will probably result in pellets to a certain extent being "shot down" into the water when the outlet pipe points away from the feed pipe, and launched further upwards resulting in a more distributed pattern in the opposite direction.

V. Results

In Figure 5, 15480 pellets were run with the attitude of the spreader driven based on the original AHRS data from [22]. In Figure 6 and 7 the amplitude of ϕ_b and θ_b has been doubled and quadrupled respectively to examine the distribution pattern at more aggressive attitudes. The spreader is positioned at $x_1^0 = 0$, $y_1^0 = 0$, the grid is 8×8 m divided in 0.25×0.25 m bins and the spreader outlet pipe is tilted up 35° at the fifth joint. The color map range is fixed $\boldsymbol{c} = \{0, 1, \cdots, 55\}$ in order to make the figures comparable and clear.

VI. Discussion

As can be observed from the surface plots in Figure 5-7, there is a substantial difference in how the pellets cover

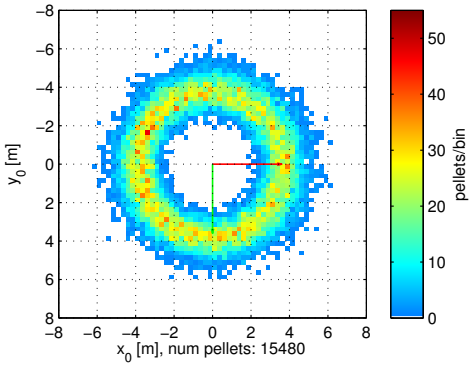

Fig. 5. Simulation result based on 30 m/s airspeed original AHRS data from [22] (CC BY-NC-SA)

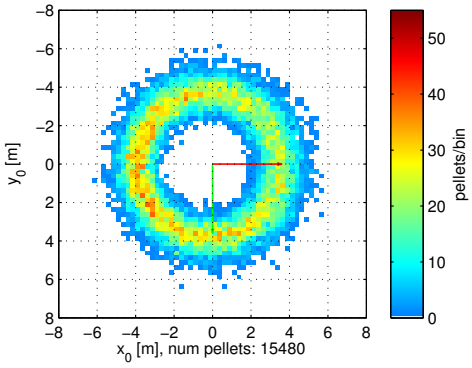

Fig. 6. Simulation result based on 30 m/s airspeed AHRS data from [22]. Roll and pitch amplitudes have been scaled by a factor 2. (CC BY-NC-SA)

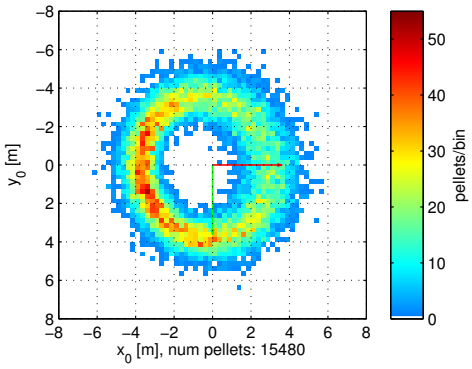

Fig. 7. Simulation result based on 30 m/s airspeed AHRS data from [22]. Roll and pitch amplitudes have been scaled by a factor 4. (CC BY-NC-SA)

the surface area of the sea cage. Comparing Figure 5 to the experimentally derived surface data from [3] reveals good correspondence. The radial distance from center corresponds well, although this is heavily dependent on the speed of the pellets at the outlet. As mentioned, k_u has been tuned based on the experiments in [3] so this correspondence is expected. The observations in [3] was based on a single line of Styrofoam boxes on the water surface placed along the direction across the spreader where the largest difference in distribution was observed. Imagining such a line in Figure 5 and comparing this to "Spreader A", with the "9 mm[1]" feed, tilt up and 20 m/s airspeed in [3] yields good correspondence. In the *dense direction* the pellets are more concentrated compared to the *dispersed direction*. This in turn corresponds well with the AHRS data from [22] which suggested that such a distribution was likely to occur. Further, in Figure 6, the roll and pitch amplitudes from Figure 4 have been doubled to investigate the effects on the spatial pellet distribution. In Figure 6, the concentration of pellets in the *dense direction* has increased further and the distribution is greater the in the opposite direction due to a more favorable outlet angle over the x_0, y_0 plane. This trend continues in Figure 7 where the amplitudes have been quadrupled. The effect of positive roll also becomes more apparent as can be seen from the *dense direction* which is now concentrated further along the positive y_0 direction. It is likely that a notably skewed distribution such as in Figure 7 will manifest itself as highly variable spatiotemporal feed concentrations within the sea cage. Simulations have also been run with $\sigma_s = 0$ in Equation 16 which yields visually very similar results to $\sigma_s = 0.25$.

Further work must be performed to determine the effects of pipe length, pellet size and the slip velocity [32] related to the vertical transport from sea level to the outlet pipe of the spreader on pellet speed. This will enable simulation of various transport configurations.

A. Limitations

As argued in [22], the empirical attitude data was obtained by fixing an Attitude Heading and Reference system (AHRS) to the center pipe of the spreader, close to the z_c axis of rotation. Some noise might be introduced due to the centripetal acceleration of the center pipe, as well as the AHRS being mounted at some distance above CF. The experimental data has been applied directly to the robot model which is a simplification due to the AHRS providing attitudes as from a single rigid rotating body, not joints at separate locations. The proposed model does not consider the Coriolis effect. The final pellet velocity at the spout is calculated as a function of variables $\boldsymbol{v} = f(\boldsymbol{q}, u)$. The linear velocity $\dot{\boldsymbol{p}}$ and angular velocity $\boldsymbol{\omega}$ of the spout will also contribute to $\boldsymbol{v}$ but this is not yet incorporated in the model. However, based on the data from [22], the variations in ϕ_b and θ_b are fairly small and slow, resulting in little contribution to $\boldsymbol{v}$. For simulations based on larger amplitudes such as in Figure 6 and 7, these effects will be of increased importance. However, ψ_c changes rapidly. Viewing the spout rotation in isolation, the 2D tangential velocity at the outlet pipe opening is given by $v_{outlet,\perp} = r\frac{d\psi_c}{dt}$. Due to the angled cut of the outlet pipe this tangential pellet velocity is

effectively arrested, and the pellet velocity is based on only $\boldsymbol{q}$ and u which is the radial component of the airspeed.

Further development and more extensive verification must be performed to ensure accurate model performance across various configurations of the spreader.

VII. Conclusion

In this study, a robotic and ballistic model has been developed in order to predict surface pellet distribution patterns from pneumatic rotary feed spreaders. The model has been parameterized based on a representative spreader design and relevant literature. Results suggest that the spreader has an annular distribution pattern which corresponds well with other empirical studies. The proposed model may be used to evaluate alternative spreader designs in order to optimize feed distribution to in turn maximize feed availability to the fish and reduce feed loss.

ACKNOWLEDGMENT

Appreciation is extended to Morten Malm and Ingolf Lygren at AKVA group for assistance and use of the rotary feed spreader.

References

[1] K. Aarseth, V. Perez, J. Bøe, and W. Jeksrud, "Reliable pneumatic conveying of fish feed," *Aquacultural Engineering*, vol. 35, no. 1, pp. 14 – 25, 2006.

[2] Norwegian Directorate of Fisheries, *Fôrforbruk 2014*, www.fiskeridir.no, 2014.

[3] M. Oehme, T. S. Aas, M. Sørensen, I. Lygren, and T. Åsgård, "Feed pellet distribution in a sea cage using pneumatic feeding system with rotor spreader," *Aquacultural Engineering*, vol. 51, no. 0, pp. 44–52, 11 2012.

[4] O.-I. Lekang, *Aquaculture Engineering*, John Wiley & Sons, 2013.

[5] F. Oppedal, T. Dempster, and L. H. Stien, "Environmental drivers of atlantic salmon behaviour in sea-cages: A review," *Aquaculture*, vol. 311, no. 1–4, pp. 1 – 18, 2011.

[6] M. O. Alver, M. Føre, K. R. Skøien, T. S. Aas, M. Oehme, and J. A. Alfredsen, "Modelling of surface and 3D pellet distribution in atlantic salmon (salmo salar l.) cages - submitted," 2015.

[7] C. J. Cromey, T. D. Nickell, and K. D. Black, "Depomod-modelling the deposition and biological effects of waste solids from marine cage farms," *Aquaculture*, vol. 214, no. 1-4, pp. 211 – 239, 2002.

[8] J. Gjøsæter, H. Otterå, E. Slinde, K. Nedreaas, and A. Ervik, "Effekter av spillfôr på marine organismer," *Kyst og Havbruk*, pp. 52–55, 2008.

[9] Norwegian Directorate of Fisheries, *Lønnsomhetsundersøkelse for matfiskproduksjon*, 2013.

[10] O. Einen, T. Mørkøre, A. M. B. Rørå, and M. S. Thomassen, "Feed ration prior to slaughter—a potential tool for managing product quality of atlantic salmon (salmo salar)," *Aquaculture*, vol. 178, no. 1–2, pp. 149 – 169, 1999.

[11] E. Brännäs, U. Berglund, and L.-O. Eriksson, "Time learning and anticipatory activity in groups of arctic charr," *Ethology*, vol. 111, no. 7, pp. 681–692, 2005.

[12] J. López-Olmeda, C. Noble, and F. Sánchez-Vázquez, "Does feeding time affect fish welfare?," *Fish Physiology and Biochemistry*, vol. 38, no. 1, pp. 143–152, 2012.

[13] C. Noble, S. Kadri, D. F. Mitchell, and F. A. Huntingford, "Influence of feeding regime on intraspecific competition, fin damage and growth in 1+ atlantic salmon parr (salmo salar l.) held in freshwater production cages," *Aquaculture Research*, vol. 38, no. 11, pp. 1137 – 1143, 2007.

[14] C. Noble, K. Mizusawa, K. Suzuki, and M. Tabata, "The effect of differing self-feeding regimes on the growth, behaviour and fin damage of rainbow trout held in groups," *Aquaculture*, vol. 264, no. 1–4, pp. 214 – 222, 2007.

[15] D. E. Ruzzante, "Domestication effects on aggressive and schooling behavior in fish," *Aquaculture*, vol. 120, pp. 1 – 24, 1994.

[16] P. E. K. Symons, "Behavioural adjustment of population density to available food by juvenile atlantic salmon," *Journal of Animal Ecology*, vol. 40, no. 3, pp. pp. 569–587, 1971.

[17] J. Attia, S. Millot, C. Di-Poï, M.-L. Bégout, C. Noble, F. Sanchez-Vazquez, G. Terova, M. Saroglia, and B. Damsgård, "Demand feeding and welfare in farmed fish," *Fish Physiology and Biochemistry*, vol. 38, pp. 107–118, 2012.

[18] C. H. Ryer and B. L. Olla, "Growth depensation and aggression in laboratory reared coho salmon: the effect of food distribution and ration size," *Journal of Fish Biology*, vol. 48, no. 4, pp. 686–694, 1996.

[19] S. Johansen and M. Jobling, "The influence of feeding regime on growth and slaughter traits of cage-reared atlantic salmon," *Aquaculture International*, vol. 6, no. 1, pp. 1–17, 1998.

[20] M. O. Alver, J. A. Alfredsen, and T. Sigholt, "Dynamic modelling of pellet distribution in atlantic salmon (salmo salar l.) cages," *Aquacultural Engineering*, vol. 31, no. 1-2, pp. 51 – 72, 2004.

[21] M. Føre, T. Dempster, J. A. Alfredsen, V. Johansen, and D. Johansson, "Modelling of atlantic salmon (salmo salar l.) behaviour in sea-cages: A lagrangian approach," *Aquaculture*, vol. 288, no. 3–4, pp. 196 – 204, 2009.

[22] K. R. Skøien and J. A. Alfredsen, "Feeding of large-scale fish farms: Motion characterization of a pneumatic rotor feed spreader," in *Oceans - St. John's, 2014*, Sept 2014, pp. 1–7.

[23] T. I. Fossen, *Handbook of marine craft hydrodynamics and motion control*, John Wiley & Sons, 2011.

[24] M. W. Spong, S. Hutchinson, and M. Vidyasagar, *Robot modeling and control*, John Wiley & Sons, Hoboken, NJ, 1 edition, 2006.

[25] L. Sciavicco and B. Siciliano, *Modelling and control of robot manipulators*, Springer, 2000.

[26] P. I. Corke, *Robotics, Vision & Control: Fundamental Algorithms in Matlab*, Springer, 2011.

[27] K. Aarseth, "Attrition of feed pellets during pneumatic conveying: the influence of velocity and bend radius," *Biosystems Engineering*, vol. 89, no. 2, pp. 197 – 213, 2004.

[28] F. M. White, *Fluid Mechanics (6th International Edition)*, McGraw-Hill, 2008.

[29] H. Schlichting, K. Gersten, and K. Gersten, *Boundary-layer theory*, Springer, 2000.

[30] S. Ray and J. Fröhlich, "An analytic solution to the equations of the motion of a point mass with quadratic resistance and generalizations," *Archive of Applied Mechanics*, pp. 1–20, 2014.

[31] MATLAB, *version 8.0.0.783 (R2012b)*, The MathWorks Inc., Natick, Massachusetts, 2012.

[32] G. Klinzing, F. Rizk, R. Marcus, and L. Leung, *Pneumatic Conveying of Solids: A Theoretical and Practical Approach*, Dordrecht: Springer Science+ Business Media BV, 2010.

Paper D Modelling of surface and 3D pellet distribution in Atlantic salmon (*Salmo salar* L.) cages

(Alver et al., 2016)
Alver, M. O., Skøien, K. R., Føre, M., Aas, T. S., Oehme, M., and Alfredsen, J. A. Modelling of surface and 3D pellet distribution in Atlantic salmon (*Salmo salar* L.) cages. *Aquacultural Engineering*, 72-73:20–29, 2016. ISSN 0144-8609. doi: http://dx.doi.org/10.1016/j.aquaeng.2016.03.003

Aquacultural Engineering 72–73 (2016) 20–29

Contents lists available at ScienceDirect

Aquacultural Engineering

journal homepage: www.elsevier.com/locate/aqua-online

Modelling of surface and 3D pellet distribution in Atlantic salmon (*Salmo salar* L.) cages

Morten O. Alver[a,b,*], Kristoffer Rist Skøien[b], Martin Føre[a,b], Turid Synnøve Aas[c], Maike Oehme[d], Jo Arve Alfredsen[b]

[a] SINTEF Fisheries and Aquaculture, NO-7465 Trondheim, Norway
[b] NTNU Department of Engineering Cybernetics, NO-7491 Trondheim, Norway
[c] Nofima, NO-6600 Sunndalsøra, Norway
[d] AllerAqua AS, Allervej 130, 6070 Christiansfeld, Denmark

ARTICLE INFO

Article history:
Received 12 February 2015
Received in revised form 8 February 2016
Accepted 5 March 2016
Available online 9 March 2016

Keywords:
Mathematical modelling
Atlantic salmon
Aquaculture
Feed distribution
Sea cage
Model validation

ABSTRACT

Feed represents the greatest single cost factor in the production of Atlantic salmon (*Salmo salar* L.). Focusing on the problem of maximising the available feed for the fish while minimising the feed waste, a mathematical model of the feeding process has been developed. The model covers the feed spreader delivering the feed, water currents, pellet sinking speed and turbulent diffusion, fish appetite as a function of temperature, gut fullness and population structure, and is intended as a tool both for optimising general feeding strategies, and to support the daily handling of the feeding process. The process of horizontal and vertical diffusion of feed pellets in the model has been parametrised and validated through two low level validation experiments. Furthermore, global distribution patterns simulated by the model were verified by comparisons with experimental data from the literature.

1. Introduction

Feed represents the most important cost factor in the production of Atlantic salmon, representing about 50% of the total production cost from hatched eggs to marketable fish meat (Directorate of Fisheries, Norway, 2011), and is also the primary driver of fish growth. One of the key challenges in the salmon industry is therefore to maximise the feed intake of the fish, while at the same time minimising the amount of wasted feed. Farmers may approach this problem in several different ways, but the most common method today is to visually monitor the fish and the feed using underwater cameras. Feeding can then be reduced or stopped when either behavioural cues indicate a reduction in appetite, or uneaten pellets are seen to sink towards the bottom of the cage. The efficiency of this method depends strongly on how well the system operator is able to interpret such signs and act accordingly. Consequently, the skills of individual operators may have a significant direct impact on fish growth and feed utilisation at fish farms.

The success of a feeding operation depends on a number of physical and biological factors. The feed delivery system plays an important role, as it determines how well the feed is dispersed over the cage surface, and how far from the cage edges the feed is delivered. Different feeder types produce different surface dispersal patterns, and Oehme et al. (2012) documented how the patterns produced by a single feeder type depend on the physical configurations of the feeder. In addition, environmental effects such as wind and waves, may affect the actual surface pellet dispersal after it leaves the nozzle of the feeder. Below the surface, sinking rate and transport of feed due to water current are the primary factors, along with the feeding behaviour of the fish.

In situations with high water temperatures and low current speeds, dissolved oxygen may become a limiting factor for the fish (Oppedal et al., 2011), with low levels causing reduced appetite (Remen et al., 2012). When aware of possible hypoxic conditions, feed distribution can be adjusted accordingly. Furthermore, the cages themselves restrict water flow and cause reduced current speeds within and downstream of each cage (Fredheim, 2005), and biofouling may reduce the permeability of the cage netting, leading to stronger effects on the current speeds (Gansel et al., 2010). Such perturbations of current patterns in and around cages may directly impact the spatial underwater distribution of pellets, and influence water exchange to and from a cage. This may again have

* Corresponding author at: SINTEF Fisheries and Aquaculture, PO Box 4762 Sluppen, NO-7465 Trondheim, Norway.
E-mail address: morten.alver@sintef.no (M.O. Alver).

http://dx.doi.org/10.1016/j.aquaeng.2016.03.003
0144-8609/

consequences for the oxygen supply within a cage, especially when several cages are placed together (Loland, 1993; Johansson et al., 2007; Gansel et al., 2011).

In the face of such a wide range of influencing factors, we believe that the best way to approach this problem is via a mathematical model. An earlier effort has been made to address this by modelling the transport of pellets in a two dimensional grid (Alver et al., 2004). The 2D model performs well, but is not well suited for representing the circular cages that have now become the industry standard in large scale production of salmon. Detailed representations of feed dispersal patterns over the cage surface are also difficult to represent in 2D.

In this work, the model developed by Alver et al. (2004) was generalised to three dimensions, and a new feed input module designed to realistically represent the feed distribution over the cage surface. Some of the basic properties of the model have been validated through experimental work (see Skøien et al., submitted for publication), and the ability of the model in predicting dispersal patterns on a cage scale were verified using experimental data from literature.

2. Materials and methods

The model equations are presented in the following sections. All model parameters, state variables and inputs are listed in Table 2.

2.1. Pellet transport in 3D

The continuous model formulation given in Eqs. (1)–(4) in Alver et al. (2004) is generalised to 3D by adding the relevant terms for the third dimension. After expanding the diffusion term, assuming omnidirectional diffusion, the full equation in 3D can be written as follows:

$$\frac{\partial c}{\partial t} + v_x \frac{\partial c}{\partial x} + v_y \frac{\partial c}{\partial y} + (v_z + u_v)\frac{\partial c}{\partial z} + \kappa\left(\frac{\partial^2}{\partial^2 x}c + \frac{\partial^2}{\partial^2 y}c + \frac{\partial^2}{\partial^2 z}c\right) = u - f_I \tag{1}$$

where $c(x, y, z, t)$ is the local feed concentration, x, y and z are the spatial coordinates along the two horizontal axes and the vertical axis, respectively, $v_x(x, y, z, t)$, $v_y(x, y, z, t)$ and $v_z(x, y, z, t)$ are the three components of the local water current, u_v is the sinking speed of the feed pellets, κ is the diffusivity, $u(x, y, z, t)$ is the feed addition and $f_I(x, y, z, t)$ is the local ingestion rate of the fish.

The model is then discretized along the three spatial dimensions using the same method as in Alver et al. (2004). The variable $c_{i,j,k}$, where $i \in \{1, \ldots, i_{max}\}$, $j \in \{1, \ldots, j_{max}\}$ and $k \in \{1, \ldots, k_{max}\}$ represent the indexes along the two horizontal dimensions and the vertical dimension, respectively, represents the amount of feed in cell (i, j, k).

The equation for c is as follows:

$$\dot{c}_{i,j,k} = f_{A(i,j,k)} + f_{D(i,j,k)} + u_{i,j,k} - f_{I(i,j,k)} \tag{2}$$

where f_A denotes the change due to advection, f_D the change due to diffusion, u the feed supply rate into cell (i, j, k) and f_I the rate of feed ingestion in the cell. The advection term is derived in the same way as for the two dimensional model, except that we must now allow for both positive and negative currents along all dimensions:

$$f_{A(i,j,k)} = |v_{x(i,j,k)}|\frac{c_{i^*,j,k}}{\Delta x} + |v_{y(i,j,k)}|\frac{c_{i,j^*,k}}{\Delta y} + |(v_{z(i,j,k)} + u_v)|\frac{c_{i,j,k^*}}{\Delta z} - \left(|v_{x(i,j,k)}|\frac{1}{\Delta x} + |v_{y(i,j,k)}|\frac{1}{\Delta y} + |(v_{z(i,j,k)} + u_v)|\frac{1}{\Delta z}\right) c_{i,j,k} \tag{3}$$

where the indexes marked by * represent a step in the opposite of the transport direction along each dimension:

$$i^* = i - \operatorname{sgn} v_{x(i,j,k)}$$

$$j^* = j - \operatorname{sgn} v_{y(i,j,k)}$$

$$k^* = k - \operatorname{sgn}(v_{z(i,j,k)} + u_v)$$

For cells along the surface, bottom and horizontal edges of the grid, some of the terms above will be outside the grid. The feed content in such outside cells is set to the ambient value, which for feed pellets equals 0.

To adapt the diffusion we simply need to add a term for the third dimension:

$$f_{D(i,j,k)} = \kappa\left(\frac{c_{i+1,j,k} - 2c_{i,j,k} + c_{i-1,j,k}}{\Delta x^2} + \frac{c_{i,j+1,k} - 2c_{i,j,k} + c_{i,j-1,k}}{\Delta y^2} + \frac{c_{i,j,k+1} - 2c_{i,j,k} + c_{i,j,k-1}}{\Delta z^2}\right) \tag{4}$$

Again, some of these terms will be outside of the grid for cells along the edges. All such cells are assumed to hold the ambient value (0 for feed pellets), except for cells above the surface ($k = 0$), which are assumed to have the same value as the cell at $k = 1$. The latter rule sets a diffusion rate of zero through the surface.

2.2. Cage shape

The discretised model is most easily implemented in a computer as a cubic array of cells. To represent the actual shape of the cage, a second cubic array of binary values is defined, where 1 denotes a cell inside the cage, and 0 denotes a cell outside. The transport equation is integrated on the entire cubic array, but only cells inside the cage are taken into account when calculating ingestion rates and feed waste.

To represent a standard salmon cage we use a circular cylinder with radius R and height D_c above a conical section with its base matching the cylinder and its tip pointing downwards and reaching a total depth of D_{tot}. The height of the conical section is thus $D_{tot} - D_c$. Cells that have their centre within this cylindro-conical shape are considered part of the cage.

2.3. Modelling the feed input

The surface distribution of the feed pellets delivered to the cage can have a significant effect on feed wastage. A higher dispersion of feed over the surface leads to lower local concentrations of feed, and in the model this will to some degree be reflected in a more even distribution of the feed between the size classes of fish. Depending on the current speed and direction, the surface distribution of feed can also affect the likelihood of feed pellets to drift out before they can be eaten.

The actual spread pattern of pellets given by a pneumatic feeding system with a rotor spreader was investigated by Oehme et al. (2012). A number of boxes were arranged diagonally across a square cage with the spreader placed in the cage centre, and the relative number of pellets landing in each box was calculated for a number of different spreader settings and various pellet sizes. In this set-up, each box covers a certain sector of the annular area representing an interval of distances from the spreader. The boxes closest to the feeder thus cover a larger angular sector compared to the boxes that are placed further away. After correcting for these differences, a probability distribution can be drawn for the distance travelled by each individual pellet. Oehme et al. (2012) found that the distribution of distance travelled by single pellets resembled a skewed normal distribution rather than being uniform for the entire range

of distances. The mean and standard deviation of this distribution was found to vary with the angle relative to the forward direction of the spreader, as well as with the air speed and tilt of the spreader nozzle (with the nozzle pointing horizontally or downwards). Pellet size was found not to have a significant effect on the distribution.

To model this spread pattern we introduce a parameterised probability distribution which is a function of airspeed (v_{air}), distance to the spreader (d), and angle relative to the forward direction of the spreader (ψ):

$$P(v_{air}, d, \psi) = \frac{1}{X_2\sqrt{2\pi}} \exp\left(-\frac{(d' - X_1)^2}{2X_2^2}\right) \tag{5}$$

which is a normal distribution with mean value (X_1) and standard deviation (X_2) determined by air speed and direction according to the following equations:

$$X_1 = (p_1 + p_2 v_{air})p_{1,tilt}\left(1 - \frac{\psi}{180}\right) + (p_3 + v_{air}p_4)p_{2,tilt}\frac{\psi}{180} \tag{6}$$

$$X_2 = (p_1 + p_2 v_{air})p_5 p_{1,tilt}\left(1 - \frac{\psi}{180}\right) + (p_3 + v_{air}p_4)p_6 p_{2,tilt}\frac{\psi}{180} \tag{7}$$

where

$$p_{1,tilt} = \begin{cases} 1: & \text{for tilt up} \\ p_7: & \text{for tilt down} \end{cases} \tag{8}$$

$$p_{2,tilt} = \begin{cases} 1: & \text{for tilt up} \\ p_8: & \text{for tilt down} \end{cases} \tag{9}$$

Parameters p_1–p_8 describe the distribution patterns in the forward ($\psi = 0$) and backward ($\psi = 180$) directions of the spreader, while $\psi \in [0, 180]$ is used to determine a weighted average between the forward and backward patterns, thereby interpolating these for any angle in between.

To produce a skewed distribution the variable d' is set equal to the distance d (from the spreader) to the power of a parameter p_9:

$$d' = d^{p_9} \tag{10}$$

This leads to a probability distribution parameterized by p_1–p_9 which describes distribution for a single type of spreader at all angles and distances for both tilt states. We then use a standard optimization function (*fminsearch* in MATLAB) to find the values of those parameters that gives distributions that are closest to the observations in a least squares sense (Table 1).

The optimised spread patterns match the measured patterns closely (Fig. 1). Spread patterns calculated over a 2D surface are ring shaped, with a more skewed pattern when the spreader is tilted up compared to when it is tilted down (Fig. 2).

2.4. Feed ingestion

Feed ingestion by fish is calculated in the same way as in Alver et al. (2004), which largely followed the model outlined by Olsen and Balchen (1992). A fish population consisting of N individual fish is modelled as a set of super-individuals, with each super-individual representing a number of fish (N_m for super-individual m) with identical individual body weights (W_m). This produces a heterogeneous population with a certain weight distribution, which resembles the situation in production sea-cages, and allows for the modelling of interactions and differences between the different size classes. Since we are looking at a time scale of minutes and hours, we assume that the body weight is constant. The only variable associated with the fish groups is thus the stomach content, denoted V_m for group m, which is modelled by Eq. (11):

$$\dot{V}_m = w_{fm} - a_1 T^{a_2} V_m \tag{11}$$

where w_{fm} is the ingestion rate, and the second term represents the stomach evacuation rate. T is water temperature, and a_1 and a_2 are constants. The feed intake rate of fish in group m is calculated as a product of a number of factors:

$$w_{fm} = P_w w_0 p_c p_{am} p_{hm} \tag{12}$$

where P_w is the weight of each pellet, and the remaining factors will be defined below.

w_0 represents the maximum ingestion rate as limited by the handling and search time per pellet:

$$w_0 = \left(T_h + \frac{k_{T_s} N P_w}{c_T}\right)^{-1} \tag{13}$$

where T_h is the handling time per pellet for the fish, k_{T_s} is a constant, and the symbol c_T denotes the total amount of feed in the cage.

The appetite factor, p_{am}, depends on the relative stomach fullness of the fish:

$$p_{am} = \begin{cases} 0.50 - \dfrac{0.57(V_{rm} - 0.3)}{V_{rm} - 0.2} & \text{if } V_{rm} > 0.3 \\ 0.50 + \dfrac{0.67(0.3 - V_{rm})}{0.4 - V_{rm}} & \text{if } V_{rm} \le 0.3 \end{cases} \tag{14}$$

where the relative stomach fullness V_{rm} is calculated based on a model of maximum stomach volume of coho salmon (*Oncorhynchus kisutch*) developed by Burley and Vigg (1989):

$$V_{rm} = \frac{V_m}{0.0007 W_m^{1.3796}} \tag{15}$$

To the authors' knowledge, no data on stomach size of Atlantic salmon has been published. Such data would be useful to improve the accuracy of this part of the model.

p_c is called the *confusion factor*, and represents confusion caused by the increased local density of fish in the areas where feed is highly concentrated. Under the assumption that the fish choose to distribute themselves similarly to the feed, we formulated an expression for p_c that depends on how well the feed is dispersed within the cage (ρ):

$$p_c = \rho^{b_1} \tag{16}$$

The parameter b_1 is a constant, and $\rho \in [0, 1]$, with a value of 0 meaning that all feed is concentrated within a single cell and a value of 1 meaning that all cells have the same amount of feed. Alver et al. (2004) calculated ρ based on the sum of the squared relative feed contents of all cells. However, this calculation does not scale well when the cage size is increased. A better approach is to consider the potential concentrations of fish is the cage. Under the assumption that the fish distribute themselves in the same pattern as the feed distribution, the feed distribution will dictate the fish densities throughout the water volume. If these densities exceed a certain threshold for a large proportion of the population, we consider the feed to be poorly distributed, and the model should use a low ρ value.

To formulate this mathematically, we first determine the relative feed content of all cells within the cage, $c_{i,j,k}/c_T$ for cell (i, j, k), where c_T is the total amount of feed in the cage. If the fish distribute similarly to the feed, the biomass of fish in cell (i, j, k) is $W_{i,j,k} = W_{total} \cdot c_{i,j,k}/c_T$. The density of fish ($FD_{i,j,k}$) can then be calculated (in kg m^{-3}) for each cell by the expression $W_{i,j,k}/(\Delta x \Delta y \Delta z)$.

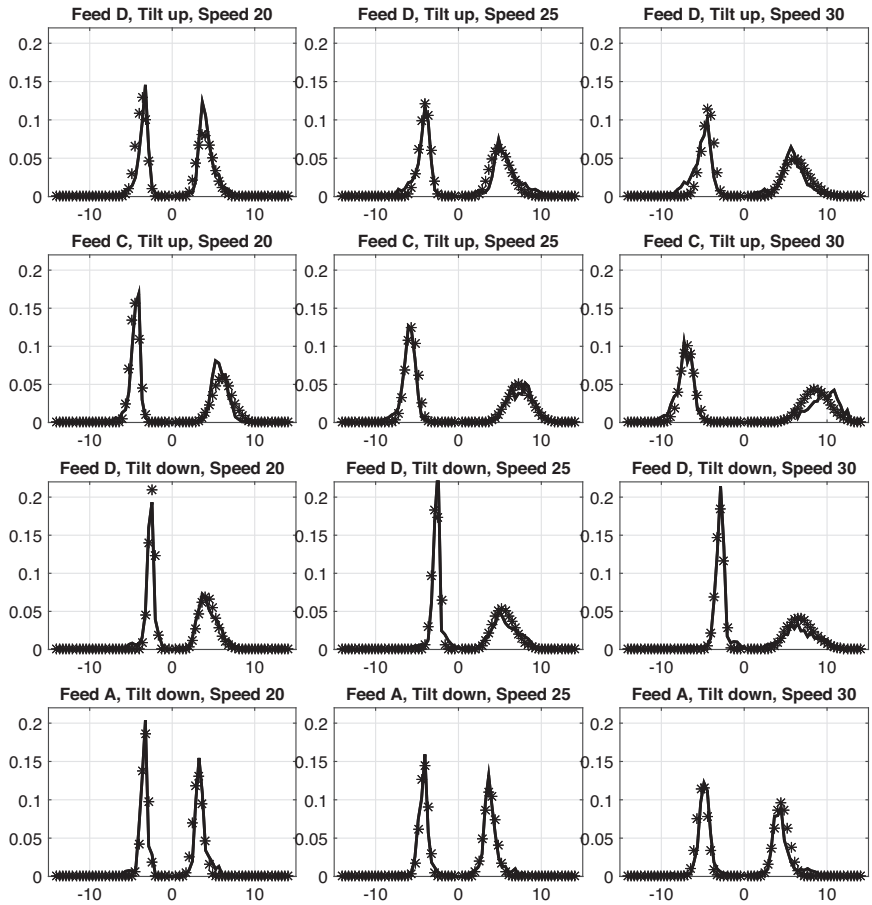

Fig. 1. Comparison between measured (solid lines) and modelled (*) pellet distributions from spreader. The *x* axes denote meters forward and backward from the spreader. The three columns show comparisons for air speed 20, 25 and 30 m s^{-1}, respectively. The two upper rows show results for tilt up, and the two lower columns for tilt down. The measurements represent tests with three different feeds (A, C and D), but no significant effect of feed type was found by Oehme et al. (2012).

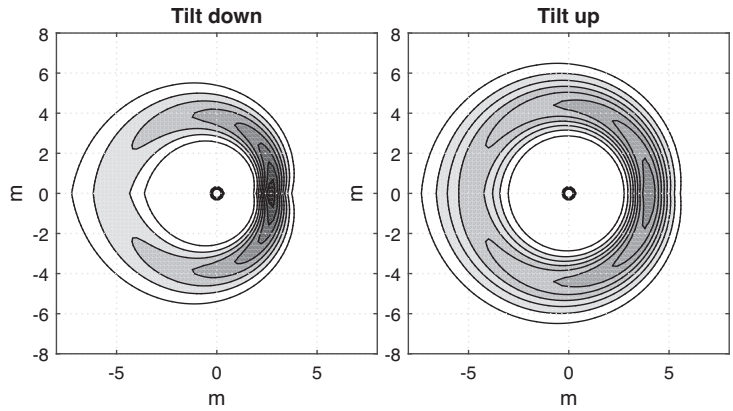

Fig. 2. Examples of modelled surface spread patterns from spreader type 1 with tilt up and down. The shades indicate different relative densities of pellets, and the total amount of feed is the same in both cases. The feeder is located at the point marked with an o, and faces to the right in the figure. Air speed was set to 25 m s^{-1}, and the model resolution is 0.1 m.

Table 1
Optimised parameter values for spreader model.

	p_1	p_2	p_3	p_4	p_5	p_6	p_7	p_8	p_9
Spreader 1	1.4145	0.0101	0.0602	1.0645	0.0297	0.0873	0.8645	1.0270	0.3608
Spreader 2	0.7373	0.1302	0.0971	1.5705	0.1351	0.1489	0.7823	0.5950	0.7912

Table 2
Summary of state variables, parameters, controlled variables and disturbances (uncontrollable inputs).

Symbol	Value	Unit	Type	Description
a_1	5.2591×10^{-6}		Parameter	Parameter for gut evacuation rate
a_2	0.7639		Parameter	Parameter for gut evacuation rate
b_1	0.4		Parameter	Parameter for confusion factor
b_2	0.5		Parameter	Parameter for hierarchy factor
$c_{i,j,k}$		g	State variable	Amount of feed in cell (i, j, k)
Δx	1	m	Parameter	Cell size in x direction
Δy	1	m	Parameter	Cell size in y direction
Δz	1	m	Parameter	Cell size in z direction (vertical)
D_c		m	Parameter	Depth of cylindrical part of cage
D_{tot}		m	Parameter	Total depth of cage
i_{max}			Parameter	Number of cells in x direction
j_{max}			Parameter	Number of cells in y direction
k_{max}			Parameter	Number of cells in z direction
κ	0.01	$m^2\,s^{-1}$	Parameter	Diffusivity constant
κ_{ref}	1.2×10^{-4}		Parameter	κ value for reference pellet diameter
k_{T_c}	1		Parameter	Parameter for maximum feed intake rate
m_{max}	7		Parameter	Number of fish size groups
N			State variable	Total number of fish
N_m			State variable	Number of fish in group m
P_s	3–12	mm	Parameter	Feed pellet diameter
$P_{s,ref}$	6	mm	Parameter	Reference feed pellet diameter
P_w	0.22	g	Parameter	Weight per feed pellet
R		m	Parameter	Radius of cage
T		°C	Disturbance	Water temperature
T_h	12	s	Parameter	Handling time per pellet
Θ	0.2		Parameter	Calibration factor for κ
U	1	BLs^{-1}	Parameter	Swimming speed of fish
u_v	0.1	$m\,s^{-1}$	Parameter	Sinking speed of pellets
V_m		g	State variable	Stomach content of fish in group m
W_m		g	State variable	Average weight of fish in group m

We then define the function $f(FD)$, giving a local ρ value based on the density in a cell:

$$f(FD) = \begin{cases} 1: & \text{for } FD < FD_{tresh} \\ 1 - \dfrac{FD - FD_{tresh}}{D_{tresh}}: & \text{for } FD_{tresh} < FD < 2 \cdot FD_{tresh} \\ 0: & \text{for } FD > 2 \cdot FD_{tresh} \end{cases} \quad (17)$$

where FD_{tresh} determines the maximum fish density that does not lead to a reduction in ρ.

The ρ factor is an average of local values, weighted by the density:

$$\rho = \sum_{i,j,k} \frac{W_{i,j,k} f(FD_{i,j,k})}{W_{total}} \quad (18)$$

This gives a ρ value that relates to the actual density of the fish, and which retains its meaning for different cage scales and population sizes.

p_{hm} is called the hierarchy factor, and represents the ability of larger fish to gain preferential access to food compared to smaller fish:

$$p_{hm} = \left(\frac{W_m}{W_{\max}}\right)^{f_a f_d} \quad (19)$$

where W_{max} is the body weight of the largest fish, and:

$$f_a = \frac{1}{W_{total}} \sum_{m=1}^{m_{\max}} N_m p_{am} W_m \quad (20)$$

$$f_d = \rho^{-b_2} \quad (21)$$

where W_{total} is the total biomass of fish in the cage, and b_2 is a constant. The factor f_a is a weighted average of the appetite of the fish, where the appetite of the largest fish is given the most weight. For the group of largest fish, $p_{hm} = 1$, and for the remaining groups it is less than 1. As the fish get more satiated, and their appetite is reduced, p_{hm} will approach 1 for all groups, causing a weakening of the hierarchical effect. The factor f_d serves to weaken the effect the more evenly the feed is distributed, since a concentration of feed makes it more easily monopolised by dominant individuals (Alarärä et al., 2001).

The total feed intake for the entire population can be calculated as:

$$w_{fT} = \sum_{m=1}^{m_{\max}} N_m w_{fm} \quad (22)$$

As in Alver et al. (2004), the relative distribution of feed intake is assumed to be equal to the relative feed distribution. Therefore, the ingestion rate in cell (i, j, k) can be calculated as follows:

$$f_{I(i,j,k)} = \frac{c_{i,j,k}}{c_T} w_{fT} \quad (23)$$

2.5. Model validation

Skøien et al. (submitted for publication) conducted a series of experiments where the horizontal (x–y plane) and vertical (z) spread of pellets in still water without fish was investigated. The data obtained from these experiments was used to validate these aspects in our model.

2.5.1. Experiment setup

The experimental feeds used by Skøien et al. (submitted for publication) were produced at Nofima Feed Technology Centre, Bergen. To cover the sizes and densities commonly used in Atlantic salmon farming, cylindrically shaped pellets were produced with 3, 6, 9 and 12 mm diameter with low, medium and high density for a total of 12 different pellet types. The production process is described in detail in (Skøien et al., submitted for publication).

The horizontal diffusion experiment was conducted at Nofima, Sunndalsøra, in a 7 m diameter 2.3 m deep tank of still seawater. Batches of 40 pellets were uniformly dropped using a quick release mechanism and guided trough a 80 mm diameter vertical pipe to the surface of the water. After impact, the pellets diffused naturally in the water and settled on a 1 m × 1 m target grid on the bottom of the tank. The resulting positions were photographed using a digital camera (FL3-GE-13S2C-CS, Point Grey Research, Inc., Richmond, Canada) equipped with an adjustable lens (focus, 3–8 mm, f/1.0-close) (M13VM308, Tamron Co., Ltd, Saitama-city, Japan). Position relative to the drop point was found for all pellets through image processing techniques. This procedure was conducted in random order for all 12 feeds with five replicates for each feed.

The vertical distribution experiment was conducted in a separate cylindrical tank, 0.79 m diameter and 2.76 m deep using the same feed types, release mechanism, guide pipe and water density as in the diffusion experiment. Images of passing pellets were captured using the same camera system, encapsulated in a watertight housing and aimed horizontally at a depth of 2.3 m. This pellet detector is further detailed in Skøien et al. (2014). Ten replicate drops were conducted for each pellet type, with 3, 20, 70 and 230 ml pellets in each batch for pellet sizes of 3, 6, 9 and 12 mm pellets respectively. This schedule was designed to ensure that each drop contained a sufficient amount of pellets for statistical analyses, while at the same time keeping the number of pellets in each captured image frame low enough to avoid adverse effects such as overlapping and clumping of pellets. A total of 3189 pellets were used in the analysis.

2.5.2. Model setup

The model was configured to simulate comparable scenarios for both experimental setups. For horizontal diffusion, a model resolution of 20 mm was used. The model was run for 120 s with constant feeding rate in a single point at the centre of the surface. At the end of the simulation, the distribution of feed in the layer at 2.28–2.3 m below the surface was recorded.

Each cell by the tank bottom was placed at a certain distance from the centre of the pellet drop, and had a certain amount of feed. The distances were organised in bin intervals of 25 mm, and the total amount of feed in each bin interval was plotted as a function of distance.

The vertical distribution experiment Skøien et al. (submitted for publication) showed how the pellets distribute in apparent sinking speed estimated by the time from the drop until they passed a certain level monitored by the pellet detector. The concept of varying sinking speeds is not directly transferable to the model, but an analogous test can be run by adding a single pulse of feed to the model, and observing the vertical spread of pellets around the level of the pellet sensor. The vertical spread of real pellets dropped at the same time can be interpreted as a variation in sinking speeds, and we can interpret the spread predicted by the model in the same way.

The model was set up with 50 mm resolution and run for 40 s with feeding in a single point at the centre of the surface, in the first time step only. The feed distribution was stored every second, and then the vertical distribution was analysed at the time when the vertical centre of mass of the feed most closely matched the 2.3 m depth where the pellet sensor was placed in the physical experiments. The feed present in cell i vertically from the drop point downwards represents feed that has travelled on average at a speed of d/t, where $d = i\Delta y$ is the distance travelled. The apparent speed distribution can therefore be plotted as the relative amounts of feed along the vertical axis, with d/t on the x axis.

2.6. Full model dynamics

In Alver et al. (2004) the 2D-version of the pellet model was validated using an experimental dataset obtained from Talbot et al. (1999). The validation was conducted with respect to the feed intake of the fish and the feed waste exiting the cage, and the model was found able to predict both these quantities over time. To ensure that the updated 3D-version of the model presented in this manuscript retained these properties, we conducted a verification study where the model was used to simulate the same setup as used in the original validation (see Alver et al., 2004, for a detailed description of the simulation setup). Although Talbot et al. (1999) did not present data on the 3D-distribution of pellets within the cages, we also ran a simulation of a modified version of the experimental setup. This simulation was intended to illustrate all aspects of our model, and was therefore set up with the new spreader model for surface distribution of pellets in a circular net cage, and water current which perturbed the underwater distribution of feed. Otherwise, the experimental parameters (e.g. feeding rates, fish population settings) matched those presented by Talbot et al. (1999).

3. Results

3.1. Model validation

Measurement results from Skøien et al. (submitted for publication) are used to validate the model's advection and diffusion properties. The measurements showed a significant positive relationship between pellet size and the mean radial distance from all pellets to the centre of mass. However, the differences in diffusion across pellet density were not significant. In contrast, the vertical distribution results implied a significant increase in sinking rate with both pellet size and density. Increased sinking rates with larger pellet size corresponds well with previous experimental findings (Findlay and Watling, 1994; Chen et al., 1999; Cromey et al., 2002; Sutherland et al., 2006).

3.1.1. Horizontal diffusion

Fig. 3 describes the comparison between model estimates of horizontal distribution for all 12 pellet types with the experimental results from Skøien et al. (submitted for publication). When run with a constant κ (diffusion coefficient) value, the model predicted a relationship between pellet size and horizontal diffusion that contradicted the observed relationship (hatched lines in Fig. 3). The model overestimated the displacement for 3 and 6 mm pellets, and underestimated displacement for 12 mm pellets, indicating that the diffusivity constant κ must be dependent on pellet size. This observation is strengthened by the positive relationship between pellet size and sinking rate identified by Skøien et al. (submitted for publication) as we assumed the same κ for vertical and horizontal diffusion in our model (Eq. (4)).

Recognising this, we introduced the following relation where the κ value is set as a function of pellet diameter in mm:

$$\kappa = \kappa_{ref}(\Theta + (P_s/P_{s,ref})^2) \tag{24}$$

We chose a reference pellet size of $P_{s,ref} = 9$ mm, while the parameters κ_{ref} and Θ were tuned based on the experimental results, giving the relation shown in Fig. 4. Repeating the model

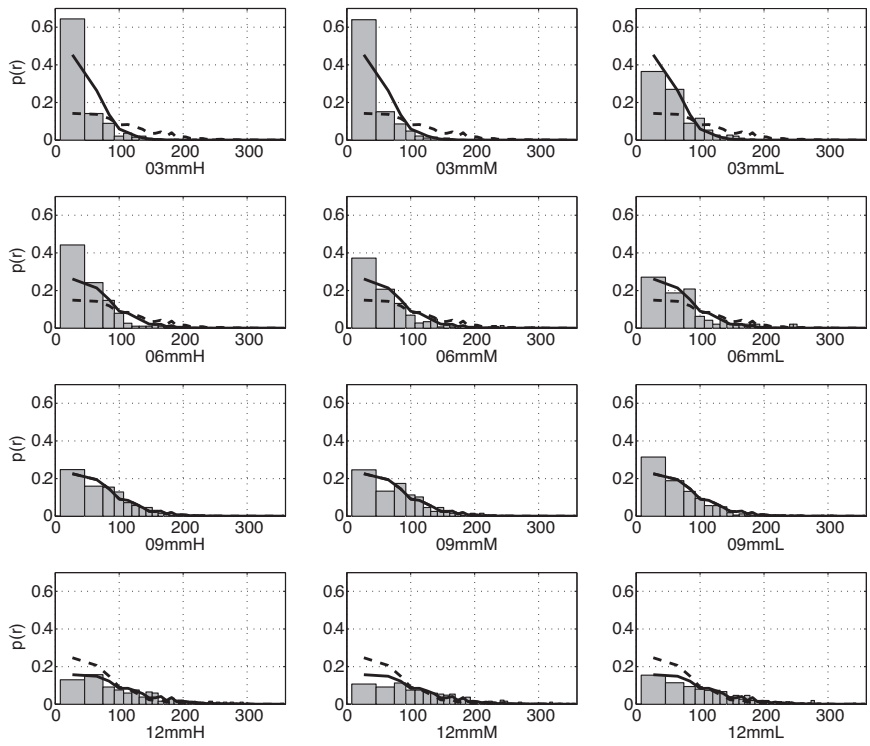

Fig. 3. Horizontal displacement in experiment (histograms) compared to model run with constant κ value (hatched lines), and with size dependent κ values (solid lines). Each row shows a single pellet size (3, 6, 9 and 12 mm), and each column shows a single pellet density (high, medium and low).

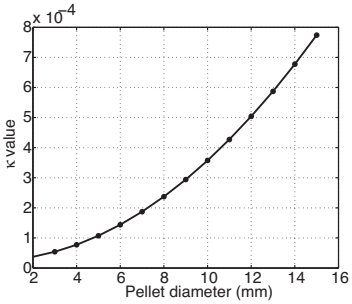

Fig. 4. Calibrated relation between pellet diameter and κ value.

simulations we now got a highly improved match between the modelled and measured distributions (solid lines in Fig. 3).

3.1.2. Vertical distribution

As vertical diffusion is modelled using the same κ as horizontal distribution (Eq. (4)), we ran vertical pellet drop tests for all pellet sizes using the κ obtained in Eq. (24). The vertical spread of pellets as predicted by our model compared well with the observation data from the physical experiments (Fig. 5).

3.2. Full model dynamics

3.2.1. Verification against original model and experimental data

Simulation output matched well with the experimental data from Talbot et al. (1999), indicating that the model was able to predict the main dynamics behind pellet distribution, feed consumption and feed wastage in a sea-cage. Furthermore, the results from the present model (Fig. 6) compared better with the experimental results than did the 2D-version model of Alver et al. (2004), implying that the modifications described in this paper improved the general performance of the model in estimating feed consumption and wastage.

3.2.2. 3D distribution of pellets in the cage volume

As described in Talbot et al. (1999), the feeding scheme lasted 15 min, with a gradual decline in feed delivery towards the end of the period. This was reflected in the 3D-visualisation of simulation output as the feed density at the surface (annular rings on the surface) stayed high at 1, 5, 10 and 13 min into the simulation, was lower at 14 min and almost zero at 15 min (Fig. 7). Feed occurring near the bottom of the the conical section of the cage in Fig. 7 represents feed that will be lost from the cage. By comparing Fig. 7 with the results presented in Fig. 6 it is apparent that the 3D-distribution followed the same pattern as the verification case. Feed loss stayed low during the first 8 min of the simulation (Fig. 6), a pattern which corresponds well to the 3D-distributions at 1 and 5 min (Fig. 7). Between 8 and 13 min, the data from Talbot et al. (1999) showed an increase in feed loss, which was also apparent in the 3D-distributions at 10 and 13 min. From 13 to 15 min, feed delivery was gradually reduced, leading to lowered feed loss in the experiments (Fig. 6). Again, this effect was seen in the 3D-distributions, in that the surface feed concentrations were gradually reduced between 13 and 15 min into the simulation (Fig. 7). Feed intensities near the bottom of the cage were also found to be lower at 14 and 15 min, which reflects the pattern towards the end of the interval in Fig. 6.

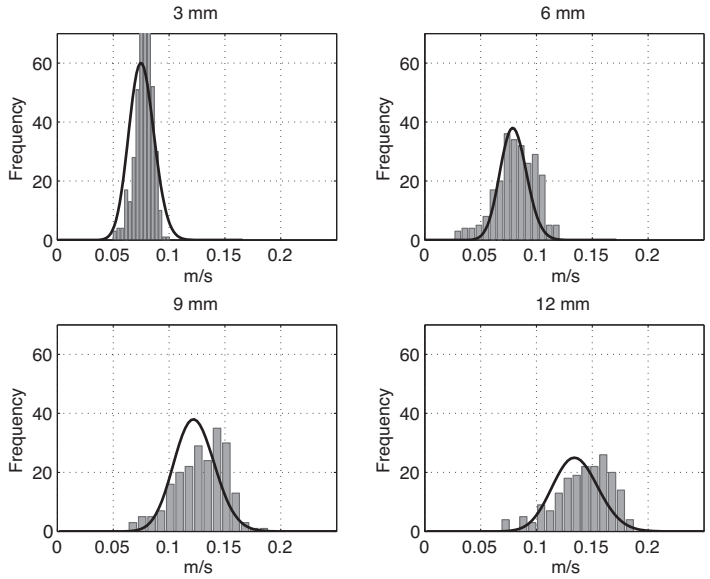

Fig. 5. Comparison of measured and modelled sinking speed distribution.

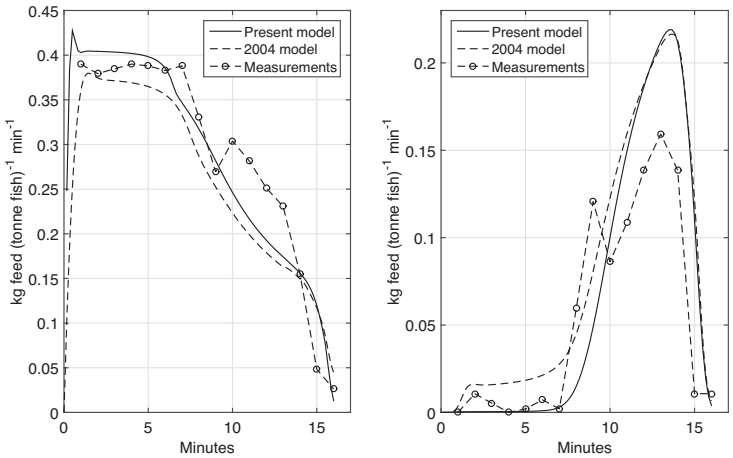

Fig. 6. Measured feed waste and estimated feed intake from salmon cage (Talbot et al., 1999, circles), compared to the output of the original pellet model (Alver et al., 2004, hatched lines) and the present model (solid lines).

The effects of water current was also visible (Fig. 7) in that the underwater distribution displayed on the slice plane that is parallel with the current was skewed towards the centre of the cage rather than propagating more directly towards the bottom.

4. Discussion

4.1. Model validation

The good match between simulation results and experimental data indicates that our model was able to capture the main mechanisms behind horizontal and vertical diffusion of pellets in water. Considering that we used identical size dependent values of κ to regulate horizontal and vertical diffusion processes, this also implies that our approach to modelling pellet diffusion (Eq. (4)) represents a realistic approximation. The pellet sizes (3, 6, 9 and 12 mm) tested by Skøien et al. (submitted for publication) cover the main range of pellet sizes used in commercial salmon aquaculture today. As the model replicated diffusion patterns for all these sizes, it is therefore likely that the model will be able to reflect the horizontal and vertical diffusion effects occurring during feed distribution in commercial rearing situations.

A limitation of the experimental setup is that it does not account for the effect of the fish on the turbulent diffusion in a commercial rearing cage. The diffusivity parameter κ may actually be somewhat higher in this setting, but it is difficult to conduct controlled experiments that take this into account.

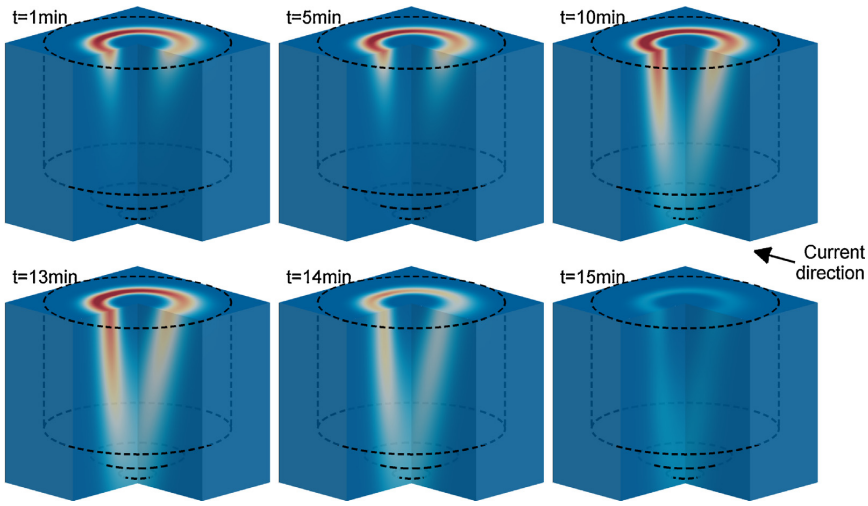

Fig. 7. Illustration of how pellets are distributed in the 3D volume of a cage at six different times during a simulated 15 min feeding trial. The simulated feeding trial is based on the feeding scheme applied in Talbot et al. (1999), but is modified to also include the new feed spreader model and water current. Different colours denote different feed pellet densities (red = high, up to 24 pellets m^{-3}; blue = low), and the thick dashed lines illustrate the outline of the circular net cage used in the simulation. (For interpretation of the references to colour in this figure legend, the reader is referred to the web version of the article.)

4.2. Verification of full model dynamics

The test of the model's prediction of the pellet consumption and wastage observed by Talbot et al. (1999) compared with the original 2D version of the model (Alver et al., 2004) verifies that the present model provides realistic full model dynamics. The most striking difference between the two models is in the initial 6 min of the feeding period, where the original model predicted an above-zero feed wastage rate, and the present model predicts no feed wastage. The data shows some variation in this period, but overall indicates a much lower wastage rate than that predicted by the original model. The general improvement in fit compared to the original model may partly be ascribed to the modification made in the expression used to compute feed ingestion, and partly to the improved estimate of the diffusivity parameter.

The 3D-visualisation of the pellet distribution at the surface and underwater demonstrated that the sub-modules in the model produced the desired effect on the model output, with the annular distribution pattern on the surface resembling those patterns observed by Oehme et al. (2012). Although feed consumption by the fish had an impact on the underwater densities for the earlier times (1–10 min) in Fig. 7, feed intake was very low for the final 3 min in the simulation experiment (Fig. 6). The reduction in pellet density with water depth seen at 13, 14 and 15 min was therefore mainly caused by the horizontal and vertical diffusion processes, and illustrates the effect of these in a 3D-volume. Since the model was found able to reproduce the feed waste observed by Talbot et al. (1999) with high precision, these observations suggest that the underwater 3D-distribution as predicted by the model bears resemblance with how pellets would distribute themselves in a physical experiment. This is, however, hard to fully verify and validate using experimental data as it would be difficult to produce a dataset which illustrates the underwater 3D distribution of pellets with sufficient resolution to compare with the outputs from our model.

4.3. Industrial applications and future work

Based on the validation and verification exercises conducted in this study, it is likely that our model would be able to provide realistic predictions of how pellets distribute themselves in the sub-surface 3D volume of a sea cage when released at the surface. Furthermore, the introduction of the parametrised model of pellet spreader distribution patterns provides the model with a more realistic pellet dispersal on the surface. We can therefore reasonably assume that our model would be able to provide realistic estimates of the feed transport occurring between feeder and fish in full-scale production cages under normal conditions.

It is likely that the spatial distribution patterns of feed pellets during feeding has an impact on the ability of the fish in capturing and ingesting the pellets, and thus also implicitly their growth rate. Different feeding strategies will lead to different underwater feed distribution patterns, but due to the difficulty in observing these patterns directly it is not easy to *a priori* evaluate which feeding strategy will result in the best growth rates at a particular site. Our model could represent an asset for such site-specific evaluations in that it could be used to estimate the distribution patterns produced by a series of different feeding strategies given the prevailing environmental conditions at the site. These predictions could then be used as a basis on which to determine which strategy or strategies are best suited to that particular site.

The model could also represent a foundation on which an operational tool for assisting feeding operations in sea cages could be based. By using inputs from the feeding system (feeder type, feeding schedule, pellet type), monitoring systems (current speed, pellet detectors), and information on the fish population (number of fish, size distribution) at the site, the model could provide a real-time estimate for the farmer on pellet distribution, ingestion and wastage. These estimates could then used as a basis for decision support in controlling and adjusting the feeding process.

The datasets used to design the surface feed distributions produced by rotor spreaders (Oehme et al., 2012) were obtained under calm weather conditions, so they do not reflect how different wind speeds impact the surface distribution patterns. This feature was consequently not taken into account in our model. This could represent a source for inaccuracy in the surface spread in pellets as estimated by our model in cases where wind significantly affects the spreader operation. Correcting the model with respect to the effects of wind could probably be realised by adding a bias to the surface distribution pattern. Ensuring that this solution produces

accurate estimates would require datasets containing both the horizontal distribution patterns and the wind conditions during the experiment. The advection effects which describe the transfer of pellets between cells in the model due to water currents has not been validated, and may thus represent an uncertainty with regard to the general performance of the model. The advection term (Eq. (3)) is based on the assumption that pellets affected by water current are given a bias in movement speed equal to the current speed. Considering the small volume and weight of individual pellets, this may be a sound assumption. Under the influence of rapidly varying currents, there may be transient deviations in the effect of the current on pellet speed, but this is not likely to be an important factor. Testing and validating such features is a challenging task, as it would require experimental setups in which both current speed and pellet movement rate are precisely monitored.

5. Conclusion

The work presented in this paper has improved the realism and applicability of the pellet distribution model in several ways. The 3D representation of the pellet field makes it possible to simulate realistic cage geometries, the surface distribution model provides representative input for the feeding equipment used in the salmon industry, and the low level adjustments and validation of the pellet diffusion rate ensures that the model accurately describes the dynamics of pellets over a variety of sizes. The full dynamics of the model shows improved fit with measurement data compared to the original model.

As a result, the present model provides a more accurate and suitable tool for understanding the feeding process and the factors determining the level of feed wastage. In combination with measurements and monitoring systems, the model can form part of a decision support system for optimising the feeding process.

Acknowledgments

This work has been financed through CREATE – the Centre for Research-based Innovation in Aquaculture Technology, which is co-funded by the Research Council of Norway and the CREATE partners.

References

Alarärä, A., Kadri, S., Paspatis, M., 2001. Feeding management. In: Food Intake in Fish. Blackwell Science Ltd., pp. 332–353.

Alver, M.O., Alfredsen, J.A., Sigholt, T., 2004. Dynamic modelling of pellet distribution in Atlantic salmon (*Salmo salar* L.) cages. Aquac. Eng. 31, 51–72, http://dx.doi.org/10.1016/j.aquaeng.2004.01.002.

Burley, C.C., Vigg, S., 1989. A method for direct measurement of the maximum volume of fish stomachs or digestive tracts. J. Fish Biol. 34 (5), 707–714, ISSN 1095-8649.

Chen, Y.-S., Beveridge, M.C., Telfer, T.C., 1999. Physical characteristics of commercial pelleted Atlantic salmon feeds and consideration of implications for modeling of waste dispersion through sedimentation. Aquac. Int. 7, 89–100, http://dx.doi.org/10.1023/A:1009249721787, ISSN 0967-6120.

Cromey, C.J., Nickell, T.D., Black, K.D., 2002. DEPOMOD-modelling the deposition and biological effects of waste solids from marine cage farms. Aquaculture 214 (1–4), 211–239, http://dx.doi.org/10.1016/S0044-8486(02)00368-X, ISSN 0044-8486.

Directorate of Fisheries, Norway, 2011. Lønnsomhetsundersøkelse for matfiskproduksjon, laks og regnbueørret (In Norwegian).

Findlay, R.H., Watling, L., 1994. Toward a process level model to predict the effects of salmon net-pen aquaculture on the benthos. In: Hargrave, B.T. (Ed.), Modelling Benthic Impacts of Organic Enrichment from Marine Aquaculture. Can. Tech. Rep. Fish. Aquat. Sci. 1949, xi + 125 p.

Fredheim, A., 2005. Current Forces on Net Structures (PhD thesis). Norwegian University of Science and Technology.

Gansel, L., McClimans, T.A., Myrhaug, D., 2010. Average flow inside and around fish cages with and without fouling in a uniform flow. ASME Conf. Proc. 2010 (January (49125)), 275–283.

Gansel, L.C., Rackebrandt, S., Oppedal, F., McClimans, T.A., 2011. Flow fields inside stocked fish cages and the near environment. ASME Conf. Proc. 2011 (44373), 201–209, http://dx.doi.org/10.1115/OMAE2011-50205.

Johansson, D., Juell, J.-E., Oppedal, F., Stiansen, J.-E., Ruohonen, K., 2007. The influence of the pycnocline and cage resistance on current flow, oxygen flux and swimming behaviour of Atlantic salmon (*Salmo salar* L.) in production cages. Aquaculture 265 (May (1–4)), 271–287, http://dx.doi.org/10.1016/j.aquaculture.2006.12.047, ISSN 0044-8486.

Løland, G., 1993. Current forces on, and water flow through and around, floating fish farms. Aquac. Int. 1 (1), 72–89, http://dx.doi.org/10.1007/BF00692665.

Oehme, M., Aas, T.S., Sørensen, M., Lygren, I., Åsgård, T., 2012. Feed pellet distribution in a sea cage using pneumatic feeding system with rotor spreader. Aquac. Eng. 51, 44–52, http://dx.doi.org/10.1016/j.aquaeng.2012.07.001.

Olsen, O.A., Balchen, J.G., 1992. Structured modeling of fish physiology. Math. Biosci. 112, 81–113.

Oppedal, F., Vågseth, T., Dempster, T., Juell, J.-E., Johansson, D., 2011. Fluctuating sea-cage environments modify the effects of stocking densities on production and welfare parameters of Atlantic salmon (*Salmo salar* L.). Aquaculture 315 (May (3–4)), 361–368, http://dx.doi.org/10.1016/j.aquaculture.2011.02.037, ISSN 0044-8486.

Remen, M., Oppedal, F., Torgersen, T., Imsland, A.K., Olsen, R.E., 2012 Jan. Effects of cyclic environmental hypoxia on physiology and feed intake of post-smolt Atlantic salmon: initial responses and acclimation. Aquaculture 326-329 (0), 148–155, http://dx.doi.org/10.1016/j.aquaculture.2011.11.036, ISSN 0044-8486.

Skøien, K.R., Alver, M.O., Alfredsen, J.A., 2014. A computer vision approach for detection and quantification of feed particles in marine fish farms. In: ICIP, pp. 1648–1652, http://dx.doi.org/10.1109/ICIP.2014.7025330.

Skøien, K.R., Aas, T.S., Alver, M.O., Romarheim, O.H., Alfredsen, J.A., 2016. Spatiotemporal distribution of extruded fish feed pellets under no-current conditions with application to aquaculture feeding models. Aquac. Eng. (submitted for publication).

Sutherland, T., Amos, C., Ridley, C., Droppo, I., Petersen, S., 2006. The settling behaviour and benthic transport of fish feed pellets under steady flows. Estuaries Coasts 29 (5), 810–819.

Talbot, C., Corneille, S., Korsøen, Ø., 1999. Pattern of feed intake in four species of fish under commercial farming conditions: implications for feeding management. Aquac. Res. 30, 509–518.

Paper E Intrinsic settling rate and spatial diffusion properties of extruded fish feed pellets

(Skøien et al., 2016a)
Skøien, K. R., Aas, T. S., Alver, M. O., Romarheim, O. H., and Alfredsen, J. A. Intrinsic settling rate and spatial diffusion properties of extruded fish feed pellets. *Aquacultural Engineering*, 74:30–37, 2016a. ISSN 0144-8609. doi: http://dx.doi.org/10.1016/j.aquaeng.2016.05.001

Errata:

- On p. 34 Table 3: [cm]
  ...should have been:
  [mm]
- On p. 34 Table 3: *6H*, under "No sig. difference", "*3H, 3M, 3L, 6M*"
  ...should have been:
  "*3H, 3M, 3L, 6M, 6L*"
- On p. 34, Chapter 3.2: "...exception of *6H* at 68 cm which is slightly less than *3L* at 70 cm."
  ...should have been:
  "...exception of *6H* at 68 mm which is slightly less than *3L* at 70 mm."

Aquacultural Engineering 74 (2016) 30–37

Contents lists available at ScienceDirect

Aquacultural Engineering

journal homepage: www.elsevier.com/locate/aqua-online

Intrinsic settling rate and spatial diffusion properties of extruded fish feed pellets

Kristoffer Rist Skøien[a,*], Turid Synnøve Aas[b], Morten Omholt Alver[a,c], Odd Helge Romarheim[d], Jo Arve Alfredsen[a]

[a] Department of Engineering Cybernetics, Norwegian University of Science and Technology (NTNU), O. S. Bragstads plass 2D, NO-7491 Trondheim, Norway
[b] Nofima, Sjølsengvegen 22, NO-6600 Sunndalsøra, Norway
[c] SINTEF Fisheries and Aquaculture, NO-7465 Trondheim, Norway
[d] Nofima, NO-5828 Bergen, Norway

ARTICLE INFO

Article history:
Received 29 January 2016
Received in revised form 29 April 2016
Accepted 5 May 2016
Available online 10 May 2016

Keywords:
Atlantic salmon (*Salmo salar*)
Aquaculture
Extruded feed pellets
Pellet distribution modelling
Pellet settling rate and diffusion

ABSTRACT

Spatial and temporal feed distribution in sea cages are important factors for the farmer, fish and environment due to the strong relation to growth, feed loss, pollution and welfare. This study presents a set of experimentally derived diffusion parameters and settling rates obtained in still water from four sizes and three densities of extruded fish feed pellets commonly used in aquaculture. It was found that pellet size is positively correlated with increased diffusion and that pellet density plays a less important role. Both the size and density of pellets had a significant impact on the settling rate. Results are compared to values obtained during feed production as well as other relevant studies. The findings suggest that parameters related to hydrodynamic behaviour of groups of feed pellets may vary across different pellet types. The results may be applied to refine and parameterize pellet motion in sea cage feeding models, improving estimates of fish behaviour, growth and feed loss.

1. Introduction

Salmon (*Salmo salar*) farming is rapidly expanding across the world with global production of just 297 tonnes in 1970 compared to over 2,087,000 tonnes in 2013 (FAO, 2015). Production has moved from moderately sized cages owned by small companies to a consolidated industry with large production sites over the last decades. Cages are usually rectangular with 20–40 m sides and 20–35 m depth, or circular with a circumference of 90–157 m up to 48 m depth (Oppedal et al., 2011). In Norway, a single cage may hold up to 200,000 fish yielding a biomass of 1000 tonnes at an typical average slaughter weight of 5 kg. A daily feed ration of 1% (Oehme et al., 2012) corresponds to 10 tons of feed per cage per day. The expenditure on feed amounts to roughly 50% of all costs in Norwegian salmon and trout farming (Norwegian Directorate of Fisheries, 2013). With the feed loss from commercial farms estimated to around 7% (Gjøsæter et al., 2008), wasted feed is a substantial economic loss for the farmer as well as poor utilization of marine and plant resources (Alfredsen et al., 2007). Feed loss may in addition have a negative impact on the surrounding marine environment. Wild fish are drawn close to the cage enabling transmission of diseases between farm sites (Dempster et al., 2009) and large amounts of wasted feed in their diet can cause changes in their filet quality (Fernandez-Jover et al., 2007).

Feed waste is one concern, but the spatiotemporal distribution of pellets within the cage is also an important parameter for the fish. Giving easy feed access for the fish by utilizing the cage volume is desirable and is likely to promote rapid growth. The spatial and temporal distribution of pellets and ration size are key factors concerning feed availability (Juell, 1995) and these factors should not be confined so the fish may forage in an unrestricted manner (Talbot et al., 1999). The spatial distribution of pellets has a considerable influence on equal feed access (Attia et al., 2012) and localized feed delivery permits resource monopolization by dominant or competitive individuals, restricting feed access to subordinates (Juell, 1995; Ryer and Olla, 1996) causing greater size variation across the population (Johansen and Jobling, 1998). Suboptimal feed intake leads to both reduced and inefficient growth in Atlantic salmon (Einen et al., 1999). Aggressive behaviour and fin damage related to feed access have been demonstrated in a range of Salmonidae (Brännäs et al., 2005; Fenderson et al., 1968; Jobling, 1985; Noble et al., 2007, 2007, 2008; Rasmussen et al., 2007; Symons, 1971; Talbot et al., 1999) and summarized by Attia et al. (2012), Ruzzante

* Corresponding author at: Department of Engineering Cybernetics, Norwegian University of Science and Technology (NTNU), NO-7491 Trondheim, Norway.
E-mail address: kristoffer.rist.skoien@itk.ntnu.no (K.R. Skøien).

http://dx.doi.org/10.1016/j.aquaeng.2016.05.001
0144-8609/

(1994) and Talbot (1993), and this aggression is in turn related to injuries and mortality (López-Olmeda et al., 2012). Optimizing the spatiotemporal pellet distribution could thus result in considerable economic, environmental and welfare benefits.

To achieve these goals more knowledge must be obtained on the interaction between the feed, fish and the environment, on which models may be created to enable simulation and optimization of feed delivery.

In Norwegian salmon farming, feed is presented to the fish in the form of cylindrical pellets where the diameter is adapted to the size of the fish, normally from 3 to 12 mm diameter (Skretting, 2012) during the ongrowth in the sea. Feed pellets are commonly produced using an extrusion process. The extrusion system has a preconditioner which mixes water and steam into the dry ingredients in order to obtain a uniformly moisturized and preheated mix for the extruder barrel (Sørensen, 2012). This barrel housing may contain one or two rotating screws which mixes and transports the feed. The heated mix obtains its final pellet shape by being forced through a die plate and cut to length by a rotating knife (Sørensen, 2012). The pellets are dried and oil is finally added to increase the energetic content and obtain the desired density of the pellets. On farms feed is conveyed from large silos onboard a barge using compressed air to propel pellets through a pipe to a rotary pneumatic spreader located on the surface in the centre of the sea cage. Pellet transport, spreader rotation and pellet throw is driven by the same airflow.

For reference, the term settling rate refers to the intrinsic sinking speed of pellets, diffusion describes how random motion causes pellets on average to move from an area of high concentration to low concentration and advection is the motion of pellets caused by the bulk motion of the surrounding water. Above surface, Oehme et al. (2012) performed the first experiment which characterized the spatial pellet distribution from a rotary spreader by collecting pellets in Styrofoam boxes on the surface. Numerical models of the spreader have also been derived to investigate effects of different designs and wind (Skoien et al., 2015, 2016). For the pellet distribution below the surface an initial numerical model was developed by Alver et al. (2004) and has since been extended with a fish behaviour and foraging model (Føre et al., 2009). The combined model has been further developed and takes into account a range of factors such as the pellet distribution pattern across the surface, pellet size and settling rate, feeding rate, water flow and temperature. It also accounts for the fish properties with respect to motion, biomass and size distribution, appetite/satiation, foraging pattern and behaviour (Alver et al., 2016).

In Alver et al. (2004, 2016) the pellet concentration of a sea cage was modelled using the transport equation to describe the spatiotemporal dynamics of its distribution.

$$\frac{\partial c}{\partial t} + v_x \frac{\partial c}{\partial x} + v_y \frac{\partial c}{\partial y} + (v_z + u_v)\frac{\partial c}{\partial z} + \kappa\left(\frac{\partial^2}{\partial^2 x}c + \frac{\partial^2}{\partial^2 y}c + \frac{\partial^2}{\partial^2 z}c\right) = u - f_I \quad (1)$$

According to Alver et al. (2016), $c(x, y, z, t)$ is the feed concentration in the coordinate system given by the horizontal plane x, y, the vertical axis z and time respectively. $v_x(x, y, z, t)$, $v_y(x, y, z, t)$ and $v_z(x, y, z, t)$ are the individual orthogonal components of the water flow, u_v is the settling rate of the pellets, κ is the diffusion factor, $u(x, y, z, t)$ is the added feed and $f_I(x, y, z, t)$ the ingestion rate of the fish at a given position and time. In the present experiments, there is no water flow or fish. Eq. (1) can thus be simplified to Eq. (2).

$$\frac{\partial c}{\partial t} + u_v \frac{\partial c}{\partial z} + \kappa\left(\frac{\partial^2}{\partial^2 x}c + \frac{\partial^2}{\partial^2 y}c + \frac{\partial^2}{\partial^2 z}c\right) = u \quad (2)$$

It is not the intention of the present study to give a detailed account of the model as a comprehensive description can be obtained from Alver et al. (2004, 2016). Both κ and u_v which are parameters of essential importance have been determined based on the findings in the current study.

Limited research has been conducted with regards to characterizing the intrinsic diffusion properties of extruded fish feed pellets. This results in a range of sea cage and deposition models such as (Alver et al., 2004; Cromey et al., 2002, 2009; Gillibrand and Turrell, 1997) being based on alternative data as opposed to experimentally derived parameters from representative feeds. There has, however, been performed extensive research in determining the vertical settling rate u_v for various fish feeds (Chen et al., 1999; Cromey et al., 2002, 2009; Findlay and Watling, 1994; Sutherland et al., 2006). There may be several factors and interactions influencing diffusion. Heavier pellets may diffuse less simply because they will be suspended in the water column for a shorter period of time compared to a lighter pellet. However, a stronger relationship may be governed by a relation between size and increased diffusion due to greater settling rate and thus a higher level of erratic motion. It is also likely that density as well as size affects the settling rate due to the non-linear relationship between surface area/mass across different sized pellets.

The contribution of this study is a description of the pellet settling rate and diffusion process obtained through experiments involving a range of pellet types with different characteristics. These results may be of importance in determining central parameters in any feeding model involving pellets. The horizontal diffusion and vertical settling rate characteristics have been derived from the same pellets giving added benefit of matched data describing the motion of a pellet along all three axes. The results have been applied to the model described by Alver et al. (2016) to improve the estimation of the spatial and temporal pellet distribution.

2. Materials and methods

The work described in this study has been conducted as two separate experiments denoted the diffusion experiment and the settling rate experiment. The former quantifies the natural diffusion of pellets in the horizontal x, y plane released from a single point until they settle on the bottom. The latter is an extensive investigation of the settling rate and the vertical (z-axis) distribution of pellets dropped from an altitude, similar to being distributed by a rotary spreader. The diffusion and settling rate experiment are described in Sections 2.2 and 2.3 respectively.

2.1. Pellet properties

The experimental pellet types were produced at Nofima Feed Technology Centre, Bergen, Norway. Four different pellet sizes of {3, 6, 9, 12} mm diameter and cylindrical shape were produced to cover a wide range commonly used in Atlantic salmon farming. Each of the four pellet sizes were coated with three different amounts of oil to obtain pellets of low, medium and high density {L, M, H}, giving a total of twelve different pellet types. Each type is denoted by its pellet size and density, e.g. *9M* denotes a 9 mm pellet of medium density. The diet formulation was similar to the average Norwegian salmon feed in 2010 (Ytrestøyl et al., 2011). One basal mix of the dry feed ingredients was made and divided into four batches prior to extrusion. The four batches were processed with similar conditions in a Wenger TX52 extruder (Wenger, KS, USA), but with die plate holes of 2.5, 4.5, 7.2 and 10.0 mm diameter. The cutting knife speed was, however, adjusted for each production to ensure pellets with a length:diameter ratio of approximately 1:1. The pellets were dried to 92% dry matter in a hot air dual layer carousel dryer (Paul

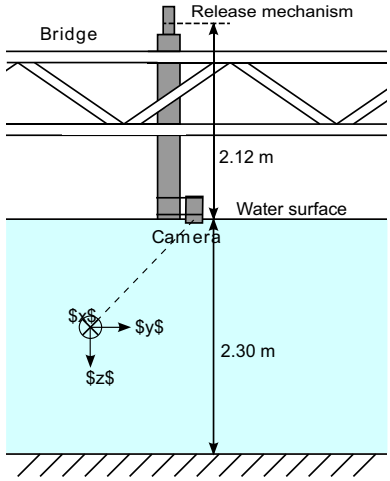

Fig. 1. The setup for the horizontal distribution experiment. Guide pipe attached vertically to a bridge crossing the tank. On top of the pipe is the quick release mechanism and the camera is mounted on the opposite end, barely breaching the water surface. The aluminium sheet is placed on the bottom of the tank. The origin of the global coordinate system is defined at the principal point of the camera, relocated in the figure for clarity.

Klöckner, Nistertal, Germany). Then each of the diets were coated in an experimental vacuum coater (Pegasus PG-10VC LAB, Dinnissen B.V., The Netherlands) with an oil blend of 43% rape seed oil and 57% fish oil. The low density diets were added an amount of oil giving slow sinking pellets, the high density diets were added the maximum amount of oil and the intermediate density diets were added an oil level halfway between the other two.

Pellet settling rate was measured at production based on 20 pellets released in a standing transparent cylinder (15 cm diameter, 1.7 m high) filled with 32 ppt NaCl salt water holding 20 °C. The measurement was started when the pellet was 5 cm below the water surface and the settling rate was calculated from the time it took a pellet to sink 1 m (Table 1). Bulk density was measured by weighing loosely poured coated pellets in a 1000 ml measuring cylinder (Table 1). Due to the differences in stacking efficiency, particle densities can not be directly compared. Diameter and length of the pellets were measured with an electronic caliper (Table 1) based on 20 pellets from each pellet size.

2.2. Horizontal distribution

The horizontal diffusion experiment was conducted at Nofima, Sunndalsøra, Norway, in a 7 m diameter octagonal 100 m^3 indoor seawater tank (Fig. 1). The x and y axes are horizontal and points towards the edges of the tank, and z points downwards. The tank bottom sloped slightly from the edge towards the drain located at the centre of the tank. Water flow was measured at 0.2, 1.2 and 2.2 m depth in both x and y direction with a propeller anemometer (0.00 m/s, handheld flow meter HFA and vane wheel, Höntzsch, Waiblingen, Germany) performed prior to experiments to ensure that the water mass was stationary. Although the water was stationary, surface particles displayed some minor motion which was attributed to the airflow from the ventilation system. The salinity was measured to 31.7 ppt (Cond 330i with a TetraCon conductivity measuring cell, WTW – Wissenschaftlich-Technische Werkstätten GmbH, Weilheim, Germany). With $T = 12$ °C, the water density was calculated to 1024 kg/m^3 Pond and Pickard (1983, pp. 310).

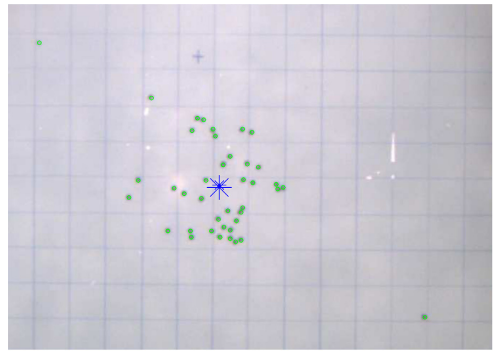

Fig. 2. Analysis of one drop of *6H* pellets superimposed on the cropped original image. All 40 pellets have settled in this drop. Circles indicate the manually marked pellet positions, the large asterisk is the centre of mass, and the small asterisk is centre of pipe projected down onto the target. Two of the pellets are far from the centre of mass probably due to surface drift before sinking.

The pellets were placed in a 70 mm diameter vertical pipe equipped with a quick release mechanism (Fig. 1). The pellets were concurrently released and guided to the water surface by an 80 mm diameter pipe ending at the surface. This resulted in a total distance from release position to water surface of 2.12 m. Disregarding friction against the pipe wall and aerodynamic resistance, this yields a free-fall time of 0.657 s from release to water impact at a rate of 6.45 m/s obtained from basic equations of motion. From the surface, pellets travelled 2.30 m through the water column before settling on a 1.00 × 1.00 m sheet of aluminium with a 50 × 50 mm grid on the bottom of the tank. A digital camera (FL3-GE-13S2C-CS, Point Grey Research, Inc., Richmond, Canada) equipped with an adjustable lens (M13VM308, Tamron Co., Ltd, Saitama-city, Japan) encapsulated in a waterproof housing was mounted at the end of the 80 mm pipe, capturing an image of the settled pellets at the end of each drop. Five replicate drops of 40 pellets each were conducted for each of the 12 pellet types, giving a total of 60 drops conducted in randomized order. There were some observations of pellets that remained afloat for an indefinite period of time or sunk later, long after the main bulk of pellets. This effect was mostly pronounced in the low density pellets. A drop was deemed finished and a picture captured as soon as there were no pellets sinking through the water column. The target grid was brushed clean of pellets after each image capture and the position of the target in relation to the pipe was verified by a laser cross and realigned if necessary. The water was left to settle for at least two minutes before the next drop was performed.

The images and pellet positions were analyzed using openCV (Bradski, 2000; MATLAB, 2014; SPSS, 2015). The position of each pellet was manually identified in the image obtained from each drop. The procedure of mapping from camera pixel coordinates $(\mathbb{R}^2)\ \boldsymbol{p} = \begin{bmatrix} u & v \end{bmatrix}^T$ to the world coordinate frame on the bottom $(_b)$ of the tank $(\mathbb{R}^2)\ \boldsymbol{q} = \begin{bmatrix} x_b & y_b \end{bmatrix}^T$ was performed by establishing the homography matrix $\boldsymbol{H}$ and calculating the transformation using the augmented vectors $\tilde{\boldsymbol{q}} = \boldsymbol{H}^{-1}\tilde{\boldsymbol{p}}$. $\boldsymbol{H}$ was obtained from a calibration image from which nine central grid points were extracted and $\boldsymbol{H}$ calculated by using the MATLAB toolbox from Corke (2011) yielding a residual of 0.89. An image example can be seen in Fig. 2.

For the purpose of statistical analysis it is assumed that there is an isotropic bivariate distribution around the centre of mass for the group of settled pellets. The centre of mass on the bottom of the tank was defined as zero $\bar{x}_b = 0$ and $\bar{y}_b = 0$ for each drop. Comparing the centre of mass to the pipe centre projected onto the bottom reference grid verifies that centre of mass was located close to pipe

Table 1
Settling rate mean ± SD [cm/s] measured in a vertical cylinder at production ($N = 20$, 20 °C water, 32 ppm NaCl), bulk density at production, mean ± SD [g/l] ($N = 3$ replicate measurements for 3 and 6 mm, $N = 4$ for 9 and 12 mm), oil content [%]. Diameter and length, mean ± SD [mm] of pelleted feed at production ($N = 20$).

		3 mm	6 mm	9 mm	12 mm
Settling rate	*H*	10.2 ± 0.5	11.8 ± 0.9	14.7 ± 0.8	16.6 ± 1.6
	M	8.1 ± 0.6	6.4 ± 1.5	10.7 ± 2.5	12.4 ± 2.4
	L	5.9 ± 1.2	5.3 ± 1.2	7.8 ± 1.5	9.7 ± 1.7
Bulk density	*H*	706 ± 7	671 ± 15	673 ± 7	637 ± 17
	M	645 ± 5	596 ± 16	623 ± 3	597 ± 5
	L	583 ± 4	556 ± 19	582 ± 11	567 ± 9
Oil content	*H*	21.0	28.0	30.0	32.0
	M	13.0	22.5	25.0	27.5
	L	5.0	17.0	20.0	23.0
Diameter		3.0 ± 0.1	6.0 ± 0.1	9.4 ± 0.2	12.8 ± 0.2
Length		3.8 ± 0.5	6.4 ± 0.4	9.0 ± 0.4	12.6 ± 0.7

centre, as is expected when there is no water flow present. The radial distance r_b from $\bar{x}_b, \bar{y}_b$ to each pellet was calculated for each drop. The vector $\boldsymbol{r}_b$ contains measured radial distances of pellets of a single type which has a Rayleigh distribution, assuming that all the x_b and y_b distances has zero mean, are normally distributed, independent and with equal variance (Forbes et al., 2011).

In the captured images it was evident that some pellets came to rest far from the centre of mass of the main cluster, as in Fig. 2. This observation was attributed to odd low-density, oddly shaped or pellets that got an air bubble attached to their surface. The latter made certain pellets float for a period of time exposing them to the previously mentioned slight surface motion caused by the ventilation system. To counter this effect, the image was captured as soon as there were no sinking pellets in the water column. However, some pellets affected by surface motion were unavoidably part of the captured image. To further limit this adverse effect, outliers were removed by visually inspecting the histogram of $\boldsymbol{r}_b$ and comparing it to a Rayleigh probability density function fitted to the data by the MATLAB command `fitdist`. This procedure defined 50 pellets (2.4%) as outliers of a total 2116 and removed them from the analysis. Small and low density pellets appeared more prone to have outliers.

For significance testing a one-way ANOVA was applied to the data set. Two-way ANOVA was not used since the particle density may be unequal for pellets of different size. $\boldsymbol{r}_b$ was square root transformed for all the pellet types and scaled so the minimum value is anchored at unity as according to (Osborne, 2002). 21 outliers were detected by box plot inspection (data points greater than 1.5 box-lengths from the edge). However, there were no extreme outliers and all outliers were situated close to the box. Some of these outliers may have been caused by one of the aforementioned reasons but they were kept in the data set as there was no clear radial separation from the remainder of the data. Normality was assessed using the Shapiro–Wilk test and found to be violated for 3*H*, 3*M*, 6*M* and 9*L* ($p < .05$). Since the group size for these four pellet types are large, (200, 198, 146 and 167 respectively), a Q–Q plot analysis was carried out as well which indicated fairly normally distributed values. The overall histogram shapes of $\sqrt{\boldsymbol{r}_b}$ looks similarly shaped, mostly with a slightly positive skewness. However, due to the robustness of ANOVA the analysis was still performed using this method. Assumption of homogeneity of variances was not satisfied which was assessed by Levine's test ($p < 0.0005$), hence, the remainder of the analysis was performed with a Welch ANOVA.

2.3. Settling rate

The vertical settling rate experiment was conducted in a cylindrical indoor tank 2.76 m high, 0.79 m diameter filled with fresh water. Sea salt was added and the salinity and temperature measured using a CTD probe (SonTek CastAway, CA, USA). Salinity and temperature readings were taken across the entire depth of the tank at three different times during the experiment. Salinity varied from 28.9 to 33.2 ppt (average 32.0 ppt), generally increasing with depth. Temperature ranged from 17.2 to 17.9 °C (average 17.6 °C). Using the average readings the water density was calculated to 1023 kg/m^3. The vertical guide pipe and release mechanism were the same as in the horizontal diffusion experiment described in Section 2.2. A camera and lens configuration as described in Section 2.2 was enclosed in a watertight housing and mounted horizontally, capturing images of passing pellets at a depth of 2.30 m. This device was positioned at the bottom of the tank and aimed towards a uniformly backlit surface where the camera captured high contrast images of pellets traversing the field of view. To guide pellets into the field of view, a 135 mm high funnel was attached to the rig giving a detection area of approximately 0.1 m^2, equivalent to 17% of the cross sectional area of the tank. This device is further detailed in Skøien et al. (2014). The camera was configured to output images of 640 × 480 pixels, 8 bit grayscale at 56 frames per second. Images were continuously transferred through an Ethernet and power umbilical and stored with a timestamp on a local computer.

Ten replicates of each pellet type were dropped in randomized order. Due to the large number of pellets, the individual pellet containers were measured by volume and 3, 20, 70 and 230 ml of 3, 6, 9 and 12 mm pellets respectively were used. The volumes were experimentally determined to provide a high number of pellets passing the sensor while keeping manual quantification manageable. The release process was identical to the one in the diffusion experiment but there was no pause between drops as there was no need to introduce foreign objects into the body of water for cleaning purposes. The duration of the recorded video for a given pellet type was determined based on the settling rate measured at production (Table 1). Assuming a normally distributed settling rate, a drop was deemed finished when four standard deviations above the mean was reached. On the rare occasion that pellets were still present in the live video stream after this period of time, the recording was extended until pellets could no longer be observed.

The recorded video and corresponding timestamps were analyzed utilizing a C++ and OpenCV (Bradski, 2000) implementation. The software traversed the video stream frame by frame with an operator signaling when a pellet passed a fictive horizontal line in the image corresponding to a depth of 2.30 m, identical to the diffusion experiment. From this the settling rate was calculated for each pellet and the results analyzed across all replicates of the 12 pellet types.

A one-way ANOVA was used for significance testing using the transformed data set using reflect and $\log_{10}$ ($\log_{10}$(max(data) + 1-data). Some outliers were present in the data but these could

Table 2
Number of pellets settling on the tank floor including pellets later classified as outliers for each pellet type. Numbers in parenthesis indicates average per replicate. <40 indicates the presence of positively buoyant pellets, >40 indicates breakage or other debris present in the image.

	3 mm	6 mm	9 mm	12 mm
H	206 (41.2)	200 (40.0)	198 (39.6)	193 (38.6)
M	202 (40.4)	152 (30.4)	198 (39.6)	193 (38.6)
L	196 (39.2)	49 (9.8)	172 (34.4)	157 (31.4)

Table 3
Average distance from centre of mass, mean ± SD [mm]. Number of pellets analyzed with outliers removed. The rightmost column indicates pellet types between which significant differences could not be established at $p < 0.05$ in relation to all other types based on results of Games–Howell analysis from the transformed data: $\sqrt{\bar{r}_b}$.

Pellet type	Mean distance [cm] ($\bar{r}_b$)	*N*	No. Sig. difference
3H	61 ± 43	200	*3M, 3L, 6H*
3M	61 ± 48	198	*3H, 3L, 6H*
3L	70 ± 40	191	*3H, 3M, 6H, 6M, 6L,*
6H	68 ± 40	197	*3H, 3M, 3L, 6M*
6M	80 ± 57	146	*3L, 6H, 6L, 9H, 9M, 9L*
6L	89 ± 57	48	*3L, 6H, 6M, 9H, 9M, 9L, 12L*
9H	92 ± 48	198	*6M, 6L, 9M, 9L*
9M	93 ± 49	197	*6M, 6L, 9H, 9L*
9L	95 ± 64	167	*6M, 6L, 9H, 9M*
12H	130 ± 70	189	*12M, 12L*
12M	140 ± 76	190	*12H, 12L*
12L	119 ± 61	145	*6L, 12H, 12M*

not be attributed to either data entry or measurement errors and were hence included in the study. Assessment of normality was performed using the Shapiro–Wilk test and found that 5 pellet types did violate the assumption of normality at $p < 0.05$. However, the ANOVA is not highly sensitive to normality deviations (McDonald, 2014). Inspection of the histograms indicated reasonable normality with mostly positive skew and some types slightly negative skewed. As stated by McDonald (2009), the one-way ANOVA is more powerful compared to the non-parametric Kruskal–Wallis test and ANOVA should be used except when the data is severely non-normal. Homogeneity of variances was tested using Levine's test and found violated at $p < 0.0005$, thus Welch ANOVA was used for the analysis.

3. Results

3.1. Production measurements

Table 1 presents the measurements obtained from Nofima Feed Technology Centre, Bergen, Norway, during feed production. These results will act as a reference for the main experiments in this study and will not be discussed in detail.

3.2. Horizontal diffusion

The number of pellets settling on the bottom and becoming part of the captured images are presented in Table 2. The average number of pellets sinking and settling on the bottom for each type was between 30.4 (76% of the 40 pellets) and 41.2 (103%), except from *6L* at 9.8 (25.5%). Across all sizes the number of pellets settling on the tank floor was positively correlated with density. In some cases the number of counted pellets exceeded 40 which was due to breakage and difficulty in separating intact pellets from fragments during the analysis. This issue was only evident the 3 mm pellet types.

As seen in Table 3, across pellet types the average radial distribution increased with size across all densities with one exception of *6H* at 68 cm which is slightly less than *3L* at 70 cm.

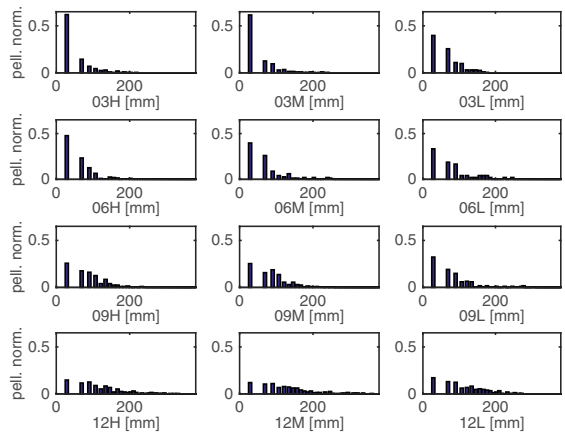

Fig. 3. Number of pellets in each annulus for each of the twelve pellet types. Each annulus and central circle are of equal area, and the number of pellets have been normalized. Distance from centre of mass in mm.

Table 4
The average and ±SD settling rate [cm/s] for all types and number of pellets analyzed. The rightmost column indicates difference in settling rate compared to the values measured at production.

Pellet type	Settling rate (u_v)	*N*	Diff. from prod.
3H	9.9 ± 0.5	506	−2%
3M	7.7 ± 0.8	435	−5%
3L	5.6 ± 1.0	376	−6%
6H	12.3 ± 0.9	329	4%
6M	8.1 ± 1.8	250	+27%
6L	6.2 ± 1.7	84	+18%
9H	14.0 ± 2.0	254	−5%
9M	12.8 ± 2.3	214	+20%
9L	9.7 ± 2.1	186	+24%
12H	17.0 ± 2.9	192	+2%
12M	14.2 ± 2.5	186	+14%
12L	11.3 ± 2.5	177	+16%

The statistical analysis stated that there were significant differences across $\sqrt{\bar{r}_b}$ for the 12 pellet types, Welch's $F(11, 667.228) = 39.859$, $p < .0005$. This result was followed up with a Games–Howell post-hoc test and the results are presented in Table 3.

To illustrate the diffusion of pellets, the radial distance $\mathbf{r}_b$ from each pellet to the centre of mass for the respective drop was concatenated across all five replicates. A circle with a radius of 380 mm was divided into 43 annuli with an additional circular central section all with equal area. Fig. 3 illustrates the normalized number of pellets in each annulus and central circle for each of the twelve pellet types.

From Fig. 3 and Table 3, diffusion was positively correlated with pellet size with the one exception of *6H* which diffused slightly less compared to *3L*. The 12 mm pellets stand out in the analysis as they in general diffused significantly more than the rest of the pellet types, with the exception of *12L* which is not significantly different from *6L*. Within the same sized pellets there is a tendency towards increased diffusion with reduced density with the exception of *12L*.

3.3. Settling rate

The average settling rates from the experiment are presented in Table 4 and corresponding normalized histograms are presented in Fig. 4. The settling rates ranged from 5.6 cm/s for *3L* to 17.0 cm/s for *12H*. Across all pellet types, increased density was positively

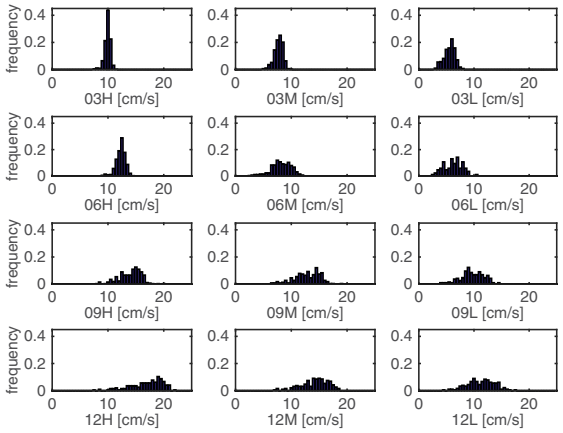

Fig. 4. Settling rate for each pellet type [cm/s], normalized count. Histograms plotted with 0.5 cm/s bin width.

correlated with settling rate. For pellets of identical density, there was also a positive correlation between size and settling rate. Upon inspection of Fig. 4 it seems that smaller pellets tend to settle as a uniform cluster whereas larger ones have a greater span in their settling rate. This observation is also evident from the standard deviations in Table 4. Comparing the settling rates from the experiment to those measured at production yields generally good correspondence. *3H*, *3M*, *3L*, *6H*, *9H* and *12H* all deviate no more than 6% from the production values. The remaining pellet types however have a faster settling compared to the production values, ranging from +14% to +27%.

Significant differences were detected between the transformed settling rates, Welch's $F(11, 916.393) = 1394$, $p < 0.0005$. Multiple comparisons were performed using the Games–Howell post-hoc test and found significant differences between all pellet types $p < 0.016$, with the exception from two pairs, *3H* and *9L* as well as *9H* and *12M*.

4. Discussion

As seen in Table 3 and the accompanying ANOVA analysis there was significant differences in the root radial diffusion $\sqrt{\bar{r}_b}$ between pellet types. There were no significant differences in $\sqrt{\bar{r}_b}$ between pellets of the same size ($p > 0.05$). Hence, it appears that pellet density is not a significant factor in determining diffusion. Since specific pellet density measurements were unavailable, the relation between this result with respect to specific density is unknown. However, between sizes the results differed greatly. These results suggest that modelling of pellet diffusion cannot be accurately represented by a generalization across all sizes and densities. However, within a given pellet size the distribution variability was limited, which may lead to satisfactory simulation results without considering the density of a given pellet type. This simplifies modelling as the pellet size is often readily available but the density may be more cumbersome to obtain. Note that the fat content described in Table 1 is not a descriptor for the specific density of a pellet. A larger pellet may expand more in percentage compared to a small pellet leaving more room for oil.

The conversion from image/pixel coordinates $\boldsymbol{p}$ to the world coordinate frame $\boldsymbol{q}$ was performed using the homography transform (Corke, 2011) based on 9 image points. This approach does not account for lens distortion but the fact that the field of view was narrow and the pellets settled close to the centre of the image greatly reduced any distortional effects. Visual inspection of the captured images showed minor distortion, which combined with the low residual value of the homography computation, gives satisfying credibility to the classification of the real life pellet positions. The $\bar{\boldsymbol{r}}_b$ in Table 3 may be used by modellers to verify that pellets originating from a point source in still water has the appropriate average Euclidean radial diffusion at 2.30 m depth. This may be achieved by adjusting the diffusion parameter, such as κ in Eq. (1). These values have already been incorporated in a sea cage model (Alver et al., 2016) for improved simulation accuracy. These parameters will likely become increasingly relevant when simulations are run under realistic conditions with a horizontal water flow field, especially for low density pellets. The slow settling rate will expose the pellets for a prolonged period of time before being eaten by fish or escaping the cage.

The obtained settling rates generally corresponded well with the values measured at production time. Interestingly, the smallest pellet types *3H*, *3M*, *3L* as well as all the high density types *6H*, *9H* and *12H* deviated no more than 6% either negatively or positively from the settling rate measured at production. For the medium and low density 6, 9 and 12 mm types, the smallest deviation from production values was 14% for *12M* and the largest deviation was 27% for *6M*. The largest differences occurred among the larger pellet types, *6M*, *6L*, *9M* and *9L* which showed positive deviations from the production measured settling rate, and *12M* and *12L* portrayed a smaller positive difference. This effect was not clearly understood. Factors which might contribute are (1) The fact that the entire cross-sectional area of the tank was not measured. Faster pellets may have travelled in the centre of the pellet cloud in the horizontal plane, resulting in a larger proportion of the faster pellets being measured. (2) The batch of pellets being released from altitude might give heavier pellets a boost compared to lighter ones. The simultaneous release of pellets was probably more realistic than single pellets measured in isolation when comparing it to a feed spreader which releases pellets in batches at 1–2 m above sea level. This though might explain the positive skew compared to the manufacturing results and the effect may be somewhat reduced if the tank was deeper.

The camera rig could not detect pellets across the entire cross sectional area of the cylindrical tank due to its limited field of view. The funnel on the camera rig accounts for the comparatively low N (Table 4) of pellet types with high diffusion as fewer of them passed the detection area. *6L* had a very low pellet count of 84 which is attributed to both a high diffusion factor as well as this particular pellet type being very buoyant with many floating pellets as was also observed in the diffusion experiment. The funnel height was only 135 mm and quite steep, which in comparison to the total settling distance is likely too modest to influence the settling rate measurements in a noticeable manner. However, such a delaying effect would manifest itself as a decrease in settling rate but the results were generally faster than the settling rates measured at production.

Inspecting the standard deviations in settling rates from Table 4 also reveals that the vertical spread of pellets increased with size. There is only one exception for ±1.0 cm/s for *3L* and ±0.9 cm/s for *6H*. This observation corresponds well with the diffusion experiment as larger pellets tended to diffuse more vertically as well as horizontally. This could be due to a positive correlation of chaotic motion and pellet size, or possibly that larger pellets have greater surface area which renders them susceptible to air bubbles attaching to the surface. A larger pellet may in turn capture either a small or a large volume of air, increasing the range of buoyancy.

Fig. 5 compares the results from the present study with production measurements as well as various feeds from Chen et al. (1999), Findlay and Watling (1994) and Sutherland et al. (2006). The agreement is quite good although the pellet types used in this study seem to have an overall slower settling rate. This effect may

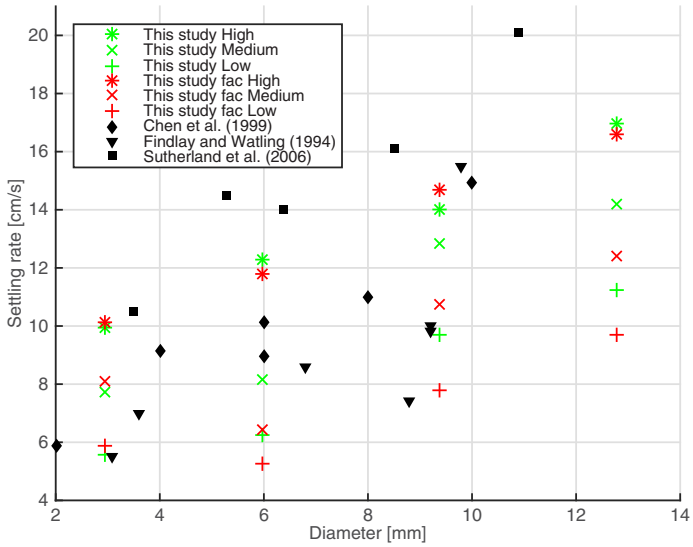

Fig. 5. Comparing settling rate and measured diameter. Comparison of experimental results, factory production measurements and studies by Chen et al. (1999), Findlay and Watling (1994) and Sutherland et al. (2006).

have been caused by the nutritional composition of the feed as well as the present pellets having a diameter/length ratio of approximately 1:1. Inspecting the results of Sutherland et al. (2006) which are overall faster, had a much lower diameter/length ratio. Pellets which are longer, more cylindrically shaped as opposed to the comparatively spherical ones used in this study may have a more stable orientation in the water column which may result in a faster settling rate. It should be noted that in Sutherland et al. (2006) their own comparison of settling rate against other pellet types showed that their pellets did indeed settle comparatively fast.

The pairwise significance analysis on the transformed data resulted in all pellet types having significantly different settling rate at $p < 0.05$ with the exception of the two pairs, *3H* and *9L* as well as *9H* and *12M*. Inspecting Table 4, other pellet types also showed very similar settling rates such as *3M* and *6M*. This may suggest that the data transformation increased the type I error rate and the significance analysis should be interpreted with caution.

For the modeller a recommendation would be to choose a suitable diffusion parameter from Table 3 based on the appropriate pellet size. As stated, no significant differences could be detected between identically sized pellet types so an average or median value might suffice. With respect to the settling rate, this value is often obtainable from the producer and should be used if available. Otherwise, a suitable settling rate from Table 1 or Table 4 could be chosen. The former table was taken from $N = 20$ at production and seems to settle slightly slower, but generally correspond well with other studies as presented in Table 5. The latter was taken from a much larger data set and released in a manner which is likely more realistic in relation to rotary spreaders in sea cage production. These results show an overall faster settling rate and these may have been more in line with the production measurements had the tank been deeper, possibly due to a faster settling rate at the shallowest section of the water column. From a pneumatic spreader, pellets will have a horizontal velocity component which has not been considered in this study. However, it is likely that this horizontal component will be quickly eliminated upon water impact and the intrinsic settling rate becoming the dominant velocity component in still water.

5. Conclusion

This study has examined the horizontal diffusion and settling rate based on experiments with four sizes and three densities of extruded salmon pellets under stationary water conditions. For horizontal diffusion only the pellet size had a significant impact on the radial distance from the centre of mass while both the size and density affected the settling rate. The results have been used to refine and parameterize a sea cage model (Alver et al., 2016) where pellet motion plays an essential role. These results allow for spatiotemporal pellet distribution and water flow induced motion to be more accurately modelled by hydrodynamics and equations of motion based on the presented experimentally derived parameters. These findings will expectedly yield improved model estimates of pellet motion within a sea cage, fish behaviour and feed loss.

Acknowledgments

Appreciation is extended to M.S. Klinge and R.E. Myrmel at Nofima for producing the experimental pellets, P.I. Snildal and T. Haugen at the Department of Engineering Cybernetics workshop at The Norwegian University of Science and Technology (NTNU) and F. Nerland at Nofima for assisting with the experiment. This research has been funded by the Centre for Research-based Innovation in Aquaculture Technology (CREATE) (Research Council of Norway, Grant number: 174842), SINTEF Sealab, NO-7645 Trondheim, Norway.

References

Alfredsen, J., Holand, B., Solvang-Garten, T., Uglem, I., 2007. Feeding activity and opercular pressure transients in Atlantic salmon (*Salmo salar* L.): application to feeding management in fish farming. In: Almeida, P., Quintella, B., Costa, M., Moore, A. (Eds.), Developments in Fish Telemetry. Developments in Hydrobiology, vol. 195. Springer, Netherlands, pp. 199–207, http://dx.doi.org/10.1007/978-1-4020-6237-7_19.

Alver, M.O., Alfredsen, J.A., Sigholt, T., 2004. Dynamic modelling of pellet distribution in Atlantic salmon (*Salmo salar* L.) cages. Aquacult. Eng. 31 (1–2), 51–72, URL http://www.sciencedirect.com/science/article/pii/S0144860904000056.

Alver, M.O., Skøien, K.R., Føre, M., Aas, T.S., Oehme, M., Alfredsen, J.A., 2016. Modelling of surface and 3D pellet distribution in Atlantic salmon (*Salmo salar* L.) cages. Aquacult. Eng. 72-73, 20–29, URL http://www.sciencedirect.com/science/article/pii/S0144860916300462.

Attia, J., Millot, S., Di-Poï, C., Bégout, M.-L., Noble, C., Sanchez-Vazquez, F., Terova, G., Saroglia, M., Damsgård, B., 2012. Demand feeding and welfare in farmed fish. Fish Physiol. Biochem. 38, 107–118, http://dx.doi.org/10.1007/s10695-011-9538-4.

Bradski, G., 2000. The OpenCV Library. Dr. Dobb's Journal of Software Tools.

Brännäs, E., Berglund, U., Eriksson, L.-O., 2005. Time learning and anticipatory activity in groups of Arctic charr. Ethology 111 (7), 681–692, http://dx.doi.org/10.1111/j. 1439-0310.2005.01094.x.

Chen, Y.-S., Beveridge, M.C., Telfer, T.C., 1999. Physical characteristics of commercial pelleted Atlantic salmon feeds and consideration of implications for modeling of waste dispersion through sedimentation. Aquacult. Int. 7, 89–100, http://dx.doi.org/10.1023/A:1009249721787.

Corke, P.I., 2011. Robotics, Vision & Control: Fundamental Algorithms in Matlab. Springer.

Cromey, C.J., Nickell, T.D., Black, K.D., 2002. DEPOMOD-modelling the deposition and biological effects of waste solids from marine cage farms. Aquaculture 214 (1–4), 211–239, URL http://www.sciencedirect.com/science/article/pii/S004484860200368X.

Cromey, C.J., Nickell, T.D., Treasurer, J., Black, K.D., Inall, M., 2009. Modelling the impact of cod (*Gadus morhua* L.) farming in the marine environment – codmod. Aquaculture 289 (1–2), 42–53, URL http://www.sciencedirect.com/science/article/pii/S004484860800999X.

Dempster, T., Uglem, I., Sanchez-Jerez, P., Fernandez-Jover, D., Bayle-Sempere, J., Nilsen, R., Bjørn, P., et al., 2009. Coastal salmon farms attract large and persistent aggregations of wild fish: an ecosystem effect. Mar. Ecol. Prog. Ser. 385 (1), 14.

Einen, O., Mørkøre, T., Rørå, A.M.B., Thomassen, M.S., 1999. Feed ration prior to slaughter – a potential tool for managing product quality of Atlantic salmon (*Salmo salar*). Aquaculture 178 (1–2), 149–169, URL http://www.sciencedirect.com/science/article/pii/S004484869900126X.

FAO, 2015. Available from: http://www.fao.org/fishery/statistics/global-aquaculture-production/en. URL http://www.fao.org/figis/servlet/SQServlet?file=/work/FIGIS/prod/webapps/figis/temp/hqp_24111803162059520 0.xml&outtype=html.

Fenderson, O., Everhart, W., Muth, K., 1968. Comparative agonistic and feeding behavior of hatchery-reared and wild salmon in aquaria. J. Fish. Board Can. 25 (1), 1–14.

Fernandez-Jover, D., Jimenez, J.A.L., Sanchez-Jerez, P., Bayle-Sempere, J., Casalduero, F.G., Lopez, F.J.M., Dempster, T., 2007. Changes in body condition and fatty acid composition of wild Mediterranean horse mackerel (*Trachurus mediterraneus*, steindachner, 1868) associated to sea cage fish farms. Mar. Environ. Res. 63 (1), 1–18.

Findlay, R.H., Watling, L., 1994. Toward a process level model to predict the effects of salmon net-pen aquaculture on the benthos. In: Hargrave, B.T. (Ed.), Modelling Benthic Impacts of Organic Enrichment from Marine Aquaculture. Can. Tech. Rep. Fish. Aquat. Sci., 1949: xi + 125 p.

Forbes, C., Evans, M., Hastings, N., Peacock, B., 2011. Statistical Distributions. John Wiley & Sons.

Føre, M., Dempster, T., Alfredsen, J.A., Johansen, V., Johansson, D., 2009. Modelling of Atlantic salmon (*Salmo salar* L.) behaviour in sea-cages: a lagrangian approach. Aquaculture 288 (3–4), 196–204, URL http://www.sciencedirect.com/science/article/pii/S0044848608008533.

Gillibrand, P., Turrell, W., 1997. Simulating the dispersion and settling of particulate material and associated substances from salmon farms. Tech. rep., Marine Laboratory, Aberdeen, Report No. 3/97, Victoria Road, Aberdeen AB11 9DB, UK.

Gjøsæter, J., Otterå, H., Slinde, E., Nedreaas, K., Ervik, A., 2008. Effekter av spillfôr på marine organismer. Kyst og Havbruk, 52–55 (in Norwegian).

Jobling, M., 1985. Physiological and social constraints on growth of fish with special reference to Arctic charr, *Salvelinus alpinus* L. Aquaculture 44 (2), 83–90, URL http://www.sciencedirect.com/science/article/pii/0044848685900110.

Johansen, S., Jobling, M., 1998. The influence of feeding regime on growth and slaughter traits of cage-reared Atlantic salmon. Aquacult. Int. 6 (1), 1–17.

Juell, J.-E., 1995. The behaviour of Atlantic salmon in relation to efficient cage-rearing. Rev. Fish Biol. Fish. 5, 320–335, http://dx.doi.org/10.1007/BF00043005.

López-Olmeda, J., Noble, C., Sánchez-Vázquez, F., 2012. Does feeding time affect fish welfare? Fish Physiol. Biochem. 38 (1), 143–152, http://dx.doi.org/10.1007/s10695-011-9523-y.

MATLAB, 2014. version 8.4.0.150421 (R2014b). The MathWorks Inc., Natick, Massachusetts.

McDonald, J.H., 2009. Handbook of Biological Statistics, vol. 2. Sparky House Publishing, Baltimore, MD.

McDonald, J.H., 2014. Handbook of Biological Statistics. Sparky House Publishing, Baltimore, MD, URL http://www.biostathandbook.com/kruskalwallis.html.

Noble, C., Kadri, S., Mitchell, D.F., Huntingford, F.A., 2007. Influence of feeding regime on intraspecific competition, fin damage and growth in 1+ Atlantic salmon parr (*Salmo salar* L.) held in freshwater production cages. Aquacult. Res. 38 (11), 1137–1143, http://dx.doi.org/10.1111/j.1365-2109.2007.01777.x.

Noble, C., Kadri, S., Mitchell, D.F., Huntingford, F.A., 2008. Growth, production and fin damage in cage-held 0+ Atlantic salmon pre-smolts (*Salmo salar* L.) fed either (a) on-demand, or (b) to a fixed satiation–restriction regime: data from a commercial farm. Aquaculture 275 (1), 163–168, URL http://www.sciencedirect.com/science/article/pii/S0044848608000069.

Noble, C., Mizusawa, K., Suzuki, K., Tabata, M., 2007. The effect of differing self-feeding regimes on the growth, behaviour and fin damage of rainbow trout held in groups. Aquaculture 264 (1–4), 214–222, URL http://www.sciencedirect.com/science/article/pii/S0044848606009276.

Norwegian Directorate of Fisheries, 2013. Lønnsomhetsundersøkelse for matfiskproduksjon, URL http://www.fiskeridir.no/statistikk/akvakultur/loennsomhet/matfiskproduksjon-laks-og-regnbueoerret.

Oehme, M., Aas, T.S., Sørensen, M., Lygren, I., Åsgård, T., 2012. Feed pellet distribution in a sea cage using pneumatic feeding system with rotor spreader. Aquacult. Eng. 51, 44–52, URL http://www.sciencedirect.com/science/article/pii/S0144860912000568.

Oppedal, F., Dempster, T., Stien, L.H., 2011. Environmental drivers of Atlantic salmon behaviour in sea-cages: a review. Aquaculture 311 (1–4), 1–18, URL http://www.sciencedirect.com/science/article/pii/S0044848610007933.

Osborne, J., 2002. Notes on the use of data transformations. Pract. Assess. Res. Eval. 8 (6).

Pond, S., Pickard, G.L., 1983. Introductory Dynamical Oceanography, 2nd ed. Butterworth-Heinemann, Oxford, ISBN 0-7506-2496-5.

Rasmussen, R.S., Larsen, F.H., Jensen, S., 2007. Fin condition and growth among rainbow trout reared at different sizes, densities and feeding frequencies in high-temperature re-circulated water. Aquacult. Int. 15, 97–107, http://dx.doi.org/10.1007/s10499-006-9070-1.

Ruzzante, D.E., 1994. Domestication effects on aggressive and schooling behavior in fish. Aquaculture 120, 1–24, URL http://www.sciencedirect.com/science/article/pii/0044848694902178.

Ryer, C.H., Olla, B.L., 1996. Growth depensation and aggression in laboratory reared coho salmon: the effect of food distribution and ration size. J. Fish Biol. 48 (4), 686–694, http://dx.doi.org/10.1111/j.1095-8649.1996.tb01464.x.

Skøien, K.R., Alver, M.O., Alfredsen, J.A., 2014. A computer vision approach for detection and quantification of feed particles in marine fish farms. In: IEEE International Conference on Image Processing (ICIP), October 2014, pp. 1648–1652.

Skøien, K.R., Alver, M.O., Alfredsen, J.A., 2015. Modelling spatial surface pellet distribution from rotary pneumatic feed spreaders. In: Proceedings of the 23rd Mediterranean Conference on Control and Automation.

Skøien, K.R., Alver, M.O., Lundregan, S., Frank, K., Alfredsen, J.A., 2016. Effects of wind on surface feed distribution in sea cage aquaculture: a simulation study. In: European Control Conference ECC16.

Skretting, 2012. Fôr. Tech. rep., Skretting (in Norwegian).

Sørensen, M., 2012. A review of the effects of ingredient composition and processing conditions on the physical qualities of extruded high-energy fish feed as measured by prevailing methods. Aquacult. Nutr. 18 (3), 233–248, http://dx.doi.org/10.1111/j.1365-2095.2011.00924.x.

SPSS, 2015. IBM SPSS Statistics for Mac, Version 23.0. Released 2015. IBM Corp., Armonk, NY.

Sutherland, T., Amos, C., Ridley, C., Droppo, I., Petersen, S., 2006. The settling behaviour and benthic transport of fish feed pellets under steady flows. Estuaries Coasts 29 (5), 810–819, URL http://eprints.soton.ac.uk/44121/.

Symons, P.E.K., 1971. Behavioural adjustment of population density to available food by juvenile Atlantic salmon. J. Anim. Ecol. 40 (3), 569–587, URL http://www.jstor.org/stable/3438.

Talbot, C., 1993. Some biological and physical constraints to the design of feeding regimes for salmonids in intensive cultivation. In: Reinertsen, H., Dahle, A.A., Jùrgensen, L., Tvinnereim, K. (Eds.), Fish Farming Technology. Balkema, Rotterdam, pp. 19–26.

Talbot, C., Corneillie, S., Korsøen, Ø., 1999. Pattern of feed intake in four species of fish under commercial farming conditions: implications for feeding management. Aquacult. Res. 30 (7), 509–518, http://dx.doi.org/10.1046/j.1365-2109.1999.00369.x.

Ytrestøyl, T., Aas, T., Berge, G., Hatlen, B., Sørensen, M., Ruyter, B., Thomassen, M., Hognes, E., Ziegler, F., Sund, V., et al., 2011. Resource utilisation and eco-efficiency of Norwegian salmon farming in 2010. Nofima Rep. 53 (2011), 65.

Paper F Effects of wind on surface feed distribution in sea cage aquaculture: A simulation study (in press)

(Skøien et al., 2016d)
Skøien, K. R., Alver, M. O., Lundregan, S., Frank, K., and Alfredsen, J. A. Effects of wind on surface feed distribution in sea cage aquaculture: A simulation study (in press). In *European Control Conference ECC16*, 2016d

Errata:

- On p. 4, Figure 3: all "%" signs
  ...should have been:
  RMSE*100

Effects of Wind on Surface Feed Distribution in Sea Cage Aquaculture: A Simulation Study

Kristoffer Rist Skøien[1,*], Morten Omholt Alver[1,2], Sarah Lundregan[2], Kevin Frank[2] and Jo Arve Alfredsen[1]

***Abstract*— This study examines the simulated effects of wind on the spatial surface distribution of pelletized feed from rotary pneumatic spreaders which are used extensively in sea cage aquaculture. A robotic model of the spreader and external ballistic description of the pellet trajectories have been extended to include wind forces, and the spatial distribution is compared for different sized pellets in various wind fields. The results show that overall effects of wind on spatial pellet distribution is limited, however, there is a negative correlation between wind and surface coverage.**

I. INTRODUCTION

Global production of farmed Atlantic salmon (Salmo salar) has expanded from 297 to more than 2,087,000 tonnes from 1970 to 2013 [1]. Norway and Chile are major producers but production is also substantial in Australia, the Faroe Islands, Great Britain and North America [2]. The final and most extensive phase of the farming process is undertaken in the marine environment employing floating rectangular or circular sea cages where the latter usually have a circumference of 90-157 m and a depth of up to 48 m [2]. The current trend in salmon aquaculture points towards even larger production volumes. In Tasmania, cages up to 240 m circumference are in use and larger facilities located at more exposed sites are emerging as a new farming alternative. A single cage unit in Norway may currently hold a maximum of 200,000 individuals at a stocking density of 25 kg/m^2 [3]. The daily feed ration is often approximated to 1% of the biomass [4] and with a slaughter weight of 5 kg up to 10 tonnes feed/day will be administered to a single sea cage towards the end of the production cycle. At Norwegian salmon and trout farms close to 1.7 million tonnes of feed was used in 2014 worth close to €200 million [5] which represents around 50% of the total farming costs [6]. 7% of the feed are estimated to be lost into the surroundings [7] giving a substantial economic loss for the farmer and poor use of valuable resources [8]. Feed in the form of 3-12 mm diameter pellets [9] is stored on a local barge where compressed air is used to convey the pellets through pipes to the individual sea cages. Pellets are distributed across the water surface by a floating rotary pneumatic spreader (Fig. 1) situated in the center of the sea cage where the rotation and throw of pellets are both driven by the airflow. Questions have been raised with respect to whether such a method of feed distribution is satisfying concerning equal feed access for all individuals, feed loss and aggression levels within the sea cage. The spatial surface distribution from the rotary spreader provides the initial positions from which currents, turbulence and sink rate further transport and diffuse the pellets within the water column, and thereby contributes fundamentally to the pellet dispersion within the cage. Feed access is determined by the spatio-temporal feed distribution and ration size [10] and suboptimal feeding is related to both reduced and inefficient growth in Atlantic salmon [10]. The surface distribution from two spreaders was quantified empirically by [4] which showed that the spatial distribution was annular in nature and skewed towards one side. One might assume that wind will significantly increase the surface coverage, but that might not be the case as argued by this study. A robotic and ballistic description of a pneumatic spreader has been constructed [11] to enable simulation of different spreader configurations and the effects on the spatial feed distribution.

This study expands the spreader model [11] with a more comprehensive robotic model, a refined description of the ballistic transport of pellets as well as including the effects of wind in the equations. Results with different wind speeds and the subsequent effects on the surface distribution are presented.

II. SPREADER MODEL

A. Reference Frames

This section is based on [11] and provides a summary of the robotic and ballistic spreader model as well as the extensions presented in this study. The reference frames in the model are based on [12], [13], [14] and are all right-hand systems. The base frame (frame of origin) is situated in the center of the sea cage, considered inertial and defined according to *North-East-Down* (NED) and given by $\{O_a\} = (x_a, y_a, z_a)$. x_a points *North*, y_a *East* and z_a *Down* into the sea normal to the x_a, y_a water surface plane. The body-fixed frame of the spreader is given by $\{O_b\} = (x_b, y_b, z_b)$ and is fixed at the center of the buoy in the water plane (Fig. 1). x_b is directed towards the pneumatic feed pipe away from the spreader, y_b to the right seen from above and z_b down towards the counterweight. Finally, the center pipe fixed frame $\{O_c\} = (x_c, y_c, z_c)$ is located above the ball bearing on the rotating part of the spreader. The roll, pitch and yaw of the spreader $\{O_b\}$ with respect to the base frame $\{O_a\}$ is given by the Euler angles $\mathbf{\Theta}_{ab} = \begin{bmatrix}\phi_b & \theta_b & \psi_b\end{bmatrix}^T$

[1]Faculty of Information Technology, Mathematics and Electrical Engineering, department of Engineering Cybernetics, Norwegian University of Science and Technology NTNU, Trondheim, NO-7491, Norway

[2]SINTEF Fisheries and Aquaculture, Trondheim, NO-7465, Norway

*Corr. author: kristoffer.rist.skoien@itk.ntnu.no

This research has been funded by the Centre for Research-based Innovation in Aquaculture Technology (CREATE), SINTEF Sealab, Trondheim, NO-7465, Norway.

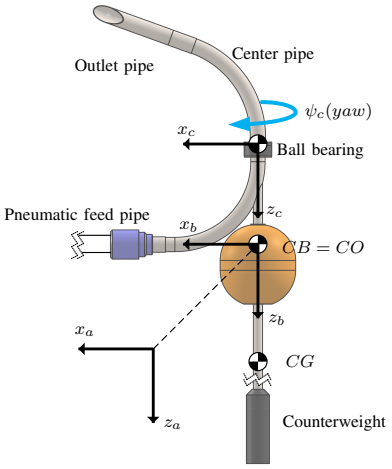

Fig. 1. Model of a pneumatic rotary feed spreader based on the "CF90 Double" (AKVA group, Bryne, Norway). A 450 mm radius center pipe and 600 mm outlet pipe was used in the experiment and the model. The base frame $\{O_a\}$ has been relocated for clarity, $\{O_b\}$ is fixed at the center of buoyancy and $\{O_c\}$ fixed to the center pipe. This figure is licensed under a Creative Commons BY-NC-SA license.

$\in \mathcal{S}^3$. Since the spreader is moored by three ropes at roughly 120° intervals to the sea cage it can not translate in the x_a, y_a plane and yaw rotation is restricted. The pseudo-sinusodial motion of the spreader caused by waves is expected to average out over time [11]. Consequently, $\psi_b = 0$ and the position vector O_a to O_b in the $\{O_a\}$ frame is given by $\boldsymbol{o}_b^a = \begin{bmatrix} x_b^a & y_b^a & z_b^a \end{bmatrix}^T = \begin{bmatrix} 0_b^a & 0_b^a & 0_b^a \end{bmatrix}^T \in \mathbb{R}^3$. The only degree of freedom between $\{O_b\}$ and $\{O_c\}$ is the rotation of the ball bearing, hence the rotation between the two can be described by $\boldsymbol{\Theta}_{bc} = \begin{bmatrix} 0 & 0 & \psi_c \end{bmatrix}^T \in \mathcal{S}^3$.

B. Kinematic Model

To determine the position and attitude of the outlet pipe opening where the pellets begin their ballistic trajectory as a function of the attitude given by $\begin{bmatrix} \phi_b & \theta_b & \psi_c \end{bmatrix}^T$, a robotic description and the Denavit-Hartenberg (DH) convention [13], [14] was used in [11]. The same model is applied here with some extensions. The spreader is modelled as a robotic manipulator with n joints and $n+1$ links. Adhering to established robotic conventions [13], [14] the joints and links are sequentially numbered starting from the base frame which is given by

$$\{O_a\} = (x_a, y_a, z_a) = \{O_0\} = (x_0, y_0, z_0) \tag{1}$$

[11] to the outlet pipe opening (end effector) $\{O_n\}$. $\{O_a\}...\{O_c\}$ is used for the physical system and $\{O_0\}...\{O_n\}$ used for the robotic description. The first joint aligns z_1 in order to adhere to the DH convention followed by two joints describing the roll and pitch of the spreader analogous to a 2 degrees of freedom (DOF) spherical wrist. This is followed by the center pipe yaw, the static center pipe bend of the spreader, a joint allowing rotation of the outlet pipe to alter the angle pellets are thrown with respect to the water and the final bend before the outlet pipe opening. As opposed to [11], in this study the stochastic angle which the pellets exit the outlet pipe is modelled as another 2 DOF spherical joint at the end of the outlet pipe allowing angular variation to be added to the attitude of the origin of the ballistic trajectory. This horizontal and vertical variance is added by

$$\theta_{w,vert} = \mathcal{N}(0, \sigma_{out}^2) u_{pel} \tag{2a}$$
$$\theta_{w,horz} = \mathcal{N}(0, \sigma_{out}^2) u_{pel} \tag{2b}$$

The rotation and translation from $\{O_0\}$ to $\{O_n\}$ is given by

$$\boldsymbol{H} = \begin{bmatrix} \boldsymbol{R}_n^0 & \boldsymbol{o}_n^0 \\ \boldsymbol{0}_{1\times 3} & 1 \end{bmatrix} \tag{3}$$

which is a homogeneous transformation matrix [13], $\boldsymbol{R}_n^0$ is a rotation matrix and $\boldsymbol{o}_n^0 = \begin{bmatrix} x_n^0 & y_n^0 & z_n^0 \end{bmatrix}^T$ is the vector giving the position of $\{O_n\}$ relative to $\{O_0\}$. $\boldsymbol{H}$ is given by a series of joints

$$\boldsymbol{H} = \boldsymbol{T}_n^0(\boldsymbol{q}) = \prod_{i=1}^{n} \boldsymbol{A}_i^{i-1}(q_i) = \prod_{i=1}^{n} \begin{bmatrix} \boldsymbol{R}_i^{i-1}(q_i) & \boldsymbol{o}_i^{i-1}(q_i) \\ \boldsymbol{0}_{1\times 3} & 1 \end{bmatrix} \tag{4}$$

$\boldsymbol{q} = \begin{bmatrix} q_1 & \cdots & q_n \end{bmatrix}^T$ is the joint variables given by either $q_i = \theta_i$ or $q_i = d_i$ if the joint is revolute or prismatic respectively. The full description as a function of the aforementioned joint variables is given by

$$\boldsymbol{H} = \boldsymbol{A}_1^0(q_1)...\boldsymbol{A}_{11}^{10}(q_{11}) \tag{5}$$

This description is not minimal as it includes two additional joints for visualization purposes and hence does not strictly adhere to the DH convention. Based on [11] the vector describing the ballistic origin of the pellets is defined as

$$\boldsymbol{\xi} = \begin{bmatrix} \xi_x & \xi_y & \xi_z \end{bmatrix}^T = \boldsymbol{o}_n^{n-2} = \boldsymbol{o}_n^0 - \boldsymbol{o}_{n-2}^0 \tag{6}$$

which is then normalized giving the vector $\hat{\boldsymbol{\xi}}$.

III. EXTERNAL BALLISTIC MODEL

The external ballistic description is based on [11] and modified with the inclusion of wind as well as a more accurate and dynamic description of the drag coefficient. Let u be the speed of a given pellet upon exiting the outlet pipe of the spreader. The two bends of the spreader will negatively affect the pellet speed as solids get separated from the transport fluid [15] and collide with the bend wall. We assume that most pellets will slide along the outer edge of the bend as they pass through the spreader. The first bend which changes the pellet direction from horizontal to vertical will negatively affect all pellets. If the following bend (the outlet pipe) points in the direction of the feed pipe ($\psi_c = 0$) or in fact the range $\psi_c = [3\pi/2, \pi/2]$ (clockwise) pellets will experience a continuous sweeping bend. On the other hand, at $\psi_c = (\pi/2, 3\pi/2)$ there will be an additional impact point

likely resulting in reduced speed which will be most extreme at $\psi_c = \pi$. This effect is modelled by Eq. 7:

$$u = \begin{cases} u_{pel} + cos(\psi_c) * k_\psi + \mathcal{N}(0, \sigma^2_{pel}) & \text{if } \frac{\pi}{2} < \psi_c < \frac{3\pi}{2} \\ u_{pel} + \mathcal{N}(0, \sigma^2_{pel}) & \text{else} \end{cases} \tag{7}$$

where u_{pel} is the speed of the pellet in the vertical section of the spreader before passing the ball bearing, $cos(\psi_c) * k_\psi$ is a simplified description of the speed reduction experienced as a function of ψ_c and k_ψ is a tuning parameter. $\mathcal{N}(0, \sigma^2_{pel})$ represents a Gaussian term to account for the variance of the pellet speed. The velocity components in $\mathbb{R}^3$ are simply obtained by

$$\boldsymbol{v} = \begin{bmatrix} v_x & v_y & v_z \end{bmatrix}^T = \hat{\boldsymbol{\xi}} u \tag{8}$$

as in [11]. A wind field is introduced and considered spatio-temporally constant with no component in z_a:

$$\boldsymbol{w} = \begin{bmatrix} w_x & w_y & 0 \end{bmatrix}^T \tag{9}$$

The relative velocity of a pellet to the wind may be expressed by

$$\Delta v = \mid \Delta \boldsymbol{v} \mid = \mid \boldsymbol{v} - \boldsymbol{w} \mid \tag{10}$$

The pellets are modelled as a point mass with weight m and area A. From [16] the drag force can be expressed as:

$$F_d = -\frac{1}{2} C_{d\infty} \rho_{air} A_{proj} \Delta v^2 \tag{11}$$

The air density is set to ρ_{air} = 1.2 kg/m^3, viscosity $\mu_{air} = 1.8{*}10^{-5}$ Ns/m^2 [16], A_{proj} is the projected (frontal) area and $C_{d\infty}$ is the drag coefficient in an unbounded fluid. $C_{d\infty} = f(R_e)$ and

$$R_e = \frac{\rho_{air} \Delta v d_{sph}}{\mu_{air}} \tag{12}$$

where d_{sph} is the diameter of a sphere which is volume equivalent to the pellet. In [11] pellets were treated as spherical particles. However, pellets are of a cylindrical shape characterized by their diameter d_p and height h_p and the standard drag curves does not describe these non-spherical particles well [15]. To describe the sphericity of a particle, a shape factor is introduced [17].

$$\psi_{sph} := A_{sph} / A \tag{13}$$

ψ_{sph} is given as the surface area of the volume equivalent sphere divided by the pellet surface area and is the most commonly used shape factor descriptor [15]. For pelleted fish feed $d_p \approx h_p \rightarrow \psi_{sph} = 0.874$. In [11] $C_{d\infty}$ was fixed as there was no wind present, hence R_e remains fairly constant through the ballistic path of a pellet and a suitable fixed value of $C_{d\infty}$ could be used. With the introduction of wind however, R_e may vary substantially and a dynamic description must be obtained. The description by [18] was used to obtain the dynamic value of $C_{d\infty}$ because of its low complexity and correspondence with empirical results [19].

$$C_{d\infty} = \frac{24}{R_e}(1 + (8.716 exp(-4.0655 \psi_{sph})) \\ R_e^{(0.0964 + 0.5565 \psi_{sph})}) + \frac{73.69 R_e exp(-5.0748 \psi_{sph})}{R_e + 5.378 exp(6.2122 \psi_{sph})} \tag{14}$$

Invoking Newton's second law and using [20] the motion of a pellet can be described on vector form

$$\frac{d\Delta \boldsymbol{v}}{dt} = -\frac{\kappa}{m} C_{d\infty}(\Delta \boldsymbol{v}, \psi_{sph}) \parallel \Delta \boldsymbol{v} \parallel \Delta \boldsymbol{v} + \boldsymbol{g} \tag{15}$$

$\kappa = \frac{1}{2} \rho_{air} A_{proj}$ and $\boldsymbol{g} = \begin{bmatrix} 0 & 0 & g \end{bmatrix}^T$, $g = 9.81$ m/s^2. Since $\boldsymbol{w}$ is constant this can be expressed as

$$\frac{dv_x}{dt} = -\frac{\kappa}{m} C_{d\infty}(\Delta v_x, \psi_{sph}) \Delta v_x ||\Delta \boldsymbol{v}|| \tag{16a}$$
$$\frac{dv_y}{dt} = -\frac{\kappa}{m} C_{d\infty}(\Delta v_y, \psi_{sph}) \Delta v_y ||\Delta \boldsymbol{v}|| \tag{16b}$$
$$\frac{dv_z}{dt} = -\frac{\kappa}{m} C_{d\infty}(\Delta v_z, \psi_{sph}) \Delta v_z ||\Delta \boldsymbol{v}|| + g \tag{16c}$$
$$\frac{ds_x}{dt} = v_x \tag{16d}$$
$$\frac{ds_y}{dt} = v_y \tag{16e}$$
$$\frac{ds_z}{dt} = v_z \tag{16f}$$

Finally, to the describe the variability in the ballistic trajectories the following description from [11] was used

$$s_{x,imp} = s_x(T) + \mathcal{N}(0, \sigma^2_s) T \tag{17a}$$
$$s_{y,imp} = s_y(T) + \mathcal{N}(0, \sigma^2_s) T \tag{17b}$$

where $s_{x,imp}$ and $s_{y,imp}$ are the impact points in the 2D water plane and T is the total flight time from $t = 0$ until $s_z(t) >= 0$.

IV. EXPERIMENT

For the purpose of tuning and model validation, an experiment was undertaken in July 2014 at Rataren (Frøya, Norway). The *CF90 Double* spreader (AKVA group, Bryne, Norway) was used for the experiment connected to the feed barge via 450 m pipe transporting 9 mm pellets (Skretting Biostar; Optiline Premium XL, 2500 50A). Styrofoam boxes measuring 40 × 80 cm clamped together on the long side were placed in a cross pattern at 90° intervals away from the spreader with 26 boxes in each direction. As there was a 0.75 m gap between the spreader and innermost boxes, the distance from the center to the end of each row of boxes totaled 11.15 m. The first row of boxes was placed as close as possible to the feed pipe in the $+x_a$ direction. Hence, the next three clockwise rows captured a 80 cm wide area in $+y_a$, $-x_a$ and $-y_a$. Three replicates were conducted at 20 m/s conveying airspeed. For all replicates the spreader was allowed to spin up using only air before feeding commenced for one minute at 20 kg/min which led to the total capture of 8287 pellets. Wind speed was low for the three replicates and measured to be 0.92, 1.14 and 1.47 m/s. The full details of this experiment have not been elaborated upon in this

study, but the experimental results from the three 20 m/s airspeed replicates have been used to tune the parameters of the model.

V. SIMULATION CONFIGURATION

To visualize the effects of pellet size and wind the simulations were run across two different pellet sizes according to Tab. I with four different wind conditions. Across all

TABLE I

EIGHT SIMULATION SCENARIOS USING TWO PELLET SIZES AND FOUR DIFFERENT WIND VELOCITIES IN THE $+x_a$ DIRECTION. *THE 9 MM 0 M/S SCENARIO WAS USED TO TUNE THE MODEL BASED ON EXPERIMENTAL DATA.

Dia. [mm]	Weight [g]	Proj. Area [mm^2]	Wind [m/s]			
9 mm	0.64	81	0*	5	10	15
6 mm	0.19	36	0	5	10	15

simulations the homogeneous wind field only acted along $+x_a$. The scenario 9 mm 0 m/s was used to tune the parameters u_{pel}, σ_{pel}, k_ψ, σ_{out} and σ_s based on the results from the experimental study. The model was run with the x_a, y_a surface plane discretized into 5 $\times$ 5 cm bins. The contents of bins corresponding to the position of the Styrofoam boxes in the experiment have been summed hence the pellet count in each virtual 40 $\times$ 80 cm box is the sum of 8 $\times$ 16 bins which is the base of the following plots. For surface coverage calculations, any pellets present in a 40 $\times$ 40 cm area is classified as covered. The results were obtained with the parameters: $u_{pel} = 6.8$ m/s, $\sigma_{pel} = 0.7$ m/s, $k_\psi = 1.1$, $\sigma_{out} = 1.5°$ and $\sigma_s = 1.25$ m. The 9 mm simulations were run with $d_p = h_p = 0.9$ mm and $m = 0.64$ g. 6 mm pellet simulations were run with identical model parameters except $d_p = h_p = 6$ mm and $m = 0.19$ g.

The proposed model was implemented in MATLAB and each ballistic trajectory calculated using *ODE45* with 360 pellets released for each revolution of ψ_c. A total of 240 revolutions $\rightarrow N = 86.400$ pellets were run for each of the simulated scenarios.

VI. RESULTS

Fig. 2 presents the manually tuned model and the corresponding experiment.

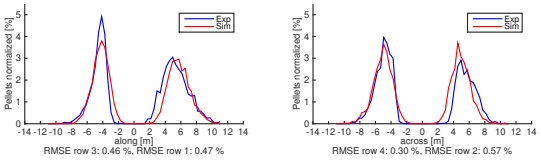

Fig. 2. Comparison of the manually tuned model with no wind present and the experimental results. Normalized concentration of pellets in virtual boxes. CC-BY-SA

Tab II presents the percentage of the surface area containing pellets in the different simulation scenarios providing insight into the effects of wind on overall pellet distribution. This measure is however quite crude as it is a binary representation of each bin and hence do not take into account the actual number of pellets in a given bin. A secondary measure of spatial uniformity in the form of global Shannon entropy (GSE) [21] given by

$$p_i = n_i / \sum_{i=1}^{N_{bin}} n_i = n_i / N \tag{18}$$

$$GSE = -\Big[\sum_{i=1}^{N_{bin}} p_i log_2(p_i)\Big] / log_2(N_{bin}) \tag{19}$$

is also presented in Tab. II. A coarser grid has been selected for this statistic with a total of $N_{bin} = 256$ bins and n_i is the number of pellets in a given bin. Given complete spatial randomness GSE = 1 and a small value of GSE indicates a low level of uniformity [21].

TABLE II

SIMULATED SURFACE COVERAGE WITH RESPECT TO A 157 M CIRCUMFERENCE SEA CAGE AND CENTER OF MASS FOR THE SURFACE DISTRIBUTION.

Dia. [mm]	Wind [m/s]	0	5	10	15
9 mm	Surface cover. [%]	14.3	14.3	13.0	12.4
	GSE	.570	.569	.548	.543
	Cnt. mass $+x_a$ [m]	0.37	1.17	2.20	3.64
6 mm	Surface cover. [%]	13.1	13.1	11.8	11.2
	GSE	.556	.555	.534	.520
	Cnt. mass $+x_a$ [m]	0.33	1.37	2.67	4.45

Fig. 3 and 4 presents the normalized concentration of pellets in the virtual boxes in the *along* and *across* directions.

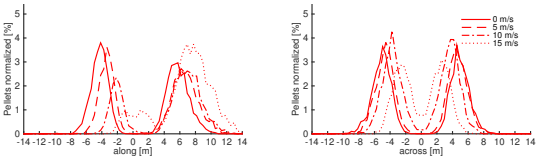

Fig. 3. Comparison of simulated effects on 9 mm pellets at 0, 5, 10 and 15 m/s wind speed. CC-BY-SA

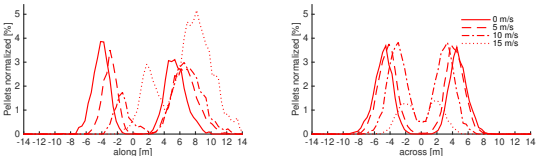

Fig. 4. Comparison of simulated effects on 6 mm pellets at 0, 5, 10 and 15 m/s wind speed. CC-BY-SA

Fig. 5 and 6 presents a heat map of the surface distribution of 9 mm pellets at 0 and 10 m/s wind respectively.

VII. DISCUSSION

A. Results

As can be observed in Fig. 2 the simulated results and experimental data correspond well which is to be expected as

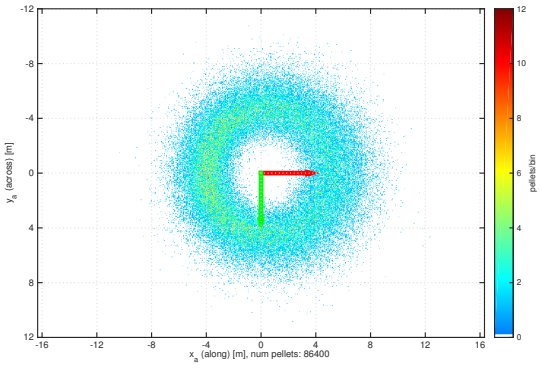

Fig. 5. Surface distribution of 86400 9 mm pellets, 5 × 5 cm grid. No wind present. x_a and y_a indicated by a red and green arrow respectively. CC-BY-SA

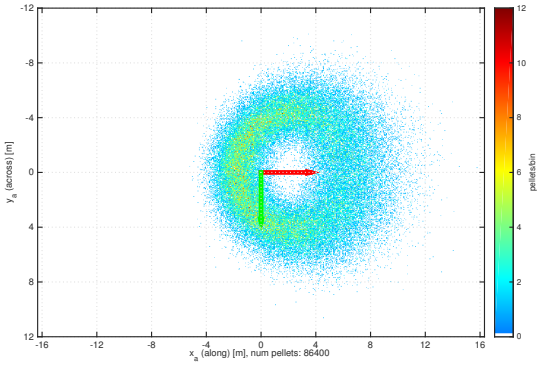

Fig. 6. Surface distribution of 86400 9 mm pellets, 5 × 5 cm grid. 10 m/s wind in the $+x_a$ direction. x_a and y_a indicated by a red and green arrow respectively. CC-BY-SA

the parameters of the model in this wind simulation study has been tuned based on this scenario. Automated tuning through for instance least squares minimization between simulated and experimental surface coverage might be an option but cumbersome due to the high number of pellets, the stochastic nature of several model parameters and the likelihood of multiple local minima. The main cause of the observed difference in Fig. 2 is probably due to the model being run with a perfectly vertical spreader. This configuration was chosen in order to generalize the results making them applicable to the most realistic or average scenario of a vertical spreader. However, the spreader is sensitive to the mounting of the feed pipe which may cause a torque and accordingly lead to an rotational offset most prominent in roll. There has probably been a roll offset in the experiments which may explain the different concentrations of pellets in the "across" boxes in Fig. 2. Taking experimental results during strong winds into account would have been greatly beneficial but such data is challenging to obtain.

The surface coverage and the respective wind speed can be seen in Tab. II. As stronger wind speeds are applied in the 9 mm scenario it is evident from Fig. 3 that wind leads to decreased concentrations and shorter throw upwind from the spreader and accordingly longer average throw lengths and increased concentrations downwind as should be expected. There is a minor decreasing trend in the corresponding surface coverage and GSE from 0 wind to 15 m/s (Tab. II). It seems that stronger wind decreases the spatial distribution upwind and increases it downwind as well as the net spatial distribution being negatively correlated with wind speed. In the across direction (Fig. 3), increased wind reduces the throw length into the virtual boxes. This result is as expected as pellets thrown in the across directions will curve towards $+x_a$. For the 6 mm simulations in Fig. 4 identical effects can be seen. The 6 mm pellets are carried further in $+x_a$ relative to the 9 mm pellets as is expected due to the large change in m relative to A_{proj}.

Accurately describing u_{pel} in such a multi-particle system is complex [15] due to gas expansion along the pneumatic transport pipe, multi-particle interactions, electrostatic effects and the combination of horizontal and vertical pellet transport. The parameter σ_{out} has been manually tuned in this study. However, experimental work has been undertaken mounting a high speed camera to the outlet pipe of the spreader providing new insight into the behavior of pellets exiting the spout as a function of ψ_c. This data is still being analyzed and will lead to a more accurate description of pellet behavior at the outlet pipe opening.

The Jacobian has not been considered in dis study since $\dot{q}_{psi}$ is the only non-zero element in $\dot{\boldsymbol{q}}$. This rotation causes a tangential velocity component at the outlet pipe opening. However, since the rotation is driven by the airflow due to the angled cut of the outlet pipe, it is assumed that the airflow will cancel this velocity component.

The simulations cover an array of wind speeds spanning what may be commonly experienced at a Norwegian fish farm. For increasing wind speed across both pellet sizes the surface coverage shows an overall decreasing trend. Due to the annular surface feed pattern created by the spreader, wind does not seem to assist in providing any increased spatial distribution of feed. Evenly distributing feed is believed to be beneficial for the fish in the form of reduced aggression levels and growth promotion [22], [23], [24], [25], [26], [27], [28], [29]. Simulation results from [30] increases this belief, albeit up to a certain point where a too extensive spread pattern combined with strong currents may lead to feed loss through the cage wall.

The results from this study indicate that wind has a limited influence on the surface pellet distribution compared to the overall area of the sea cage. In addition, winds up to 15 m/s generally lead to a decrease in spatial distribution but also seems to result in higher local concentrations of feed pellets. This suggests that design of spreaders may not rely on wind to further increase the feed distribution. Finally, it is evident that wind may shift the center of pellet mass by over 4 meters. The spreader tends to be mounted in the center of the cage, so any surface translation of pellets will lead to

feed being thrown closer to the cage wall, increasing the likelihood of feed loss in high currents.

B. Further work

Analysing the results of the high speed camera at the outlet pipe will provide new insight into the pellet velocity and the angles from which pellets exit the spreader. A more thorough investigation should also be performed with respect to the external ballistic properties of feed pellets. The roughness of the pellet should be determined more accurately as this will affect the drag, and a more accurate model of wind diffusion should be implemented. Further investigation into the effects from these simulations on fish behaviour, subsurface feed distribution and feed loss are planned. The results from the current model will be used to seed the surface distribution in a full sea cage model [30], [31] and the effects of wind and spreader configurations can be investigated in depth.

VIII. CONCLUSION

In this study, a pneumatic rotary feed spreader model has been extended by implementing a new representation of how pellets leave the spreader, taking into account the sphericity factor and providing a new manner of calculating the drag coefficient. The present study also provides verification through an experiment performed with a rotary spreader identical to the one the model is based upon. Simulations of various pellet sizes in wind fields have been performed and elaborated upon. The results indicate that wind has a limited effect on surface coverage, however, increasing wind is negatively correlated with coverage. The center of mass of the pellet cloud may be shifted by over four meters at 15 m/s winds depending on the pellet size.

ACKNOWLEDGMENT

We appreciate the assistance of Morten Malm and Ingolf Lygren at AKVA group.

REFERENCES

[1] fao.org, "Available from: http://www.fao.org/fishery/statistics/global-aquaculture-production/en," 2015.

[2] F. Oppedal, T. Dempster, and L. H. Stien, "Environmental drivers of atlantic salmon behaviour in sea-cages: A review," *Aquaculture*, vol. 311, no. 1–4, pp. 1 – 18, 2011.

[3] Norwegian Ministry of Fisheries and Coastal Affairs, "Aquaculture operations regulations with remarks. https://lovdata.no/dokument/SF/forskrift/2008-06-17-822 (In Norwegian)," 2008.

[4] M. Oehme, T. S. Aas, M. Sørensen, I. Lygren, and T. Åsgård, "Feed pellet distribution in a sea cage using pneumatic feeding system with rotor spreader," *Aquacultural Engineering*, vol. 51, no. 0, pp. 44–52, 11 2012.

[5] Norwegian Directorate of Fisheries, *Fôrforbruk 2014*, www.fiskeridir.no, 2014.

[6] Norwegian Directorate of Fisheries, *Lønnsomhetsundersøkelse for matfiskproduksjon*, 2013.

[7] J. Gjøsæter, H. Otterå, E. Slinde, K. Nedreaas, and A. Ervik, "Effekter av spillfôr på marine organismer (In Norwegian)," *Kyst og Havbruk*, pp. 52–55, 2008.

[8] J. Alfredsen, B. Holand, T. Solvang-Garten, and I. Uglem, "Feeding activity and opercular pressure transients in atlantic salmon (salmo salar l.): application to feeding management in fish farming," in *Developments in Fish Telemetry*, P. Almeida, B. Quintella, M. Costa, and A. Moore, Eds., vol. 195 of *Developments in Hydrobiology 195*, pp. 199–207. Springer Netherlands, 2007.

[9] Skretting, "Fôr (In Norwegian)," Tech. Rep., Skretting, 2012.

[10] J.-E. Juell, "The behaviour of atlantic salmon in relation to efficient cage-rearing," *Reviews in Fish Biology and Fisheries*, vol. 5, pp. 320–335, 1995.

[11] K. R. Skøien, M. O. Alver, and J. A. Alfredsen, "Modelling spatial surface pellet distribution from rotary pneumatic feed spreaders," in *Proceedings of the 23rd Mediterranean Conference on Control and Automation*, 2015.

[12] T. I. Fossen, *Handbook of marine craft hydrodynamics and motion control*, John Wiley & Sons, 2011.

[13] M. W. Spong, S. Hutchinson, and M. Vidyasagar, *Robot modeling and control*, John Wiley & Sons, Hoboken, NJ, 1 edition, 2006.

[14] B. Siciliano, L. Sciavicco, L. Villani, and G. Oriolo, *Robotics: modelling, planning and control*, Springer Science & Business Media, 2009.

[15] G. Klinzing, F. Rizk, R. Marcus, and L. Leung, *Pneumatic Conveying of Solids: A Theoretical and Practical Approach*, Dordrecht: Springer Science+ Business Media BV, 2010.

[16] F. White, *Fluid mechanics*, McGraw-Hill Higher Education, 2011.

[17] H. Wadell, "The coefficient of resistance as a function of reynolds number for solids of various shapes," *Journal of the Franklin Institute*, vol. 217, no. 4, pp. 459 – 490, 1934.

[18] A. Haider and O. Levenspiel, "Drag coefficient and terminal velocity of spherical and nonspherical particles," *Powder Technology*, vol. 58, no. 1, pp. 63 – 70, 1989.

[19] R. Chhabra, L. Agarwal, and N. Sinha, "Drag on non-spherical particles: an evaluation of available methods," *Powder Technology*, vol. 101, no. 3, pp. 288 – 295, 1999.

[20] S. Ray and J. Fröhlich, "An analytic solution to the equations of the motion of a point mass with quadratic resistance and generalizations," *Archive of Applied Mechanics*, pp. 1–20, 2014.

[21] K. M. Kam, L. Zeng, Q. Zhou, R. Tran, and J. Yang, "On assessing spatial uniformity of particle distributions in quality control of manufacturing processes," *Journal of Manufacturing Systems*, vol. 32, no. 1, pp. 154–166, 2013.

[22] J. Attia, S. Millot, C. Di-Poï, M.-L. Bégout, C. Noble, F. Sanchez-Vazquez, G. Terova, M. Saroglia, and B. Damsgård, "Demand feeding and welfare in farmed fish," *Fish Physiology and Biochemistry*, vol. 38, pp. 107–118, 2012.

[23] B. Olla, M. Davis, and C. Ryer, "Foraging and predator avoidance in hatchery-reared pacific salmon: achievement of behavioral potential," *The Importance of Feeding Behaviour for the Efficient Culture of Salmonid Fishes*, pp. 5–13, 1992.

[24] C. Ryer and B. Olla, "Agonistic behavior in a schooling fish: form, function and ontogeny," *Environmental Biology of Fishes*, vol. 31, no. 4, pp. 355–363, 1991.

[25] J. Thorpe, C. Talbot, M. Miles, C. Rawlings, and D. Keay, "Food consumption in 24 hours by atlantic salmon (salmo salar l.) in a sea cage," *Aquaculture*, vol. 90, no. 1, pp. 41 – 47, 1990.

[26] S. Kadri, F. Huntingford, N. Metcalfe, and J. Thorpe, "Social interactions and the distribution of food among one-sea-winter atlantic salmon (salmo salar) in a sea-cage," *Aquaculture*, vol. 139, pp. 1 – 10, 1996.

[27] J. Thorpe and C. Y. Cho, "Minimising waste through bioenergetically and behaviourally based feeding strategies," *Water Science and Technology*, vol. 31, no. 10, pp. 29–40, 1995.

[28] C. H. Ryer and B. L. Olla, "Growth depensation and aggression in laboratory reared coho salmon: the effect of food distribution and ration size," *Journal of Fish Biology*, vol. 48, no. 4, pp. 686–694, 1996.

[29] J. Thomassen and O. Lekang, "Optimal distribution of feed in sea cages," *Fish Farming Technology, Balkema, Rotterdam*, pp. 439–442, 1993.

[30] M. O. Alver, J. A. Alfredsen, and T. Sigholt, "Dynamic modelling of pellet distribution in atlantic salmon (salmo salar l.) cages," *Aquacultural Engineering*, vol. 31, no. 1-2, pp. 51 – 72, 2004.

[31] M. O. Alver, K. R. Skøien, M. Føre, T. S. Aas, M. Oehme, and J. A. Alfredsen, "Modelling of surface and 3d pellet distribution in atlantic salmon (salmo salar l.) cages," *Aquacultural Engineering*, vol. 72-73, pp. 20 – 29, 2016.

Paper G Feed spreaders in sea cage aquaculture - Motion characterization and measurement of spatial pellet distribution using an unmanned aerial vehicle.

(Skøien et al., 2016e)
Skøien, K. R., Alver, M. O., Zolich, A. P., and Alfredsen, J. A. Feed spreaders in sea cage aquaculture - Motion characterization and measurement of spatial pellet distribution using an unmanned aerial vehicle. *Computers and Electronics in Agriculture*, 129:27 – 36, 2016e. ISSN 0168-1699. doi: http://dx.doi.org/10.1016/j.compag.2016.08.020

Computers and Electronics in Agriculture 129 (2016) 27–36

Contents lists available at ScienceDirect

Computers and Electronics in Agriculture

journal homepage: www.elsevier.com/locate/compag

Feed spreaders in sea cage aquaculture – Motion characterization and measurement of spatial pellet distribution using an unmanned aerial vehicle

Kristoffer Rist Skøien [a,*], Morten Omholt Alver [a,b], Artur Piotr Zolich [a,c], Jo Arve Alfredsen [a,c]

[a] NTNU, Norwegian University of Science and Technology, Department of Engineering Cybernetics, NO-7491 Trondheim, Norway
[b] SINTEF Fisheries and Aquaculture, NO-7465 Trondheim, Norway
[c] Centre for Autonomous Marine Operations and Systems (NTNU AMOS), Department of Engineering Cybernetics, NTNU, Norwegian University of Science and Technology, NO-7491 Trondheim, Norway

ARTICLE INFO

Article history:
Received 27 May 2016
Received in revised form 6 July 2016
Accepted 22 August 2016

Keywords:
Computer vision
Feed distribution
Pneumatic rotary feed spreader
Sea cage aquaculture
Unmanned aerial vehicle

ABSTRACT

Pneumatic rotary feed spreaders represent essential equipment in the feeding system of present day industrial-scale sea cage aquaculture. This study presents experimentally obtained attitude measurements and corresponding surface distribution patterns of pellets in order to characterize the dynamic behavior and performance of such spreaders. Spreader attitude and direction were measured by employing an attitude and heading reference system along with a rotary encoder. In addition, an unmanned aerial vehicle (UAV) was used to record pellet surface impacts from the air, and the position and direction of the spreader was obtained by applying computer vision methods to the recorded video. The proposed UAV method was fast to deploy, requires minimal equipment installation and presents a viable alternative to the approach of collecting pellets manually using Styrofoam boxes as reported in earlier studies. The findings from this study may be used as a base for further development and refinement with respect to using an UAV to observe the performance and spatial pellet distribution from various feed spreaders used in aquaculture. Such a tool may be valuable for farmers and equipment producers which may easily evaluate the performance of various spreader designs. In addition, the results serve as valuable input for parametrization and validation of mathematical feed spreader models.

1. Introduction

Atlantic salmon (*Salmo salar*) farming has over the last few decades grown to become a major source of food and the business has become a significant employer and contributor to the national income of several countries (Oppedal et al., 2011). Annual global production has been able to increase to over 2,087,000 tonnes (FAO, 2015) due to continuous knowledge-based improvements and optimizations of the farming process. After an initial hatching and growth period which takes place in indoor tanks, the salmon smolts are transferred to floating sea cages where the main part of the grow-out phase takes place. These cages are typically cylindrical with a diameter of 29–50 m and depth down to 48 m (Oppedal et al., 2011). However, 76 m diameter cages are currently in use in Tasmania, and efforts are being directed towards development of even larger structures for deployment in more exposed coastal and offshore locations. According to Norwegian legislation, one cage may hold a maximum of 200,000 individuals and the stocking density is limited to 25 kg/m^3 (Norwegian Ministry of Fisheries and Coastal Affairs, 2008). Given a slaughter weight of 5 kg/fish and a daily feed ration of 1% (Oehme et al., 2012), 10 tonnes of feed per day may be distributed in a single cage with each farming site typically consisting of 4–16 cages. Feed constitutes close to 50% of all farming costs (Norwegian Directorate of Fisheries, 2015) and about 1.7 million tonnes of feed were used at Norwegian salmon and Trout farms in 2014, worth close to €2000 million (Norwegian Directorate of Fisheries, 2014). Substantial economic incentives thus exist with respect to optimization of feed utilization.

Feed pellets are cylindrical, 3–12 mm in diameter with a specific density that is slightly higher than salt water allowing the pellets to sink at 6–20 cm/s. For the majority of the growth phase, a centrally located pneumatic rotary spreader (Fig. 1) handles the feed distribution across the water surface. Feed is transported to the site by ship and offloaded into silos on a local barge which

* Corresponding author.
E-mail address: kristoffer.rist.skoien@itk.ntnu.no (K.R. Skøien).

http://dx.doi.org/10.1016/j.compag.2016.08.020
0168-1699/

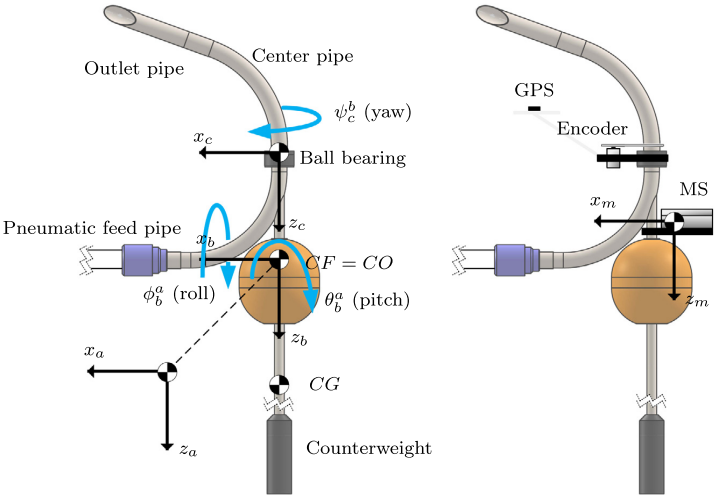

Fig. 1. The spreader with reference system definitions and with the measurement system (MS) mounted. Figure based on Skøien et al. (2016). In this figure the center pipe points in the direction of the feed pipe, $\psi_c^b = 0$ or known as a "*U*" configuration due to the single U-bend the pellets experience through the spreader.

typically handles feed delivery and monitoring of an array of sea cages. A set of blowers supply compressed air which propels pellets along feed pipes to the individual sea cages. The outlet pipe of the spreader has a spiral shape and is cut at an angle which causes the airflow to create a torque about the vertical (z_c) axis, inducing the rotation of the center and outlet pipe. The airflow is the driving force for both the rotation as well as the feed throw and pellets are expected to leave the spreader at about 6.6–9.4 m/s (Kevin Frank, pers. comm.) depending on airspeed, spreader configuration and length of the feed pipe. As a result the spreader creates an annular feed distribution pattern across the surface (Oehme et al., 2012; Skøien et al., 2016).

The spatiotemporal feed distribution within the sea cages is an important factor as it links to fish welfare, aggression, growth rate and feed loss. In Atlantic salmon, suboptimal feed intake is related to inefficient and reduced growth (Einen et al., 1999). Confinement of spatial and temporal availability or the amount of feed should not occur so fish may forage unrestrictedly (Talbot et al., 1999) and these factors also affect growth variation and aggression (Olla et al., 1992). The feed availability is a central factor in achieving efficient production (Juell, 1995) and a highly localized delivery of feed may lead to monopolization by dominant individuals (Juell, 1995).

Summaries by Ruzzante (1994), Attia et al. (2012) and Talbot (1993) discusses relations between agonistic behavior and feeding in salmonids, and it is likely that large distribution of feed will reduce agonistic behavior and positively affect growth (Thorpe et al., 1990; Ryer and Olla, 1991; Olla et al., 1992; Thomassen and Lekang, 1993; Thorpe and Cho, 1995; Ryer and Olla, 1996; Kadri et al., 1996; Attia et al., 2012). However, one should keep in mind that salmonids do well at adapting to different feeding regimes (Talbot, 1993; Thorpe and Cho, 1995; Talbot et al., 1999; López-Olmeda et al., 2012). Feed loss from commercial farms have been estimated to 7% (Gjøsæter et al., 2008) which results in poor resource utilization (Thorpe and Cho, 1995; Alfredsen et al., 2007).

These studies warrant the belief that spatiotemporal feed distribution is an important topic that should be studied closely and optimized. To investigate the complicated joint effects of fish physiology, behavior, feed distribution and environmental factors, a range of sea cage and fish models have been created (Alver et al., 2004; Føre et al., 2009; Alver et al., 2016). The feed distribution from the spreader seeds the initial surface distribution used in these models and is thus of importance. Oehme et al. (2012) showed that the surface feed distribution from a rotary spreader only covered a limited percentage of the surface area and was skewed to one side. This result warranted a further inquiry into the behavior and performance of the spreader itself. Measurements of spreader attitude has been made in Skøien and Alfredsen (2014) and physical models of its behavior has been created in Skøien et al. (2015, 2016).

Experiments obtaining the spatial surface pellet distribution from a rotary feed spreader have been conducted earlier by Oehme et al. (2012) and Skøien et al. (2016). Both studies employed Styrofoam boxes floating on the water surface to capture pellets and subsequently deducing the surface spread pattern from a section of the surface area. Oehme et al. (2012) used two rows of boxes attached to each other on the long side on each side of the spreader, forming a single line. In Skøien et al. (2016) this arrangement was expanded to four rows, effectively capturing pellets in a cross formation. The experimental setup proved able to accurately quantify the pellet distribution in the area covered by each box, however, with limited spatial resolution. The majority of pellets land outside the boxes leaving a substantial area of the surface unmapped. This method is also expensive and laborious due to the time it takes to count or photograph the contents of each box and empty them for each replicate run of an experiment. The position of the boxes are difficult to maintain in high winds and requires personnel inside the sea cage at almost all times.

This study presents an alternative method of determining surface pellet distribution using an unmanned aerial vehicle (UAV) and also provides attitude data obtained from a representative rotary pneumatic spreader (*CF90 Double*, AKVA group, Bryne, Norway) across different operating conditions. The results are then compared and discussed in relation with previously obtained attitude measurements from Skøien and Alfredsen (2014). In addition, a novel method of obtaining the surface pellet distribution is presented, using an UAV to observe the surface of the sea cage. Both experiments were run simultaneously to obtain corresponding data for later use in simulations, model parametrisation and verification of spreader models. The spreader models may in turn be

used together with sea cage models which enable simulation of different spreader configurations and the causal effect on parameters such as growth rate and feed loss which might be a valuable tool for farmers, farming equipment designers and the research community.

2. Materials and methods

2.1. Definitions

This section presents the reference frames which are used to describe the relative position and orientation between the sea cage, spreader and UAV. The definitions are identical to Skøien et al. (2015, 2016) based on Fossen (2011) and all systems are right-handed. See Table 3 for the definition of commonly used symbols. The rotation and translation of the spreader is determined with respect to a North-East-Down (NED) reference frame which is considered inertial, positioned in the sea cage at the location of the spreader and given by $\{O_a\} = (x_a, y_a, z_a)$ (Fig. 3). x_a is directed towards true north, y_a towards east, and z_a points down towards the earth center from the water surface plane spanned by x_a, y_a. The body fixed reference frame is given as $\{O_b\} = (x_b, y_b, z_b)$ and is fixed to the main body of the spreader (Fig. 1). x_b points towards the feed pipe, y_b is directed to starboard when looking in the $+x_b$ direction and finally z_b is positive down toward the submerged counterweight. Not considering the feed pipe leading to the spreader, the origin O_b of $\{O_b\}$ is fixed at the center of the water plane area (A_{wp}) of the spreader. This is the point which the spreader rolls and pitches about (Fossen, 2011). Hence, the center of origin (CO) equals the center of flotation (CF), and CO = CF = O_b. $\{O_c\} = (x_c, y_c, z_c)$ denotes the center pipe reference system, fixed just above the ball bearing which allows the center and outlet pipe to rotate. The spreader attitude which is described between $\{O_a\}$ and $\{O_b\}$ is given by $\boldsymbol{\Theta}_b^a = \begin{bmatrix} \phi_b^a & \theta_b^a & \psi_b^a \end{bmatrix}^T \in \mathcal{S}^3$ or the roll, pitch and yaw. Likewise, the attitude between $\{O_b\}$ and $\{O_c\}$ is given by $\boldsymbol{\Theta}_c^b = \begin{bmatrix} \phi_c^b & \theta_c^b & \psi_c^b \end{bmatrix}^T \in \mathcal{S}^3$. Further, the position of the spreader is given by the vector from O_a to O_b in the $\{O_a\}$ frame given by $\boldsymbol{o}_b^a = \begin{bmatrix} x_b^a & y_b^a & z_b^a \end{bmatrix}^T \in \mathbb{R}^3$.

As stated in Skøien et al. (2015) the 6 degrees of freedom (DOF) describing the rotation and translation of the spreader is given by

$$\boldsymbol{\eta} = \begin{bmatrix} \boldsymbol{o}_b^a & \boldsymbol{\Theta}_b^a \end{bmatrix}^T \in \mathbb{R}^3 \times \mathcal{S}^3 \tag{1}$$

The spreader is moored to the floating collar of the sea cage by ropes, which ensures that no translational motion can occur with respect to the sea cage. Hence $x_b^a = y_b^a = 0$. In addition, the effect of waves on the vertical translation averages out over time and it is stated that $z_b^a = 0$. The same ropes also restrict the rotation of the spreader meaning that ψ_b^a will be constant. Hence we define $\psi_b^a = 0$. Finally, the center pipe of the spreader has only 1 DOF in relation to the main body which is described by ψ_c^b. This reduces the system to

$$^*\boldsymbol{o}_b^a = \begin{bmatrix} 0 & 0 & 0 \end{bmatrix}^T \tag{2a}$$

$$\boldsymbol{\Theta}_b^a = \begin{bmatrix} \phi_b^a & \theta_b^a & 0 \end{bmatrix}^T \tag{2b}$$

$$\boldsymbol{\Theta}_c^b = \begin{bmatrix} 0 & 0 & \psi_c^b \end{bmatrix}^T \tag{2c}$$

according to Skøien et al. (2015) which are three central parameters obtained in this study. * indicates a constant variable. To provide a visual reference for the camera on the UAV, the floating collar of the sea cage was used. A separate reference frame is located on the sea cage in the water plane denoted $\{O_{cage}\}$ (Fig. 3). Since the plane spanned by x_a, y_a and x_{cage}, y_{cage} are identical, their relation can be described by

$$^*\boldsymbol{o}_{cage}^a = \begin{bmatrix} ^*x_{cage}^a & ^*y_{cage}^a & 0 \end{bmatrix}^T \tag{3a}$$

$$^*\boldsymbol{\Theta}_{cage}^a = \begin{bmatrix} 0 & 0 & ^*\psi_{cage}^a \end{bmatrix}^T \tag{3b}$$

2.2. Hardware for attitude measurement

To obtain the attitude of the spreader, a custom measurement system (MS) was constructed (Fig. 2). At the heart of the system is a self contained attitude and heading reference system (AHRS) (MTi-G, Xsens, Enschede, the Netherlands) providing Kalman filtered estimates of the Euler angles between the inertial system and the sensor $\boldsymbol{\Theta}_m^a$ (X-Y-Z rotation sequence) as well as GPS time. In addition to GPS, the sensor fusion algorithms draw upon measurements from a total of $3 * 3$ orthogonal accelerometers, gyroscopes and magnetometers. A 3D magnetic field mapping was performed prior to the experiment to compensate for any static offsets caused by the spreader. In order to reduce the effect of centripetal acceleration, the MS was mounted as close to the buoy as possible. Since the AHRS is mounted close to the CO and the dynamics of the spreader are slow (<2 Hz), this will limit the effect of centripetal acceleration on the attitude estimation. Thus $\boldsymbol{\Theta}_m^a \approx \boldsymbol{\Theta}_b^a$ but it is assumed that $\boldsymbol{\Theta}_m^a = \boldsymbol{\Theta}_b^a$. The latter will be used for simplicity.

To obtain the angular position of the center pipe (ψ_c^b) an absolute rotary encoder was used (VERT-X 2831-736-221-102, Contelec AG, Biel, Switzerland) attached via a 1:1 synchronous belt from the center pipe of the spreader. The encoder has an internal 12 bit resolution which is converted to an analog output in the range $0.1U_b = U_{low} \leqslant U_{out} \leqslant U_{high} = 0.9U_b$, corresponding to $0^\circ < \psi_c^b \leqslant 360^\circ$. U_b = 5 V supply voltage. The angle is given by

$$\psi_c^b = (U_{out} - U_{low}) * 360^\circ / (U_{high} - U_{low}) \tag{4}$$

Due to noise issues, U_b could not be supplied directly from USB power. In order to provide a low noise power supply, a data acquisition (DAQ) unit (USB-6009, National Instruments, Austin, TX, USA) was used. U_{out} was connected to both external analog inputs of the AHRS as well as to the DAQ as a backup. The GPS antenna was mounted 0.8 m above the water surface on a metal plane to reduce the likelihood of adverse multipath issues. Power was supplied via a USB hub from a computer in a small dinghy situated along side the spreader which had access to additional power via a 12 V lead battery and a 230 V inverter.

Let *without feed* denote the experiments run with only air and *with feed* describe the experiments where feed was introduced into the airstream as would be done during normal operation. For the *without feed* experiments AHRS log analysis started at least 15 s after the spreader started to rotate to ensure stable operational conditions. Similarly for the experiments *with feed*, the spreader was allowed to spin up before feed was added to the airflow and hence analysis started when feed first appeared at the spreader. In order to gain insight into the effect of the position of the outlet pipe on the spreader's attitude, $\phi_b^a(\psi_c^b)$ and $\theta_b^a(\psi_c^b)$ was derived, or in other words, the roll and pitch as a function of the angular position of the outlet pipe. This was done by rounding of integer degrees $\psi_c^b(t) \in (0, 360] \in \mathbb{R} \rightarrow \psi_c^b(t) \in [1, 360] \in \mathbb{Z}^+$ and then traversing $\psi_c^b(t), t = [t_{start}, t_{end}]$ for each replicate, storing the corresponding ϕ_b^a and θ_b^a which were averaged.

2.3. Aerial platform and image analysis

A Phantom 2 Vision+ (DJI, Shenzhen, China) quadcopter UAV was used for aerial observation of the feed distribution patterns in the experiment. This UAV was equipped with a three-axis gimbal stabilized 140° field of view (FOV) $1080 * 1920$ pixel camera

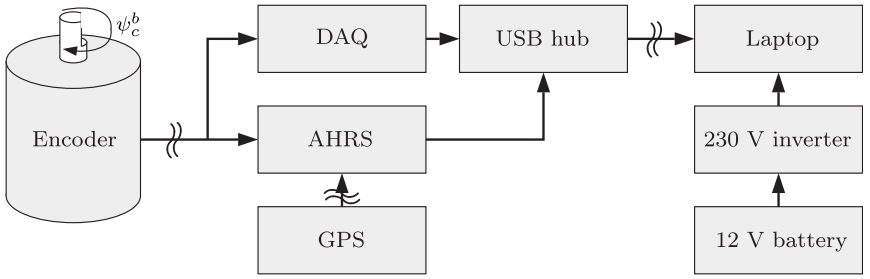

Fig. 2. Overview of the measurement system (MS). The encoder was attached to the center pipe of the spreader using a 1:1 synchronous belt. The AHRS captured the spreader attitude and also stored encoder data via external analog inputs. The DAQ acted as a power supply for the encoder and as redundant data storage. The waterproof laptop and power supply system was situated in a dinghy beside the spreader.

recording at 30 FPS. The orientation of the UAV camera (denoted "$_u$", Fig. 3) in relation to the spreader and the sea cage origin is given by $\boldsymbol{\Theta}_u^{cage} = \begin{bmatrix} \phi_u^{cage} & \theta_u^{cage} & \psi_u^{cage} \end{bmatrix}^T \in \mathcal{S}^3$ which can be described by a rotation matrix $\boldsymbol{R}_u^{cage}$ Fossen (2011) and the position given by $\boldsymbol{o}_u^{cage} = \begin{bmatrix} x_u^{cage} & y_u^{cage} & z_u^{cage} \end{bmatrix}^T \in \mathbb{R}^3$. These parameters are important as the orientation and translation of the camera relative to the water surface and spreader must be known to obtain the world coordinates of pellets from the image coordinates. The problem is simplified by assuming $\phi_u^{cage} = 0$ and $\theta_u^{cage} = 0$ which is handled by the UAV gimbal, always keeping the camera perpendicular to the water surface. Due to the short time frame of each recording, the spreader and sea cage are considered inertial and the position of the UAV is kept constant by the on board navigation system. Hence, the translation may be considered constant ${}^*\boldsymbol{o}_u^{cage}$ but unknown. In order to quantify the position of pellets in the image in relation to the spreader, the homography matrix between the image coordinates $(x_u, y_u) \in \mathbb{R}^2$. and the water surface plane $(x_a, y_a) \in \mathbb{R}^2$ must be determined. A set of 18 chequerboard

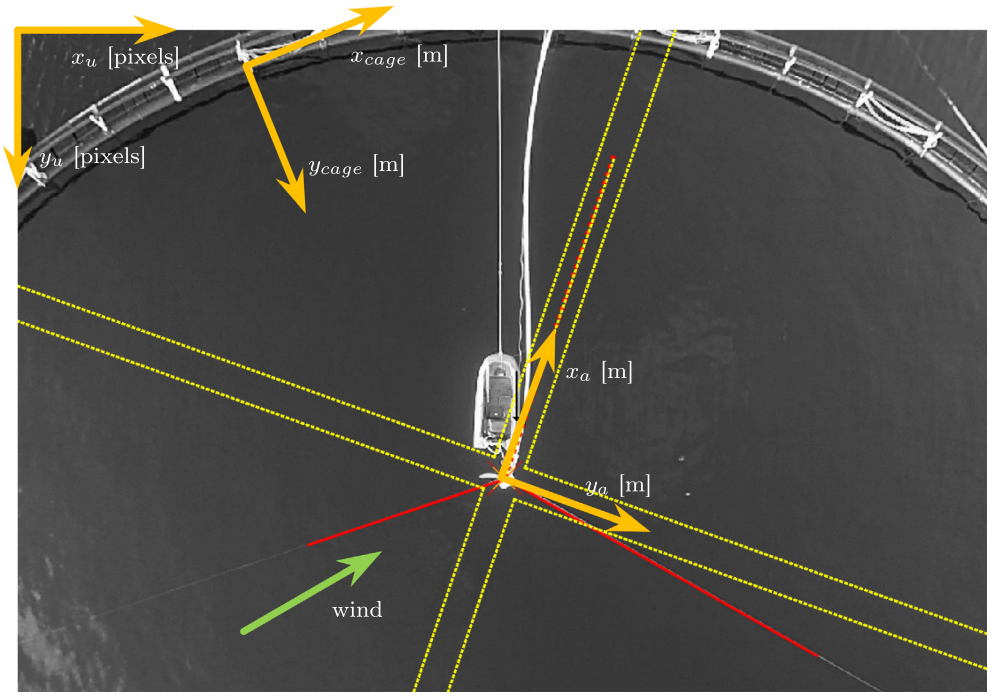

Fig. 3. Aerial footage from the UAV. The spreader is located centrally in the image with the buoy and outlet pipe which is pointing left barely visible. The three mooring ropes tying the spreader to the floating collar are readily visible. Two pellet impacts are distinguishable just to the right of the spreader. A support dinghy was situated close to the spreader and due to the proximity almost no pellets ended up inside. The red lines were obtained from the Hough transform and the position of the spreader was analytically determined. The yellow cross indicates the position of the virtual Styrofoam boxes and pellet impacts were only determined within this area. Three reference frames are indicated in the image. $\{O_u\}$ is the image coordinate frame given in pixels, $\{O_{cage}\}$ is the cage coordinate frame and $\{O_a\}$ the inertial base frame. The average wind vector is indicated, contributing to a positive shift of pellet impacts along x_a and y_a. (For interpretation of the references to color in this figure legend, the reader is referred to the web version of this article.)

calibration images at 1–3 m distance were extracted from a video sequence and run through the MATLAB (2014) camera calibration procedure, yielding the internal camera parameters at a mean error of 0.34 pixels. The chequerboard calibration distance should ideally be representative of the altitude of the UAV during the experiment which were in the order of 30–36 m, but basic tests yielded length errors of maximum 1.3%. All images were undistorted using the obtained camera parameters. ${}^{*}\boldsymbol{o}_u^{cage}$ and ${}^{*}\boldsymbol{R}_u^{cage}$ was determined by the MATLAB command `extrinsics` which takes the camera parameters, and a set of points in the image frame x_u, y_u and world cage frame x_{cage}, y_{cage} as inputs. Corresponding points were obtained by calculating the position of the vertical beams between the floating collar and handrail of the sea cage (Fig. 3). There were 60 vertical beams assumed equally spaced along the circumference of 50 m diameter circle and four of these were used for the calculations. These four points in the image coordinate frame were manually marked in the first image of each experiment to correspond with the vertical beams.

From the recordings it was determined that pellet impacts remained visible on the water surface for 10.4 images on average. To reduce the storage requirement and computational load, every fifth frame from the original recording was undistorted and stored in 8-bit grayscale format.

In order to determine the position of the spreader the three clearly visible mooring ropes were used as a reference (Fig. 3). To detect the ropes, images were run through a Canny edge detector (Canny, 1986) before K number of lines $\boldsymbol{L} = [\mathcal{L}_1, \mathcal{L}_2, \ldots, \mathcal{L}_K]$ were extracted using the Hough transform (Hough and Paul, 1962). $\boldsymbol{L}$ is sorted by length so $\mathcal{L}_1$ is the longest line in $\boldsymbol{L}$. Each line is a candidate for a mooring rope and is described by a six scalar element structure

$$\mathcal{L}_k = \left\{ \begin{bmatrix} x_{u,k,end1} & y_{u,k,end1} \end{bmatrix}, \begin{bmatrix} x_{u,k,end2} & y_{u,k,end2} \end{bmatrix}, \psi_{u,k}, \rho_{u,k} \right\} \tag{5}$$

where $[x_u, y_u] \in \mathbb{N}^2$ represents the two end points of the line in the image coordinate frame and $\psi_{u,k} \in \mathbb{Z}, \rho_{u,k} \in \mathbb{N}$ are part of a parametric line representation given by

$$\rho = x\cos(\psi) + y\sin(\psi) \tag{6}$$

on general form. To obtain the position and yaw of the spreader, the two lines that most probably represent the mooring ropes named $\mathcal{L}_{left}, \mathcal{L}_{right}$ must be extracted from the candidate lines $\boldsymbol{L}$. As can be seen in Fig. 3, the top rope is also attached to the dinghy and is not necessarily directed straight towards the spreader. Hence, only the left and right mooring rope was used as descriptors. $\mathcal{L}_{left}$ and $\mathcal{L}_{right}$ are found and extracted by Algorithm 1.

Algorithm 1. Traverse Hough lines by length and extract the longest lines which are candidates for the left and right mooring rope

```
maxLinesToTraverse ← 7
L_left, L_right ← ∅
for k = 1 to min(K, maxLinesToTraverse) do
  if ψ_{u,k} ∈ A_left && L_left == ∅ then
    L_left ← L_k
  else if ψ_{u,k} ∈ A_right && L_right == ∅ then
    L_right ← L_k
  end if
end for
```

In Algorithm 1 $\mathcal{A}_{left}$ and $\mathcal{A}_{right}$ are sets of valid angles for the lines to be classified as mooring ropes. The two angle sets were manually determined from images. The values were set to filter out spurious lines with very different orientation to the mooring ropes whilst allowing for some UAV yaw rotation. Let ${}^{*}\psi_{u,left,fix}$ and ${}^{*}\psi_{u,right,fix}$ be the fixed angle of the left and right mooring rope respectively in relation to a vertical image line, manually determined from the video. Then,

$$\{\mathcal{A}_{left} \in \mathbb{Z} | {}^{*}\psi_{u,left,fix} - a \leqslant \mathcal{A}_{left} \leqslant {}^{*}\psi_{u,left,fix} + a\} \tag{7a}$$

$$\{\mathcal{A}_{right} \in \mathbb{Z} | {}^{*}\psi_{u,left,fix} - a \leqslant \mathcal{A}_{right} \leqslant {}^{*}\psi_{u,right,fix} + a\} \tag{7b}$$

where $a = 20^{\circ}$. This method gives valid info for none, one or both $\mathcal{L}_{left}, \mathcal{L}_{right}$ depending on the results of the Hough transform and line angles. The position of the spreader in the image frame is calculated by inserting $\psi_{u,left}, \psi_{u,right}, \rho_{u,left}, \rho_{u,right}$ into two line equations (6) and solving analytically for the position $[x_{u,spread}\ y_{u,spread}]$. This is converted to world coordinates with respect to the sea cage using the MATLAB function `pointsToWorld`:

$$\begin{bmatrix} x_{cage} & y_{cage} \end{bmatrix} = f\left({}^{*}o_u^{cage}, {}^{*}R_u^{cage}, [x_u \quad y_u]\right) \tag{8}$$

The heading of the spreader in $\{O_{cage}\}$ is computed by converting the end points of $\mathcal{L}_{left}$ and $\mathcal{L}_{right}$ to the $\{O_{cage}\}$ frame according to Eq. (8) and applying Eq. (9)

$$\psi_{cage,spread} = mean\left({}^{*}\psi_{cage,left,fix} + atan\left(\frac{x_{cage,left,end1} - x_{cage,left,end2}}{y_{cage,left,end2} - y_{cage,left,end1}}\right), {}^{*}\psi_{cage,right,fix} + atan\left(\frac{x_{cage,right,end1} - x_{cage,right,end2}}{y_{cage,right,end2} - y_{cage,right,end1}}\right)\right) \tag{9}$$

The two fixed parameters are manually determined and represent the angle between the left and right mooring rope respectively and the feed pipe. In order to make the solution more robust against missing data and smooth out the position and angle, an averaging sliding window filter on the simplified form

$\bar{\epsilon} = \frac{1}{N}\sum_{i-N}^{i}\epsilon_i$ was used where i is the current image in the video sequence and ϵ symbolizes $x_{cage,spread}, y_{cage,spread}$ and $\psi_{cage,spread}$. $N = 24$ frames = 6 s (every fifth frame stored). In case the algorithm is unable to compute the current position or angle of the spreader, an empty value is added to the filter.

Through these calculations the position and rotation of the spreader has been determined in the $\{O_{cage}\}$ frame. However, this frame is only used as an intermediate in order to map from pixels to world coordinates whilst the position of pellets in relation to the spreader is the desired metric. By definition:

$$x_{a,spread} := 0, y_{a,spread} := 0, \psi_{a,spread} := 0 \tag{10}$$

When a pellet impacts the water it is observed in the $\{O_u\}$ frame which has now been converted to world coordinates in $\{O_{cage}\}$ and must finally be rotated and translated into $\{O_a\}$. This is performed by taking the pellet impact position $x_{u,imp}, y_{u,imp}$, applying Eq. (8) and converting from $\{O_{cage}\}$ to $\{O_a\}$ using polar coordinates:

$$r = \sqrt{(x_{cage,imp} - \bar{x}_{cage,spreader})^2 + (y_{cage,imp} - \bar{y}_{cage,spreader})^2} \tag{11}$$

$$\alpha = \operatorname{atan}\left(\frac{y_{cage,imp} - \bar{y}_{cage,spreader}}{x_{cage,imp} - \bar{x}_{cage,spreader}}\right) \tag{12}$$

and factoring in the angle of the spreader

$$x_{a,imp} = r\cos\left(\alpha - \bar{\psi}_{cage,spread} + \pi/2\right) \tag{13a}$$

$$y_{a,imp} = r\sin\left(\alpha - \bar{\psi}_{cage,spread} + \pi/2\right) \tag{13b}$$

which is the world position of a pellet impact in relation to the spreader.

The determination of pellet impacts in the image was performed manually in this study. A sequence of 300 frames (50 s, every fifth frame stored from the UAV) from each replicate was used and pellet impacts manually marked in the image.

Table 1
The average roll and pitch of the spreader and angular velocity of the outlet pipe for the different experiments. All values ±1 SD. Results given *without feed* and *with feed*.

Airspeed [m/s]	Roll $\bar{\phi}_b^a$ [deg]	Pitch $\bar{\theta}_b^a$ [deg]	Angular velocity $\bar{\dot{\psi}}_c^b = \bar{\omega}_c^b$ [RPM]
Wo. feed			
20	−0.7 ± 1.9	−2.2 ± 0.8	36.0 ± 1.9
25	−0.9 ± 1.1	−2.2 ± 0.3	63.4 ± 0.9
29	−1.1 ± 0.7	−2.2 ± 0.4	77.3 ± 1.2
With feed			
20	−3.1 ± 0.9	−1.8 ± 1.0	39.5 ± 1.7
25	−3.5 ± 1.3	−1.8 ± 0.5	55.7 ± 3.2
29	−2.5 ± 1.0	−1.9 ± 0.5	72.5 ± 2.7
29 tilt	−16.4 ± 0.4	−0.9 ± 0.6	78.6 ± 2.8

2.4. Experiment

The experiment was carried out at a fish farm in Halsa (Møre og Romsdal, Norway) from 3rd to 6th November 2015. The spreader was mounted in a 50 m diameter sea cage, moored via three ropes to the floating collar and connected via a 423 m long 90 mm diameter feed pipe to the local feed barge. A bend radius of 450 mm on the center pipe and 600 mm outlet pipe was mounted to the base of the spreader. The airflow was driven by a 30 kW Omega CB131 C compressor (Kaeser Compressors, Inc., Fredericksburg, VA, USA), capable of shifting 10.85 m^3/min at a maximum pressure difference of 1 bar. 9 mm feed pellets (Optiline S L 2500-50A, Skretting, Stavanger, Norway) was introduced into the airflow from silos via a feed doser valve (AKVA group, Bryne, Norway) before being sent to the sea cage. Continuous temperature, pressure and airspeed monitoring was available from sensors mounted at the barge. The feeding system was calibrated without feed to enable mapping from the applied power to a given airspeed. It was found that 100%, 81% and 60% corresponded to 29, 25 and 20 m/s airspeed respectively. Three replicates were run at each power setting in randomized order with *without feed* experiments run on November 5th and experiments *with feed* and UAV on November 6th. The spreader was allowed to spin up using only air before feed was added and run at 10 kg/min. To investigate the spreader behavior and feed distribution at extreme attitudes, an additional experiment was undertaken where the spreader was forced down (rolled) to an extreme angle. Average and maximum wind speed was recorded on all experiments involving feed using an anemometer (Windmaster 2, Kaindl, Rohrbach, Germany).

3. Results

3.1. Spreader attitude

The experimental results include data on the attitude of the spreader as well as the position of the outlet pipe at three different airspeeds for the feeder running *without feed* and *with feed*. The average roll, pitch and rotational speed of the outlet pipe are given in Table 1. $\phi_b^a(\psi_c^b)$ and $\theta_b^a(\psi_c^b)$ are given in Figs. 4 and 5.

3.2. Pellet distribution

Fig. 6 shows the manually plotted pellet positions from all three replicates at 20 m/s airspeed. This Figure is mainly intended as a

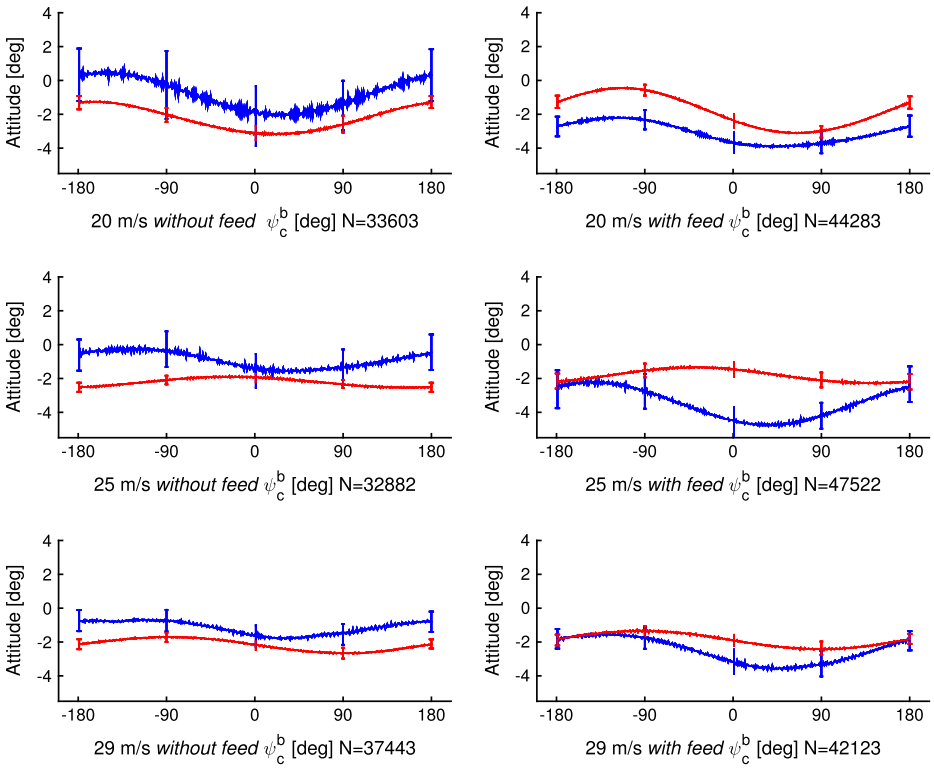

Fig. 4. The spreader roll $\phi_b^a(\psi_c^b)$ (blue) and pitch $\theta_b^a(\psi_c^b)$ (red). The error bars depict ±1 SD at 90° intervals. *N* denotes the total number of samples from all three replicates. (For interpretation of the references to color in this figure legend, the reader is referred to the web version of this article.)

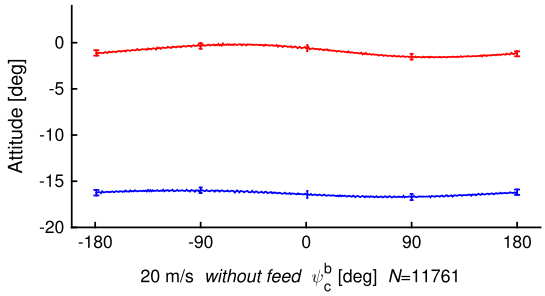

Fig. 5. The spreader roll $\phi_b^a(\psi_c^b)$ (blue) and pitch $\theta_b^a(\psi_c^b)$ (red) when the spreader was forced to an extreme roll using an additional rope. The error bars depict ±1 SD at 90° intervals. *N* denotes the total number of samples. (For interpretation of the references to color in this figure legend, the reader is referred to the web version of this article.)

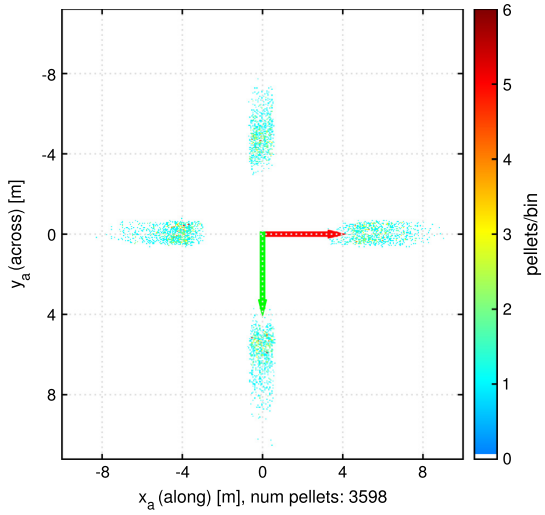

Fig. 6. Manually plotted pellet impacts from all replicates at 20 m/s airspeed. The number of pellets is higher in this image compared to Fig. 7 since the virtual Styrofoam box mask has not yet been applied.

visual reference to better comprehend the following plots and discussion. Fig. 7 presents the normalized pellet count in all replicates present in 40 × 80 cm boxes placed in a cross pattern as indicated in Fig. 3. Fig. 8 presents the experiment where the spreader was tilted to an extreme roll angle. The average throw and center of mass calculations are presented in Table 2.

4. Discussion

From Table 1 the average angular velocity ($\bar{\omega}_c^b$) increases monotonically as a function of airspeed. $\bar{\omega}_c^b$ is generally higher for experiments *without feed* with the exception of 20 m/s where $\bar{\omega}_c^b$ is slightly higher with feed in the system. $\bar{\omega}_c^b$ is comparable to the results *without feed* from Skøien and Alfredsen (2014), where 15, 20, 25 and 30 m/s corresponded to 14.6, 41.7, 60.8 and 79 RPM respectively.

$\bar{\phi}_b^a$ is closer to zero, i.e. the spreader is in a more upright position during the *without feed* experiments. This effect is most likely not related to feed being present but rather daily variations in water currents and weather. Unfortunately, the *without feed* and *with feed* experiments had to be conducted on two separate days. This in turn allowed for changes in wind and currents to translate and rotate the feed pipe which would easily affect the attitude of the spreader, especially roll. $\bar{\theta}_b^a$ is quite constant with no more than 0.4° variation across all independent variables.

Inspecting Fig. 4 allows for a more detailed understanding of the effect of ψ_c^b on the spreader attitude. The $\bar{\phi}_b^a$ shift from about −0.9 to −3.5 for the *with feed* experiments may be easily observed in these plots as well and $\bar{\theta}_b^a$ is quite stable across all experiments. It is expected that the center pipe pointing in a certain direction will force the spreader down due to the mass of the center and outlet pipe. In other words $\psi_c^b = 0° \rightarrow \min(\theta_b^a), \psi_c^b = 90° \rightarrow \max(\phi_b^a)$, $\psi_c^b = 180° = -180° \rightarrow \max(\theta_b^a)$ and $\psi_c^b = -90° \rightarrow \min(\phi_b^a)$. This effect was observed during compressor start where ω_c^b was low. However, as ω_c^b increased, the inertia of the spreader and feed pipe caused a phase shift between ψ_c^b and the observed attitude. At 20 m/s (Fig. 4) ϕ_b^a and θ_b^a are close to in phase which is not the case for the rest of the experiments. This might be due to differences in inertia around x_b and y_b as well as the feed pipe and spreader having certain harmonic frequencies. At 20 m/s $\min(\theta_b^a)$ occurs at about 17° and 65° *without feed* and *with feed* respectively. This corresponds very well with the experiments performed in Skøien and Alfredsen (2014) and is reasonable. At higher airspeeds this phase shift was enlarged, and $\min(\theta_b^a)$ lags about 93°–173° behind ψ_c^b. However, the differences in θ_b^a amplitude were small. $\min(\phi_b^a)$ on the other hand was fairly constant across all experiments at 120°–129° shift. The phase shift effect was confirmed by video recordings of the spreader during the experiment. In summary, comparing these results to the previously obtained AHRS data from Skøien and Alfredsen (2014) yields good agreement. $\theta_b^a(\psi_c^b)$ corresponds well at 20 m/s between the studies. The phase shift is larger

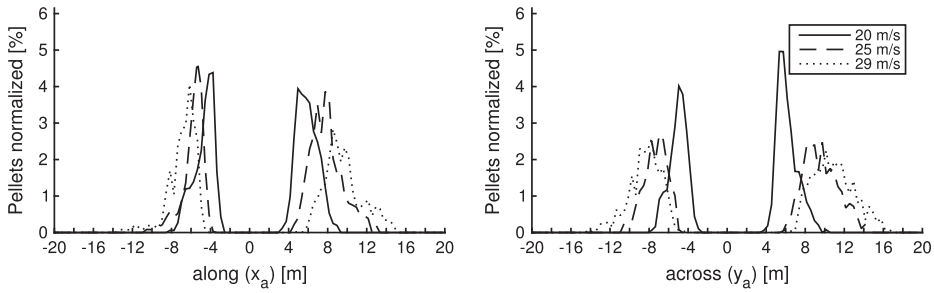

Fig. 7. Normalized pellet distribution in the virtual 40 × 80 cm boxes at 20, 25 and 29 m/s airspeed based on 2605, 1732 and 1939 pellets respectively.

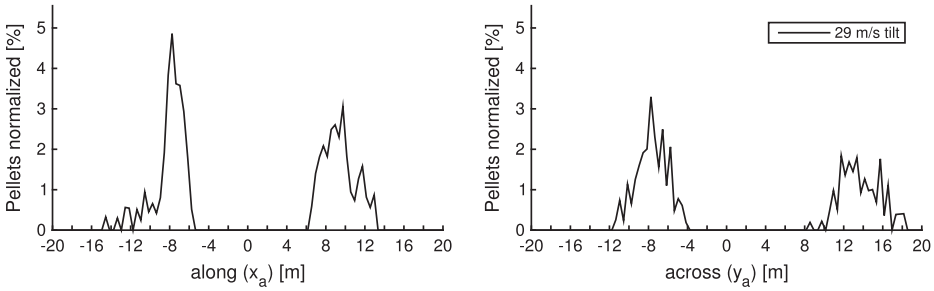

Fig. 8. Normalized pellet distribution in the virtual 40 × 80 cm boxes at 29 m/s airspeed with the spreader forced into a negative roll. Based on 701 pellets.

Table 2
Airspeed, average pellet throw length from spreader and center of mass.

Airspeed	Avg. throw [m]	Cnt. mass x_a [m]	Cnt. of mass y_a [m]
20 m/s	5.3 ± 1.2	0.27	0.30
25 m/s	7.3 ± 1.9	0.84	0.55
29 m/s	8.5 ± 2.2	0.22	0.59
29 m/s tilt	8.8 ± 2.5	0.04	0.49

Table 3
Commonly used symbols.

Description	Symbol	Unit
A given frame (a) consisting of three orthogonal unit vectors (x_a, y_a, z_a)	$\{O_a\}$	–
The origin (center) of a frame	O_a	–
Rotation about the x-axis (roll)	ϕ	deg
Rotation about the y-axis (pitch)	θ	deg
Rotation about the z-axis (yaw)	ψ	deg
Angular velocity of the outlet pipe	$\dot{\psi}_c^b = \omega_c^b$	deg/s or RPM
Rotation of $\{O_b\}$ with respect to $\{O_a\}$ given as a Euler angle vector: $[\phi_b^a \quad \theta_b^a \quad \psi_b^a]^T$	$\mathbf{\Theta}_b^a$	deg
Translation of O_b with respect to O_a expressed in $\{O_a\}$ given as a distance vector: $[x_b^a \quad y_b^a \quad z_b^a]^T$	o_b^a	m
A line represented in a six-scalar element structure according to Eq. (5)	$\mathcal{L}$	

overall for ϕ_b^a. $\bar{\phi}_b^a$ varies greatly in these experiments. Although $-3.5^\circ \leqslant \bar{\phi}_b^a \leqslant -0.7^\circ$ individual replicates showed a wider spectrum. Hence, it seems that $\bar{\phi}_b^a$ is highly variable, likely due to linear forces and torques exerted on the spreader from the feed pipe. $\bar{\phi}_b^a$ may also be affected by the mounting of the spreader as it is usually hauled on board a service vessel to connect the feed pipe. When hoisted back into the sea cage, this will likely manifest itself as a roll offset. A notable difference between this study and (Skøien and Alfredsen, 2014) is that the positive shift in $\bar{\theta}_b^a$ with increasing ω_c^b can not be observed here. It is likely that the centripetal acceleration exerted on the AHRS due to being mounted to the rotating center pipe may have caused this positive shift with increased angular velocity in the previous study. The dynamics of the spreader are still not fully understood and comparisons of results are difficult due to noise and possible attitude drift. Overall, variations in roll (ϕ_b^a) seem to be highly influenced by the torque of the feed pipe and the pitch (θ_b^a) tends to be fairly stable.

The 29 m/s experiment must be treated separately from the remainder of the discussion as an external force was applied to alter the attitude of the spreader. The effect of the additional rope used to force the spreader into a negative roll offset is apparent in Table 1. $\bar{\phi}_b^a$ was −16.4°, a significant difference from the remaining experiments. The angular velocity of the spreader increased slightly during this experiment for which there was no apparent explanation as all the other variables were unaltered.

Based on the current study and observations from Skøien and Alfredsen (2014) it is probable that for simulations, values in the range of $-5^\circ \leqslant \bar{\phi}_b^a \leqslant 5^\circ$ and $-2.2^\circ \leqslant \bar{\theta}_b^a \leqslant 1^\circ$ may be used to describe the attitude of this type of pneumatic rotary feed spreader. Attitude offsets will likely affect the spatial pellet distribution and create an unsymmetrical pattern across the surface. This may in turn lead to high concentrations of pellets in one area and thus increased crowding of fish during feeding which may negatively influence growth, feed loss and welfare.

The 2D surface plot at 20 m/s airspeed in the $\{O_a\}$ frame can be viewed in Fig. 6. Naturally, the pellet distribution covers an annular (doughnut-shaped) area but the quantified area was restricted to a cross section to be in line with previous studies and decrease the amount of manual plotting. The surface plots results in Figs. 6 and 7 presents an annular surface distribution similar to what was observed in experiments by Oehme et al. (2012) and Skøien et al. (2016). The average pellet throw increased as a function of airspeed (Table 2) from 5.3 through 7.3 and 8.5 m for 20, 25 and 29 m/s airspeed respectively as expected. The standard deviation of throw length also increased with airspeed which is plausible as there might be more randomness in the motion of a pellet and increased headroom for variability.

The surface pellet cloud center of mass results is more elaborate as there are three factors affecting this metric. Firstly, the attitude of the spreader will affect where pellets land. The attitude will cause a translation of the outlet pipe, directly affecting the throw length in relation to O_b. Inversely, the outlet pipe pointing down will lead to a shorter ballistic path with pellets being shot down into the water. On the other hand, with the outlet pipe pointing upwards, pellets will have a more favourable ballistic angle and will be thrown further. Secondly, the configuration of the spreader itself affects the pellet speed and hence the length of throw. When the outlet pipe points in the direction of the feed pipe ($\psi_c^b = 0$) pellets will experience a long sweeping "*U*" bend before being released. Oppositely at $\psi_c^b = 180^\circ$ pellets will experience a 90° bend at the bottom of the spreader before impacting the center pipe bend and experience another change of direction ("*S*" configuration). The latter is known to reduce the overall pellet speed and will result in shorter throw. In addition, it must be considered that a pellet experiencing the most significant speed reduction at $\psi_c^b = 180^\circ$ will not land exactly on the $-x_a$ axis. It takes some time for the pellet to reach the outlet opening of the spreader and by then some rotation has occurred. Lastly, the curvature of the outlet pipe of 36° means that the trajectory of pellets projected down in the water plane can not be represented by a straight line away from $x_a = 0, y_a = 0$ (O_a). This outlet pipe curve is not visible in

Fig. 1 as it curves out towards $-y_a$. However, it is believed that the tangential velocity component from the spreader rotation largely cancels out the effect of the curved shape of the outlet pipe as discussed in Skøien et al. (2015, 2016). This assumption appears reasonable when observing pellet trajectories from UAV videos and hence the water plane projected trajectories may be approximated by a straight line away from O_a.

The center of mass was calculated from the normalized pellet count across all boxes. During the experiment it was observed that the spreader releases pellets in a fairly continuous stream, randomly interrupted by a batch of clustered pellets. If many of these batches land in the same region, the resulting center of mass calculation will obviously be shifted towards that area. For all experiments except 29 m/s tilt the number of replicates and revolutions of the spreader were high, so the effect of batch pellets are assumed negligible. However, for the 29 m/s tilt only one replicate could be performed due to unforeseen events at the farming site. This gives some uncertainty with respect to the results from this single experiment.

Wind was low for all replicates with an average value of 0.6–2.3 m/s and directed towards $+x_a, +y_a$, 40° to the right of $+x_a$. Hence, the wind contributed to a positive shift in pellet impacts along both x_a and y_a. With this in mind, the pellet cloud center of mass along x_a and y_a was positive across all replicates. The wind may have contributed to this result but the exact amount is unknown and it is likely to be very limited. For y_a this result is reasonable since roll ($\bar{\phi}_b^a$) in Table 1 was negative for all replicates resulting in a more favourable ballistic trajectory in the $+y_a$ direction. Oppositely, the pitch ($\bar{\theta}_b^a$) was also negative in all experiments suggesting that the center of mass should be located in $-x_a$. Observing Table 2 the result was the opposite. The reason for this is believed to be the aforementioned spreader bend configuration. Since $\bar{\theta}_b^a$ is fairly small, the effect of "*U*" vs. "*S*" will be more influential and hence the throw will be longer in $+x_a$ due to the higher pellet speed. Since the balance between these two factors is unknown the results must be interpreted with caution. The 29 m/s tilt experiment must again be treated separately. Pellet cloud center of mass according to Table 2 is close to 0 as expected along the x_a direction. However, the center of mass along y_a was only 0.49 m. Due to the more favourable ballistic angle in $+y_a$ this result is not intuitive. Investigating Fig. 8 it is indeed evident that the throw was longer in $+y_a$ compared to $-y_a$ but there are more pellets closer to the spreader in $-y_a$. This effect may be attributed to the aforementioned batch pellet release, or that the spreader spent more time with the outlet pipe pointing in the general $-y_a$ direction due to the negative roll offset caused by the external force and the weight of the outlet pipe.

Using an UAV to observe the surface pellet distribution appears to be a viable alternative to collecting pellets in boxes as was done in Oehme et al. (2012) and Skøien et al. (2016). The method was significantly faster to deploy, easier to maintain and has much higher spatial resolution. Pellet impacts were easily observable on the surface in calm weather conditions. Smaller pellets and fragments may have gone undetected in the proposed method as these impacts are difficult to observe. The advantage of being able to observe the entire annular impact region has not been fully utilized in this study. Manual plotting of pellet impacts was time consuming and hence only a cross-shaped area of the surface was classified. Automatic detection of pellet impacts would have been a significant benefit to the solution. However, with the manually marked impacts from a section of the image now available, a reference exists which may be used later to validate an automatic detection algorithm.

The assumption of regarding the translation ${}^*o_u^{cage}$ and rotation ${}^*R_u^{cage}$ as constant does not completely hold as the UAV is affected by wind. Although the GPS position was recorded for both the spreader and UAV, this measurement was far too inaccurate for use in this study. However, in this experimental configuration, positioning of pellets relative to the spreader is possible without direct knowledge of the rotation and translation: $\phi_u^{cage} = 0$ and $\theta_u^{cage} = 0$ are kept constant by the UAV camera gimbal. Since x_a, y_a and x_{cage}, y_{cage} exists in the same water surface plane, the camera will be perpendicular to this plane as well. The UAV may translate and rotate (x_u^{cage}, y_u^{cage} and ψ_u^{cage}) and these values are unknown. This renders direct relative mapping from the camera $\{O_u\}$ to the real world $\{O_{cage}\}$ or $\{O_a\}$ impossible. However, we are only concerned with the relation of pellet impacts relative to the position of the spreader and by extracting the spreader position and rotation in the image, relative calculations may still be performed. Hence, x_u^{cage}, y_u^{cage} and ψ_u^{cage} may remain unknown. The UAV altitude (z_u^{cage}) is calculated back from the `extrinsics` command based on four points from the sea cage. Since this calculation is only performed on the first frame from each replicate it is assumed that the altitude of the UAV is constant for the 50 s of video used. No altitude drift could be observed in the videos or the flight logs. The initial calibration in relation to the cage was based on the vertical supports connecting the floating collar to the handrail being equidistant along the circumference of the sea cage. Upon closer inspection, this is not perfectly true as there was a joint in the sea cage. However, the cage is believed to be the best visual reference available in the videos. Having a large floating calibration pattern attached to the spreader would have rendered it possible to get a more accurate reference as well as continuous updates for each frame.

5. Conclusion

This study has presented measurements characterizing the dynamic motion of a pneumatic rotary feed spreader which are frequently used in sea cage aquaculture. The results indicate that the spreader pitch is generally stable but roll on the other hand varies more, possibly due to forces and torques from the feed pipe. An UAV has been used to observe and determine the surface pellet distribution from the same spreader. Well established computer vision methods have been used in order to resolve the position and rotation of the spreader within the image as well as pellet impacts relative to the position of the spreader. The UAV approach seems to be a viable alternative compared to placing Styrofoam boxes on the surface to collect pellets as has been reported in previous studies. The proposed method is considerably faster to deploy and to operate whilst requiring a minimal amount of personnel. The results from the present study may be used to analyze pellet distributions from other spreaders and act as a foundation for further expansion with an automated pellet impact detection implementation. The results may also be used to parametrize and verify pneumatic spreader models in order to obtain more accurate and realistic results. This study has elevated the understanding of how a feed spreader behaves and the results may aid in design of new and alternative methods of feed distribution in sea cage aquaculture.

Acknowledgments

Appreciation is extended to Terje Haugen and Daniel Bogen at the department of Engineering Cybernetics workshop for their assistance with assembling the measurement system. We thank Morten Malm at AKVA group for providing the rotary spreader. This work has been conducted as part of Centre for Research-based Innovation in Aquaculture Technology (CREATE) (Research

Council of Norway, Grant No.: 174842), SINTEF Sealab, NO-7645 Trondheim, Norway.

References

Alfredsen, J.A., Holand, B., Solvang-Garten, T., Uglem, I., 2007. Feeding activity and opercular pressure transients in Atlantic salmon (*Salmo salar* L.): application to feeding management in fish farming. In: Almeida, P., Quintella, B., Costa, M., Moore, A. (Eds.), Developments in Fish Telemetry, Developments in Hydrobiology, vol. 195. Springer, Netherlands, pp. 199–207. http://dx.doi.org/10.1007/978-1-4020-6237-7_19.

Alver, M.O., Alfredsen, J.A., Sigholt, T., 2004. Dynamic modelling of pellet distribution in Atlantic salmon (*Salmo salar* L.) cages. Aquacult. Eng. 31, 51–72. http://dx.doi.org/10.1016/j.aquaeng.2004.01.002.

Alver, M.O., Skøien, K.R., Føre, M., Aas, T.S., Oehme, M., Alfredsen, J.A., 2016. Modelling of surface and 3D pellet distribution in Atlantic salmon (*Salmo salar* L.) cages. Aquacult. Eng., 20–29 http://dx.doi.org/10.1016/j.aquaeng.2016.03.003.

Attia, J., Millot, S., Di-Poï, C., Bégout, M.L., Noble, C., Sanchez-Vazquez, F., Terova, G., Saroglia, M., Damsgård, B., 2012. Demand feeding and welfare in farmed fish. Fish Physiol. Biochem. 38, 107–118. http://dx.doi.org/10.1007/s10695-011-9538-4.

Canny, J., 1986. A computational approach to edge detection. IEEE Trans. Pattern Anal. Machine Intell. PAMI-8, 679–698. http://dx.doi.org/10.1109/TPAMI.1986.4767851.

Einen, O., Mørkøre, T., Rørå, A.M.B., Thomassen, M.S., 1999. Feed ration prior to slaughter—a potential tool for managing product quality of Atlantic salmon (*Salmo salar*). Aquaculture 178, 149–169. http://dx.doi.org/10.1016/S0044-8486(99)00126-X.

FAO, 2015. Fishery statistical collections, global aquaculture production. <http://www.fao.org/fishery/statistics/global-aquaculture-production/en>.

Føre, M., Dempster, T., Alfredsen, J.A., Johansen, V., Johansson, D., 2009. Modelling of Atlantic salmon (*Salmo salar* L.) behaviour in sea-cages: a lagrangian approach. Aquaculture 288, 196–204. http://dx.doi.org/10.1016/j.aquaculture.2008.11.031.

Fossen, T.I., 2011. Handbook of Marine Craft Hydrodynamics and Motion Control. John Wiley & Sons.

Gjøsæter, J., Otterå, H., Slinde, E., Nedreaas, K., Ervik, A., 2008. Effekter av spillfôr på marine organismer (in Norwegian). Kyst og Havbruk, 52–55.

Hough, V., Paul, C., 1962. Method and means for recognizing complex patterns. US Patent 3,069,654.

Juell, J.E., 1995. The behaviour of Atlantic salmon in relation to efficient cage-rearing. Rev. Fish Biol. Fisheries 5, 320–335. http://dx.doi.org/10.1007/BF00043005.

Kadri, S., Huntingford, F., Metcalfe, N., Thorpe, J., 1996. Social interactions and the distribution of food among one-sea-winter Atlantic salmon (*Salmo salar*) in a sea-cage. Aquaculture 139, 1–10. http://dx.doi.org/10.1016/0044-8486(95)01163-3.

López-Olmeda, J., Noble, C., Sánchez-Vázquez, F., 2012. Does feeding time affect fish welfare? Fish Physiol. Biochem. 38, 143–152. http://dx.doi.org/10.1007/s10695-011-9523-y.

MATLAB, 2014. version 8.4.0.150421 (R2014b). The MathWorks Inc., Natick, Massachusetts.

Norwegian Directorate of Fisheries, 2014. Fôrforbruk 2014. <http://www.fiskeridir.no/content/download/17752/150515/version/61/file/biostat-forforbruk-tab01-20150115.xlsx>.

Norwegian Directorate of Fisheries, 2015. Kostnad per kilogram 2008–2014. <http://www.fiskeridir.no/Akvakultur/Statistikk-akvakultur/Loennsomhetsundersoekelse-for-laks-og-regnbueoerret/Matfiskproduksjon-laks-og-regnbueoerret>.

Norwegian Ministry of Fisheries and Coastal Affairs, 2008. Aquaculture operations regulations with remarks (in Norwegian). <https://lovdata.no/dokument/SF/forskrift/2008-06-17-822>.

Oehme, M., Aas, T.S., Sørensen, M., Lygren, I., Åsgård, T., 2012. Feed pellet distribution in a sea cage using pneumatic feeding system with rotor spreader. Aquacult. Eng. 51, 44–52. http://dx.doi.org/10.1016/j.aquaeng.2012.07.001.

Olla, B., Davis, M., Ryer, C., 1992. Foraging and predator avoidance in hatchery-reared pacific salmon: achievement of behavioral potential. In: The Importance of Feeding Behaviour for the Efficient Culture of Salmonid Fishes. The World Aquaculture Society, pp. 5–12.

Oppedal, F., Dempster, T., Stien, L.H., 2011. Environmental drivers of Atlantic salmon behaviour in sea-cages: a review. Aquaculture 311, 1–18. http://dx.doi.org/10.1016/j.aquaculture.2010.11.020.

Ruzzante, D.E., 1994. Domestication effects on aggressive and schooling behavior in fish. Aquaculture 120, 1–24. http://dx.doi.org/10.1016/0044-8486(94)90217-8.

Ryer, C., Olla, B., 1991. Agonistic behavior in a schooling fish: form, function and ontogeny. Environ. Biol. Fishes 31, 355–363. http://dx.doi.org/10.1007/BF00002360.

Ryer, C.H., Olla, B.L., 1996. Growth depensation and aggression in laboratory reared coho salmon: the effect of food distribution and ration size. J. Fish Biol. 48, 686–694. http://dx.doi.org/10.1111/j.1095-8649.1996.tb01464.x.

Skøien, K.R., Alfredsen, J.A., 2014. Feeding of large-scale fish farms: motion characterization of a pneumatic rotor feed spreader. In: Oceans – St. John's, 2014, pp. 1–7. http://dx.doi.org/10.1109/OCEANS.2014.7003103.

Skøien, K.R., Alver, M.O., Alfredsen, J.A., 2015. Modelling spatial surface pellet distribution from rotary pneumatic feed spreaders. In: 23th Mediterranean Conference on Control and Automation (MED), pp. 883–888. http://dx.doi.org/10.1109/MED.2015.7158857.

Skøien, K.R., Alver, M.O., Lundregan, S., Frank, K., Alfredsen, J.A., 2016. Effects of wind on surface feed distribution in sea cage aquaculture: a simulation study (in press). In: European Control Conference ECC16.

Talbot, C., 1993. Some biological and physical constraints to the design of feeding regimes for salmonids in intensive cultivation. In: Reinertsen, H., Dahle, L.A., Jørgensen, L., Tvinnereim, K. (Eds.), Fish Farming Technology. Balkema, Rotterdam, pp. 19–26. ISBN 9054103264.

Talbot, C., Corneillie, S., Korsøen, Ø., 1999. Pattern of feed intake in four species of fish under commercial farming conditions: implications for feeding management. Aquac. Res. 30, 509–518. http://dx.doi.org/10.1046/j.1365-2109.1999.00369.x.

Thomassen, J., Lekang, O., 1993. Optimal distribution of feed in sea cages. In: Reinertsen, H., Dahle, L.A., Jørgensen, L., Tvinnereim, K. (Eds.), Fish Farming Technology. Balkema, Rotterdam, pp. 439–442. ISBN 9054103264.

Thorpe, J., Cho, C.Y., 1995. Minimising waste through bioenergetically and behaviourally based feeding strategies. Water Sci. Technol. 31, 29–40. http://dx.doi.org/10.1016/0273-1223(95)00424-L.

Thorpe, J., Talbot, C., Miles, M., Rawlings, C., Keay, D., 1990. Food consumption in 24 hours by Atlantic salmon (*Salmo salar* L.) in a sea cage. Aquaculture 90, 41–47. http://dx.doi.org/10.1016/0044-8486(90)90281-Q.

Paper H Modelling and simulation of rotary feed spreaders with application to sea cage aquaculture - a study of common and alternative designs (Manuscript)

(Skøien et al., 2016b)
Skøien, K. R., Alver, M. O., and Alfredsen, J. A. Modelling and simulation of rotary feed spreaders with application to sea cage aquaculture - a study of common and alternative designs (manuscript). 2016b

Modelling and simulation of rotary feed spreaders with application to sea cage aquaculture - a study of common and alternative designs

Kristoffer Rist Skøien[a,*], Morten Omholt Alver[a,b], Jo Arve Alfredsen[a]

[a]*NTNU, Norwegian University of Science and Technology, Faculty of Information Technology, Mathematics and Electrical Engineering, department of Engineering Cybernetics, NO-7491 Trondheim, Norway*
[b]*SINTEF Fisheries and Aquaculture, Trondheim, NO-7465, Norway*

Abstract

Rotary feed spreaders are extensively used in large scale fish aquaculture and are tasked with distributing pelletized feed in a spatially uniform manner over the water surface. Questions have been raised with respect to the performance of classical spreader designs regarding the size and uniformity of the covered area as well as their inability to adapt to changing environmental conditions. This study presents a robotic model of rotary spreaders with experimental validations. Classical rotary spreaders are simulated as well as two alternative designs in the form of a spreader releasing pellets at an optimal initial ballistic angle and a motorized version to increase throw length and provide a more spatially homogeneous surface feed distribution. The alternative designs both yielded improved surface coverage without the need of higher conveying airspeed which may lead to increased pellet attrition. In addition, the motorized design may be used to position pellets at a given location within the sea cage, such as into the wind and current so that pellets can reside inside the sea cage for a prolonged period of time. The model may be of interest to researchers and equipment manufacturers who desire to explore performance of a given spreader design.

Keywords: Atlantic salmon, feed distribution, modelling, rotary spreader, sea cage aquaculture.

*NTNU, Norwegian University of Science and Technology, Faculty of Information Technology, Mathematics and Electrical Engineering, department of Engineering Cybernetics, NO-7491 Trondheim, Norway. Tel.: +47 90580496, E-mail address: kristoffer.rist.skoien@itk.ntnu.no

Preprint submitted to Elsevier *November 11, 2016*

1. Introduction

Continuous improvement and optimization of farming systems and technology have been instrumental in the formidable increase of Atlantic salmon (Salmo salar) production, growing from 294 tonnes in 1970 to over 2,087,000 tonnes in 2013 (FAO, 2015). Production of Atlantic salmon is mostly undertaken in Norway and Chile, but Australia, the Faroe Islands, Great Britain and North America are also significant producers (Oppedal et al., 2011). The salmon are typically farmed in rectangular or square floating sea cages with 20-40 m sides, 20 to 35 m deep, or in circular cages with a circumference of 90-157 m up to 48 m deep (Oppedal et al., 2011). 240 m circumference cages are currently in use in Tasmania and the tendency to move towards more exposed farming locations has increased interest for even larger structures. In Norway, a single cage may be populated by up to 200,000 individuals at a maximum stocking density of 25 kg/m^3 (Norwegian Ministry of Fisheries and Coastal Affairs, 2008). Given a slaughter weight of 5 kg the biomass in one sea cage may be 1000 tonnes which at a daily feed ration of 1 % body weight (Oehme et al., 2012) results in 10 tonnes feed a day per cage. In 2014, almost 1.7 million tonnes of feed were administered at Norwegian salmon and trout farms at a total value of about €2000 million (Norwegian Directorate of Fisheries, 2014). Feed loss is a cumbersome figure to obtain, but between 5 % from recent publications and up to 15 % from earlier sources are indicated (Brooks and Mahnken, 2003; Cromey et al., 2002; Gjøsæter et al., 2008; Milewski, 2001; Otterå et al., 2009). This is poor utilization of resources (Alfredsen et al., 2007; Thorpe and Cho, 1995) and as feed compromises about 50 % of all farming costs (Norwegian Directorate of Fisheries, 2013) this over time becomes a significant financial loss for the farmer.

Feed is administered in the form of extruded pellets, 3-12 mm in diameter (Skretting, 2012) stored in a local barge which handles feed distribution to all cages on site, typically 4-16. A blower compresses air which is cooled through submerged piping before feed is added to the air stream through a feed doser valve and routed to the individual cages. Floating flexible piping runs from the barge to the sea cages which can be up to 800 m long (Aarseth et al., 2006) before terminating at the spreader. In Norway, the most common method of feed distribution at the cage surface is by use of a pneumatic rotary spreader. A typical design is depicted in Figure 1 which illustrates the *CF90 Double* rotary spreader (AKVA Group, Bryne, Norway) which will be referred to as *CF90*. A flotation

device such as a ring or buoy keeps the spreader afloat and this particular design features a submerged counterweight to maintain an upright attitude. A ball bearing allows the center pipe to rotate with respect to the body of the spreader. The rotary motion is achieved through the spiral shape of the outlet pipe and the airflow drives this rotation as well as the pellet throw.

The behaviour of salmon during feeding is a complex combination of environmental and biotic factors such as light, temperature, hunger level, competition and predation risk (Juell, 1995). A suboptimal intake of feed is linked to reduced and inefficient growth in Atlantic salmon (Einen et al., 1999). The amount as well as spatial and temporal availability of feed should not be confined, so the fish can forage in their unrestricted, desired manner (Talbot et al., 1999) and the availability of feed is a crucial factor in order to achieve efficient production (Juell, 1995). Key factors in determining food availability is the spatial and temporal distribution as well as ration size (Juell, 1995). These factors also affect variation in growth and level of aggression (Olla et al., 1992). Highly localized delivery of feed permits dominant individuals to monopolize the food supply, restricting feed access to subordinate individuals (review by Juell (1995)). Olla et al. (1992) states and identical argument, but emphasized that this occurs at underfeeding. A suboptimal feeding method may lead to increased nutrient discharge with respect to the produced biomass and reduced growth (Einen et al., 1995), increased aggression and growth depensation (variation) (Davis and Olla, 1987; Talbot, 1993; Thorpe and Cho, 1995). On the other hand, no growth depensation was found in a separate study (Noble et al., 2008), but still witnessed reduced growth and increased fin damage, especially in smaller fish as a result of restricted ration size. Ryer and Olla (1996) found increased growth depensation as a result of localized delivery of food as opposed to spatially and temporally distributed food.

Limited knowledge exists on the relation between feed access, growth and welfare in full scale sea-cages. However, several studies of salmonids mostly conducted on a smaller scale have shown aggressive behavior related to feed access (Brännäs et al., 2005; Fenderson et al., 1968; Jobling, 1985; Noble et al., 2007a,b, 2008; Rasmussen et al., 2007; Symons, 1971; Talbot et al., 1999) and general summary by (Attia et al., 2012; Ruzzante, 1994; Talbot, 1993), and aggression is linked to increased injury and mortality (López-Olmeda et al., 2012).

On the other hand, some studies have shown no effect of spatial distribution on aggressiveness or growth (Aas et al., 2015) and fish do show an array of behavioral responses in order to adapt to different feeding regimes (López-Olmeda et al., 2012; Talbot, 1993; Talbot et al., 1999; Thorpe and Cho, 1995).

In summary, although empirical results on Atlantic salmon in large scale sea

cages are limited, it is likely that maximizing the spatial distribution of feed will promote growth and minimize tendencies of agonistic behaviour (Attia et al., 2012; Juell, 1995; Kadri et al., 1996; Olla et al., 1992; Ryer and Olla, 1991, 1996; Thomassen and Lekang, 1993; Thorpe et al., 1990; Thorpe and Cho, 1995). Simulation results from (Alver et al., 2004) also suggest that a distributed feed delivery method is preferred over localized delivery. However, an extensive distribution pattern from a spreader may cause feed to end up outside the cage, or escape the cage before being eaten due to currents (Alver et al., 2004).

As shown by Oehme et al. (2012), high conveying airspeed increases the pellet distribution across the surface and the throw length. Nontheless, even at 30 m/s conveying airspeed the pellets are usually concentrated within 8 m of the spreader. In relation to a 50 m diameter sea cage this equates to less than a third of the diameter and a surface coverage of just 6.1 to 26.8 % over the 1960 m^2 cage surface area. Simply increasing the airspeed by running the blower at higher power or using a high performance blower does itself present challenges such as increased energy expenditure and increased demand of cooling. Higher airspeed in pneumatic conveying is also linked to increased levels of pellet attrition (Aarseth et al., 2006; Aarseth, 2004). Low airspeed and increased feed amount reduces the creation of fine particles of feeds of low quality (Aas et al., 2011). Small particles and dust are not desired as they have no value as feed (Aas et al., 2011).

Based on the previous argumentation, it is likely that the optimal spatial feed distribution is one that covers the surface of the sea cage in calm conditions, is reduced or moved to compensate for high winds or currents and ensures that breakage is kept to a minimum. It is unlikely that the current basic design and static placement of feed spreaders are able to facilitate such an increased and adaptable spatial distribution. By introducing the concept of a motorized spreader, the throw length may be increased without the need for higher conveying airspeed.

In order to experiment with new spreader designs a model was developed by Skøien et al. (2016a, 2015). The model uses a robotic description of the spreader combined with an extrinsic ballistic model to predict the surface distribution pattern. Such a model enables experimentation of different spreader configurations, transport airspeeds as well as the influence of wind. This study expands the model presented in Skøien et al. (2016a, 2015) with new experimental results. Specifically, new attitude data combined with aerial footage of the spreader in action (Skøien et al., 2016b) has been used for model verification. In addition, preliminary results from a high speed camera mounted on the spreader outlet pipe has been used to more accurately describe the effect of the spreader's curved pipes. This study compares the performance of the updated spreader model to

experimentally obtained surface pellet distributions. In addition, the concept of two alternative spreader configurations are introduced. In the first configuration the model is altered to represent a spreader with a 45° initial angle of pellet throw. The second configuration features a motorized design where the rotation of the spreader is driven independently from the conveying air. By increasing the rotational velocity of the spreader, the speed of the pellets are increased at the very end of the pneumatic transport path without the need for higher airspeed which may lead to increased attrition. Model performance and the two alternative spreader configurations are compared and discussed.

The results may be of interest to the research community as well as equipment manufacturers as a tool to evaluate alternative spreader designs and the resulting surface pellet distribution pattern. Simulations from the presented model may be used to seed the initial pellet distribution in sea cage models (Alver et al., 2016, 2004; Føre et al., 2016) to evaluate the impact of spreader performance on central factors such as growth, aggression indicators and feed loss.

2. Materials and methods

2.1. Definitions

The *CF90* model definitions and reference frames are based on (Fossen, 2011; Siciliano et al., 2009; Skøien et al., 2016a, 2015; Spong et al., 2006) and are illustrated in Figure 1. The translational and rotational spreader motion as well as all subsequent plots are given with respect to the inertial *North-East-Down* (NED) base frame $\{O_a\} = (x_a, y_a, z_a)$ located at the centroid of the sea cage surface area. x_0 is directed towards *North*, y_0 *East* and z_0 points *Down* into the water, normal to the x_0, y_0 water plane. With respect to the pellet distribution, x_0 is defined as *along* since this vector runs along the feed pipe and y_0 *across*. For the kinematic spreader model, the base frame is defined as $\{O_0\} = (x_0, y_0, z_0) = \{O_a\}$. The Latin subscripts are used in relation to attitude measurements and the sea cage, and numerical subscripts for the robotic model. The body reference frame $\{O_b\} = (x_b, y_b, z_b)$ is fixed to the main body of the spreader located at the water level. x_b is directed along the feed pipe away from the spreader, y_b is positive to starboard when viewed from above and z_b positive down (Fossen, 2011; Skøien et al., 2016a, 2015). The attitude of the spreader body with respect to the base frame is given by the Euler angles $\mathbf{\Theta}_b^a = \begin{bmatrix}\phi_b^a & \theta_b^a & \psi_b^a\end{bmatrix}^T \in \mathcal{S}^3$, using the X-Y-Z rotation sequence. Finally, the center pipe reference frame $\{O_c\} = (x_c, y_c, z_c)$ is located above the ball bearing which allows for the rotational motion of the spreader. There is only one degree of freedom between $\{O_b\}$ and $\{O_c\}$: $\mathbf{\Theta}_c^b = \begin{bmatrix}0 & 0 & \psi_c^b\end{bmatrix}^T$. $\psi_c^b = 0$ when the outlet

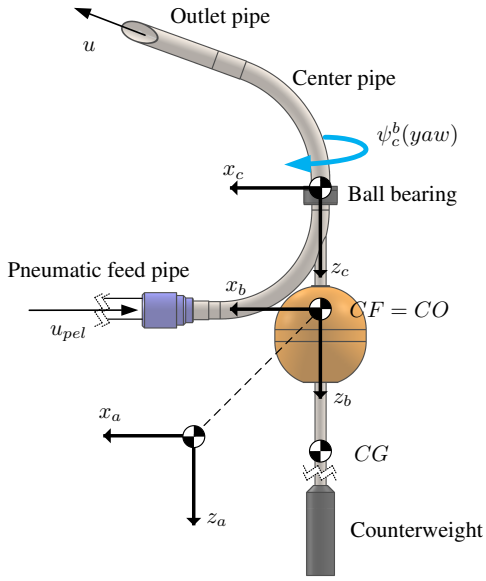

Figure 1: Model of the *CF90 Double* rotary spreader (AKVA group, Bryne, Norway). Figure based on (Skøien et al., 2016a). The spreader floats on the buoy and is kept upright by a submerged counterweight. The feed pipe from the barge is connected to the blue flange on the left. A ball bearing allows the center pipe to rotate and the spiral shape of the outlet pipe directs the airflow which results in a rotary motion. In this image, $\psi_c^b = 0$ which yields a characteristic *"U"* shape of the pellet path through the spreader. This figure is licensed under a Creative Commons CC-BY-SA license.

pipe points in the direction of the feed pipe as in Figure 1. This angular position is also denoted *"U"* due to the shape of the spreader where pellets follow an almost continuous bend. Consequently, $\psi_c^b = 180°$ or $-180°$ is called *"S"*. It is assumed that only the buoy is in contact with the water surface, accordingly, the centroid of the water plane area which is the point about which roll and pitch occurs is the center of flotation (CF) (Fossen, 2011; Skøien et al., 2015) CF = CO = O_b. The vector $\boldsymbol{o}_b^a = \begin{bmatrix} x_b^a & y_b^a & z_b^a \end{bmatrix}^T \in \mathbb{R}^3$ quantifies the distance O_a to O_b in the $\{O_a\}$ frame. The position and attitude of the spreader body is given by

$$\boldsymbol{\eta} = \begin{bmatrix} \boldsymbol{o}_b^a & \boldsymbol{\Theta}_b^a \end{bmatrix}^T \in \mathbb{R}^3 \times \mathcal{S}^3 \tag{1}$$

However, this can be simplified due to the spreader being tied to the floating collar,
130 fixing its position in the plane with respect to the cage and the fish, $x_b^a = 0$ and

$y_b^a = 0$, and also prohibiting rotation of the body $\psi_b^a = 0$. Waves cause the spreader to move up and down in the water but over time this effect will be averaged out Skøien et al. (2015), $z_b^a = 0$. Accordingly, the translation and attitude is defined as (Skøien et al., 2015):

$$\boldsymbol{o}_b^a = \begin{bmatrix} 0 & 0 & 0 \end{bmatrix}^T \tag{2a}$$

$$\boldsymbol{\Theta}_b^a = \begin{bmatrix} \phi_b^a & \theta_b^a & 0 \end{bmatrix}^T \tag{2b}$$

$$\boldsymbol{\Theta}_c^b = \begin{bmatrix} 0 & 0 & \psi_c^b \end{bmatrix}^T \tag{2c}$$

2.2. Forward kinematics

In order to determine where pellets impact the water, the ballistic path must be calculated and hence the position and orientation of the ballistic origin which is the outlet pipe opening O_n must be known. n denotes the last spreader joint. To determine the position and orientation of O_n with respect to the origin $\{O_0\} = \{O_a\}$, forward kinematics and the Denavit-Hartenberg (DH) convention was used (Siciliano et al., 2009; Spong et al., 2006). The model was based on the description in Skøien et al. (2016a) which was a series of joints and links to represent the robotic configuration of the spreader. Briefly described, the roll (ϕ_b^a) and pitch (θ_b^a) of the spreader is modelled as a 2 degrees of freedom (DOF) spherical joint at the water surface, a 1 DOF revolute joint represents the ball bearing (ψ_c^b) followed by a sequence of revolute joints which represents the center pipe bend (θ_{cnt}), outlet pipe twist (θ_{twi} - not used in this study) and the outlet pipe curve (θ_{cur}) which alters the direction of airflow to create the rotary motion. At the very end of the outlet pipe is another spherical joint consisting of two revolute joints controlled by $\theta_{w,vert}$ and $\theta_{w,horz}$ representing the angular variability in the initial pellet trajectory. The lengths and angles are based on the *CF90* spreader and the full set of DH parameters are given in Table 3 and 4. The robotic spreader model is depicted in Figure 2.

The rotation and translation of $\{O_n\}$ relative to $\{O_0\}$ is given by the transformation matrix (Spong et al., 2006)

$$\boldsymbol{H} = \begin{bmatrix} \boldsymbol{R}_n^0 & \boldsymbol{o}_n^0 \\ \boldsymbol{0}_{1\times 3} & 1 \end{bmatrix} \tag{3}$$

$\boldsymbol{R}_n^0$ being a 3×3 rotation matrix. $\boldsymbol{H}$ is given by the series of joints

$$\boldsymbol{H} = \boldsymbol{T}_n^0(\boldsymbol{q}) = \prod_{i=1}^{n} \boldsymbol{A}_i^{i-1}(q_i) \tag{4}$$

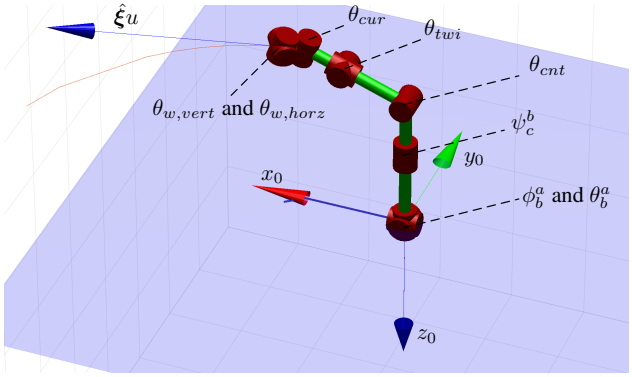

Figure 2: The 3D rendered spreader model based on the DH parameters in Table 3. The spreader attitude in this image is identical to Figure 1, with $\phi_b^a = 0$, $\theta_b^a = 0$ and $\psi_c^b = 0$. The blue arrow shows the initial pellet velocity vector and a simulated curved pellet trajectory in red below. Visualization by the RVC Toolbox (Corke, 2011).

$\boldsymbol{T}$ is a transformation matrix, $\boldsymbol{q} = \begin{bmatrix} q_1 & \cdots & q_n \end{bmatrix}^T$ are the joint variables, either defined by $q_i = \theta_i$ for revolute joints or $q_i = d_i$ for prismatic joints (Siciliano et al., 2009). For each joint, the homogeneous transformation matrix is given by

$$\boldsymbol{A}_i^{i-1}(q_i) = \begin{bmatrix} \boldsymbol{R}_i^{i-1}(q_i) & \boldsymbol{o}_i^{i-1}(q_i) \\ \boldsymbol{0}_{1\times 3} & 1 \end{bmatrix} \tag{5}$$

a_i, α_i, d_i and θ_i represents the link length, link twist, link offset and joint angle respectively (Spong et al., 2006) and given in Table 3.

From $\boldsymbol{H}$, $\boldsymbol{o}_n^0$ and $\boldsymbol{o}_{n-2}^0$ are given which are the position of the end pipe opening and the joint before angular variability is introduced. From this it follows that $\boldsymbol{o}_n^0$ is the origin of the ballistic trajectory and

$$\boldsymbol{\xi} = \begin{bmatrix} \xi_x & \xi_y & \xi_z \end{bmatrix}^T = \boldsymbol{o}_n^{n-2} = \boldsymbol{o}_n^0 - \boldsymbol{o}_{n-2}^0 \tag{6}$$

gives the vector between these two points. $n-2$ and n are used since the last two joints are non-physical, describing the variability in pellet angles when exiting the outlet pipe (Equation 8). $\hat{\boldsymbol{\xi}} = \boldsymbol{\xi}/||\boldsymbol{\xi}||$ yields the normalized attitude of the ballistic path origin, based on Skøien et al. (2015).

In this study, the differential kinematics of the spreader has been derived in order to facilitate simulation of motorized spreaders. This concept is based on an electrical, pneumatic or hydraulic motor attached to or part of the rotating joint

where the ball bearing is located, which drives the rotation of the center pipe. The mapping from joint velocities $\dot{\boldsymbol{q}}$ to the linear velocity $\dot{\boldsymbol{o}}_n^0$ and angular velocity $\dot{\boldsymbol{\omega}}_n^0$ of the outlet pipe is done via the Jacobian $\boldsymbol{J} \in \mathbb{R}^{6\times n}$ (Siciliano et al., 2009)

$$\begin{bmatrix} \dot{\boldsymbol{o}}_n^0 \\ \boldsymbol{\omega}_n^0 \end{bmatrix} = \boldsymbol{J}(\boldsymbol{q})\dot{\boldsymbol{q}} \tag{7}$$

With respect to the robotic configuration there are two notable alterations compared to Skøien et al. (2015) and Skøien et al. (2016a). Firstly, with respect to the angle of spiral shaped outlet pipe seen from above θ_{cur}. This angle is barely visible in Figure 2 and this bend rotates the airstream left which gives the rotation of the spreader. θ_{cur} was not present in either Skøien et al. (2015) or Skøien et al. (2016a) since the resulting curved path of the pellets given by this twist was assumed canceled by the tangential velocity of the outlet opening. Hence, pellets were thrown almost perfectly radially away from the spreader in relation to the water plane. However, with the introduction of a motorized spreader this twist must be taken into account.

Secondly, the two last joints of the robotic model which describes the variability of the exit angle of pellets from the spreader are given by Equation 8(a,b) and the parameters $\bar{\theta}_{out,vert}$ and $\sigma_{out,vert}$ which were previously unknown.

$$\theta_{w,vert} = \mathcal{N}(\bar{\theta}_{out,vert}, \sigma^2_{out,vert}) \tag{8a}$$

$$\theta_{w,horz} = \mathcal{N}(\bar{\theta}_{out,horz}, \sigma^2_{out,horz}) \tag{8b}$$

This gives the vertical and horizontal angular variability modelled as a Gaussian distribution.

Estimates of the angular variability was obtained from an experiment to be published by (Kevin Frank, 2016, pers. comm.). A high speed camera was mounted on the outlet pipe of the *CF90* spreader, enabling observation of the speed and angle of individual pellets. A 600 mm radius central pipe was used in this study as opposed to the model which uses a 450 mm radius pipe. Kevin Frank(2016, pers. comm.) used a 317 m feed pipe from the barge to the spreader and all experiments were performed in triplicate at 16 and 20 m/s airspeed with the spreader in both *"S"* and *"U"* configuration. A one second recording at 1000 frames per second was performed for each of the replicates. The preliminary results are stated in Table 1.

Since experimental attitude and surface distribution data was obtained at 20, 25 and 29 m/s in Skøien et al. (2016b), the 20 m/s results were mainly used from Table 1. As can be observed from the pellet angle, at higher speeds the average angle becomes smaller. Since no data exists at airspeeds higher than 20 m/s, $\theta_{w,vert}$

Table 1: Preliminary results from (Kevin Frank, 2016, pers. comm.). Average pellet speed and angle ±1 SD from the *CF90* spreader. Three replicates of 1 second each at 1000 FPS from each configuration and airspeed.

Config.	Airspeed [m/s]	Speed (u) [m/s]	Angle ($\theta_{w,vert}$) [°]	N
CF90 S	16	6.60 ± 0.62	-3.59 ± 8.30	830
CF90 U	16	7.29 ± 0.91	-8.10 ± 6.00	491
CF90 S	20	8.45 ± 0.81	-1.67 ± 7.76	1359
CF90 U	20	9.36 ± 0.98	-4.57 ± 7.60	339

was defined by $\bar{\theta}_{out,vert} = -3.1°$ and $\sigma_{out,vert} = 7.7°$. The high speed camera could only observe the vertical exit angle and the magnitude of the horizontal variability component is still unknown. It is, however, likely that in the horizontal plane $\theta_{w,horz} = 0$ and $\sigma_{out,horz}$ was set at $4°$. There is uncertainty in $\sigma_{out,horz}$, but this parameter is of far less importance due to the rotation of the spreader having a more dominant effect in the horizontal plane.

2.3. External ballistic model

Essential to the ballistic model is the speed u pellets have upon exiting the spreader. Although some data exists on average values for of u from the barge to spreader (Oehme et al., 2012), the airspeed and thus pellet speed at the spreader may vary significantly due to fluid expansion along the feed pipe (Aarseth et al., 2006; Klinzing et al., 2010). u can be obtained through modelling based on the operational parameters at the barge which are often well known, but calculations may become severely involved in such a multiparticle system (Klinzing et al., 2010). Factors such as drag, gravity, friction, compressibility, particle collisions and electrostatics may have to be considered in order to achieve an accurate model. In this study, the pellet speed is obtained by fitting model parameters to empirical results. Such an approach yield a comparatively simple and satisfactory approximation given that the remainder of the model is correct but limits the ability of the model to describe systems with widely different configurations accurately. The model in Equation 9 is used to determine the pellet speed at the outlet pipe. This based on Skøien et al. (2016a) was built upon the assumption that pellets will experience a continuous sweeping bend when $\psi_c^b = 0°$ or *"U"* configuration, whilst at $\psi_c^b = 180°$ (*"S"*) the pellets will experience an extra impact and an abrupt

alteration to their velocity component which reduces the speed.

$$u = \begin{cases} u_{pel} * -cos(2 * \psi_c^b) * \frac{(1-k_\psi)}{2} + 1 - \frac{(1-k_\psi)}{2} + \mathcal{N}(0, \sigma_{pel}^2) & \text{if } \frac{\pi}{2} < \psi_c^b < \frac{3\pi}{2} \\ u_{pel} + \mathcal{N}(0, \sigma_{pel}^2) & \text{else} \end{cases} \tag{9}$$

u_{pel} denotes the base speed of pellets right before entering the spreader (Figure 1). The need for such a description as Equation 9 is warranted based on the results in Table 1. The speed in the *"S"* configuration is 90.5 % and 90.3 % of *"U"* for 16 and 20 m/s respectively. Since 20 m/s is closest to the experimental attitude and surface distribution data, $k_\psi = 8.45/9.36 = 0.903$. The normally distributed variability term was set based on the average value at 20 m/s in Table 1, $\sigma_{pel} = 0.90$.

The scalar pellet speed must be converted into velocity components in $\mathbb{R}^3$. This is based on Skøien et al. (2015), but extended with the velocity of the outlet pipe opening $\dot{\boldsymbol{o}}_n^0$. The individual components were calculated by

$$\boldsymbol{v} = \begin{bmatrix} v_x & v_y & v_z \end{bmatrix}^T = \hat{\boldsymbol{\xi}} u + \dot{\boldsymbol{o}}_n^0 \tag{10}$$

In Skøien et al. (2016a) wind components ($\boldsymbol{w}$) and the relative velocity of a pellet in relation to the wind was introduced by

$$\boldsymbol{w} = \begin{bmatrix} w_x & w_y & 0 \end{bmatrix}^T \tag{11}$$

$$\Delta v = \parallel \Delta \boldsymbol{v} \parallel = \parallel \boldsymbol{v} - \boldsymbol{w} \parallel \tag{12}$$

Wind is used in this study only to replicate experimental conditions, and a detailed description of the effect of wind on surface pellet distribution can be obtained from Skøien et al. (2016a). The basic force of aerodynamic drag in a stationary unbounded fluid is given by White (2011)

$$F_d = -\frac{1}{2} C_{d\infty} \rho_{air} A_{proj} \Delta v^2 \tag{13}$$

A_{proj} is the frontal or projected area of the pellet, ρ_{air} = 1.2 kg/m^3 which is the air density and the kinematic viscosity $\mu_{air} = 1.8 * 10^{-5}$ Ns/m^2 as also stated in Table 4. The drag coefficient $C_{d\infty}$ is given by a non-linear function of the Reynolds number R_e White (2011)

$$C_{d\infty} = f(R_e) \tag{14}$$

often obtained via empirically established charts.

$$R_e = \frac{\rho_{air} \Delta v d_{sph}}{\mu_{air}} \tag{15}$$

d_{sph} denotes the diameter of a sphere which is volume equivalent to the pellet. In Skøien et al. (2015) the motion of the pellet was considered in a stationary fluid. However, in this extended model the effects of wind has been included and the wind velocity components may be large compared to u. Because of this, Equation 13 must be altered (Skøien et al., 2016a). In order to obtain a more accurate and dynamic description of the drag coefficient, a sphereicity parameter was introduced (Haider and Levenspiel, 1989; Wadell, 1934) which is the most commonly used shape factor (Klinzing et al., 2010).

$$\psi_{sph} := A_{sph}/A \approx 0.874 \tag{16}$$

based on a pellet with a diameter:height ratio of 1. And as in (Skøien et al., 2016a) based on (Haider and Levenspiel, 1989) the drag is described by Equation 17 which is of fairly low complexity and corresponds well with empirical studies (Chhabra et al., 1999).

$$\begin{aligned} C_{d\infty} = \frac{24}{R_e}(1 + (8.716exp(-4.0655\psi_{sph})) \\ R_e^{(0.0964+0.5565\psi_{sph})} + \frac{73.69 R_e exp(-5.0748\psi_{sph})}{R_e + 5.378exp(6.2122\psi_{sph})} \end{aligned} \tag{17}$$

Equation 17 can then be used in Equation 13 which when taking into account the wind (Ray and Fröhlich, 2015) gives

$$\boldsymbol{F}_d = -\frac{1}{2} C_{d\infty} \rho_{air} A_{proj} \parallel \Delta \boldsymbol{v} \parallel \Delta \boldsymbol{v} \tag{18}$$

Using Newton's second law the acceleration of the pellet can be written as

$$\frac{d\Delta \boldsymbol{v}}{dt} = -\frac{\kappa}{m} C_{d\infty}(\Delta \boldsymbol{v}, \psi_{sph}) \parallel \Delta \boldsymbol{v} \parallel \Delta \boldsymbol{v} + \boldsymbol{g} \tag{19}$$

on vectorial form, where $\kappa = \frac{1}{2}\rho_{air} A_{proj}$ and $\boldsymbol{g} = \begin{bmatrix} 0 & 0 & g \end{bmatrix}^T$, g = 9.81 m/s^2. With $\boldsymbol{w}$ being a constant vector, Equation 18 can be rewritten on component form

(Equations 20a-20c) and the position-velocity description given by Equations 20d - 20f.

$$\frac{dv_x}{dt} = -\frac{\kappa}{m} C_{d\infty}(\Delta v_x, \psi_{sph}) \Delta v_x ||\Delta \boldsymbol{v}|| \tag{20a}$$

$$\frac{dv_y}{dt} = -\frac{\kappa}{m} C_{d\infty}(\Delta v_y, \psi_{sph}) \Delta v_y ||\Delta \boldsymbol{v}|| \tag{20b}$$

$$\frac{dv_z}{dt} = -\frac{\kappa}{m} C_{d\infty}(\Delta v_z, \psi_{sph}) \Delta v_z ||\Delta \boldsymbol{v}|| + g \tag{20c}$$

$$\frac{ds_x}{dt} = v_x \tag{20d}$$

$$\frac{ds_y}{dt} = v_y \tag{20e}$$

$$\frac{ds_z}{dt} = v_z \tag{20f}$$

It is assumed that during the flight along the ballistic path, the pellets will be subject to some random motion not yet described in the model. To capture this stochastic behavior, a random factor is added upon water impact as defined in Skøien et al. (2015):

$$s_{x,imp} = s_x(T) + \mathcal{N}(0, \sigma_s^2) T \tag{21a}$$

$$s_{y,imp} = s_y(T) + \mathcal{N}(0, \sigma_s^2) T \tag{21b}$$

$s_{x,imp}$, $s_{y,imp}$ is the final impact point on the water surface, and T denotes the total time of flight which runs from $t = 0$ to pellet impact $s_z(t) >= 0$. The model was implemented in MATLAB (2014) and Equations 20a-20f solved using *ode45*. 360 ballistic simulations were run for one revolution of the spreader.

2.4. Experimental determination of surface coverage and spreader attitude

Oehme et al. (2012) conducted the first study which empirically obtained the surface distribution of two different rotary spreaders with varying twist (θ_{twi}) configuration and airspeed. Pellets were collected on the surface using Styrofoam boxes placed in a single line with the spreader in the centre. The study revealed a non-uniform annular surface distribution where increased airspeed resulted in a more uniform pattern and longer throw. These results could be used to parameterize the model, however, this approach has three limitations. Firstly, the two spreaders used in Oehme et al. (2012) are similar but not identical to the *CF90* which the model is based upon. Secondly, Oehme et al. (2012) only used a single row of

boxes to collect pellets giving limited information on the two dimensional surface distribution. Finally, the box row placement was not explicitly specified with respect to the orientation of the spreader. A second study was conducted as part of Skøien et al. (2016a) where two box rows were used, effectively capturing pellets in a cross formation. This study used the same *CF90* spreader the model is based upon and the orientation of the boxes are known in relation to the spreader. However, attitude data is unavailable from Skøien et al. (2016a), which would result in the attitude and surface data originating from different experiments. The current model is parameterized from the findings in Skøien et al. (2016b) where an unmanned aerial vehicle (UAV) observed the surface pellet distribution, while the spreader attitude was recorded using an Attitude and Heading Reference System (AHRS).

2.5. Simulations

The simulations in this study have been named as follows: *SIMxx* denotes the simulations that were run with attitude data from Skøien et al. (2016b) and the resulting surface distribution compared to the empirical results from the same study. xx denotes the RPM of the spreader, also obtained from Skøien et al. (2016b). Table 2 compares the simulated and experimental results by root mean square error, and a visual comparison is presented in Figure 3. *SIM78TILT* is identical to the above, with the exception that this simulation is based on the attitude data from Skøien et al. (2016b) where the spreader was offset at an extreme roll angle. This scenario sheds light on model performance when beyond normal operating conditions and these simulations conclude the part where experimental attitude and surface distribution data was used.

With the current definition of the robotic and ballistic model, the only difference in model inputs between different airspeeds was the spreader attitude and the initial speed of the pellets u_{pel}. Data for the spreader attitude and rotational speed was taken from Skøien et al. (2016b). u_{pel} was found by minimizing the difference between the experimentally determined surface distributions and the simulation results. Simulations with 172800 pellets or 480 revolutions of the spreader was run for all scenarios in this study and the results have been compared to the surface distributions in Skøien et al. (2016b) and presented in Table 2. Since the experimental results were presented the in the form of virtual boxes on the water surface, pellet counts were drawn from simulated boxes in the x_a, y_a plane, 0.8 m wide $\times$ 0.4 m deep identical to the previous experiments. Simulations were run with a water plane bin size of 5×5 cm. Consequently, the number of pellets in each simulated box was summarized across 8×16 bins. The wind field was set

based to the average windspeeds in the experiments form Skøien et al. (2016a), resulting in 1.3 m/s in $+x_a$ and 1.1 m/s in $+y_a$.

In *SIMxxB* an optimal ballistic spreader (45° initial angle over the horizontal plane) was introduced. The center pipe bend has been configured to $\theta_{cnt} = 45°$ as opposed to the original design where $\theta_{cnt} = 20°$ providing an optimal initial pellet trajectory. The aim of this configuration was to determine if such a minor alteration to the design may improve the spatial pellet distribution. Attitude data was not used for this simulation, no wind, and the spreader was fixed in a perfectly vertical position. Three simulations were run denoted *SIM39B*, *SIM55B* and *SIM72B* with otherwise identical configuration to their *SIMxx* counterparts. Results are presented in Table 2 and Figure 4.

In the final scenarios a motorized spreader is envisioned where the rotation is driven by an external force. *SIM39CAL* simulates a perfectly vertical spreader as a baseline for the following motorized simulations. This simulation is identical to *SIM39*, but run without attitude data i.e. the spreader was set perfectly vertical and the wind was set to zero. *SIMxxM* presents the results for the motorized spreader. In these simulations the final bend of the outlet pipe has been straightened so pellets will be thrown radially out from the spreader base over the water plane. The rotation in these studies was driven at a constant angular velocity by a fictive external motor, which enables control of ψ_c^b and $\dot{\psi}_c^b$ effectively decoupling the influence of airspeed on the rotational velocity of the spreader. All experiments were run at a fixed pellet velocity into the spreader u_{pel} = 9.13 m/s, identical to *SIM39*. The results are presented in Table 2 and Figure 5.

3. Results

Table 2 lists the results from all simulations. The table presents the angular velocity of the spreader, airspeed measured at the barge and u_{pel}. The airspeed is heavily dependent on the feeding system and is meant as an indication. Surface coverage is based on a 50 m diameter sea cage, and 0.4 × 0.4 bins where a bin is classified as covered as long as the number of pellets are $>= 1$. This is a crude measurement, so the Global Shannon Entropy (GSE) is presented as well (Kam et al., 2013). This metric also takes into account the number of pellets present in each bin, and a value of 1 indicates a perfectly homogeneous spatial distribution. GSE was also based on a 50 m diameter sea cage divided into 256 surface bins. This is followed by the mean throw length from the spreader and the root mean squared error between the virtual boxes of the simulations and experimental results from Skøien et al. (2016b) where applicable.

Figure 3 compares the simulations and experimental results from the *SIM39*, *SIM55*, *SIM72* and *SIM78TILT* scenario. Figure 4 compares the three simulations *SIM39B*, *SIM55B* and *SIM72B* with the optimal ballistic trajectory. Finally, Figure 5 shows the results from the motorized spreader *SIM39M*, *SIM80M* and *SIM160M*. Surface distribution heatmaps are depicted in Figure 6 corresponding to *SIM39M* and *SIM160M*.

Table 2: The angular velocity, airspeed at barge, pellet speed into the spreader, surface coverage, global Shannon entropy (GSE), average throw length and the resulting root mean square error summed across the four virtual box rows.

Name	Angular vel. $\dot{\psi}_c^b$ [RPM]	Airspeed [m/s]	Pel.speed u_{pel} [m/s]	Surf. coverage [%]	GSE [0-1]	Mean throw [m]	RMSE
Standard configuration with experimental data							
SIM39	39.5	20	9.1	13.9	.567	5.5 ± 1.1	.0034
SIM55	55.7	25	12.5	22.7	.665	7.5 ± 1.6	.0050
SIM72	72.5	29	14.4	28.5	.709	8.6 ± 1.8	.0039
SIM78TILT	78.6	29	17.5	37.1	.753	10.0 ± 3.2	.0064
Optimal initial ballistic trajectory							
SIM39B	39.5	20	9.1	18.6	.628	6.6 ± 1.3	-
SIM55B	55.7	25	12.5	28.1	.706	9.4 ± 1.5	-
SIM72 B	72.5	29	14.4	33.5	.739	10.6 ± 1.6	-
Motorized spreader							
SIM39CAL	39.5	20	9.1	14.0	.571	5.5 ± 1.1	-
SIM39M	39.5	20	9.1	18.1	.624	6.7 ± 1.2	-
SIM80M	80.0	20	9.1	20.4	.645	7.5 ± 1.2	-
SIM160M	160.0	20	9.1	27.4	.706	9.6 ± 1.4	-

4. Discussion

4.1. Model performance

The predictive ability of the model is good at *SIM39* with an RMSE of only .0034. Figure 3 at *SIM39* also shows good correspondence in all four directions. However, this is expected as the high speed data for the pellet speed and angles are obtained from experiments during similar operating conditions. The peak along $+y_a$ is not properly captured by the model. This experimental pellet peak is odd since the spreader had a slight negative roll during the experiments in

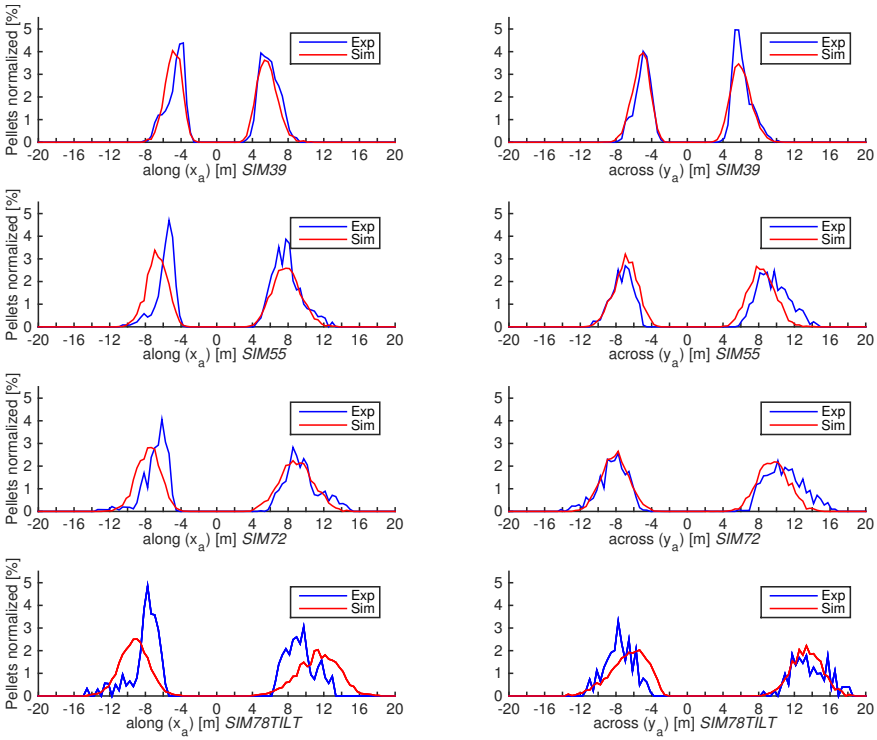

Figure 3: Experimental results from Skøien et al. (2016b) compared to simulation results from this study. Plots are taken from virtual 40 $\times$ 80 cm Styrofoam boxes placed in a cross formation along the x_a and y_a axis of the sea cage. Plots have been normalized across all boxes.

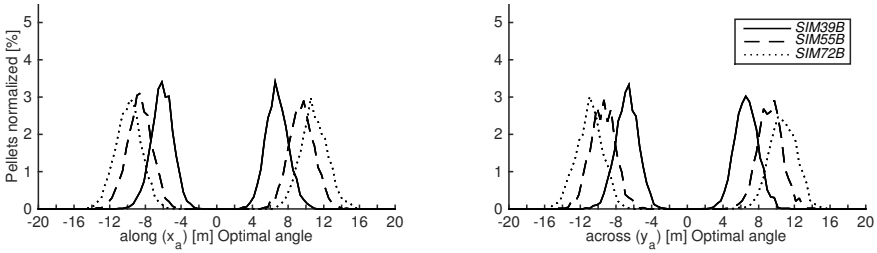

Figure 4: Experimental results using a center pipe bend angle of 45°. Plots are taken from virtual 40 $\times$ 80 cm Styrofoam boxes placed in a cross formation along the x_a and y_a axis of the sea cage. Plots have been normalized across all boxes.

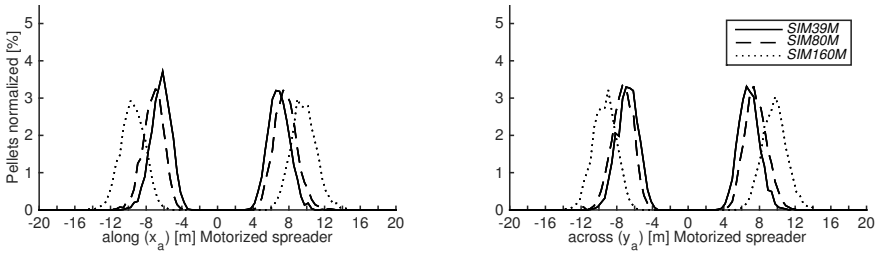

Figure 5: Experimental results using a spreader where the rotation is driven by a motor. Plots are taken from virtual 40 $\times$ 80 cm Styrofoam boxes placed in a cross formation along the x_a and y_a axis of the sea cage. Plots have been normalized across all boxes.

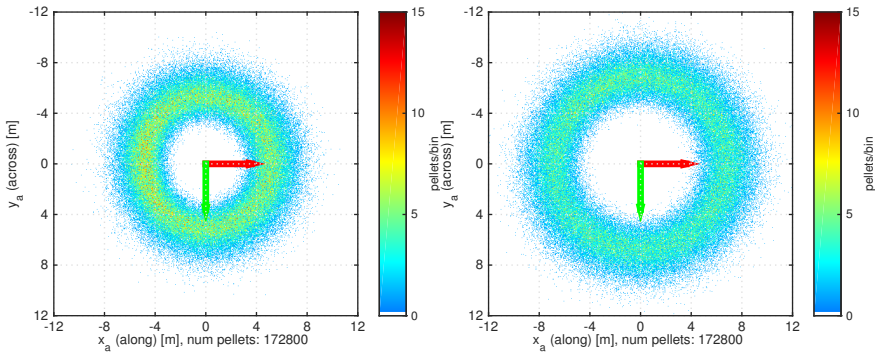

Figure 6: 2D simulated spatial surface distributions using a motorized spreader based on a 5×5 cm bin grid and the heatmap corresponds to the actual number of pellets in a given bin. Motorized spreader at 39.5 RPM (*SIM39M*) on the left side and motorized spreader at 160 RPM (*SIM160M*) on the right.

Skøien et al. (2016b) which suggests that pellets should me more concentrated and a peak more likely to occur in $-y_a$. This peak may thus be attributed to the spreader releasing pellets in batches/lumps, which is often observed, and several of these batches landing around the 4.8 m mark along $+y_a$ in the experiment. In *SIM55* the correspondence is still decent, but most notably, the simulated throw is overestimated along $-x_a$. This effect is also evident in *SIM72*. Since no high speed experimental footage exist at high airspeeds, it is not possible to know the exact pellet behaviour at such speeds. This effect may be attributed to the erratic pellet motion through the spreader increasing as a non linear function with airspeed, and thus the pellet speed out from the spreader (u) being lower than anticipated at high airspeeds.

In the tilted simulation *SIM78TILT* the spreader had an average roll offset of -16.4°. The RMSE at .0064 is the highest of all the simulated scenarios. This is expected, being quite far from normal operating conditions from which some of the experimental data was obtained. Along y_a the prediction is overall good (Figure 3) with the throw along +y_a being about four meters longer compared to $-y_a$. This indicates that the model is able to capture the effect roll has on pellet trajectory. On the other hand, along x_a the prediction is less accurate. This may indeed be a simple tuning issue as u_{pel} was tuned to minimize the difference between the experimental and simulated box distributions for each of the scenarios. Hence, a lower u_{pel} would have caused a better fit along x_a and reduced the correspondence along y_a. This overall discrepancy may be related to a number of effects. Firstly, the model releases one pellet for each degree of ψ_c^b. In the experiment, due to the negative roll offset and the weight of the center and outlet pipe, the spreader probably spent more time pointing in the general $-y_b$ direction compared to $+y_b$. This would likely result in more pellets being released in the former direction. Secondly, the number of data points from Skøien et al. (2016b) was limited for the roll offset experiment. Only one replicate could be conducted and since the spreader at times released pellets in batches (Skøien et al., 2016b) this might have skewed the results. Finally, the large roll offset may introduce new undefined effects or alter existing parameters in an unknown manner. For instance, the speed of pellets being shot down may be greater than pellets being shot upwards in the $+y_a$ direction.

4.2. Optimal ballistic configuration

In the *SIMxxB* simulations, a center pipe bend of 45° provided an optimal initial pellet trajectory. From Table 2 the surface coverage, GSE and mean throw all increased compared to the standard configuration. The mean throw length

increased by 1.1, 1.9 and 2.0 m for *SIM39B*, *SIM55B* and *SIM72B* respectively. This result indicates that longer throw may be achieved simply by altering the angle of the spreader center pipe from 20° to 45°. However, such a design alteration will increase the maximum altitude of the pellet trajectory. This increases the possibility of pellets colliding with the bird net and pellets being eaten by birds if they stray outside the bird net at some point along their trajectory. The increased elevation and flight time of pellets would also leave them more susceptible to wind. Such caveats may be avoided by reducing the airspeed in high winds or making the spreader lower. In case of a lower spreader, care must be taken to avoid sharp bends which may lead to an increase in attrition (Aarseth, 2004).

4.3. Motorized spreader

The results from the motorized spreader (Table 2) also shows a monotonically increasing pellet coverage and throw length with increased angular velocity. The initial simulation *SIM39CAL* is based on *SIM39* but with a perfectly vertical spreader and no wind. As expected, the results from these two simulations are almost identical. In *SIM39M* all variables were equivalent to *SIM39CAL* but the spreader was motorized. This alteration was simulated by straightening the last bend ($\theta_{end} = 0$) and hence the force of the air is no longer used to drive the spreader rotation. In addition an imaginary motor drives $\dot{\psi}_c^b$ at 39.5 RPM, identical to *SIM39CAL*. These alterations alone provide an increase in surface coverage from 14.0% to 18.1% and the mean throw length was 1.2 m longer. This increasing trend continues when an external motor drives the rotation at 80 and 160 RPM where the latter provides a longer mean throw and comparable surface coverage and GSE to *SIM72* whilst maintaining the same low airspeed. This result indicates that a motorized spreader may indeed outperform the classical design with respect to spatial feed distribution even at low airspeeds.

Transporting the pellets at low speed will likely lead to decreased attrition and chipping (Aarseth et al., 2006; Aarseth, 2004; Aas et al., 2011) resulting in reduced feed loss.

Although not part of this study, a motorized spreader may also yield benefits in conditions such as high wind, high water flow and when the spreader is not centred in the sea cage. The motor enables guiding of feed towards single static point or to a section of the sea cage. Pellets may be directed into the wind or current which may lead to pellets residing for a longer period of time within the water column of the sea cage, increasing the temporal availability to the fish. Directing the feed into the current may be beneficial at high current sites where the fish may abandon

their usual circular schooling pattern and congregate towards the net facing into the current (Johansson et al., 2014).

4.4. Summary

Overall the model shows good performance and corresponds well with empirical results. For further work it is recommended to develop a full pneumatic transport model. This would greatly increase the versatility of the model, as based on the pellet characteristics, conveying airspeed, pressure and pipe length one would be able to obtain the pellet speed (u_{pel}) at the end of the pipe. The current solution is tuned based on u_{pel} and this value is heavily dependent on the pneumatic transport system. The natural next step is development of a full kinetic model, taking into account such factors as the mass of the spreader, non-linear hydrodynamic drag on the counterweight, inertia of the spreader and feed pipe and ball bearing friction. The presented model performs best for certain and small deviations from the standard configuration. However, a full kinetic model would allow for simulation of an even wider array of designs and render the model independent of experimentally obtained attitude data.

5. Conclusions

This study has presented a parametrized and refined model of a pneumatic rotary feed spreader which are commonly used in sea cage aquaculture. New experimental results has been taken into account, the model has been altered and the performance evaluated. The model performs well under normal operating conditions. In addition, two experimental spreader designs have been evaluated. Firstly, the pellets were given an optimal initial ballistic angle by altering the center pipe bend of the spreader. Secondly, a motorized spreader design was evaluated based on an external force driving the rotation of the spreader. Both designs show promising simulation results with improved spatial pellet coverage compared to the standard spreader configuration. The proposed models allows researchers and equipment manufacturers to simulate alternative spreader designs and evaluate their performance.

Table 3: Denavit-Hartenberg parameters based on Skøien et al. (2015) and expanded. This is a verbose representation as links subscripted with # are added to visually position joints at the same physical position as the spreader itself. Links marked with $\star$ are not physically present, but a means to represent variability in the angle of which pellets leave the outlet pipe.

Link	a_i	α_i	d_i	θ_i
1	0	$\pi/2$	0	$\pi/2$
2	0	$-\pi/2$	0	$-\pi/2 + \phi_b^a$
3	0	$-\pi/2$	0	$-\pi/2 + \theta_b^a$
$4_\#$	0	0	$l_{\overline{CO\,BB}}$	$-\pi/2$
5	0	$\pi/2$	$l_{\overline{BB\,CNT}}$	$\pi/2 - \psi_c^b$
$6_\#$	$l_{\overline{CNT\,TWI}}$	0	0	θ_{cnt}
7	0	$\pi/2$	0	$\pi/2$
8	0	$\pi/2$	$l_{\overline{TWI\,CUR}}$	$\pi/2 + \theta_{twi}$
9	$l_{\overline{CUR\,NOI}}$	$\pi/2$	0	$\pi/2 + \theta_{cur}$
$10_\star$	0	$-\pi/2$	0	$\theta_{w,vert}$
$11_\star$	$l_{\overline{NOI\,OUT}}$	0	0	$\theta_{w,horz}$

Appendix

Denavit-Hartenberg model description

Model Parameters

Acknowledgements

The authors would like to thank Morten Malm and Ingolf Lygren at AKVA group for their assistance. This work has been supported by the Centre for Research-based Innovation in Aquaculture Technology (CREATE)(Research Council of Norway, Grant number: 174842), SINTEF Sealab, NO-7645 Trondheim, Norway.

Aarseth, K., 2004. Attrition of feed pellets during pneumatic conveying: the influence of velocity and bend radius. Biosystems Engineering 89 (2), 197--213. URL http://www.sciencedirect.com/science/article/pii/S1537511004001217

Aarseth, K., Perez, V., Bøe, J., Jeksrud, W., 2006. Reliable pneumatic conveying of fish feed. Aquacultural Engineering 35 (1), 14--25. URL http://www.sciencedirect.com/science/article/pii/S0144860905000798

Table 4: Simulation parameters. EXP indicates value obtained from the experimental results found in Skøien et al. (2016b), "-" denotes dimensionless or non-existent.

	Description	Symbol	Unit	Value
Spreader configuration	CO to ball bearing	$l_{\overline{CO\,BB}}$	cm	51
	Ball bearing to center bend	$l_{\overline{BB\,CNT}}$	cm	38
	Center bend to outlet pipe twist	$l_{\overline{CNT\,TWI}}$	cm	43
	Outlet pipe twist to outlet pipe curve	$l_{\overline{TWI\,CUR}}$	cm	26
	Outlet pipe curve to noise	$l_{\overline{CUR\,NOI}}$	cm	14
	Noise to outlet opening (leverage)	$l_{\overline{NOI\,OUT}}$	cm	≈ 0
	Angle main bend	θ_{cnt}	°	variable (20 or 45)
	Angle twist	θ_{twi}	°	0
	Angle outlet	θ_{cur}	°	variable (0 or 35.7)
	Mean horizontal pellet angle	$\bar{\theta}_{out,vert}$	°	-3.1
	Horizontal SD pellet angle	$\sigma_{out,vert}$	°	7.7
	Mean vertical pellet angle	$\bar{\theta}_{out,horz}$	°	0
	Vertical SD pellet angle	$\sigma_{out,horz}$	°	4
Ballistic properties	Air density	ρ_{air}	kg/m^3	1.2
	Air viscosity	μ_{air}	Ns/m	1.8*10^{-5}
	Gravitational acceleration	g	m/s^2	9.81
	Pellet diameter	d_p	mm	9
	Pellet height	h_p	mm	9
	Pellet mass	m_p	g	0.64
	Wind x-direction	w_x	m/s	EXP or 0
	Wind y-direction	w_y	m/s	EXP or 0
	Impact variability	σ_s	m	0.8
	Pellet speed variability	σ_{pel}	m/s	0.9
	Yaw speed effect	k_ψ	-	0.903
Other	Roll	ϕ_b^a	°	EXP or 0
	Pitch	θ_b^a	°	EXP or 0
	Outlet yaw	ψ_c^b	°	variable (-179 to 180)
	Outlet yaw rate	$\dot{\psi}_c^b$ or ω_c^b	RPM	EXP or variable (39.5 to 160)
	Cage diameter	o_{cage}	m	50
	Surface grid resolution	-	cm	5
	Pellets pr simulation	-	-	172800 (480 revolutions)
	Base pellet speed	u_{pel}	m/s	tuned (9.1 to 17.5)

Aas, T. S., Oehme, M., Sørensen, M., He, G., Lygren, I., Åsgård, T., 2011. Analysis of pellet degradation of extruded high energy fish feeds with different physical qualities in a pneumatic feeding system. Aquacultural Engineering 44 (1), 25--34.
URL http://www.sciencedirect.com/science/article/pii/S014486091000083X

Aas, T. S., Ytrestøyl, T., Åsgård, T. E., Skøien, K. R., Alver, M. O., Alfredsen, J. A., 2015. Feed intake in Atlantic salmon fed with two different spreading patterns of feed. Tech. rep., Nofima.

Alfredsen, J. A., Holand, B., Solvang-Garten, T., Uglem, I., 2007. Feeding activity and opercular pressure transients in Atlantic salmon (*Salmo salar* L.): application to feeding management in fish farming. In: Almeida, P., Quintella, B., Costa, M., Moore, A. (Eds.), Developments in Fish Telemetry. Vol. 195 of Developments in Hydrobiology. Springer Netherlands, pp. 199--207.

Alver, M. O., Alfredsen, J. A., Sigholt, T., 2004. Dynamic modelling of pellet distribution in Atlantic salmon (*Salmo salar* L.) cages. Aquacultural Engineering 31 (1-2), 51--72.

Alver, M. O., Skøien, K. R., Føre, M., Aas, T. S., Oehme, M., Alfredsen, J. A., 2016. Modelling of surface and 3D pellet distribution in Atlantic salmon (*Salmo salar* L.) cages. Aquacultural Engineering 72-73, 20--29.

Attia, J., Millot, S., Di-Poï, C., Bégout, M.-L., Noble, C., Sanchez-Vazquez, F., Terova, G., Saroglia, M., Damsgård, B., 2012. Demand feeding and welfare in farmed fish. Fish Physiology and Biochemistry 38, 107--118.

Brännäs, E., Berglund, U., Eriksson, L.-O., 2005. Time learning and anticipatory activity in groups of Arctic charr. Ethology 111 (7), 681--692.

Brooks, K. M., Mahnken, C. V. W., 2003. Interactions of Atlantic salmon in the Pacific northwest environment: II. Organic wastes. Fisheries Research 62 (3), 255--293.

Chhabra, R., Agarwal, L., Sinha, N., 1999. Drag on non-spherical particles: an evaluation of available methods. Powder Technology 101 (3), 288--295.

Corke, P. I., 2011. Robotics, Vision & Control: Fundamental Algorithms in Matlab. Springer.

Cromey, C. J., Nickell, T. D., Black, K. D., 2002. DEPOMOD-modelling the deposition and biological effects of waste solids from marine cage farms. Aquaculture 214 (1-4), 211--239.

Davis, M. W., Olla, B. L., 1987. Aggression and variation in growth of Chum salmon (*Oncorhynchus keta*) juveniles in seawater: Effects of limited ration. Canadian Journal of Fisheries and Aquatic Sciences 44 (1), 192--197.

Einen, O., Holmefjord, I., Åsgård, T., Talbot, C., 1995. Auditing nutrient discharges from fish farms: theoretical and practical considerations. Aquaculture Research 26 (9), 701--713.

Einen, O., Mørkøre, T., Rørå, A. M. B., Thomassen, M. S., 1999. Feed ration prior to slaughter---a potential tool for managing product quality of Atlantic salmon (*Salmo salar*). Aquaculture 178 (1-2), 149--169.

FAO, 2015. Fishery statistical collections, global aquaculture production. URL `http://www.fao.org/fishery/statistics/global-aquaculture-production/en`

Fenderson, O., Everhart, W., Muth, K., 1968. Comparative agonistic and feeding behavior of hatchery-reared and wild salmon in aquaria. Journal of the Fisheries Board of Canada 25 (1), 1--14.

Føre, M., Alver, M., Alfredsen, J. A., Marafioti, G., Senneset, G., Birkevold, J., Willumsen, F. V., Lange, G., Espmark, Å., Terjesen, B. F., 2016. Modelling growth performance and feeding behaviour of Atlantic salmon (*Salmo salar* L.) in commercial-size aquaculture net pens: Model details and validation through full-scale experiments. Aquaculture 464, 268--278.

Fossen, T. I., 2011. Handbook of marine craft hydrodynamics and motion control. John Wiley & Sons.

Gjøsæter, J., Otterå, H., Slinde, E., Nedreaas, K., Ervik, A., 2008. Effekter av spillfôr på marine organismer (in Norwegian). Kyst og Havbruk, 52--55.

Haider, A., Levenspiel, O., 1989. Drag coefficient and terminal velocity of spherical and nonspherical particles. Powder Technology 58 (1), 63--70.

Jobling, M., 1985. Physiological and social constraints on growth of fish with special reference to Arctic charr, *Salvelinus alpinus* L. Aquaculture 44 (2), 83--90.

Johansson, D., Laursen, F., Fernö, A., Fosseidengen, J. E., Klebert, P., Stien, L. H., Vågseth, T., Oppedal, F., 2014. The interaction between water currents and salmon swimming behaviour in sea cages. PloS one 9 (5), e97635.

Juell, J.-E., 1995. The behaviour of Atlantic salmon in relation to efficient cage-rearing. Reviews in Fish Biology and Fisheries 5, 320--335.

Kadri, S., Huntingford, F., Metcalfe, N., Thorpe, J., 1996. Social interactions and the distribution of food among one-sea-winter Atlantic salmon (*Salmo salar*) in a sea-cage. Aquaculture 139, 1--10.

Kam, K. M., Zeng, L., Zhou, Q., Tran, R., Yang, J., 2013. On assessing spatial uniformity of particle distributions in quality control of manufacturing processes. Journal of Manufacturing Systems 32 (1), 154--166.

Klinzing, G., Rizk, F., Marcus, R., Leung, L., 2010. Pneumatic Conveying of Solids: A Theoretical and Practical Approach. Dordrecht: Springer Science+ Business Media BV.

López-Olmeda, J., Noble, C., Sánchez-Vázquez, F., 2012. Does feeding time affect fish welfare? Fish Physiology and Biochemistry 38 (1), 143--152.

MATLAB, 2014. version 8.4.0.150421 (R2014b). The MathWorks Inc., Natick, Massachusetts.

Milewski, I., 2001. Impacts of salmon aquaculture on the coastal environment: a review. In: MF Tlusty, DA Bengston, HO Halvorson, SD Oktay, JB, Pearce and RB Rheault Jr.,(eds). Marine aquaculture and the environment: A meeting for stakeholders in the Northeast. Cape Cod Press, Falmouth, MA. Univ of Massachusetss Pcmbt, pp. 166--197.

Noble, C., Kadri, S., Mitchell, D. F., Huntingford, F. A., 2007a. Influence of feeding regime on intraspecific competition, fin damage and growth in 1+ Atlantic salmon parr (*Salmo salar* L.) held in freshwater production cages. Aquaculture Research 38 (11), 1137--1143.

Noble, C., Kadri, S., Mitchell, D. F., Huntingford, F. A., 2008. Growth, production and fin damage in cage-held 0+ Atlantic salmon pre-smolts (*Salmo salar* L.) fed either a) on-demand, or b) to a fixed satiation-restriction regime: Data from a commercial farm. Aquaculture 275 (1), 163--168.

Noble, C., Mizusawa, K., Suzuki, K., Tabata, M., 2007b. The effect of differing self-feeding regimes on the growth, behaviour and fin damage of rainbow trout held in groups. Aquaculture 264 (1-4), 214--222.

Norwegian Directorate of Fisheries, 2013. Lønnsomhet-sundersøkelse for matfiskproduksjon. Available from: http://www.fiskeridir.no/statistikk/akvakultur/loennsomhet/matfiskproduksjon-laks-og-regnbueoerret.
URL http://www.fiskeridir.no/statistikk/akvakultur/loennsomhet/matfiskproduksjon-laks-og-regnbueoerret

Norwegian Directorate of Fisheries, 2014. Fôrforbruk 2014.
URL http://www.fiskeridir.no/content/download/17752/150515/version/61/file/biostat-forforbruk-tab01-20150115.xlsx

Norwegian Ministry of Fisheries and Coastal Affairs, 2008. Aquaculture operations regulations with remarks (in Norwegian).
URL https://lovdata.no/dokument/SF/forskrift/2008-06-17-822

Oehme, M., Aas, T. S., Sørensen, M., Lygren, I., Åsgård, T., 11 2012. Feed pellet distribution in a sea cage using pneumatic feeding system with rotor spreader. Aquacultural Engineering 51 (0), 44--52.

Olla, B., Davis, M., Ryer, C., 1992. Foraging and predator avoidance in hatchery-reared Pacific salmon: Achievement of behavioral potential. In: The Importance of Feeding Behaviour for the Efficient Culture of Salmonid Fishes. Vol. 2. The World Aquaculture Society, pp. 5--12.

Oppedal, F., Dempster, T., Stien, L. H., 2011. Environmental drivers of Atlantic salmon behaviour in sea-cages: A review. Aquaculture 311 (1-4), 1--18.

Otterå, H., Karlsen, Ø., Slinde, E., Olsen, R. E., 2009. Quality of wild-captured saithe (*Pollachius virens* L.) fed formulated diets for 8 months. Aquaculture Research 40 (11), 1310--1319.

Rasmussen, R. S., Larsen, F. H., Jensen, S., 2007. Fin condition and growth among rainbow trout reared at different sizes, densities and feeding frequencies in high-temperature re-circulated water. Aquaculture International 15, 97--107.

Ray, S., Fröhlich, J., 2015. An analytic solution to the equations of the motion of a point mass with quadratic resistance and generalizations. Archive of Applied Mechanics 85 (4), 395--414.

Ruzzante, D. E., 1994. Domestication effects on aggressive and schooling behavior in fish. Aquaculture 120, 1--24.

Ryer, C., Olla, B., 1991. Agonistic behavior in a schooling fish: form, function and ontogeny. Environmental Biology of Fishes 31 (4), 355--363.

Ryer, C. H., Olla, B. L., 1996. Growth depensation and aggression in laboratory reared coho salmon: the effect of food distribution and ration size. Journal of Fish Biology 48 (4), 686--694.

Siciliano, B., Sciavicco, L., Villani, L., Oriolo, G., 2009. Robotics: modelling, planning and control. Springer Science & Business Media.

Skøien, K. R., Alver, M. O., Alfredsen, J. A., June 2015. Modelling spatial surface pellet distribution from rotary pneumatic feed spreaders. In: 23th Mediterranean Conference on Control and Automation (MED). pp. 883--888.

Skøien, K. R., Alver, M. O., Lundregan, S., Frank, K., Alfredsen, J. A., 2016a. Effects of wind on surface feed distribution in sea cage aquaculture: A simulation study (in press). In: European Control Conference ECC16.

Skøien, K. R., Alver, M. O., Zolich, A. P., Alfredsen, J. A., 2016b. Feed spreaders in sea cage aquaculture - Motion characterization and measurement of spatial pellet distribution using an unmanned aerial vehicle. Computers and Electronics in Agriculture 129, 27 -- 36.

Skretting, 2012. Fôr (in Norwegian). Tech. rep., Skretting.

Spong, M. W., Hutchinson, S., Vidyasagar, M., 2006. Robot modeling and control, 1st Edition. John Wiley & Sons, Hoboken, NJ.

Symons, P. E. K., 1971. Behavioural adjustment of population density to available food by juvenile Atlantic salmon. Journal of Animal Ecology 40 (3), 569--587. URL `http://www.jstor.org/stable/3438`

Talbot, C., 1993. Some biological and physical constraints to the design of feeding regimes for salmonids in intensive cultivation. In: Reinertsen, H., Dahle, L. A.,

Jørgensen, L., Tvinnereim, K. (Eds.), Fish Farming Technology. No. ISBN 9054103264. Balkema, Rotterdam, pp. 19--26.

Talbot, C., Corneillie, S., Korsøen, Ø., 1999. Pattern of feed intake in four species of fish under commercial farming conditions: implications for feeding management. Aquaculture Research 30 (7), 509--518.

Thomassen, J., Lekang, O., 1993. Optimal distribution of feed in sea cages. In: Reinertsen, H., Dahle, L. A., Jørgensen, L., Tvinnereim, K. (Eds.), Fish Farming Technology. No. ISBN 9054103264. Balkema, Rotterdam, pp. 439--442.

Thorpe, J., Cho, C. Y., 1995. Minimising waste through bioenergetically and behaviourally based feeding strategies. Water Science and Technology 31 (10), 29--40.

Thorpe, J., Talbot, C., Miles, M., Rawlings, C., Keay, D., 1990. Food consumption in 24 hours by Atlantic salmon (*Salmo salar* L.) in a sea cage. Aquaculture 90 (1), 41--47.

Wadell, H., 1934. The coefficient of resistance as a function of reynolds number for solids of various shapes. Journal of the Franklin Institute 217 (4), 459--490.

White, F., 2011. Fluid mechanics. McGraw-Hill Higher Education.

Paper I Optimizing feed delivery in salmon sea cage culture for growth and fish welfare - a simulation study (Manuscript)

(Skøien et al., 2016c)
Skøien, K. R., Alver, M. O., and Alfredsen, J. A. Optimizing feed delivery in salmon sea cage culture for growth and fish welfare - a simulation study (manuscript). 2016c

Optimizing feed delivery in salmon sea cage culture for growth and fish welfare - a simulation study

Kristoffer Rist Skøien[a,*], Morten Omholt Alver[a,b], Jo Arve Alfredsen[a]

[a] *Faculty of Information Technology, Mathematics and Electrical Engineering, department of Engineering Cybernetics, Norwegian University of Science and Technology NTNU, Trondheim, NO-7491, Norway*
[b] *SINTEF Fisheries and Aquaculture, Trondheim, NO-7465, Norway*

Abstract

This study investigates the influence of spatial feed distribution across the surface of a sea cage on central production parameters such as feed loss, growth and welfare using two different models. A model of the feed spreader produced a two dimensional surface pattern which seeded the second model of the sea cage which takes into account central factors such as feed diffusion, advection, fish crowding and appetite. Feed delivery ranging from sharply localized distributions to large uniform surface coverage has been simulated as well as various spreader configurations. The results indicate that feed should be distributed over a large surface area and that a dynamically positioned feed spreader may produce favorable results compared to a spreader in a fixed position. Results can be used by farmers, equipment producers and researchers interested in developing technology and feeding regimes to improve feed utilization and fish welfare.
Keywords: Atlantic salmon (*Salmo salar*), aquaculture, modelling, feed distribution

1. Introduction

1.1. Salmonid farming

Farming of Atlantic salmon (*Salmo salar*) begun in Norway in the 1960's and may still be considered in its infancy compared to cattle, sheep, pig and chicken farming (Føre, 2011). On a global basis, production of farmed Atlantic salmon has increased dramatically from 294 metric tonnes in 1970 to over 2.3 million tonnes in 2014 (FAO,

*Corresponding author

2016). Norway and Chile are major producers while Australia, the Faroe Islands, Great Britain and North America also feature a substantial contribution (Oppedal et al., 2011). In Norway, farmed salmon are first cultivated in indoor tanks and post smolts are transferred to floating fish farms for the major ongrowth period of up to 18 months. A sea cage is typically circular with a circumference of 90-157 m and up to 48 m deep (Oppedal et al., 2011) but even larger 240 m circumference cages are in use in Tasmania. Farms are often located in a fjord which offers some protection from the harsh coastal environment whilst providing sufficient water currents for maintaining the required level of dissolved oxygen and waste dispersal. Farms are also to some degree placed in open waters, but close to the coast to facilitate simple transport of feed, personnel, materials and fish. Efforts are directed towards development of even larger structures intended for more exposed farming outside the relative protection of fjords. Present Norwegian legislation allows for up to 200.000 individuals in a single cage at 25 kg/m^3 stocking density (Norwegian Ministry of Fisheries and Coastal Affairs, 2008). Feeding is of essential importance in the sea cage. Feed should ideally be equally available to all individuals, each fish should be able to eat until satiated, there should be no competition for feed and no feed should escape the cage. Given an average weight of 5 kg/fish prior to slaughter and a daily feed ration of 1 % (Oehme et al., 2012) 10 tonnes of feed is supplied per cage each day. Close to 1.7 million tonnes of feed was administered at Norwegian trout and salmon farms in 2014 costing up towards €2000 million (Norwegian Directorate of Fisheries, 2014a,b). The cost of feed amounts to about 50 % or more of the total farming costs (Norwegian Directorate of Fisheries, 2013) and a feed loss of 5 % to up to 15 % has been suggested (Brooks and Mahnken, 2003; Cromey et al., 2002; Gjøsæter et al., 2008; Milewski, 2001; Otterå et al., 2009) implying a substantial financial loss and poor utilization of nutritional resources (Alfredsen et al., 2007; Thorpe and Cho, 1995).

The feed itself is delivered in the form of firm extruded pellets 3-12 mm in diameter (Skretting, 2012) adapted to the present size of the fish. Feed is transported to site and offloaded into a local floating barge which handles feed distribution and monitoring of 4-16 sea cages. A pneumatic transport system transports feed to the sea cages. An array of blowers compresses ambient air and feed is introduced to the airflow through a

doser valve before being transported through floating pipes up to 800 m long (Aarseth et al., 2006) to the individual sea cages.

Located in the center of the sea cage is a pneumatic rotor feed spreader which purpose is to spread the feed over a large portion of the surface area (Figure 1). The design of this device varies. A common arrangement consists of a floating bouy or ring, sometimes with a submerged counterweight for stabilization and a ball bearing which allows the center pipe of the spreader to rotate. A spiral shaped outlet pipe redirects the air causing the spreader to rotate. Both the pellet transport, the spreader rotation and pellet throw are all driven by the same airflow.

As shown by experimental results from Oehme et al. (2012) and Skøien et al. (2016d), such a design produces an annular (donut shaped) pellet distribution covering a limited area of the sea cage surface. Oehme et al. (2012) investigated the performance of two rotor spreaders collecting pellets in Styrofoam boxes across the surface with one row of boxes on either side of the spreader. Looking at these two box rows together yielded a surface coverage of 20.5 to 66.5 %, that is boxes which contained >0 pellets. However, Oehme et al. (2012) used a 14.5 m radius cage as a reference and in relation to a standard 50 m diameter cage the surface coverage ranged from 6.9 to 22.4 % across all pellet types, airspeeds and outlet tilt configurations. Simulation results from Skøien et al. (2016b) based on empirical results from Skøien et al. (2016d) showed a surface coverage of 13.9 % to 28.5% depending on airspeed. The latter result was in relation to a 5×5 cm grid where a cell was considered covered if only one pellet landed in that cell. It addition, the skewness of the surface pattern must be considered as well as the fact that the number of pellets in a covered cell varies considerably. In summary, it seems that many spreaders may cover a limited annular section of the surface area, possibly also with the concentration skewed to one side. These results raise interest as to whether such a method of feed distribution is adequate in relation to feed loss, welfare and growth. The present study sheds new light on this topic as several different spreader configurations are simulated and key parameters are extracted from a sea cage model (Alver et al., 2016, 2004).

1.2. Feeding and behaviour

The behaviour of salmonids during feeding is influenced by the environment such as temperature and light as well as biotic factors (e.g. predation risk, hunger level and competition) (Juell, 1995). Einen et al. (1999) states that suboptimal feed intake is related to both reduced as well as inefficient growth and feed availability is crucial for efficient production (Juell, 1995). Feed should be both spatially and temporally available so the fish may forage as they desire in an unrestricted manner (Talbot et al., 1999). Ration size and the method of which feed is introduced to the fish is related to monopolization of the food supply and growth depensation (i.e. variation) (Olla et al., 1992). A highly localized feed delivery renders the food supply defensible by dominant individuals, giving a smaller ration size to subordinates (review by) Juell (1995), especially in cases of underfeeding (Olla et al., 1992). Feeding suboptimally can cause elevated levels of nutrient discharge as well as reduced growth (Einen et al., 1995) in addition to increased levels of aggression and growth depensation (Davis and Olla, 1987; Talbot, 1993; Thorpe and Cho, 1995). Noble et al. (2008) found no significant growth depensation but reduced growth and elevated levels of fin damage when the fish was administered a restricted ration. Ryer and Olla (1996) on the other hand witnessed depensation when comparing a localized feed delivery to temporally and spatially distributed feeding.

In full scale sea cages, the effect of spatially and temporally restrictive feeding versus distributed feeding on growth, growth variation, feed loss and aggression is largely unknown. This is likely related to the vast economical and welfare risks in conducting such a large scale experiment. Smaller scale studies has on the other hand demonstrated a relation between feed access and aggression (Brännäs et al., 2005; Fenderson et al., 1968; Jobling, 1985; Noble et al., 2007a,b, 2008; Rasmussen et al., 2007; Symons, 1971; Talbot et al., 1999), summarized by (Attia et al., 2012; Ruzzante, 1994; Talbot, 1993). Injury and mortality is also linked to aggressive behaviour (López-Olmeda et al., 2012). A study by Aas et al. (2015) investigated a spatially localized versus a distributed feed pattern on tank reared Atlantic salmon and found no differences in aggressiveness or growth. However, the duration of the study was too short to show any definite growth differences. The fish does show a great deal of adaptability to the feed-

ing regime they are presented with (López-Olmeda et al., 2012; Talbot, 1993; Talbot et al., 1999; Thorpe and Cho, 1995).

Overall, it seems plausible that maximizing the spatial feed distribution within the sea cage will keep agonistic behaviour to a minimum and promote rapid and efficient growth (Attia et al., 2012; Juell, 1995; Kadri et al., 1996; Olla et al., 1992; Ryer and Olla, 1991, 1996; Thomassen and Lekang, 1993; Thorpe et al., 1990; Thorpe and Cho, 1995).

1.3. Scope

This study is focused towards gaining additional insight into the effect of the spreader and the spatial surface distribution on growth, feed loss and aggression indicators. The two dimensional surface distribution is of importance as this seeds the three dimensional shape of the pellet cloud within the water column. This study simulates different 2D feed distributions, investigates and discusses the causal effect on central production parameters. The results may be of importance to farmers, equipment producers and researchers looking for methods of optimizing the farming process with respect to feed loss, growth and welfare.

2. Materials and Methods

2.1. Models

The present study combines two models to obtain the overall results. The first model is denoted $\mathcal{M}_1$ (Skøien et al., 2015, 2016b,c) and describes the spatial distribution of pellets across the water surface from a rotor feed spreader. The model is based on a robotic description of the spreader combined with an extrinsic ballistic model to calculate the trajectory of pellets through the air. $\mathcal{M}_1$ is based upon the *CF90 Double* rotor pneumatic spreader by AKVA group (Bryne, Norway) and this fundamental design is widely used in sea cage aquaculture. $\mathcal{M}_1$ is capable of simulating different airspeeds, spreader attitudes, bend configurations, wind and spreaders where the rotational motion is driven independently from the airflow. Different configurations of $\mathcal{M}_1$ produce a 2D surface distribution pattern which is given as input to the sea cage model

$\mathcal{M}_2$. $\mathcal{M}_2$ (Alver et al., 2016, 2004) simulates the sub-surface mechanisms of pellet feeding in sea cages and takes into account the sinking speed, advection and diffusion of pellets in the water column (Skøien et al., 2016a), currents and the feeding behaviour of Atlantic salmon such as foraging behaviour and feed ingestion. $\mathcal{M}_2$ gives insight into the spatiotemporal feed distribution within the sea cage, fish growth, aggression levels and feed loss. These two models will not be extensively detailed in this study as specific descriptions may be found in Skøien et al. (2015, 2016b,c) and Alver et al. (2004, 2016). Figure 1 illustrates the respective domains of $\mathcal{M}_1$ and $\mathcal{M}_2$.

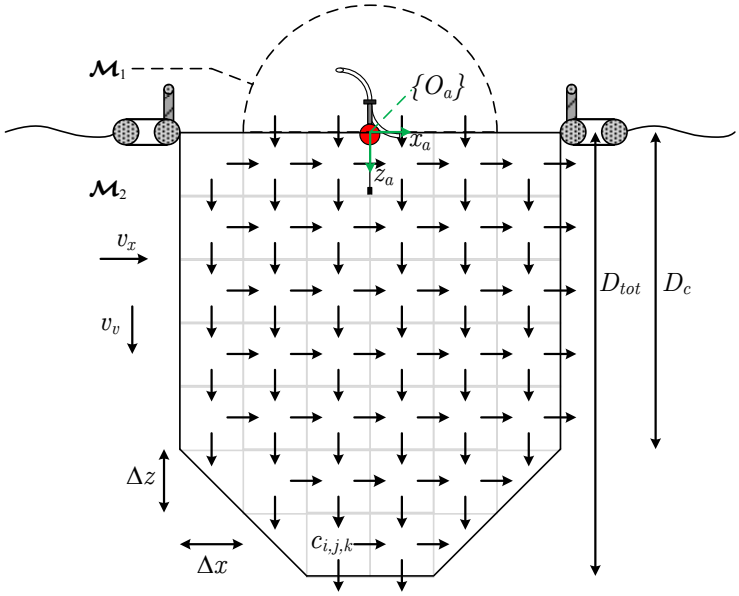

Figure 1: Overview of a sea cage and the two models. The dotted semicircle indicates the domain of $\mathcal{M}_1$ which encompasses the spreader and an extrinsic ballistic model. $\mathcal{M}_2$ operates from the water surface down. Fish and feed exist in a three dimensional quadratic grid and the feed concentration in a cell is represented by $c_{i,j,k}$. Current is given by v_x, pellet settling rate by v_v. D_{tot} and D_c represents the depth of the cylindrical section and total depth of the cage respectively.

The combination of $\mathcal{M}_1$ and $\mathcal{M}_2$ enable simulation of a range of spreader configurations and external environmental properties and the corresponding effect on central

production parameters such as growth and feed loss.

2.2. Physical representation

The origin of $\mathcal{M}_1$ and $\mathcal{M}_2$ is given by the reference frame $\{O_a\} = (x_a, y_a, z_a)$ and is considered stationary, inertial and situated at the centroid of the sea cage at the water surface. $\{O_a\}$ is defined according to the *North-East-Down* (NED) coordinate system, where x_a is directed towards *North*, y_a towards *East* and z_a *Down* normal to the water plane x_a, y_a (Fossen, 2011; Skøien et al., 2015). The reference system of the spreader is given by $\{O_b\} = (x_b, y_b, z_b)$ and fixes at the water level. Since the spreader is moored to the sea cage during typical production and we assume that the vertical motion caused by waves averages out over time, the position of the spreader with relation to the sea cage is fixed. Hence, there is no translation between $\{O_a\}$ and $\{O_b\}$.

The attitude of the spreader is given by $\mathbf{\Theta}_b^a = \begin{bmatrix}\phi_b^a & \theta_b^a & 0\end{bmatrix}$ where ϕ_b^a and θ_b^a describes the roll and pitch of the spreader respectively and $\psi_b^a = 0$ due the moorings restricting rotation of the spreader body. Since the only degree of freedom between the body and outlet pipe is the rotation of the ball bearing, the final degree of freedom is described by $\mathbf{\Theta}_c^b = \begin{bmatrix}0 & 0 & \psi_c^b\end{bmatrix}$ which is the angular position of the outlet pipe. For simplicity when referring to positions inside the sea cage, non-subscripted x, y, z will be used.

Taking into account the spreader attitude, airspeed, aerodynamic drag and the pellet characteristics, a normalized 2D surface distribution is obtained from $\mathcal{M}_1$ denoted $\boldsymbol{D}$. $\boldsymbol{D}$ is considered temporally constant as the dynamics of the feed spreader with a angular velocity ($\dot{\psi}_c^b = \omega_c^b$) of roughly 40 to 110 RPM for airspeeds >= 20 m/s (Oehme et al., 2012; Skøien and Alfredsen, 2014; Skøien et al., 2016d) is notably faster compared to the feeding dynamics of the fish. Salmonids may ingest 2 pellets/fish/min (Talbot, 1993) and maybe more at first feeding, down to 0.7 - 1.4 depending on fish size towards the end of a feeding period (Talbot et al., 1999). At 60 RPM a new batch of pellets will impact the same section of surface each second. This combined with variability in the ballistic pellet path and turbulent water caused by the erratic fish motion during feeding will likely render the temporal spreader dynamics insignificant.

Hence, $\boldsymbol{D}$ is only a spatial descriptor held constant throughout a simulation in $\mathcal{M}_2$. The spatial resolution of $\mathcal{M}_1$ is $\Delta x_a, \Delta y_a = 1/20$ m which is then adapted to the resolution of $\mathcal{M}_2$, $\Delta x, \Delta y, \Delta z = 1$ m and run to obtain the final results.

The feed transportation, feed ingestion and loss is simulated from t_0 to t_{end}. This process is mainly governed by Equation 1

$$\frac{\partial c}{\partial t} + v_x \frac{\partial c}{\partial x} + v_y \frac{\partial c}{\partial y} + (v_z + u_v)\frac{\partial c}{\partial z} + \kappa \left(\frac{\partial^2}{\partial^2 x} c + \frac{\partial^2}{\partial^2 y} c + \frac{\partial^2}{\partial^2 z} c \right) = u - f_I \quad (1)$$

(Alver et al., 2016). $c(x, y, z, t)$ is the feed concentration in a given cell, the local water current speed is given by $v_x(x, y, z, t)$, $v_y(x, y, z, t)$, $v_z(x, y, z, t)$. The sinking speed of pellets is given by u_v and κ is a constant describing the pellet diffusivity based on Skøien et al. (2016a). The added feed $u(x, y, z, t)$ is based on the surface distribution $\boldsymbol{D}$ multiplied by a given amount of feed over a certain time. Finally, f_I denotes the fish ingestion rate.

2.3. Model Configuration

In both $\mathcal{M}_1$ and $\mathcal{M}_2$ there is a vast number of possible configurations available to customize the simulation. A list of parameter values are presented in Table 3 and the variables set according to the scenario given in Table 1. In this study the primary objective is to investigate the effect on central production parameters due to different spreader configurations and spreader positioning.

The physical robotic spreader description in $\mathcal{M}_1$ was based on *CF90 Double* spreader but altered according to the given scenario. According to Skøien et al. (2016d) the mean roll and pitch of a spreader may be described by $-5^\circ \leqslant \bar{\phi}_b^a \leqslant 5^\circ$ and $-2.2^\circ \leqslant \bar{\theta}_b^a \leqslant 1^\circ$. To represent the most generic scenario, both the roll and pitch were set to zero for all simulations, i.e. the spreader was perfectly vertical. The airspeed was based on a 20 m/s airspeed scenario from Skøien et al. (2016b) which corresponded to an actual pellet speed at the spreader of 9.1 m/s. Further details regarding $\mathcal{M}_1$ may be obtained from Skøien et al. (2016b).

With respect to $\mathcal{M}_2$, a selection of the most central parameters are discussed in this section. The physical properties of the sea cage was based on common production parameters, 50 m diameter (157 m circumference) (Oppedal et al., 2011) with $D_c = 40$

m deep cylindrical section before narrowing in an inverted cone shape to a depth of $D_{tot} = 50$ m. The model resolution was set to $\Delta x = \Delta y = \Delta z = 1$ m. The cage was populated with $N = 200,000$ fish, which is the highest allowed number of individuals in Norway (Norwegian Ministry of Fisheries and Coastal Affairs, 2008). The fish population is assumed to have a normal distribution of body weights. The population was divided into 7 groups with different weights and fish counts, approximating the normal distribution. Fish positions are not explicitly modelled, but feed intake for each group is calculated taking into account the current appetite of each group, the availability of feed, the spatial distribution of feed and the competition between fish groups. The feeding regime and surface distribution of the feed will affect the distribution of feed intake between the groups. The average weight was set to 1.2 ± 0.32 kg to represent a typical weight during a production cycle. The standard deviation was based on actual measurements from a Norwegian fish farm (0.845 ± 0.224 kg, N = 160) scaled by a linear factor to represent the standard deviation at 1.2 kg. The pellet diameter was set to 9 mm based on the fish size as suggested by Skretting (2012) and the diffusivity parameter $\kappa = 1.44 * 10^{-4}$ according to Alver et al. (2016) based on the experimental results from Skøien et al. (2016a). Further, the sinkrate is set to $u_v = 12.8$ cm/s (Skøien et al., 2016a) and the mass $m_p = 0.64$ g/pellet (Oehme et al., 2012). The meal duration was set from t_0 to $t_{fstop} = 120$ minutes during which 2.64 tonnes of feed corresponding to 1.1 % of the total biomass was delivered uniformly in time. The total simulation time $t_{end} = 150$ min and all individuals were initialized with zero stomach content. Remaining parameters may be obtained from Alver et al. (2016) and have been left unaltered.

2.4. Scenarios

In order to investigate the effect from different surface distributions $\boldsymbol{D}$ on feed loss and spatial feed distribution, a range of scenarios was defined. Each scenario is identified by $\mathcal{S}$ subscripted with the given scenario identifier and additional information if applicable according to Table 1.

$\mathcal{S}_1$: This scenario does not use $\mathcal{M}_1$ but establishes a baseline by distributing all the feed into a single cell, corresponding to 1 m^2 or 0.05 % of the total surface area.

$\mathcal{S}_2$: Similar to $\mathcal{S}_1$ except here the feed was uniformly distributed into the cage in the form of a disk covering close to 85 % of the total surface area. This represents a near ideal spatial homogeneous distribution.

$\mathcal{S}_3$: $\mathcal{M}_1$ is introduced based on the standard *CF90 Double* spreader. $\mathcal{S}_3$ represents the most realistic feed distribution pattern with respect to production at a farm. This scenario is based on a pneumatic rotor spreader running at 40 RPM stationary located at the center of the sea cage. This surface distribution has been verified with empirical results (Skøien et al., 2016b) and represents an airspeed of 20 m/s. This configuration is realistic but the accuracy dependent on the length of the feed pipe as well as the configuration of the feeding system. 20 m/s airspeed is in the normal but lower range of airspeeds used at large scale farms. Farms running their feeding systems at higher airspeeds may produce a surface feed pattern closer to $\mathcal{S}_{4,80\text{RPM}}$.

$\mathcal{S}_4$ is a continuation based on $\mathcal{S}_3$ where the effect of a spreader with longer throw was investigated. This was obtained through the concept of a motorized spreader where the rotation of the center pipe ψ_c^b is driven by some external force such as a pneumatic or hydraulic motor. The idea of a motorized design originates from Skøien et al. (2016b). Such a solution decouples the spreader rotation from the transport airflow and hence the transport air is only used to transport and throw pellets. The added centripetal acceleration also contributes to a longer pellet throw. Such a design may allow for longer throw without increased pellet attrition and breakage. The increased throw may also be compared to an ordinary rotor spreader being run at higher airspeeds.

$\mathcal{S}_5$: Feeding into the current. The scenario is similar to $\mathcal{S}_3$ but a current of 0.1 m/s in $+x$ direction is introduced in $\mathcal{M}_2$. This velocity is well within what has been measured inside a cage in an exposed location Johansson et al. (2014). NS9415 (Standards Norway, 2009) classifies a midcurrent of 0.1 m/s between current class c "Substantial exposure" and d "High exposure". This scenario investigates the effect of moving the spreader further up in the direction of current and the consequent simulation results at several spreader positions. The second subscript denotes the number of meters the spreader was moved into the current.

The complete list of scenarios and corresponding parameters are given in Table 1, and the central nomenclature given in Table 3. Table 3 gives the mean radius of pellets

Table 1: The scenarios as defined in Section 2.4 and corresponding metrics of the surface coverage. The average pellet impact distance from the spreader, percentage of cells containing ≥ 1 pellet and global Shannon entropy (GSE) of the spatial surface feed distribution.

Scenario	Config. summary	Mean radius [m]	Surface coverage [%]	Surface GSE [0,1]
$\mathcal{S}_1$	Feed in single cell	-	≈ 0	0
$\mathcal{S}_{1,0.1\text{m/s}}$	0.1 m/s current	-	≈ 0	0
$\mathcal{S}_{1,0.2\text{m/s}}$	0.2 m/s current	-	≈ 0	0
$\mathcal{S}_2$	Uniform distribution	-	85	0.98
$\mathcal{S}_3$	Standard spreader 40 RPM	5.5	16	0.66
$\mathcal{S}_{4,80\text{RPM}}$	Motorized 80 RPM	7.5	23	0.72
$\mathcal{S}_{4,160\text{RPM}}$	Motorized 160 RPM	9.6	31	0.77
$\mathcal{S}_{5,0\text{m}}$	Spreader in center	5.5	16	0.66
$\mathcal{S}_{5,5\text{m}}$	Spreader moved 5 m	5.5	16	0.66
$\mathcal{S}_{5,10\text{m}}$	Spreader moved 10 m	5.5	16	0.66

where the spreader has been used and the percentage of surface area containing any pellets with respect to a 1×1 m grid. This parameter is simple to comprehend, but coarse as it does not take into account the number of pellets in each cell. Hence, the global Shannon entropy (GSE) is introduced (Kam et al., 2013) where a value of 1 equals perfect spatial uniformity and 0 is all feed exist is a singe cell.

3. Results

Table 2 presents the results from the simulated scenarios. The Table shows the feed loss at the end of the simulation calculated as the supplied feed minus total ingested feed. This metric was obtained at t_{end} ensuring that all feed had left the cage. Table 2 further lists the minimum appetite and at what time this occurred. The maximum difference in appetite was defined as $max|\Delta appetite(t)|\forall t$, which in practice is the largest difference in appetite between the smallest and largest fish group given in per-

Table 2: The scenario and corresponding results. The total feed loss, minimum average appetite across fish groups, the largest difference in appetite between group 1 and 7 given in percent points, percentage of cells within the sea cage containing more than 0.66 g feed (one pellet) and the global Shannon entropy of the spatial feed distribution. The two latter metrics were obtained from simulations without fish present in the sea cage.

Scenario	Feed loss	Min appetite	Max diff. appetite	Vol. coverage	Vol. GSE
	[%]	[%]	[pp]	[%]	[0,1]
$\mathcal{S}_1$	31.0	6.6 (@125 min)	83.2 (@40 min)	0.7	0.38
$\mathcal{S}_{1,0.1\text{m/s}}$	22.9	4.4 (@123 min)	78.6 (@36 min)	2.6	0.56
$\mathcal{S}_{1,0.2\text{m/s}}$	32.8	6.7 (@122 min)	83.0 (@47 min)	1.6	0.52
$\mathcal{S}_2$	7.2	1.9 (@125 min)	25.4 (@36 min)	85.1	0.99
$\mathcal{S}_3$	7.6	1.9 (@124 min)	59.9 (@34 min)	14.3	0.78
$\mathcal{S}_{4,80\text{RPM}}$	7.2	1.9 (@125 min)	52.1 (@34 min)	20.4	0.82
$\mathcal{S}_{4,160\text{RPM}}$	7.2	1.9 (@125 min)	45.3 (@34 min)	26.8	0.85
$\mathcal{S}_{5,0\text{m}}$	8.7	2.0 (@123 min)	56.0 (@34 min)	18.1	0.81
$\mathcal{S}_{5,5\text{m}}$	8.1	2.0 (@124 min)	56.1 (@34 min)	21.5	0.83
$\mathcal{S}_{5,10\text{m}}$	7.8	1.9 (@124 min)	56.1 (@34 min)	24.4	0.84

centage points [pp] at any time during the simulation. This metric gives insight into the largest difference in satiation between fish groups, and if sizeable, indicates that feed is not ingested uniformly. In addition, though not modelled explicitly, this variable may indicate occurrence of crowding and agonistic behaviour as a high concentration of feed in one place leads to confusion in the model and larger individuals consume a a disproportionate share of the food supply. The second to last metric in Table 2 gives the number of cells containing more than 0.66 g feed corresponding to one pellet and the GSE for the entire cage volume.

Figure 2 shows the distribution of feed inside the sea cage with no fish present in scenario $\mathcal{S}_{5,0\text{m}}$. The 0.1 m/s current clearly affects the pellet cloud forcing almost all the feed out through the side of the cage instead of the bottom.

Figure 3 illustrates the appetite of all seven fish groups through the duration of a

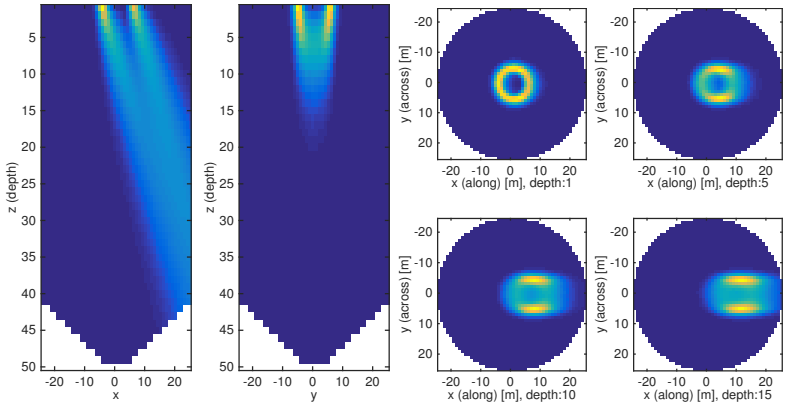

(a) Side view of sea cage (b) Top view of sea cage

Figure 2: Simulation of scenario $\mathcal{S}_{5,0\mathrm{m}}$ with no fish and continuous feeding. The surface distribution from the spreader was exported from $\mathcal{M}_1$.

feeding session. In the localized delivery scenario (Figure 3a, $\mathcal{S}_1$) the largest group feeds first, restricting feed access for the smaller fish which are forced to await their turn at the dense localized feed cloud. On the other hand, in Figure 3b when the feed is distributed over a large section of the surface area ($\mathcal{S}_2$) the fish groups feed in a more uniform manner and obtain an overall higher level of satiation.

4. Discussion

4.1. Spatially localized and spatially distributed feeding

There was as expected a significant difference between $\mathcal{S}_1$ and $\mathcal{S}_2$ in terms of all metrics in Table 2. These two scenarios represent the extremes with a fully localized and a almost maximally distributed feeding pattern across the surface. Most notably, the number of sea cage cells containing pellets increased from 0.7 to 85.1 %. Such a high concentration of feed makes it difficult for the fish to obtain pellets due to the amount of crowding and the feed loss reflects this. 31.0 % feed loss was recorded during the spatially concentrated delivery as opposed to only 7.2 % when feed was distributed across almost the entire surface. The min. appetite decreased from 6.6 % to

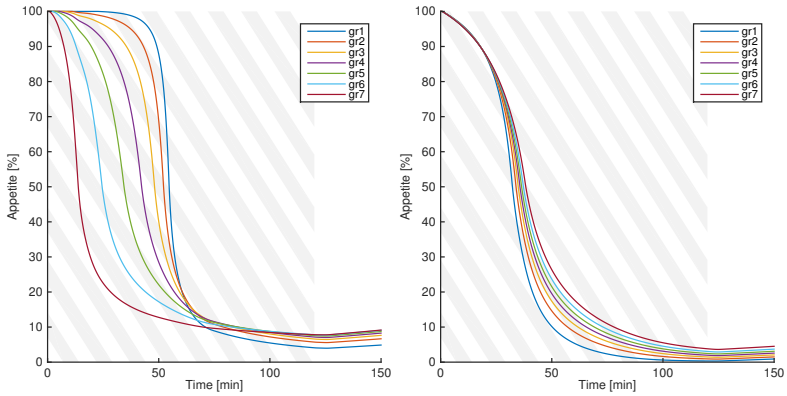

(a) Localized feeding ($\mathcal{S}_1$) (b) Distributed feeding ($\mathcal{S}_2$)

Figure 3: The appetite of the seven fish groups with time. The hatched area indicates the 120 minutes during which feed was administered.

1.9 % indicating that the fish experienced a higher degree of satiation. There is a large gap in the max diff. appetite which was reduced from 83.2 to 25.4 pp during $\mathcal{S}_2$. This indicates that large fish may have dominated the food supply at the beginning when feed is delivered in the spatially restricted fashion. Later in the feeding process as the larger fish become satiated and lose interest in the feed, the smaller fish gain increased access to the food (Figure 3). Hence, it seems that there may be large differences in satiation during feeding but at the end of the feeding period the difference in appetite has diminished. Although appetite is not directly related to aggression it may serve as an indicator. Looking at the differences between $\mathcal{S}_1$ and $\mathcal{S}_2$, the former localized delivery method indicates that differences in appetite are large during the course of a meal. More advanced behavioural models must be included before any links to agonistic behaviour can be made, but large differences in satiation may indicate heightened levels of aggression. More clearly, such a large difference in satiation may lead to size differences which increases the need for size grading during production and makes it difficult to produce the fish size which is of highest value to the market. This problem can possibly be overcome by overfeeding which again will cause increased feed

loss. Across all metrics, the results signal that a sharply localized feed delivery method is discouraged. This result also highlights the importance of the spatial surface distribution as it seeds the 3D distribution within the sea cage. However, the modelled scenario is somewhat idealized, as only the natural diffusion of pellets is included. The fish induce their own currents and it remains unclear how this affects water velocities, turbulence and flow patterns (review by Klebert et al. (2013)) which are likely to further add to the subsurface feed diffusion but this is not yet incorporated in $\mathcal{M}_2$.

4.2. Spatially localized feeding with water current

In order to investigate a more realistic scenario, a 0.1 and 0.2 m/s current in $+x$ was added to $\mathcal{S}_1$ denoted $\mathcal{S}_{1,0.1\text{ m/s}}$ and $\mathcal{S}_{1,0.2\text{m/s}}$ respectively. As can be seen from Table 2 the feed loss and appetite is reduced from $\mathcal{S}_1$ to $\mathcal{S}_{1,0.1\text{m/s}}$ due to a higher degree of spatiotemporal feed availability. The added current aids in spreading the pellets, covering the cage volume more efficiently. As a result, the volume coverage and GSE also increases. Interestingly, in $\mathcal{S}_{1,0.2\text{m/s}}$ all metrics are inferior to $\mathcal{S}_{1,0.1\text{m/s}}$. Although diffusion increased, feed loss through the cage wall becomes a dominant factor. Fish are unable to catch the pellets before they escape through the cage wall. This effect is likely to further increase with stronger currents which may be experienced at exposed sites (Johansson et al., 2014).

4.3. Using a rotor feed spreader

$\mathcal{S}_3$ yields a feed loss of 7.6 % which is very similar to the approximated feed loss of 7 % from commercial farms by Gjøsæter et al. (2008) and the 5 % to 15 % loss suggested earlier. The overall feed loss increased from 7.2 % to 7.6 % compared to the highly distributed $\mathcal{S}_2$ and min appetite remained unaltered. This limited difference is somewhat unexpected as the volume coverage is vastly contrasted, 85.1 % compared to just 14.3 % for $\mathcal{S}_3$. Even though the feed is made available to the fish through a relatively small volume, is seems to be enough for the fish to catch most of the pellets. This indicates that the distribution pattern from an ordinary rotor spreader is sufficient to satiate the fish at a slightly higher feed loss compared to $\mathcal{S}_2$. However, there is a large difference in max diff. appetite which increased from 25.4 to 59.9

pp from $\mathcal{S}_2$ to $\mathcal{S}_3$ indicating that although feed loss is limited, there may be strong hierarchical effects inside the sea cage. At 34 minutes the largest difference in appetite occurs between the smallest and largest group. Although the exact implications of this difference is unknown, it is possible that this indicates increased levels of aggressive bouts as the feed supply appears to be defensible by dominant individuals. Viewing this from another perspective, is seems that feed loss and/or FCR is not a satisfying indicator of welfare inside the sea cage. Although all fish forage until satiated at the end of feeding, the transition period shows large differences which cannot be discovered by inspecting feed loss or FCR at the end of a production cycle. This result highlights the importance of inspecting the fish for large size differences, wounds and fin damage as part of the on-site assessment of a given feeding method.

4.4. Feed spreader with increased spatial surface distribution

According to Table 1, $\mathcal{S}_{4,80\text{RPM}}$ and $\mathcal{S}_{4,160\text{RPM}}$ respectively produced a feed pattern that covered 23 % and 31 % of the surface compared to the base scenario $\mathcal{S}_3$ at 16 %. This in turn yielded an increased cage volume coverage of 20.4 % and 26.8 % for $\mathcal{S}_{4,80\text{RPM}}$ and $\mathcal{S}_{4,160\text{RPM}}$ respectively opposed to just 14.3 % for the base scenario. Interestingly, the feed loss is almost unaffected by this increased spatial distribution and the min appetite remains unchanged. This again indicates that the fish were able to reach full satiation despite the difference in distribution. However, the max diff. appetite decreases monotonically with the increased spatial distribution. As was seen in $\mathcal{S}_1$ and $\mathcal{S}_3$ the concentrated feed restricts access to subordinate individuals possibly raising aggression levels and injuries.

4.5. Movable feed spreader

Finally, across $\mathcal{S}_{5,x\text{m}}$ the concept of a movable spreader was introduced. As expected, the feed loss and min appetite was higher in this scenario with a 0.1 m/s current compared to $\mathcal{S}_3$ where the water was stationary. Some feed escaped through the cage side before being eaten. On the other hand, the max diff. appetite is lower in $\mathcal{S}_{5,0\text{m}}$ compared to $\mathcal{S}_3$ since the water current distributed the pellets over a larger volume. Moving the spreader into the current 5 or 10 m leads to a monotonically decreasing

trend in both feed loss and min appetite. Although the reduction in feed loss seems limited in Table 2, given that 8.7 % loss is the baseline value, a reduction to 7.8 % equates to a 10.8% reduction in feed loss. The new spreader location ensures that pellets remain for longer within the sea cage before becoming inaccessible to the fish on the down-current side of the sea cage.

4.6. Summary

The highly localized feed delivery method ($\mathcal{S}_1$) gave the least favorable results across all metrics. This indicates that feed should not be delivered in a spatially localized manner. A spatially large distribution is likely to promote growth and keep agonistic behaviour to a minimum (Attia et al., 2012; Juell, 1995; Kadri et al., 1996; Olla et al., 1992; Ryer and Olla, 1991, 1996; Thomassen and Lekang, 1993; Thorpe et al., 1990; Thorpe and Cho, 1995). The maximum spatial distribution ($\mathcal{S}_2$) yielded the best scores across all measured result parameters. However, producing such a large uniform feed pattern is an engineering challenge which may be too difficult or expensive to implement on floating fish farms. The added pellet transport and diffusion by currents and fish may also render $\mathcal{S}_2$ less desirable as pellets entering the water near the cage wall may easily be lost. The standard spreader ($\mathcal{S}_3$) gave good results despite the significantly reduced volume coverage compared to $\mathcal{S}_2$. However, the max diff. appetite is large but gradually reduced through the increased surface coverage of $\mathcal{S}_{4,80\text{RPM}}$ and $\mathcal{S}_{4,160\text{RPM}}$. This suggests that a spreader should cover a large surface area. Simply raising the conveying airspeed increases the surface coverage (Oehme et al., 2012; Skøien et al., 2016d) but increases pellet attrition and breakage (Aarseth, 2004; Aarseth et al., 2006). The dust may be carried away by the wind and small particles have no value as feed (Aas et al., 2011). A motorized spreader may overcome these challenges as stated by Skøien et al. (2016b). $\mathcal{S}_{5,0\text{m}}$ is identical to $\mathcal{S}_3$ and should be viewed as a more realistic scenario as a current of 0.1 m/s is present. Moving the spreader further up into the current shows promising results as it offers an improvement in feed loss and min appetite whilst max diff. appetite is almost unaltered. Realization of such a system should be fairly simple and low cost as a single winch may handle the positioning of the spreader along the axis of dominant water flow. Such winch solutions

exist and are already in place in many locations to position underwater camera systems. The positioning may be fully automated based on current measurements and/or known tidal variations. Such a solution can be even more valuable at high-current locations where the fish congregate towards the current (Johansson et al., 2014) and a traditional stationary spreader may deliver feed behind the fish which are facing in the opposite direction.

4.7. Further work

Several elements of both $\mathcal{M}_1$ and $\mathcal{M}_2$ have been verified against empirical results (Skøien et al., 2016b; Alver et al., 2004, 2016). However, the results would greatly benefit from a full scale experiment where different feeding methods are tested over time and consequent effects on feed loss, growth and injuries recorded. More complex behaviour models of fish may also be included in $\mathcal{M}_2$ such as Føre et al. (2009) and work has begun on this topic. A more advanced model may also take into account the positioning of fish in high currents (Johansson et al., 2014), and cage deformation (Klebert et al., 2015).

5. Conclusions

This study has presented the combined results of two models, one describing the behaviour of a rotor feed spreader and the other focused on the subsurface dynamics of a sea cage. The results indicate that the spatial feed distribution over the surface has a powerful influence on the volumetric coverage of feed inside the sea cage, feed loss, growth and appetite. It is possible that the disproportionate amount of attained food witnessed in some of the scenarios indicate presence of crowding and aggressive behaviour. Single point feeding is discouraged based on the simulated results as it resulted in high feed loss and substantial differences in appetite throughout the feeding session. A spatially large uniform coverage of feed across the cage surface yielded the best results, but may be difficult to achieve in practice and may result in additional feed loss in high currents. A spreader covering a large surface area combined with dynamic positioning within the sea cage is a feasible solution in practice and likely to produce good results.

Appendix

5.1. Central simulation parameters

Acknowledgements

This study has been performed with support from the Centre for Research-based Innovation in Aquaculture Technology (CREATE)(Research Council of Norway, Grant number: 174842), SINTEF Sealab, NO-7645 Trondheim, Norway.

Aarseth, K., 2004. Attrition of feed pellets during pneumatic conveying: the influence of velocity and bend radius. Biosystems Engineering 89 (2), 197–213.
URL http://www.sciencedirect.com/science/article/pii/S1537511004001217

Aarseth, K., Perez, V., Bøe, J., Jeksrud, W., 2006. Reliable pneumatic conveying of fish feed. Aquacultural Engineering 35 (1), 14–25.
URL http://www.sciencedirect.com/science/article/pii/S0144860905000798

Aas, T. S., Oehme, M., Sørensen, M., He, G., Lygren, I., Åsgård, T., 2011. Analysis of pellet degradation of extruded high energy fish feeds with different physical qualities in a pneumatic feeding system. Aquacultural Engineering 44 (1), 25–34.
URL http://www.sciencedirect.com/science/article/pii/S014486091000083X

Aas, T. S., Ytrestøyl, T., Åsgård, T. E., Skøien, K. R., Alver, M. O., Alfredsen, J. A., 2015. Feed intake in Atlantic salmon fed with two different spreading patterns of feed. Tech. rep., Nofima.

Alfredsen, J. A., Holand, B., Solvang-Garten, T., Uglem, I., 2007. Feeding activity and opercular pressure transients in Atlantic salmon (*Salmo salar* L.): application to feeding management in fish farming. In: Almeida, P., Quintella, B., Costa, M., Moore, A. (Eds.), Developments in Fish Telemetry. Vol. 195 of Developments in Hydrobiology. Springer Netherlands, pp. 199–207.

Table 3: Central simulation parameters. Symbols are for the most part based on the original description of the models (Alver et al., 2016, 2004; Skøien et al., 2015, 2016d,b). Detailed descriptions of the individual model configurations may also be obtained from here.

Description	Symbol	Unit	Value
Spreader model ($\mathcal{M}_1$)			
Pellet speed at spreader	u_{pel}	m/s	9.1
Angular spreader speed	$\dot{\psi}_c^b$	deg/s or RPM	variable (40, 80, 160 RPM)
Subsea model ($\mathcal{M}_2$)			
Depth of cylindrical cage section	D_c	m	40
Total cage depth	D_{tot}	m	50
Cell size x	Δx	m	1
Cell size y	Δy	m	1
Cell size z	Δz	m	1
Diffusion constant for 9 mm pellet	κ	m^2/s	$1.44*10^{-4}$
Number of fish size groups	m_{max}	-	7
Total number of fish in cage	N	-	200 000
Pellet diameter	D_p	mm	9
Individual pellet weight	m_p	g	0.66
Cage radius	R	25	m
Water temperature	T	° C	14
Pellet settling rate	u_v	cm/s	12.8
Current x direction	v_x	m/s	variable (0, 0.1, 0.2)
Current y direction	v_y	m/s	0
Current z direction	v_z	m/s	0
Average fish weight	W_{fish}	kg	1.2 ± 0.318

- Denotes dimensionless

Alver, M. O., Alfredsen, J. A., Sigholt, T., 2004. Dynamic modelling of pellet distribution in Atlantic salmon (*Salmo salar* L.) cages. Aquacultural Engineering 31 (1-2), 51–72.

Alver, M. O., Skøien, K. R., Føre, M., Aas, T. S., Oehme, M., Alfredsen, J. A., 2016. Modelling of surface and 3D pellet distribution in Atlantic salmon (*Salmo salar* L.) cages. Aquacultural Engineering 72-73, 20–29.

Attia, J., Millot, S., Di-Poï, C., Bégout, M.-L., Noble, C., Sanchez-Vazquez, F., Terova, G., Saroglia, M., Damsgård, B., 2012. Demand feeding and welfare in farmed fish. Fish Physiology and Biochemistry 38, 107–118.

Brännäs, E., Berglund, U., Eriksson, L.-O., 2005. Time learning and anticipatory activity in groups of Arctic charr. Ethology 111 (7), 681–692.

Brooks, K. M., Mahnken, C. V. W., 2003. Interactions of Atlantic salmon in the Pacific northwest environment: II. Organic wastes. Fisheries Research 62 (3), 255–293.

Cromey, C. J., Nickell, T. D., Black, K. D., 2002. DEPOMOD-modelling the deposition and biological effects of waste solids from marine cage farms. Aquaculture 214 (1-4), 211–239.

Davis, M. W., Olla, B. L., 1987. Aggression and variation in growth of Chum salmon (*Oncorhynchus keta*) juveniles in seawater: Effects of limited ration. Canadian Journal of Fisheries and Aquatic Sciences 44 (1), 192–197.

Einen, O., Holmefjord, I., Åsgård, T., Talbot, C., 1995. Auditing nutrient discharges from fish farms: theoretical and practical considerations. Aquaculture Research 26 (9), 701–713.

Einen, O., Mørkøre, T., Rørå, A. M. B., Thomassen, M. S., 1999. Feed ration prior to slaughter—a potential tool for managing product quality of Atlantic salmon (*Salmo salar*). Aquaculture 178 (1-2), 149–169.

FAO, 2016. Food and Agriculture Organization of the United Nations. Available from http://www.fao.org/fishery/statistics/global-aquaculture-production/query/en.

Fenderson, O., Everhart, W., Muth, K., 1968. Comparative agonistic and feeding behavior of hatchery-reared and wild salmon in aquaria. Journal of the Fisheries Board of Canada 25 (1), 1–14.

Føre, M., 2011. Individual based modelling and observation of atlantic salmon (salmo salar l.) behaviour in sea cages. Ph.D. thesis, NTNU, Norwegian University of.

Føre, M., Dempster, T., Alfredsen, J. A., Johansen, V., Johansson, D., 2009. Modelling of Atlantic salmon (*Salmo salar* L.) behaviour in sea-cages: A lagrangian approach. Aquaculture 288 (3-4), 196–204.

Fossen, T. I., 2011. Handbook of marine craft hydrodynamics and motion control. John Wiley & Sons.

Gjøsæter, J., Otterå, H., Slinde, E., Nedreaas, K., Ervik, A., 2008. Effekter av spillfôr på marine organismer (in Norwegian). Kyst og Havbruk, 52–55.

Jobling, M., 1985. Physiological and social constraints on growth of fish with special reference to Arctic charr, *Salvelinus alpinus* L. Aquaculture 44 (2), 83–90.

Johansson, D., Laursen, F., Fernö, A., Fosseidengen, J. E., Klebert, P., Stien, L. H., Vågseth, T., Oppedal, F., 2014. The interaction between water currents and salmon swimming behaviour in sea cages. PloS one 9 (5), e97635.

Juell, J.-E., 1995. The behaviour of Atlantic salmon in relation to efficient cage-rearing. Reviews in Fish Biology and Fisheries 5, 320–335.

Kadri, S., Huntingford, F., Metcalfe, N., Thorpe, J., 1996. Social interactions and the distribution of food among one-sea-winter Atlantic salmon (*Salmo salar*) in a sea-cage. Aquaculture 139, 1–10.

Kam, K. M., Zeng, L., Zhou, Q., Tran, R., Yang, J., 2013. On assessing spatial uniformity of particle distributions in quality control of manufacturing processes. Journal of Manufacturing Systems 32 (1), 154–166.

Klebert, P., Lader, P., Gansel, L., Oppedal, F., 2013. Hydrodynamic interactions on net panel and aquaculture fish cages: A review. Ocean Engineering 58, 260–274.

Klebert, P., Patursson, Ø., Endresen, P. C., Rundtop, P., Birkevold, J., Rasmussen, H. W., 2015. Three-dimensional deformation of a large circular flexible sea cage in high currents: Field experiment and modeling. Ocean Engineering 104, 511–520.

López-Olmeda, J., Noble, C., Sánchez-Vázquez, F., 2012. Does feeding time affect fish welfare? Fish Physiology and Biochemistry 38 (1), 143–152.

Milewski, I., 2001. Impacts of salmon aquaculture on the coastal environment: a review. In: MF Tlusty, DA Bengston, HO Halvorson, SD Oktay, JB, Pearce and RB Rheault Jr.,(eds). Marine aquaculture and the environment: A meeting for stakeholders in the Northeast. Cape Cod Press, Falmouth, MA. Univ of Massachusetss Pcmbt, pp. 166–197.

Noble, C., Kadri, S., Mitchell, D. F., Huntingford, F. A., 2007a. Influence of feeding regime on intraspecific competition, fin damage and growth in 1+ Atlantic salmon parr (*Salmo salar* L.) held in freshwater production cages. Aquaculture Research 38 (11), 1137–1143.

Noble, C., Kadri, S., Mitchell, D. F., Huntingford, F. A., 2008. Growth, production and fin damage in cage-held 0+ Atlantic salmon pre-smolts (*Salmo salar* L.) fed either a) on-demand, or b) to a fixed satiation-restriction regime: Data from a commercial farm. Aquaculture 275 (1), 163–168.

Noble, C., Mizusawa, K., Suzuki, K., Tabata, M., 2007b. The effect of differing self-feeding regimes on the growth, behaviour and fin damage of rainbow trout held in groups. Aquaculture 264 (1-4), 214–222.

Norwegian Directorate of Fisheries, 2013. Lønnsomhetsundersøkelse for matfiskproduksjon. Available from: http://www.fiskeridir.no/statistikk/akvakultur/loennsomhet/matfiskproduksjon-laks-og-regnbueoerret.
URL `http://www.fiskeridir.no/statistikk/akvakultur/loennsomhet/matfiskproduksjon-laks-og-regnbueoerret`

Norwegian Directorate of Fisheries, 2014a. Fôrforbruk 2014.
URL http://www.fiskeridir.no/content/download/17752/150515/version/61/file/biostat-forforbruk-tab01-20150115.xlsx

Norwegian Directorate of Fisheries, 2014b. Lønnsomhetsundersøkelse for laks og regnbueørret: Matfiskproduksjon. www.fiskeridir.no.
URL http://www.fiskeridir.no/Akvakultur/Statistikk-akvakultur/Loennsomhetsundersoekelse-for-laks-og-regnbueoerret/Matfiskproduksjon-laks-og-regnbueoerret

Norwegian Ministry of Fisheries and Coastal Affairs, 2008. Aquaculture operations regulations with remarks (in Norwegian).
URL https://lovdata.no/dokument/SF/forskrift/2008-06-17-822

Oehme, M., Aas, T. S., Sørensen, M., Lygren, I., Åsgård, T., 11 2012. Feed pellet distribution in a sea cage using pneumatic feeding system with rotor spreader. Aquacultural Engineering 51 (0), 44–52.

Olla, B., Davis, M., Ryer, C., 1992. Foraging and predator avoidance in hatchery-reared Pacific salmon: Achievement of behavioral potential. In: The Importance of Feeding Behaviour for the Efficient Culture of Salmonid Fishes. Vol. 2. The World Aquaculture Society, pp. 5–12.

Oppedal, F., Dempster, T., Stien, L. H., 2011. Environmental drivers of Atlantic salmon behaviour in sea-cages: A review. Aquaculture 311 (1-4), 1–18.

Otterå, H., Karlsen, Ø., Slinde, E., Olsen, R. E., 2009. Quality of wild-captured saithe (*Pollachius virens* L.) fed formulated diets for 8 months. Aquaculture Research 40 (11), 1310–1319.

Rasmussen, R. S., Larsen, F. H., Jensen, S., 2007. Fin condition and growth among rainbow trout reared at different sizes, densities and feeding frequencies in high-temperature re-circulated water. Aquaculture International 15, 97–107.

Ruzzante, D. E., 1994. Domestication effects on aggressive and schooling behavior in fish. Aquaculture 120, 1–24.

Ryer, C., Olla, B., 1991. Agonistic behavior in a schooling fish: form, function and ontogeny. Environmental Biology of Fishes 31 (4), 355–363.

Ryer, C. H., Olla, B. L., 1996. Growth depensation and aggression in laboratory reared coho salmon: the effect of food distribution and ration size. Journal of Fish Biology 48 (4), 686–694.

Skøien, K. R., Aas, T. S., Alver, M. O., Romarheim, O. H., Alfredsen, J. A., 2016a. Intrinsic settling rate and spatial diffusion properties of extruded fish feed pellets. Aquacultural Engineering 74, 30–37.

Skøien, K. R., Alfredsen, J. A., Sept 2014. Feeding of large-scale fish farms: Motion characterization of a pneumatic rotor feed spreader. In: Oceans - St. John's, 2014. pp. 1–7.

Skøien, K. R., Alver, M. O., Alfredsen, J. A., June 2015. Modelling spatial surface pellet distribution from rotary pneumatic feed spreaders. In: 23th Mediterranean Conference on Control and Automation (MED). pp. 883–888.

Skøien, K. R., Alver, M. O., Alfredsen, J. A., 2016b. Modelling and simulation of rotary feed spreaders with application to sea cage aquaculture - a study of common and alternative designs (manuscript).

Skøien, K. R., Alver, M. O., Lundregan, S., Frank, K., Alfredsen, J. A., 2016c. Effects of wind on surface feed distribution in sea cage aquaculture: A simulation study (in press). In: European Control Conference ECC16.

Skøien, K. R., Alver, M. O., Zolich, A. P., Alfredsen, J. A., 2016d. Feed spreaders in sea cage aquaculture - Motion characterization and measurement of spatial pellet distribution using an unmanned aerial vehicle. Computers and Electronics in Agriculture 129, 27 – 36.

Skretting, 2012. Fôr (in Norwegian). Tech. rep., Skretting.

Standards Norway, N., 2009. Ns9415 marine fish farms – requirements for site survey, risk analyses, design, dimensioning, production, installation and operation. ics 65.150;67.260.
URL http://www.standard.no

Symons, P. E. K., 1971. Behavioural adjustment of population density to available food by juvenile Atlantic salmon. Journal of Animal Ecology 40 (3), 569–587.
URL http://www.jstor.org/stable/3438

Talbot, C., 1993. Some biological and physical constraints to the design of feeding regimes for salmonids in intensive cultivation. In: Reinertsen, H., Dahle, L. A., Jørgensen, L., Tvinnereim, K. (Eds.), Fish Farming Technology. No. ISBN 9054103264. Balkema, Rotterdam, pp. 19–26.

Talbot, C., Corneillie, S., Korsøen, Ø., 1999. Pattern of feed intake in four species of fish under commercial farming conditions: implications for feeding management. Aquaculture Research 30 (7), 509–518.

Thomassen, J., Lekang, O., 1993. Optimal distribution of feed in sea cages. In: Reinertsen, H., Dahle, L. A., Jørgensen, L., Tvinnereim, K. (Eds.), Fish Farming Technology. No. ISBN 9054103264. Balkema, Rotterdam, pp. 439–442.

Thorpe, J., Cho, C. Y., 1995. Minimising waste through bioenergetically and behaviourally based feeding strategies. Water Science and Technology 31 (10), 29–40.

Thorpe, J., Talbot, C., Miles, M., Rawlings, C., Keay, D., 1990. Food consumption in 24 hours by Atlantic salmon (*Salmo salar* L.) in a sea cage. Aquaculture 90 (1), 41–47.

References

Aarseth, K. Attrition of feed pellets during pneumatic conveying: the influence of velocity and bend radius. *Biosystems Engineering*, 89(2):197–213, 2004. ISSN 1537-5110. doi: http://dx.doi.org/10.1016/j.biosystemseng.2004.06.008.

Aarseth, K., Perez, V., Bøe, J., and Jeksrud, W. Reliable pneumatic conveying of fish feed. *Aquacultural Engineering*, 35(1):14–25, 2006. ISSN 0144-8609. doi: http://dx.doi.org/10.1016/j.aquaeng.2005.06.006.

Aas, T. S., Oehme, M., Sørensen, M., He, G., Lygren, I., and Åsgård, T. Analysis of pellet degradation of extruded high energy fish feeds with different physical qualities in a pneumatic feeding system. *Aquacultural Engineering*, 44(1):25–34, 2011. ISSN 0144-8609. doi: http://dx.doi.org/10.1016/j.aquaeng.2010.11.002.

Aas, T. S., Ytrestøyl, T., Åsgård, T. E., Skøien, K. R., Alver, M. O., and Alfredsen, J. A. Feed intake in Atlantic salmon fed with two different spreading patterns of feed. Technical report, Nofima, 2015.

Alfredsen, J. A., Holand, B., Solvang-Garten, T., and Uglem, I. Feeding activity and opercular pressure transients in Atlantic salmon (*Salmo salar* L.): application to feeding management in fish farming. In Almeida, P., Quintella, B., Costa, M., and Moore, A., editors, *Developments in Fish Telemetry*, volume 195 of *Developments in Hydrobiology*, pages 199–207. Springer Netherlands, 2007. ISBN 978-1-4020-6236-0. doi: http://dx.doi.org/10.1007/978-1-4020-6237-7_19.

Alver, M. O., Alfredsen, J. A., and Sigholt, T. Dynamic modelling of pellet distribution in Atlantic salmon (*Salmo salar* L.) cages. *Aquacultural Engineering*, 31(1-2):51–72, 2004. ISSN 0144-8609. doi: http://dx.doi.org/10.1016/j.aquaeng.2004.01.002.

Alver, M. O., Skøien, K. R., Føre, M., Aas, T. S., Oehme, M., and Alfredsen, J. A. Modelling of surface and 3D pellet distribution in Atlantic salmon (*Salmo salar* L.) cages. *Aquacultural Engineering*, 72-73:20–29, 2016. ISSN 0144-8609. doi: http://dx.doi.org/10.1016/j.aquaeng.2016.03.003.

Attia, J., Millot, S., Di-Poï, C., Bégout, M.-L., Noble, C., Sanchez-Vazquez, F., Terova, G., Saroglia, M., and Damsgård, B. Demand feeding and welfare in farmed fish. *Fish Physiology and Biochemistry*, 38:107–118, 2012. ISSN 0920-1742. doi: http://dx.doi.org/10.1007/s10695-011-9538-4.

Ayer, N. W. and Tyedmers, P. H. Assessing alternative aquaculture technologies: life cycle assessment of salmonid culture systems in Canada. *Journal of Cleaner Production*, 17(3):362–373, 2009. ISSN 0959-6526. doi: http://dx.doi.org/10.1016/j.jclepro.2008.08.002.

Bradski, G. The OpenCV Library. *Dr. Dobb's Journal of Software Tools*, 2000.

Brännäs, E., Berglund, U., and Eriksson, L.-O. Time learning and anticipatory activity in groups of Arctic charr. *Ethology*, 111(7):681–692, 2005. ISSN 1439-0310. doi: http://dx.doi.org/10.1111/j.1439-0310.2005.01094.x.

Brooks, K. M. and Mahnken, C. V. W. Interactions of Atlantic salmon in the Pacific northwest environment: II. Organic wastes. *Fisheries Research*, 62(3): 255–293, 2003.

Buchspies, B., Tölle J, S., and Jungbluth, N. Life cycle assessment of high-sea fish and salmon aquaculture. Technical report, ESU-services Ltd., 2011.

Canny, J. A computational approach to edge detection. *IEEE Transactions on Pattern Analysis and Machine Intelligence*, PAMI-8(6):679–698, Nov 1986. ISSN 0162-8828. doi: http://dx.doi.org/10.1109/TPAMI.1986.4767851.

Chen, Y.-S., Beveridge, M. C., and Telfer, T. C. Physical characteristics of commercial pelleted Atlantic salmon feeds and consideration of implications for modeling of waste dispersion through sedimentation. *Aquaculture International*, 7: 89–100, 1999. ISSN 0967-6120. doi: http://dx.doi.org/10.1023/A:1009249721787. 10.1023/A:1009249721787.

Cho, C. Y. and Bureau, D. P. A review of diet formulation strategies and feeding systems to reduce excretory and feed wastes in aquaculture. *Aquaculture Research*, 32:349–360, 2001. ISSN 1365-2109. doi: http://dx.doi.org/10.1046/j.1355-557x.2001.00027.x.

Corke, P. I. *Robotics, Vision & Control: Fundamental Algorithms in Matlab*. Springer, 2011. ISBN 978-3-642-20143-1.

Costa-Pierce, B. A. *Ecological aquaculture: the evolution of the blue revolution*. John Wiley & Sons, 2008.

Cromey, C. J., Nickell, T. D., and Black, K. D. DEPOMOD-modelling the deposition and biological effects of waste solids from marine cage farms. *Aquaculture*, 214(1-4):211–239, 2002. ISSN 0044-8486. doi: http://dx.doi.org/10.1016/S0044-8486(02)00368-X.

Cromey, C. J., Nickell, T. D., Treasurer, J., Black, K. D., and Inall, M. Modelling the impact of cod (*Gadus morhua* L.) farming in the marine environment - CODMOD. *Aquaculture*, 289(1-2):42–53, 2009. ISSN 0044-8486. doi: http://dx.doi.org/10.1016/j.aquaculture.2008.12.020.

Davis, M. W. and Olla, B. L. Aggression and variation in growth of Chum salmon (*Oncorhynchus keta*) juveniles in seawater: Effects of limited ration. *Canadian Journal of Fisheries and Aquatic Sciences*, 44(1):192–197, 1987.

Dempster, T., Sanchez-Jerez, P., Fernandez-Jover, D., Bayle-Sempere, J., Nilsen, R., Bjørn, P.-A., and Uglem, I. Proxy measures of fitness suggest coastal fish farms can act as population sources and not ecological traps for wild gadoid fish. *PLoS ONE*, 6(1):1–9, 01 2011. doi: http://dx.doi.org/10.1371/journal.pone.0015646.

Einen, O., Holmefjord, I., Åsgård, T., and Talbot, C. Auditing nutrient discharges from fish farms: theoretical and practical considerations. *Aquaculture Research*, 26(9):701–713, 1995.

Einen, O., Mørkøre, T., Rørå, A. M. B., and Thomassen, M. S. Feed ration prior to slaughter—a potential tool for managing product quality of Atlantic salmon (*Salmo salar*). *Aquaculture*, 178(1-2):149–169, 1999. ISSN 0044-8486. doi: http://dx.doi.org/10.1016/S0044-8486(99)00126-X.

Ellingsen, H., Olaussen, J., and Utne, I. Environmental analysis of the norwegian fishery and aquaculture industry—A preliminary study focusing on farmed salmon. *Marine Policy*, 33(3):479–488, 2009. ISSN 0308-597X. doi: http://dx.doi.org/10.1016/j.marpol.2008.11.003.

FAO. *The state of world fisheries and aquaculture*. Number ISBN 978-92-5-107225-7. FAO - Food and agriculture organization of the united nations, Fisheries and Aquaculture Department, 2012.

FAO. *The state of world fisheries and aquaculture*. Number ISBN 978-92-5-108275-1. FAO - Food and agriculture organization of the united nations, Fisheries and Aquaculture Department, 2014a.

FAO. Food and Agriculture Organization of the United Nations. Available from http://www.fao.org/ag/againfo/themes/en/meat/backgr_sources.html, 2014b.

FAO. Food and Agriculture Organization of the United Nations. Available from http://www.fao.org/fishery/statistics/global-aquaculture-production/query/en, 2016a.

FAO. Food and Agriculture Organization of the United Nations. Available from http://faostat3.fao.org/, 2016b.

Fenderson, O., Everhart, W., and Muth, K. Comparative agonistic and feeding behavior of hatchery-reared and wild salmon in aquaria. *Journal of the Fisheries Board of Canada*, 25(1):1–14, 1968.

Fernandez-Jover, D., Martinez-Rubio, L., Sanchez-Jerez, P., Bayle-Sempere, J. T., Jimenez, J. A. L., Lopez, F. J. M., Bjørn, P.-A., Uglem, I., and Dempster, T. Waste feed from coastal fish farms: A trophic subsidy with compositional side-effects for wild gadoids. *Estuarine, Coastal and Shelf Science*, 91(4):559–568, 2011. ISSN 0272-7714. doi: http://dx.doi.org/10.1016/j.ecss.2010.12.009.

Fernö, A., Huse, I., Juell, J.-E., and Bjordal, Å. Vertical distribution of Atlantic salmon (*Salmo salar* L.) in net pens: trade-off between surface light avoidance and food attraction. *Aquaculture*, 132(3):285–296, 1995. ISSN 0044-8486. doi: http://dx.doi.org/10.1016/0044-8486(94)00384-Z.

FHL and EFF. Norsk havbruk (in Norwegian). Technical report, The Norwegian Seafood Federation and the Norwegian Seafood Export Council, 2011.

Findlay, R. H. and Watling, L. Toward a process level model to predict the effects of salmon net-pen aquaculture on the benthos. *Hargrave, B.T,[ed.]. Modelling benthic impacts of organic enrichment from marine aquaculture. Can. Tech. Rep. Fish. Aquat. Sci. 1949: xi + 125 p*, 1994.

Føre, M., Dempster, T., Alfredsen, J. A., Johansen, V., and Johansson, D. Modelling of Atlantic salmon (*Salmo salar* L.) behaviour in sea-cages: A lagrangian approach. *Aquaculture*, 288(3-4):196–204, 2009. ISSN 0044-8486. doi: http://dx.doi.org/10.1016/j.aquaculture.2008.11.031.

Føre, M., Dempster, T., Alfredsen, J. A., and Oppedal, F. Modelling of Atlantic salmon (*Salmo salar* L.) behaviour in sea-cages: Using artificial light to control swimming depth. *Aquaculture*, 388–391:137 – 146, 2013. ISSN 0044-8486. doi: http://dx.doi.org/10.1016/j.aquaculture.2013.01.027.

Føre, M., Alver, M., Alfredsen, J. A., Marafioti, G., Senneset, G., Birkevold, J., Willumsen, F. V., Lange, G., Espmark, Å., and Terjesen, B. F. Modelling growth performance and feeding behaviour of Atlantic salmon (*Salmo salar* L.) in commercial-size aquaculture net pens: Model details and validation through full-scale experiments. *Aquaculture*, 464:268–278, 2016.

Forster, J. Cost trends in farmed salmon. Technical report, 533 East Park Port Angeles, Washington 98362, June 1995.

Fossen, T. I. *Handbook of marine craft hydrodynamics and motion control*. John Wiley & Sons, 2011.

Foster, M., Petrell, R., Ito, M., and Ward, R. Detection and counting of uneaten food pellets in a sea cage using image analysis. *Aquacultural Engineering*, 14(3): 251–269, 1995. ISSN 0144-8609. doi: http://dx.doi.org/10.1016/0144-8609(94)00006-M.

Gillibrand, P. and Turrell, W. Simulating the dispersion and settling of particulate material and associated substances from salmon farms. Technical report, Marine Laboratory, Aberdeen , Report No 3/97, Victoria Road, Aberdeen AB11 9DB, UK, 1997.

Gjøsæter, J., Otterå, H., Slinde, E., Nedreaas, K., and Ervik, A. Effekter av spillfôr på marine organismer (in Norwegian). *Kyst og Havbruk*, pages 52–55, 2008.

González, A. D., Frostell, B., and Carlsson-Kanyama, A. Protein efficiency per unit energy and per unit greenhouse gas emissions: Potential contribution of diet choices to climate change mitigation. *Food Policy*, 36(5):562–570, 2011. ISSN 0306-9192. doi: http://dx.doi.org/10.1016/j.foodpol.2011.07.003.

Goulão, M., Andrade, C., Gouveia, N., Gomes, J., Timóteo, V., and Soares, F. Evaluación de pérdidas de piensos en una piscifactoría en mar abierto y su uso en modelos del crecimiento de peces de cultivo y de la ración diaria (in Spanish). In *Publicación Previa al VIII Congreso Nacional de Acuicultura*, 2001.

Grøttum, J. A. and Beveridge, M. *A review of cage aquaculture: northern Europe*. Number 498. FAO - Food and agriculture organization of the united nations, Fisheries and Aquaculture Department, Fisheries Technical Paper, 2007.

Handeland, S. O., Imsland, A. K., and Stefansson, S. O. The effect of temperature and fish size on growth, feed intake, food conversion efficiency and stomach evacuation rate of Atlantic salmon post-smolts. *Aquaculture*, 283(1-4):36 – 42, 2008. ISSN 0044-8486. doi: http://dx.doi.org/10.1016/j.aquaculture.2008.06.042.

Hansen, L. P. Migration and survival of farmed Atlantic salmon (*Salmo salar* L.) released from two norwegian fish farms. *ICES Journal of Marine Science: Journal du Conseil*, 63(7):1211–1217, 2006. doi: http://dx.doi.org/10.1016/j.icesjms.2006.04.022.

Harwood, A. J., Armstrong, J. D., Metcalfe, N. B., and Griffiths, S. W. Does dominance status correlate with growth in wild stream-dwelling Atlantic salmon (*Salmo salar*)? *Behavioral Ecology*, 14(6):902–908, 2003. doi: http://10.1093/beheco/arg080.

Hoar, W. S. The endocrine regulation of migratory behavior in anadromous teleosts. In *Proceedings of the XVI International Congress of Zoology*, volume 3, pages 14–20, 1963.

Hough, V. and Paul, C. Method and means for recognizing complex patterns, Dec. 18 1962. US Patent 3,069,654.

Jobling, M. Physiological and social constraints on growth of fish with special reference to Arctic charr, *Salvelinus alpinus* L. *Aquaculture*, 44(2):83–90, 1985. ISSN 0044-8486. doi: http://dx.doi.org/10.1016/0044-8486(85)90011-0.

Johansson, D., Laursen, F., Fernö, A., Fosseidengen, J. E., Klebert, P., Stien, L. H., Vågseth, T., and Oppedal, F. The interaction between water currents and salmon swimming behaviour in sea cages. *PloS one*, 9(5):e97635, 2014.

Juell, J.-E. The behaviour of Atlantic salmon in relation to efficient cage-rearing. *Reviews in Fish Biology and Fisheries*, 5:320–335, 1995. ISSN 0960-3166. doi: http://dx.doi.org/10.1007/BF00043005.

Kadri, S., Huntingford, F., Metcalfe, N., and Thorpe, J. Social interactions and the distribution of food among one-sea-winter Atlantic salmon (*Salmo salar*) in a sea-cage. *Aquaculture*, 139:1–10, 1996. ISSN 0044-8486. doi: http://dx.doi.org/10.1016/0044-8486(95)01163-3.

Kam, K. M., Zeng, L., Zhou, Q., Tran, R., and Yang, J. On assessing spatial uniformity of particle distributions in quality control of manufacturing processes. *Journal of Manufacturing Systems*, 32(1):154–166, 2013.

Klebert, P., Patursson, Ø., Endresen, P. C., Rundtop, P., Birkevold, J., and Rasmussen, H. W. Three-dimensional deformation of a large circular flexible sea cage in high currents: Field experiment and modeling. *Ocean Engineering*, 104:511–520, 2015. ISSN 0029-8018. doi: http://dx.doi.org/10.1016/j.oceaneng.2015.04.045.

Klinzing, G., Rizk, F., Marcus, R., and Leung, L. *Pneumatic Conveying of Solids: A Theoretical and Practical Approach*. Dordrecht: Springer Science+ Business Media BV, 2010.

Kuhn, H. W. The hungarian method for the assignment problem. *Naval research logistics quarterly*, 2(1-2):83–97, 1955.

López-Olmeda, J., Noble, C., and Sánchez-Vázquez, F. Does feeding time affect fish welfare? *Fish Physiology and Biochemistry*, 38(1):143–152, 2012. ISSN 0920-1742. doi: http://dx.doi.org/10.1007/s10695-011-9523-y.

MATLAB. *version 8.4.0.150421 (R2014b)*. The MathWorks Inc., Natick, Massachusetts, 2014.

McGinnity, P., Prodöhl, P., Ferguson, A., Hynes, R., Maoiléidigh, N. ó., Baker, N., Cotter, D., O'Hea, B., Cooke, D., Rogan, G., Taggart, J., and Cross, T. Fitness reduction and potential extinction of wild populations of Atlantic salmon, *Salmo salar*, as a result of interactions with escaped farm salmon. *Proceedings of the Royal Society of London B: Biological Sciences*, 270(1532):2443–2450, 2003. ISSN 0962-8452. doi: http://dx.doi.org/10.1098/rspb.2003.2520.

Milewski, I. Impacts of salmon aquaculture on the coastal environment: a review. In *MF Tlusty, DA Bengston, HO Halvorson, SD Oktay, JB, Pearce and RB Rheault Jr.,(eds). Marine aquaculture and the environment: A meeting for stakeholders in the Northeast. Cape Cod Press, Falmouth, MA*, pages 166–197. Univ of Massachusetss Pcmbt, 2001.

Munkres, J. Algorithms for the assignment and transportation problems. *Journal of the Society for Industrial & Applied Mathematics*, 5(1):32–38, 1957.

Noble, C., Kadri, S., Mitchell, D. F., and Huntingford, F. A. Influence of feeding regime on intraspecific competition, fin damage and growth in 1+ Atlantic salmon parr (*Salmo salar* L.) held in freshwater production cages. *Aquaculture Research*, 38(11):1137–1143, 2007a. ISSN 1365-2109. doi: http://dx.doi.org/10.1111/j.1365-2109.2007.01777.x.

Noble, C., Mizusawa, K., Suzuki, K., and Tabata, M. The effect of differing self-feeding regimes on the growth, behaviour and fin damage of rainbow trout held in groups. *Aquaculture*, 264(1-4):214–222, 2007b. ISSN 0044-8486. doi: http://dx.doi.org/10.1016/j.aquaculture.2006.12.028.

Noble, C., Kadri, S., Mitchell, D. F., and Huntingford, F. A. Growth, production and fin damage in cage-held 0+ Atlantic salmon pre-smolts (*Salmo salar* L.) fed either a) on-demand, or b) to a fixed satiation-restriction regime: Data from a commercial farm. *Aquaculture*, 275(1):163–168, 2008. ISSN 0044-8486. doi: http://dx.doi.org/10.1016/j.aquaculture.2007.12.028.

Norwegian Directorate of Fisheries. Profitability survey on the production of Atlantic salmon and rainbow trout (in norwegian). Technical Report ISSN 1894-2881, www.fiskeridir.no, 2015a.

Norwegian Directorate of Fisheries. Number of employees 1994-2015 (juvenile production). Available from: http://www.fiskeridir.no/english/aquaculture/statistics/atlantic-salmon-and-rainbow-trout, 2015b.

Norwegian Directorate of Fisheries. Kostnad per kilogram 2008-2014. Available from: http://www.fiskeridir.no/akvakultur/statistikk-akvakultur/loennsomhetsundersoekelse-for-laks-og-regnbueoerret/matfiskproduksjon-laks-og-regnbueoerret, 2015c.

Norwegian Directorate of Fisheries. Number of licenses per 31.12 1994-2015. Available from: http://www.fiskeridir.no/english/aquaculture/statistics/atlantic-salmon-and-rainbow-trout, 2016a.

Norwegian Directorate of Fisheries. Number of employees 1994-2015. Available from: http://www.fiskeridir.no/english/aquaculture/statistics/atlantic-salmon-and-rainbow-trout, 2016b.

Norwegian Directorate of Fisheries. Sale 1994-2015. Available from: http://www.fiskeridir.no/english/aquaculture/statistics/atlantic-salmon-and-rainbow-trout, 2016c.

Norwegian Ministry of Fisheries and Coastal Affairs. Aquaculture operations regulations with remarks (in Norwegian), 2008.

Oehme, M., Aas, T. S., Sørensen, M., Lygren, I., and Åsgård, T. Feed pellet distribution in a sea cage using pneumatic feeding system with rotor spreader. *Aquacultural Engineering*, 51(0):44–52, 11 2012. doi: http://dx.doi.org/10.1016/j.aquaeng.2012.07.001.

Olla, B., Davis, M., and Ryer, C. Foraging and predator avoidance in hatchery-reared Pacific salmon: Achievement of behavioral potential. In *The Importance of Feeding Behaviour for the Efficient Culture of Salmonid Fishes*, volume 2, pages 5–12. The World Aquaculture Society, 1992.

Oppedal, F., Dempster, T., and Stien, L. H. Environmental drivers of Atlantic salmon behaviour in sea-cages: A review. *Aquaculture*, 311(1-4):1–18, 2011. ISSN 0044-8486. doi: http://dx.doi.org/10.1016/j.aquaculture.2010.11.020.

Otterå, H., Karlsen, Ø., Slinde, E., and Olsen, R. E. Quality of wild-captured saithe (*Pollachius virens* L.) fed formulated diets for 8 months. *Aquaculture Research*, 40(11):1310–1319, 2009. ISSN 1365-2109. doi: http://dx.doi.org/10.1111/j.1365-2109.2009.02230.x.

Øverland, M., Sørensen, M., Storebakken, T., Penn, M., Krogdahl, Å., and Skrede, A. Pea protein concentrate substituting fish meal or soybean meal in diets for Atlantic salmon (*Salmo salar*) - Effect on growth performance, nutrient digestibility, carcass composition, gut health, and physical feed quality. *Aquaculture*, 288(3-4):305 – 311, 2009. ISSN 0044-8486. doi: http://dx.doi.org/10.1016/j.aquaculture.2008.12.012.

Parsonage, K. D. Detection of fish-food pellets in highly-cluttered underwater images with variable illumination. Master's thesis, The University of British Columbia, 2001.

Parsonage, K. D. and Petrell, R. J. Accuracy of a machine-vision pellet detection system. *Aquacultural Engineering*, 29(3–4):109–123, 2003. ISSN 0144-8609. doi: http://dx.doi.org/10.1016/S0144-8609(03)00049-9.

Pelletier, N. and Tyedmers, P. Feeding farmed salmon: Is organic better? *Aquaculture*, 272(1):399–416, 2007.

Pelletier, N., Tyedmers, P., Sonesson, U., Scholz, A., Ziegler, F., Flysjo, A., Kruse, S., Cancino, B., and Silverman, H. Not all salmon are created equal: Life cycle assessment (LCA) of global salmon farming systems. *Environmental Science & Technology*, 43(23):8730–8736, 2009. doi: http://dx.doi.org/10.1021/es9010114. PMID: 19943639.

Rasmussen, R. S., Larsen, F. H., and Jensen, S. Fin condition and growth among rainbow trout reared at different sizes, densities and feeding frequencies in high-temperature re-circulated water. *Aquaculture International*, 15:97–107, 2007. ISSN 0967-6120. doi: http://dx.doi.org/10.1007/s10499-006-9070-1.

Ruzzante, D. E. Domestication effects on aggressive and schooling behavior in fish. *Aquaculture*, 120:1–24, 1994. ISSN 0044-8486. doi: http://dx.doi.org/10.1016/0044-8486(94)90217-8.

Ryer, C. and Olla, B. Agonistic behavior in a schooling fish: form, function and ontogeny. *Environmental Biology of Fishes*, 31(4):355–363, 1991. ISSN 0378-1909. doi: http://dx.doi.org/10.1007/BF00002360.

Ryer, C. H. and Olla, B. L. Growth depensation and aggression in laboratory reared coho salmon: the effect of food distribution and ration size. *Journal of Fish Biology*, 48(4):686–694, 1996. ISSN 1095-8649. doi: http://dx.doi.org/10.1111/j.1095-8649.1996.tb01464.x.

Seymour, E. and Bergheim, A. Towards a reduction of pollution from intensive aquaculture with reference to the farming of salmonids in Norway. *Aquacultural*

Engineering, 10(2):73–88, 1991. ISSN 0144-8609. doi: http://dx.doi.org/10.1016/0144-8609(91)90001-Z.

Siciliano, B., Sciavicco, L., Villani, L., and Oriolo, G. *Robotics: modelling, planning and control*. Springer Science & Business Media, 2009.

Skøien, K. R. and Alfredsen, J. A. Feeding of large-scale fish farms: Motion characterization of a pneumatic rotor feed spreader. In *Oceans - St. John's, 2014*, pages 1–7, Sept 2014. doi: http://dx.doi.org/10.1109/OCEANS.2014.7003103.

Skøien, K. R., Alver, M. O., Føre, M., Solvang-Garten, T., Aas, T. S., Åsgård, T., and Alfredsen, J. A. Modellbasert pelletplassering i stormerd - neste skritt? Presentation. In *TEKMAR*, 2013a.

Skøien, K. R., Alver, M. O., Føre, M., Solvang-Garten, T., Aas, T. S., and Åsgård, T. E. Modelling and measurement of feed concentrations in salmon cages – tools for optimization of feeding. Abstract and presentation. *Presented at European Aquaculture Society (EAS 2013)*, 2013b.

Skøien, K. R., Alver, M. O., Føre, M., Solvang-Garten, T., Aas, T. S., Åsgård, T. E., and Alfredsen, J. A. Pellet distribution modelling: a tool for improved feed delivery in sea cages. Technical report, International Aquafeed, 2013c.

Skøien, K. R., Alver, M. O., and Alfredsen, J. A. A computer vision approach for detection and quantification of feed particles in marine fish farms. In *2014 IEEE International Conference on Image Processing (ICIP)*, pages 1648–1652, Oct 2014a. doi: http://dx.doi.org/10.1109/ICIP.2014.7025330.

Skøien, K. R., Alver, M. O., Føre, M., and Alfredsen, J. A. Modellbasert fôrdistribusjon i oppdrett. *Fiskeri og havbruk (Addition to Teknisk Ukeblad)*, page 14, 2014b.

Skøien, K. R., Alver, M. O., and Alfredsen, J. A. Modelling spatial surface pellet distribution from rotary pneumatic feed spreaders. In *23th Mediterranean Conference on Control and Automation (MED)*, pages 883–888, June 2015. doi: http://dx.doi.org/10.1109/MED.2015.7158857.

Skøien, K. R., Aas, T. S., Alver, M. O., Romarheim, O. H., and Alfredsen, J. A. Intrinsic settling rate and spatial diffusion properties of extruded fish feed pellets. *Aquacultural Engineering*, 74:30–37, 2016a. ISSN 0144-8609. doi: http://dx.doi.org/10.1016/j.aquaeng.2016.05.001.

Skøien, K. R., Alver, M. O., and Alfredsen, J. A. Modelling and simulation of rotary feed spreaders with application to sea cage aquaculture - a study of common and alternative designs (manuscript). 2016b.

Skøien, K. R., Alver, M. O., and Alfredsen, J. A. Optimizing feed delivery in salmon sea cage culture for growth and fish welfare - a simulation study (manuscript). 2016c.

Skøien, K. R., Alver, M. O., Lundregan, S., Frank, K., and Alfredsen, J. A. Effects of wind on surface feed distribution in sea cage aquaculture: A simulation study (in press). In *European Control Conference ECC16*, 2016d.

Skøien, K. R., Alver, M. O., Zolich, A. P., and Alfredsen, J. A. Feed spreaders in sea cage aquaculture - Motion characterization and measurement of spatial pellet distribution using an unmanned aerial vehicle. *Computers and Electronics in Agriculture*, 129:27 – 36, 2016e. ISSN 0168-1699. doi: http://dx.doi.org/10.1016/j.compag.2016.08.020.

Skretting. Fôr (in Norwegian). Technical report, Skretting, 2012.

Spong, M. W., Hutchinson, S., and Vidyasagar, M. *Robot modeling and control*. John Wiley & Sons, Hoboken, NJ, 1 edition, 2006.

SPSS. *IBM SPSS Statistics for Mac, Version 23.0.* Released 2015. : IBM Corp., Armonk, NY, 2015.

Sutherland, T., Amos, C., Ridley, C., Droppo, I., and Petersen, S. The settling behaviour and benthic transport of fish feed pellets under steady flows. *Estuaries and Coasts*, 29(5):810–819, 2006.

Suzuki, S. and Abe, K. Topological structural analysis of digitized binary images by border following. *Computer Vision, Graphics, and Image Processing*, 30(1):32–46, 1985. ISSN 0734-189X. doi: http://dx.doi.org/10.1016/0734-189X(85)90016-7.

Symons, P. E. K. Behavioural adjustment of population density to available food by juvenile Atlantic salmon. *Journal of Animal Ecology*, 40(3):569–587, 1971. ISSN 00218790.

Talbot, C. Some biological and physical constraints to the design of feeding regimes for salmonids in intensive cultivation. In Reinertsen, H., Dahle, L. A., Jørgensen, L., and Tvinnereim, K., editors, *Fish Farming Technology*, number ISBN 9054103264, pages 19–26. Balkema, Rotterdam, 1993.

Talbot, C., Corneillie, S., and Korsøen, Ø. Pattern of feed intake in four species of fish under commercial farming conditions: implications for feeding management. *Aquaculture Research*, 30(7):509–518, 1999. ISSN 1365-2109. doi: http://dx.doi.org/10.1046/j.1365-2109.1999.00369.x.

Taranger, G. L., Svåsand, T., Kvamme, B. O., Kristiansen, T., and Boxaspen, K. K. e. Risikovurdering norsk fiskeoppdrett 2012 (in Norwegian). Technical Report Fisken og havet, særnummer 2-2012, Institute of marine research, 2012.

Thomassen, J. and Lekang, O. Optimal distribution of feed in sea cages. In Reinertsen, H., Dahle, L. A., Jørgensen, L., and Tvinnereim, K., editors, *Fish Farming Technology*, number ISBN 9054103264, pages 439–442. Balkema, Rotterdam, 1993.

Thorpe, J. and Cho, C. Y. Minimising waste through bioenergetically and behaviourally based feeding strategies. *Water Science and Technology*, 31(10): 29–40, 1995. doi: http://dx.doi.org/10.1016/0273-1223(95)00424-L.

Thorpe, J., Talbot, C., Miles, M., Rawlings, C., and Keay, D. Food consumption in 24 hours by Atlantic salmon (*Salmo salar* L.) in a sea cage. *Aquaculture*, 90(1):41–47, 1990. ISSN 0044-8486. doi: http://dx.doi.org/10.1016/0044-8486(90)90281-Q.

Torstensen, B., Espe, M., Sanden, M., Stubhaug, I., Waagbø, R., Hemre, G.-I., Fontanillas, R., Nordgarden, U., Hevrøy, E., Olsvik, P., and Berntssen, M. Novel production of Atlantic salmon (*Salmo salar*) protein based on combined replacement of fish meal and fish oil with plant meal and vegetable oil blends. *Aquaculture*, 285(1-4):193 – 200, 2008. ISSN 0044-8486. doi: http://dx.doi.org/10.1016/j.aquaculture.2008.08.025.

Tuya, F., Sanchez-Jerez, P., Dempster, T., Boyra, A., and Haroun, R. Changes in demersal wild fish aggregations beneath a sea-cage fish farm after the cessation of farming. *Journal of Fish Biology*, 69(3):682–697, 2006.

Uglem, I., Karlsen, Ø., Sanchez-Jerez, P., and Sæther, B.-S. Impacts of wild fishes attracted to open-cage salmonid farms in Norway. *Aquaculture Environment Interactions*, 6:91–103, 2014. doi: http://dx.doi.org/10.3354/aei00112.

Vigne, J.-D. The origins of animal domestication and husbandry: A major change in the history of humanity and the biosphere. *Comptes Rendus Biologies*, 334(3):171 – 181, 2011. ISSN 1631-0691. doi: http://dx.doi.org/10.1016/j.crvi.2010.12.009.

Wathes, C., Kristensen, H., Aerts, J.-M., and Berckmans, D. Is precision livestock farming an engineer's daydream or nightmare, an animal's friend or foe, and a farmer's panacea or pitfall? *Computers and Electronics in Agriculture*, 64(1):2 – 10, 2008. ISSN 0168-1699. doi: http://dx.doi.org/10.1016/j.compag.2008.05.005.

Ytrestøyl, T., Aas, T., Berge, G., Hatlen, B., Sørensen, M., Ruyter, B., Thomassen, M., Hognes, E., Ziegler, F., Sund, V., et al. Resource utilisation and eco-efficiency of Norwegian salmon farming in 2010. *Nofima Report*, 53(2011):65, 2011.

Ytrestøyl, T., Aas, T. S., and Åsgård, T. E. Resource utilisation of Norwegian salmon farming in 2012. 2014.

Ytrestøyl, T., Aas, T. S., and Åsgård, T. Utilisation of feed resources in production of Atlantic salmon (*Salmo salar*) in norway. *Aquaculture*, 448:365–374, 2015. ISSN 0044-8486. doi: http://dx.doi.org/10.1016/j.aquaculture.2015.06.023.

Zolich, A., Alfredsen, J. A., Johansen, T. A., and Skøien, K. R. A communication bridge between underwater sensors and unmanned vehicles using a surface wireless sensor network – design and validation. In *OCEANS 2016 - Shanghai*, pages 1–9, April 2016. doi: http://dx.doi.org/10.1109/OCEANSAP.2016.7485493.